SYNTHESIS OF TRIAZOLE DERIVATIVES AS ANTI-TUBERCULAR AND ANTICANCER AGENTS

Thesis submitted to

THE KLE ACADEMY OF HIGHER EDUCATION AND RESEARCH,

BELAGAVI

(KLE DEEMED UNIVERSITY)

[Declared as Deemed-to-be-University u/s 3 of the UGC Act, 1956 vide

Govt. of India Notification No.F.9-19/2000-U.3 (A)]

(Accredited 'A+' Grade by NAAC)(3rdCycle)

[Placed in Category 'A' by MHRD (GoI)]

For the award of the degree of

Doctor of Philosophy

In the Faculty of

Pharmacy

by

ARNIKA DAS, M. Pharm.

(Registration No: KLEU/Ph.D./14-15/D01214007)

Under the Guidance of

DR. SUBHAS S. KARKI, M. Pharm., Ph. D

Professor

JANUARY-2023

UNDERTAKING

I, **ARNIKA DAS** hereby declare that the information and the data mentioned in my thesis entitled "**Synthesis of Triazole Derivatives As Anti-Tubercular And Anticancer Agents"** belongs to me and is original.

I am aware of definition of plagiarism as detailed below:

- An act or instance of using or closely imitating the language and thoughts of another author without authorization and the representation of that author's work as one's own, as by not crediting the original author.
- A piece of writing or other work reflecting such unauthorized use or imitation.
- The deliberate or reckless representation of another's words, thoughts or ideas as one's own without attribution in connection with submission of academic work, whether graded or otherwise.

I hereby declare that the thesis prepared by me is original-one and does not involve plagiarism anywhere. In case at a later stage it is found that I have indulged in plagiarism, then I am solely responsible for the same and the Institution is at liberty to take any disciplinary action against me including cancellation of dissertation or any other penalties imposed by the University.

Signature of the Research Scholar

Place: Bengaluru

Arnika Das, M. Pharm.

Date:

KLE College of Pharmacy,

Bengaluru-560010.

KLE ACADEMY OF HIGHER EDUCATION AND RESEARCH
(Formerly known as KLE University)
(Deemed-to-be-University established u/s 3 of the UGC Act, 1956)
Accredited A+ Grade by NAAC (3rd Cycle) Placed in Category 'A' by MHRD (GoI)
JNMC Campus, Nehru Nagar, Belagavi-590 010, Karnataka State, India
☎: 0831-2444444 Web: http://www.kledeemeduniversity.edu.in E-mail: info@kledeemeduniversity.edu.in

Ref. No. KAHER/AA/22-23/D- 229 12th December 2022

Madam,

The soft copy of Ph.D. research thesis of **Ms. Arnika Das, Faculty of Pharmacy, KAHER,** has been submitted for anti-plagiarism check at the office of the undersigned through "Turn-it-in" package. The scan has been carried out and the scanned output reveals a match percentage of **3%** which is within the acceptable limit of 10%.

To obtain the comprehensive report of the plagiarism test, research scholar can send a mail to **diracademic@kledeemeduniversity.edu.in** along with the Registration Number, Name of the Scholar, Name of Guide/Co-guide and title of the thesis.

DIRECTOR ACADEMIC AFFAIRS Deemed-to-be-University

Dr.(Mrs.) Roopa M. Bellad
Director, Academic Affairs

To,
Ms. Arnika Das
Full-Time Research Scholar
2014-15 Batch, Faculty of Pharmacy,
College of Pharmacy,
KAHER, **Bengaluru**.

KLE ACADEMY OF HIGHER EDUCATION AND RESEARCH,

(KLE DEEMED UNIVERSITY)

[Declared as Deemed-to-be-University u/s 3 of the UGC Act, 1956 vide Govt. of India Notification No.F.9-19/2000-U.3 (A)]

(Accredited 'A+' Grade by NAAC) (3rdCycle)

[Placed in Category 'A' by MHRD (GoI)]

BELAGAVI

COPYRIGHT DECLARATION

We hereby declare that **KLE ACADEMY OF HIGHER EDUCATION AND RESEARCH, BELAGAVI, KARNATAKA,** *shall have the rights to preserve, use and disseminate this thesis in print or electronic format for academic/research purpose.*

Signature of Research Scholar
Arnika Das, **M. Pharm.**

Signature of Research Guide
Dr. Subhas S. Karki, **M. Pharm., Ph. D**
Professor & Head
Department of Pharmaceutical Chemistry
KLE College of Pharmacy
Bengaluru-560010.

Place: Bengaluru

Date:

KLE ACADEMY OF HIGHER EDUCATION AND RESEARCH,

(KLE DEEMED UNIVERSITY)

[Declared as Deemed-to-be-University u/s 3 of the UGC Act, 1956 vide Govt. of India Notification No.F.9-19/2000-U.3 (A)]

(Accredited 'A+' Grade by NAAC) (3rd Cycle)

[Placed in Category 'A' by MHRD (GoI)]

BELAGAVI

DECLARATION

*I hereby declare that the thesis entitled "**Synthesis of Triazole Derivatives As Anti-tubercular And Anticancer Agents**" is a bonafide and original research carried out by me under the guidance of Dr. Subhas S. Karki, Professor & Head Dept. of Pharmaceutical Chemistry, KLE College of Pharmacy, Bengaluru. The thesis or any part thereof has not formed the basis for the award of any degree/fellowship or similar title to any candidate of any University.*

Place : Bengaluru
Date :

Signature of Research Scholar
Arnika Das, M. Pharm.
KLE College of Pharmacy,
Bengaluru-560010.

KLE ACADEMY OF HIGHER EDUCATION AND RESEARCH,

(KLE DEEMED UNIVERSITY)

[Declared as Deemed-to-be-University u/s 3 of the UGC Act, 1956 vide Govt. of India Notification No.F.9-19/2000-U.3 (A)]

(Accredited 'A+' Grade by NAAC) (3rd Cycle)

[Placed in Category 'A' by MHRD (GoI)]

BELAGAVI

CERTIFICATE

*This is to certify that the thesis entitled "**Synthesis of triazole derivatives as anti-tubercular and anticancer agents**" is a bonafide and genuine research carried out by Arnika Das under the guidance of Dr. Subhas S. Karki, Ph.D, Professor & Head Dept. of Pharmaceutical Chemistry, KLE College of Pharmacy, Bengaluru.*

Place : Belagavi
Date :

Signature
Dr. M.S Ganachari, Dean
Faculty of Pharmacy
KLE Academy Of Higher Education& Research Belagavi, Karnataka.

KLE ACADEMY OF HIGHER EDUCATION AND RESEARCH,

(KLE DEEMED UNIVERSITY)

[Declared as Deemed-to-be-University u/s 3 of the UGC Act, 1956 vide Govt. of India Notification No.F.9-19/2000-U.3 (A)]

(Accredited 'A+' Grade by NAAC) (3rd Cycle)

[Placed in Category 'A' by MHRD (GoI)]

BELAGAVI

CERTIFICATE

*This is to certify that the thesis entitled "**Synthesis of triazole derivatives as anti-tubercular and anticancer agents" is** a bonafide record of original research carried out by Arnika Das for the award of degree of DOCTOR OF PHILOSOPHY IN FACULTY OF PHARMACY under my supervision and guidance.*

Place : Bengaluru
Date :

Signature
Dr. Subhas S. Karki, M. Pharm, Ph.D
Professor & Head
Department of Pharmaceutical Chemistry
KLE College of Pharmacy, Bengaluru-5600010.

KLE ACADEMY OF HIGHER EDUCATION AND RESEARCH,
(KLE DEEMED UNIVERSITY)

[Declared as Deemed-to-be-University u/s 3 of the UGC Act, 1956 vide Govt. of India Notification No.F.9-19/2000-U.3 (A)]

(Accredited 'A+' Grade by NAAC) (3rd Cycle)

[Placed in Category 'A' by MHRD (GoI)]

BELAGAVI

CERTIFICATE

*This is to certify that the thesis entitled "**Synthesis of triazole derivatives as anti-tubercular and anticancer agents**" is a bonafide record of original research carried out by ARNIKA DAS under the guidance of Dr. Subhas S. Karki, Professor & Head Dept. Of Pharmaceutical Chemistry, KLE College of Pharmacy, Bengaluru.*

Place : Bengaluru
Date :

Signature
Dr. Rajamma A.J, M. Pharm, Ph.D
Principal
KLE College of Pharmacy,
Bengaluru-5600010.

ACKNOWLEDGMENT

This dissertation would not have been possible without the guidance and help of intellectuals who contributed and extended their support to complete this study.

I would like to express my sincere thanks to my Guide ***Dr. Subhas S. Karki****, Professor,& Head, Dept. of Pharmaceutical Chemistry, KLE College of Pharmacy-Bengaluru, for the supervision during the research.*

My Sincere thanks to ***Dr. A.J. Rajamma,*** *Principal, KLE College of Pharmacy Bengaluru, for the support to complete this research.*

Sincere thanks to ***Dr. H.N Shivakumar****, Vice-Principal, KLE College of Pharmacy, Bengaluru and* ***Dr. Sujeet Kumar,*** *Associate Professor, Department of Pharmaceutical Chemistry, KLE College of Pharmacy, Bengaluru, for the assistance in synthesis.*

I would like to express my gratitude to the ***Office of the Director****, Academic Affairs, KAHER, Belagavi.*

A, Special thanks to ***Giulia Greco, Elena Catanzaro, Rita Morigi, Alessandra Locatelli, Dominique Schols, Camella Fimognari, Hakan Alici, Hakan Tahtaci, Drik Daelemans, Lentjee Persoons*** *and other overseas collaboratorsfor biological evaluation support.*

My Sincere thanks to ***Febina Ravindran,*** *IBAB, Bengaluru, for the in-vitro normal cell line study during the research.*

My special thanks to ***Mr. J.N. Biradar,*** *Store in-charge, KLE College of Pharmacy, Bengaluru for the timely availability of reagents and solvents during the research.*

I am thankful to ***Agilent Technologies****, Bengaluru and* ***NMR Research Centre IISc.-Bengaluru*** *for the LC-MS and NMR spectra.*

Last but not least "Thank you my Better-Half, My Parents, In-Laws, Sister, Friends and, The Almighty GOD" for everything you gave me.

Signature of the Research Scholar

Date : **Arnika Das.**

Place:

TABLE OF CONTENTS

ABBREVIATIONS & SYMBOLS

%: Percentage

&: And

α: Alpha

δ: Delta

°C: Degree Celsius

µ: Micro

3D: Three-dimensional

7-AAD: 7-Aminoactinomycin D

ACE: Angiotensin converting enzyme

ADME: Absorption, distribution, metabolism and excretion

ALA: Alanine

ali: Aliphatic

ANOVA: Analysis of variance

ar.: Aromatic

ASP: Aspartase

ATCC: American type cancer collection

BCL: Beta cell leukemia/lymphoma

C: Carbon

Caco: Cancer coli

CCCP: Carbonylcyanide 3-chlorphenylhydrazone

CCP: Citrullinated peptide

CDK: Cyclin-dependent kinase

Cm: Centimeter

CoV: Corona virus

Cpt: Camptothecin

d: Deuterated

DCF: 2,7-Dichlorofluorescein

DFO: Deferoxamine mesylate

DHA: Docosahexaenoic acid

DMF: Dimethyl formamide

DMSO: Dimethyl sulfoxide

DNA: Deoxyribonucleic acid

DSMZ: Deutsche Sammlung von mikroorganismen und zellkulturen

DTT: Dithiothreitol

Em: Emission

ESOL: Estimated solubility

ETO: Etoposide

EtOH: Ethanol

Ex: Extinction

Ferr: Ferrostatin

Fsp3: Fraction of sp3 carbon

FTIR: Fourier transform infrared

g: Gram

G: Growth

GMCSF: Granulocyte-macrophage colony stimulating factor

h: Hour

H: Hydrogen

H2DCFDA: 2',7'-dichlorodihydrofluorescein diacetate

HAS: Human albumin serum

HBA: Hydrogen bonds acceptor

HBD: Hydrogen bonds donor

HCT: Human colorectal carcinoma

HeLa: Henrietta Lacks

Hep: Hepatoma/Hepatocellular

HL: Human leukemia

IC: Inhibitory concentration

IL: Interleukin

IUPAC: International union of pure and applied chemistry

L: Liter

LCMS: Liquid chromatography-mass spectrometry

LEU: Leucine

LGA: Lamarckian genetic algorithm

m.p: Melting point

m/z: Mass/charge

m: Mili

M: Mole

MCF: Michigan cancer foundation

MCR: Mobile colistin resistance

MeOH: Methanol

MET: Methionine

MF: Molecular formula

MFI: Mean fluorescence intensity

MG: Malignant glioma

MHz: Mega-Hertz

MIC: Minimum inhibitory concentration

MMFF: Merck molecular force field

M-phase: Mitosis phase

Mpro: Main protease

MR: Molar refractivity

MTCC: Microbial type culture collection

MW: Molecular weight

n: Nano

N: Nitrogen

N: Normal

NCIM: National collection of industrial microorganism

NCP: National cancer registry program

Nec: Necrostatin

NMR: Nuclear magnetic resonance

No.: Number

OADC: Oleic acid albumin-dextrose catalase

Obs: Observed

OD: Optical density

Ola: Olaparib

OPN: Osteopontin

P: Para

PBS: Phosphate buffer saline

PC: Protease cancer cell line

PLpro: Papain-like protease

pNA: Peptide nucleic acid

ppm: Parts per million

PyRx: Python prescription

RB: Rotatable bonds

R_f: Retardation factor

ROS: Reactive oxygen species

RPMI: Rosewell Park Memorial Institute

S: Synthesis

SARS: Severe acute respiratory syndrome

SEM: Standard error of the mean

Sl.: Serial

STS: Staurosporine

TB: Tuberculosis

TLC: Thin layer chromatography

TMS: Tetramethyl silane

TNF: Tumor necrosis factor

tPSA: Topological polar surface area

USA: United States of America

UV: Ultra-violet

v: Volume

VAD-FMK: Valyl-alanyl-aspartyl-[O-methyl]-fluoromethylketone

VEGFR: Vascular endothelial growth factor receptor

Vit: Vitamin

WB: Wash buffer

WHO: World health organization

List of Tables

List of Figures

Abstract

Background:

Cancer and tuberculosis are India's biggest health concerns. The National Cancer Registry Program 2022 reports an estimated 14,61,427 cancer patients in India by 2025 while WHO finds India as the country with the maximum number of tuberculosis cases. The government of India vowed to eradicate TB by 2025. The chemotherapeutic agents available to treat cancer bear one or the other untoward effects. At the same time, the emergence of multi-drug resistance Mycobacterium strains are limiting the effectiveness of existing anti-tubercular drugs.

Objectives:

To design and develop1,2,3-triazole analogs as a *lead* against cancer and tuberculosis.

Methodology:

The stilbene-linked 1-benzyl-4-((4-styrylphenoxy)methyl)-1*H*-1,2,3-triazoles**AD 1-24** were obtained by refluxing 4-((1-benzyl-1*H*-1,2,3-triazol-4-yl)methoxy)benzaldehydes **7a-d** with aralkyl triphenylphosphonium halides **10a-f**involving Wittig reaction while the Knovenagal condensation of **7a-d** with indoline-2-ones **13a-f** gave 3-(4-((1-benzyl-1*H*-1,2,3-triazol-4-yl)methoxybenzylidene)indolin-2-ones **AD 25-48.** The 4-((1-benzyl-1*H*-1,2,3-triazol-4-yl) methoxy)benzaldehydes **7a-d**were obtained in a regioselective copper (Cu)-catalyzed dipolar-1,3-cycloaddition of 4-(prop-2-benzyloxy)benzaldehyde **(3)** with benzyl azides **6a-d.** Compounds **3, 6a-d** and **13a-f** were prepared as per the literature. The *in-vitro* cytotoxicity was performed and mechanism of action was established thereafter. *In-silico* ADME and the drug-likeness prediction were done using the Swiss-ADME webserver. Docking studies were performed on Tubulin Alpha-Beta Dimer 1TUB and TGFR receptor 6P8Q using PyRx and AutoDockVina with the Lamarckian genetic algorithm using

Discovery Studio as visualizing tool.One-way analysis of variance (ANOVA) was used to measure inter-group data variation (mean ± SEM) using Graph Pad Prism 6.01.

Results:

Analytical data summarized in **Tables 4.13-4.20** and **Figures4.1-4.14** confirm the structure of newly synthesized derivatives. Compound **AD 03** (IC_{50}: 19.30 µM, K-562), **AD 05** (IC_{50}:13.5 µM, HCT-116), **AD 08** (IC_{50}: 12.2 µM, HCT-116 & 11.6 µM, NCI H460), **AD 11** (IC_{50}: 12.6µM, HCT-116) **AD 18** (IC_{50}: 16.2 µM, NCI H460), **AD 23** (IC_{50}: 12.2 µM, NCI-H460), **AD 30** (IC_{50}: 1.5±0.6 µM, CEM), and, **AD-45** (1.7±0.8 µM, CEM) were the active molecules from the series. Biological investigations found apoptosis induction and caspase-3 activation by **AD-30**. No ROS production and mitochondrial membrane potential alteration was observed during the study. Docking results were found to be in coherence with *in-vitro* cytotoxicity data.

Conclusion:

A total of, forty-eight 1,2,3-triazole derivatives**(AD 1-48)** were synthesized, characterized, and, screened for *in-vitro* cytotoxicity. The stilbene-linked derivatives **AD-08** and **AD-18** had shown good *in-vitro* cytotoxicity.Most of the compounds were found selective towards carcinoma cells. The indolin-2-one linked analogs **(AD 25-48)** were found to be active against CEM and HeLa cells. Compound **7c/AD-30** was found to be the most potent in the series with no genotoxicity. Biological data reveals **7c/AD-30**&**7w/AD-45** have the potential to become a lead against cancer. Further study is warranted to establish it. No anti-mycobacterial properties were observed during the study.

Keywords:

Cancer; Tuberculosis; 1,2,3-Triazole; Stilbene; Indole; Cytotoxicity; Molecular Docking; 1TUB; 6P8Q.

1.0 INTRODUCTION

Cancer is responsible for one in six deaths globally.[1] In the United States of America, it is second only to cardiovascular disease in terms of mortality.[2] Indian health sector receives approximately 800,000 cancer patients annually.[3] The NCRP (National cancer registry program) 2022 report estimate 14, 61, 427 cancer patients in India with a 12.8 % hike by 2025.[4] Credit goes to multiple factors such as late diagnosis, infection, pollution, smoking, excessive alcohol consumption, genetic changes, etc. Scientifically, cancer is defined as the uncontrolled growth of cells affecting every organ system of the body.[5] The cancer cell growth can be controlled or reduced either by surgery, radiation, chemotherapy, and immunotherapy or, by a combination of these methods. Depending on the cancer cell loading the treatment protocol **(Figure 1.1)** is followed.[6] Each method has its own merits and demerits. Surgery and radiation therapy are site-specific and localized while the chemotherapeutic agents **(Figure 1.2)** are cytotoxic in nature.[7]

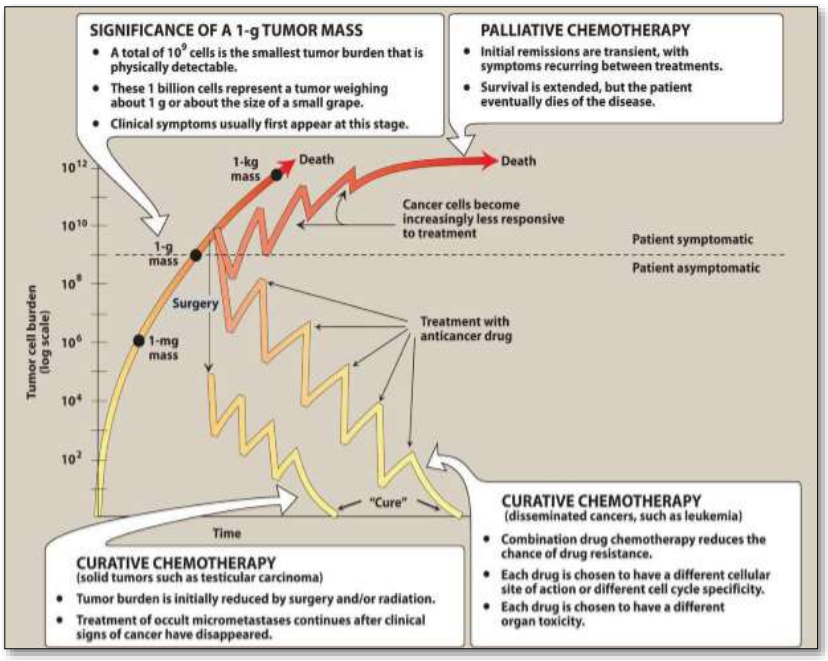

Figure 1.1. Effects of various treatments on the cancer cell burden in a hypothetical patient.[6]

However, despite the toxicity, the chemotherapeutic agents are used to relieve cancer symptoms and improve the quality of life. No therapy can claim to eradicate cancer cells completely.

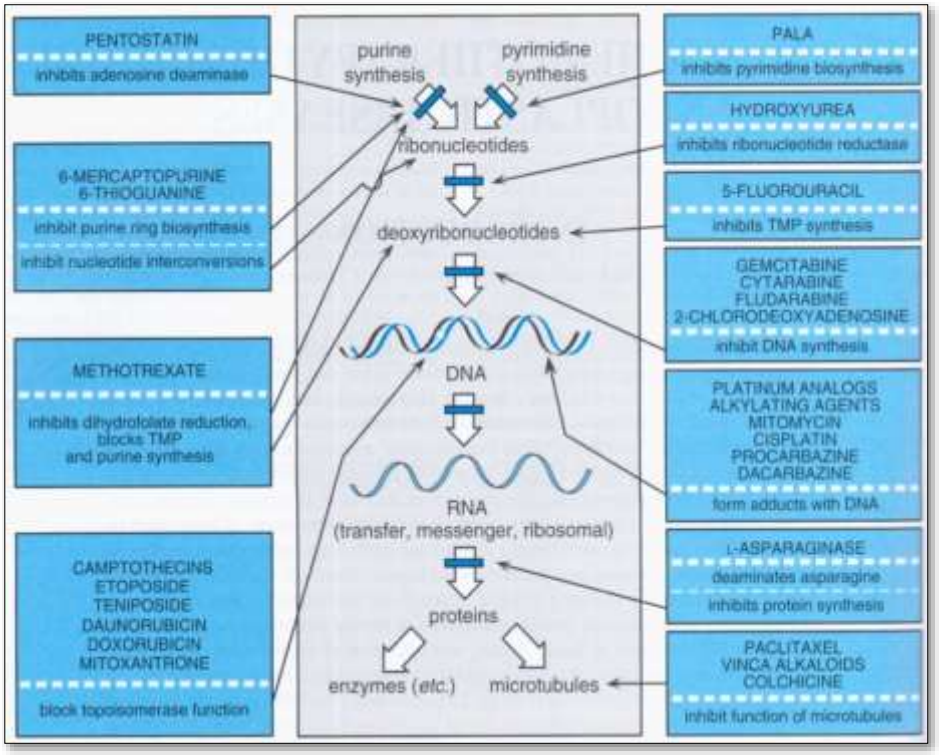

Figure 1.2. Chemotherapeutic agents affecting RNA and DNA synthesis process.[7]

TB (Tuberculosis) is India's biggest health concern, second to cancer. It caused approximately 10.6 million deaths globally in 2021 with the highest contribution from India **(Figure 1.3)**.[8, 9] The government of India vowed to eradicate TB by 2025.[10]

1.1 Background:

Chemotherapeutic agents, **Figure 1.2** cause cytotoxic effects and arrest the tumor cell progression. It may be DNA (Deoxyribonucleic acid) targeted or against metabolic pathways. An ideal chemotherapeutic agent should have high selectivity for cancer cells over normal cells. Unfortunately, the traditionally used anticancer drugs are devoid of it and cause severe toxicity. Metastasis is another obstacle in cancer therapy.[6, 7]

In the case of TB, the currently prescribed anti-tubercular drugs are not effective alone. The silent killer (TB) may affect the larger section of society, especially, the economically deprived and ill-educated segment of India. The emergence of multi-drug resistance *Mycobacterial* strains is limiting the effectiveness of existing 1st and 2nd line anti-tubercular isoniazid, rifampin, aminoglycosides, etc.[6]

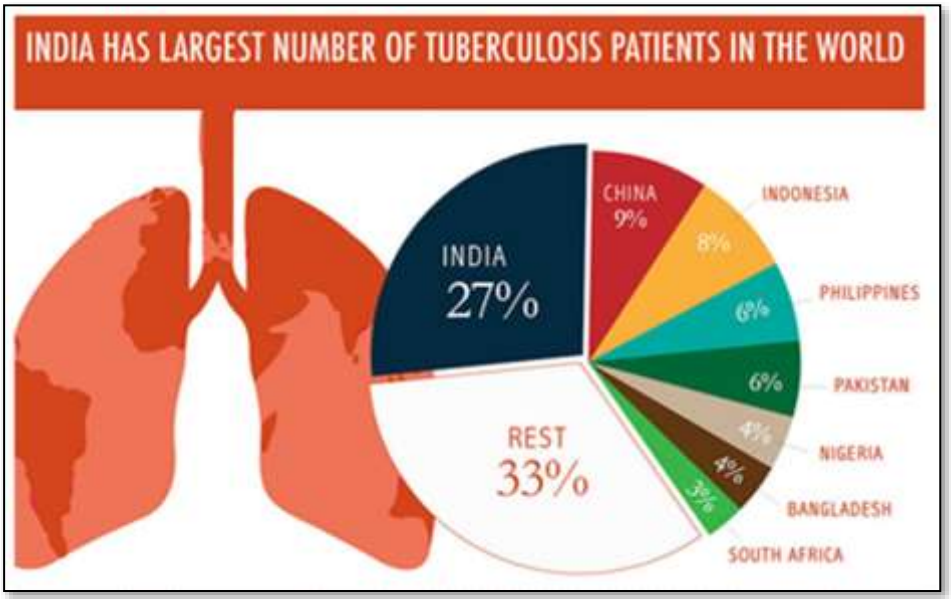

Figure 1.3: WHO (World Health Organization) India's tuberculosis report.[8]

Hence, extensive research is needed to find the future lead against TB. Hence, there is a need for rapid and effective drug discovery to tackle cancer and TB.

Heterocycles & drug discovery

Heterocyclic chemistry plays important role in the drug discovery process. Low cytotoxicity, synthetic feasibility, reactivity, and greater receptor affinity make nitrogen heterocycles the first choice substrate in the process **(Figure 1.4).**[11] Among nitrogen-bearing molecules, imidazole, and triazoles are the most studied **(Figure 1.5).**[12] Considering the biological importance of nitrogenous heterocyclic moieties in medicinal chemistry, it was decided to develop some 1,2,3-triazole analogs with possible anticancer and anti-tubercular properties.

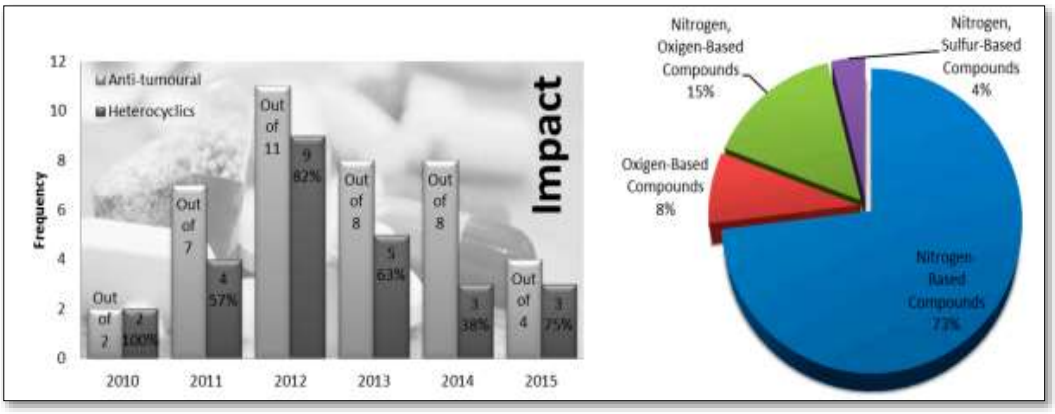

Figure 1.4. Role of heterocycles in anticancer drug discovery.[11]

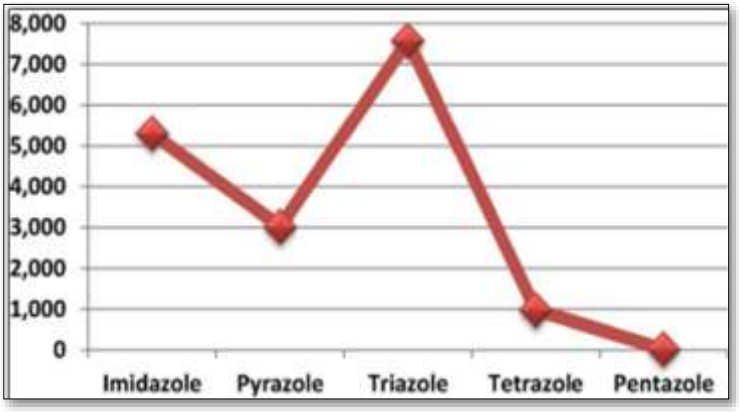

Figure 1.5. Nitrogen-containing heterocycles in drug discovery.[12]

1.3 Justification:

Triazole

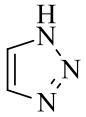

1,2,3-Triazole **(1.1)**

1,2,3-Triazole is a synthetically versatile moiety. Chemically, it is a five-membered ring with three nitrogen in a row **(1.1).** It can be prepared by 1,3-dipolar cycloaddition reaction between alkyne and azide **(1.2).**[13]

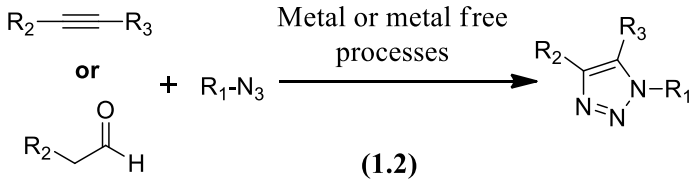

(1.2)

In aqueous solution, *triazole* exists in three tautomeric form **(1.3).**[13]

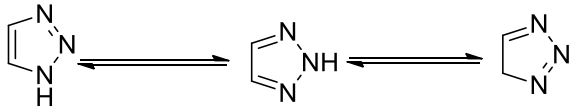

1,2,3-1*H*-Triazole **1,2,3-2*H*-Triazole** **1,2,3-4*H*-Triazole**

(1.3)

1,2,3-Triazole acts as an useful isostere known for its diverse biological properties such as anticancer, antiviral, anti-tubercular etc. **(1.4).**[14]

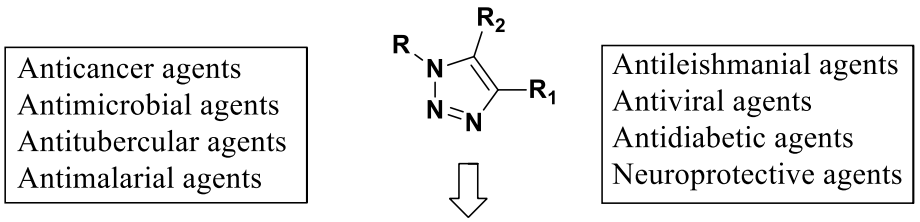

(1.4)

Indole

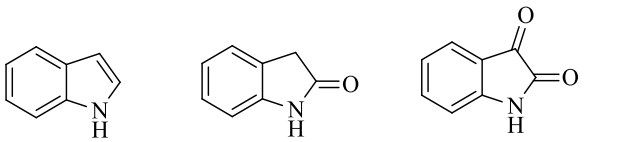

1*H*-indole **Indolin-2-one** **Indoline-2,3-dione**

(I.5) **(1.6)** **(1.7)**

Among heterocycles, indoles **(1.5-1.7)** are the most promising moieties and, are considered golden scaffolds in drug design. It's widely distributed in nature, less toxic and, synthetically versatile. Many indole derivatives have been reported with diverse pharmacological properties such as sunitinib **(1.8),** and indomethacin **(1.9).**[6, 15] Further, design of Disarib **(1.10)** a BCL2 (Beta cell leukemia) inhibitor by Iyer et al.[16] made us to synthesize some more indole derivatives with possible anticancer and antitubercular properties.

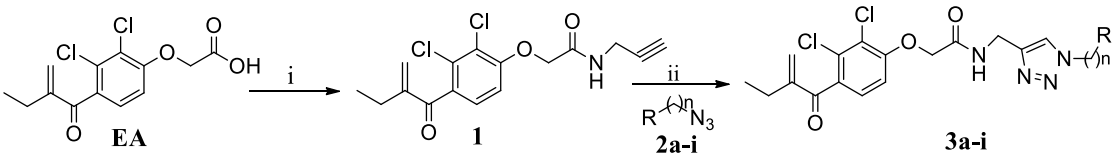

(Where, n= -CH_2, -CH_2CH_2-, R= Phenyl, Pyridyl, 4-NH_2-phenyl, 4-Anisyl, 4-F-Phenyl, 4-NO_2-Phenyl)

(2.6)

Stilbene

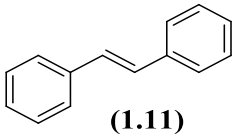

(1.11)

Stilbene or (*E*)-1,2-Diphenylethene

Stilbene **(1.11)** based compounds (hydroxylated) are widely available in nature and have attracted many researchers. *Trans* resveratrol **(1.12)** present in grapes **(Figure 1.6)** prevent coronary disorders effectively.[17, 18] Besides this, it is also known for its chemo-preventive, antioxidant, antineoplastic, and anti-estrogenic property.[19] Tamoxifen **(1.13)** is a stilbene derivative used to treat breast cancer.[20]

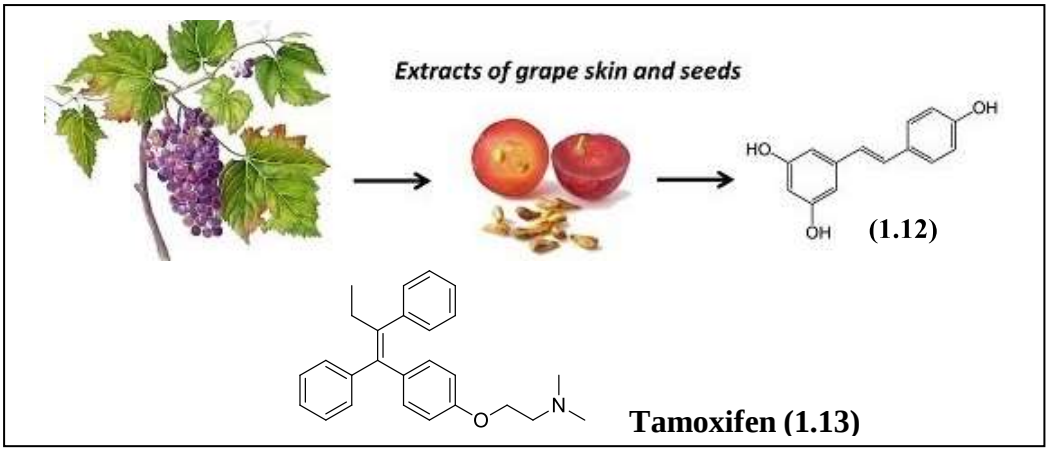

Figure 1.6: Isolation of resveratrol from Grapes.[18]

Considering the biological importance of triazole, indole and stilbene nucleus, the fused analogs were designed by incorporating the stilbene and indole moieties on 1,2,3-triazole through a linker (methylene) to get new lead with advanced physicochemical and biological properties against cancer and tuberculosis.

2.0 REVIEW OF LITERATURE

Triazole is the most explored molecule among 5-membered heterocycles. Below are the excerpts from the literature survey done on anticancer and antimicrobial properties of the triazole.

Othman et al.[21] (2022) have reported semicarbazone and thiosemicarbazone derivatives bearing1,2,3-triazole nuclei **(2.1)** as VEGFR-2 (Vascular endothelial growth factor receptor-2) inhibitors. The synthesized derivatives were active against leukemic cell line HL 60 (Human leukemia). The VEGFR-2 inhibitory property of molecule **21, 26,** and **30,** were at 0.128, 0.413, and 0.067 µM (micromole) respectively, compared to Sorafenib (0.048 µM [Micromole]). Early apoptosis was reported by molecule **30.**

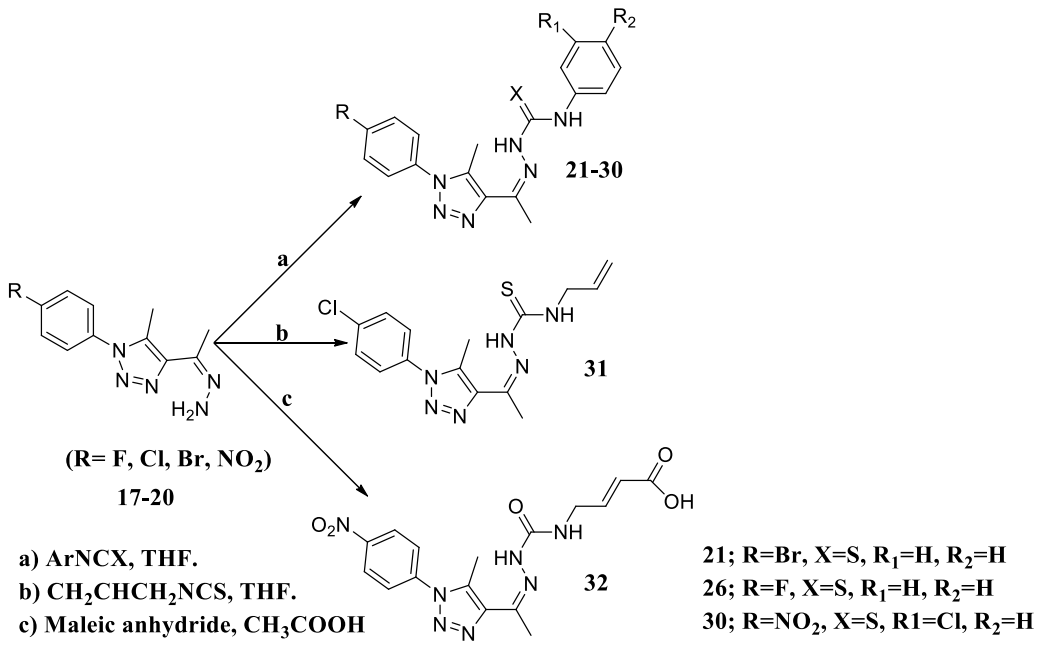

(2.1)

Aouad et al.[22] (2022) have reported triazole analogs bearing sulphonamide moiety **(2.2).** Synthesized derivatives were screened for their anticancer property against HepG-2 (Hepatoma G-2), Caco-2 (Cancer coli-2) and, MDA-MB-231 cells. Doxorubicin was used as reference.

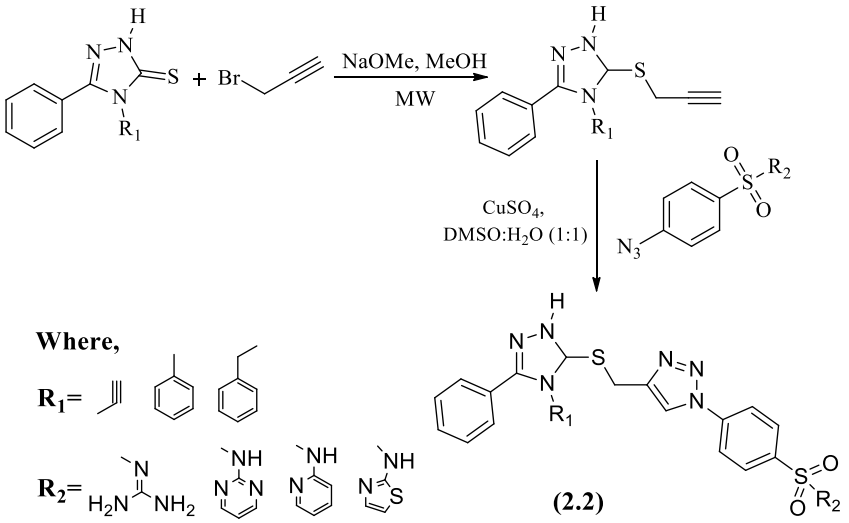

Tan A have (2022) reported phthalimides linked 1,2,3-triazoles as potential SARS-CoV-2 (Severe acute respiratory syndrome-corona virus-2) inhibitors **(2.3).** Molecular docking performed on SARS-CoV-2 (Mpro [Main protease] and PLpro [Papain like protease]) proteins find stable interaction in 8a-Mpro, 8b-PL-pro, and 9a-'ACE2-S1' (Angiotensin converting enzyme-2) interactions. The compounds may also inhibit the progression of the Mpro, and PL-pro proteins of SARS-CoV-2.[23]

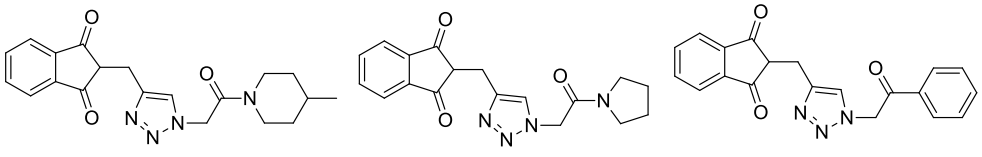

(2.3)

Mlakic et al.[24] (2022) had reported stilbene linked 1,2,3-triazoles **(2.4)** for anti-inflammatory and anticholinesterase (acetyl, butyl) properties. Reduction in TNFα (Tumour necrosis factor-α) production was observed as cholinesterase inhibitory marker.

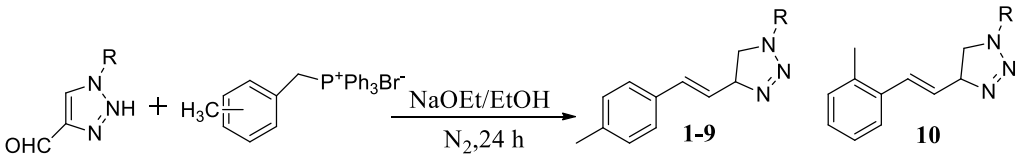

(Where, R= Isopropyl, n-Butyl, 1-Butene, 2-Butene, n-Pentanol, 2-Ethylindole, Benzyl, *N*-Ethyl aniline).

(2.4)

Narul et al.[25] (2022) had reported synthesis and immunomodulatory property of 1,4-disubstituted-bis-1,2,3-triazoles. The immunomodulatory properties of newly synthesized derivatives was studied by evaluating TNF-α, GMCSF (Granulocyte macrophage colony-stimulating factor) IL6 (Interleukin-6), and IL12p40 cellular release and, found to be supressed. Some of the molecules were effective through PI3K pathway.

Oubella et al.[26] (2021) have reported thiazolidinone-linked-1,2,3-triazoles **(2.5)** as potential cytotoxic moiety against A-549, MDA-MB-23, HT-1080 and, MCF-7 (Michigan Cancer Foundation-7) cells. The obtained IC_{50} (Inhibitory concentration) showed mild anti-proliferative activity (IC_{50}: 15.04 ± 0.71 to 42.22 ± 1.20 µM). Caspase-3/7 activation, and S/G2 (Synthesis/Growth-2) phase arrest was observed suggesting apoptosis.

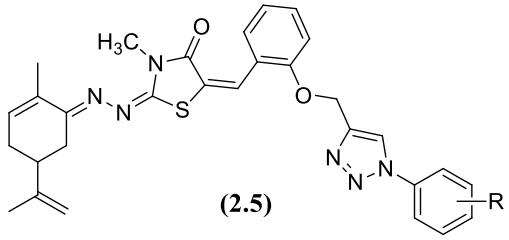

(2.5)

Abbouchi et al.[27] (2021) had reported cytotoxicity of ethacrynic acid bearing triazoles **(2.6 a, b)** against HL60 cell line. Later, molecule **3a, 3c** tested against cancerous HCT116 (Human colorectal carcinoma 116), SKOV3, PC3 (Protease cancer cell line-3), U87-MG, A549, MCF7 and normal MCR5 (Mobile colistin resistance-5) cells. Good antitumor activities expressed in nm (Nano mole) by **3c** against A549, PC3 and U87-MG (Malignant glioma) cell lines respectively (IC_{50}: 20.2, 56.5 and 76.8 nM). Compound **3c** found to 1.3 and 2.8 times more potent than doxorubicin against U87-MG and A549 cells, respectively. Mitochondrial dysfunctions leading to caspase-induced apoptosis was observed for **3c** during the study.

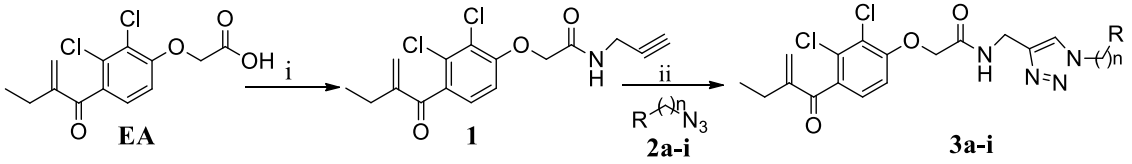

(Where, n= -CH_2, -CH_2CH_2-, R= Phenyl, Pyridyl, 4-NH_2-phenyl, 4-Anisyl, 4-F-Phenyl, 4-NO_2-Phenyl)

(2.6)

Kumar et al.[28] (2021) have reported synthesis, anti-tubercular and HAS (Human albumin serum) binding property of imidazole based 1,2,3-triazole derivatives **(2.7)** against *M. tuberculosis* H37Rv. The cytotoxicity was performed against mammalian Vero cell lines. The compounds **3d** and **3e** displayed potent *in-vitro* anti-tubercular activity. Further, HAS binding was observed by molecule **3a (2.7).**

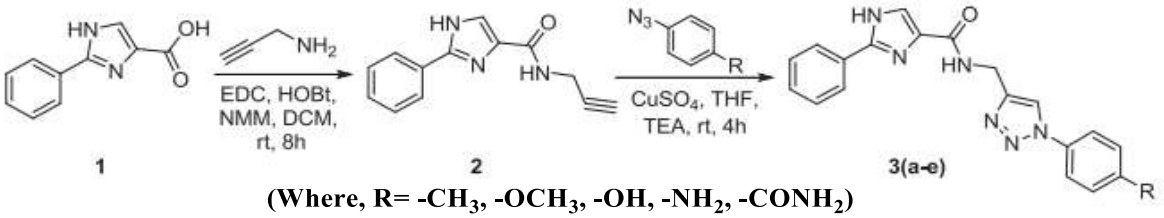

(Where, R= -CH_3, -OCH_3, -OH, -NH_2, -$CONH_2$)

(2.7)

Oliveira et al.[29] (2021) had synthesized and screened glycoconjugates of oxadiazole linked 1,2,3-triazoles against *M. tuberculosis* H37RV and lung carcinoma. A series of 43 molecules were synthesized. Anticancer screening was done for 17 molecules against NCIH-460, AGP-01, PC-3, SKMEL-103 and, HCT-116 cells. Molecule 7 **(2.8)** had shown *in-vitro* inhibitory activity against H37Rv (23.9 mM).

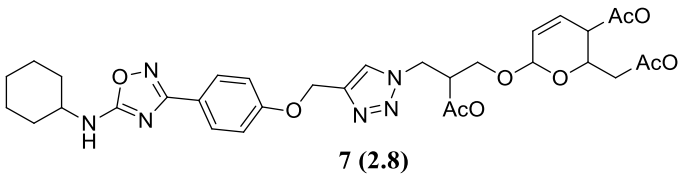

7 (2.8)

Ashour et al.[30] (2020) have synthesized 1,2,3-triazole-chalcones **(2.9)** and screened on NCI cell lines. Molecule **4d** was most potent from the series inhibiting SR leukemic cells by 94.95% (10 µM) concentration. It also inhibited the growth of MCF7, K-562

and, M14 cells by more than 80% at the same test concentration. Compound **4d** showed better activity than methotrexate and gefitinib against K-562 cells.

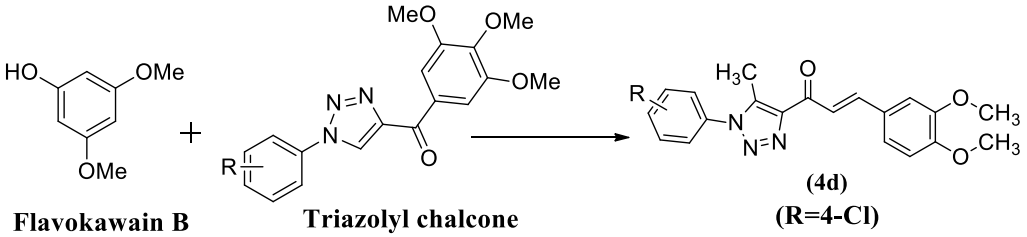

Flavokawain B **Triazolyl chalcone** **(4d) (R=4-Cl)**

(2.9)

Kaur et al.[31] (2020) synthesized newer β-lactam derivatives of triazoles. Synthesized derivatives **(2.10)** were characterized and screened for antibacterial property on *S. aureus* ATCC29213 (American type culture collection), *B. subtilis* MTCC441 (Microbial type culture collection) and *P. aeruginosa* (MTCC1034). Compound **7a** found most active with MIC (Minimum inhibitory concentration) of 1.25 µg/mL. Ampicillin was used as reference standard.

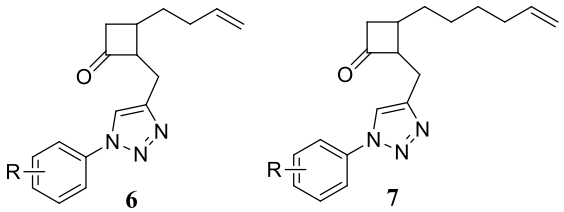

(6a, 7a = R= 3-NO_2, 6b, 7b = R= 4-NO_2, 6c, 7c R = 3-Cl, 6 d,7d R= 4-Cl, 6e, 7e =R= -3OCH_3, 6f=R= H).

(2.10)

Pasupuleti et al.[32] (2020) had reported OPN (Osteopontin) expression of trioxane-linked triazoles **(2.11)** in MDA-MB-435 breast cancer cells. Synthesized derivatives were found to down regulate OPN expression better than artimisinin and, can control breast cancer cells metastasis effectively.

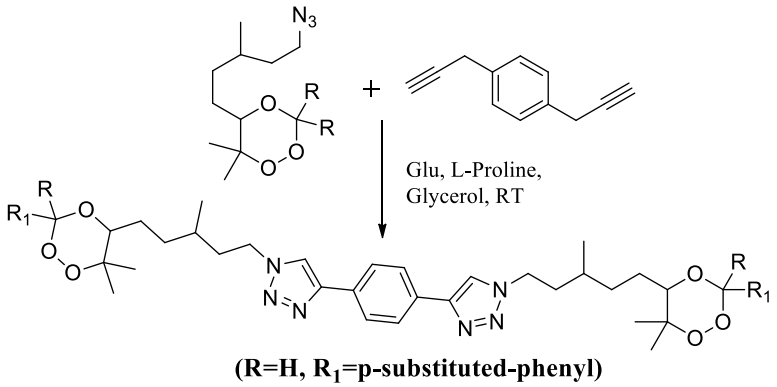

(R=H, R_1=p-substituted-phenyl)

2.11

Pinheiro et al.[33] (2020) have reported some chalcone based 1,2,3-triazoles **(2.12)** as cytotoxic agents. Molecules **4a, c** and **e** found to reduce cell growth with IC_{50} of 28.55, 15.64 and 25.56 µM, respectively against PC 3 prostate cancer cells.

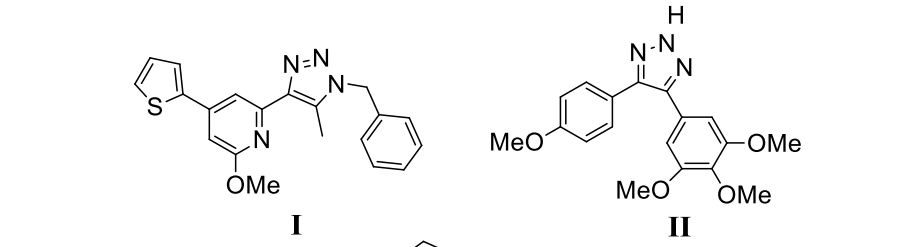

2.12

Holanda et al.[34] (2020) had reported antileishmanial property (IC_{50}:30.76±3.25) of phthalidomide linked triazole **(2.13).** *In-silico* study showed **2.13** interaction of leishmanial protein with lanosterol 14 α-demethylase. Increase in ROS (Reactive oxygen species) production and decrease in mitochondrial membrane potential observed during the study as root cause for parasite death.

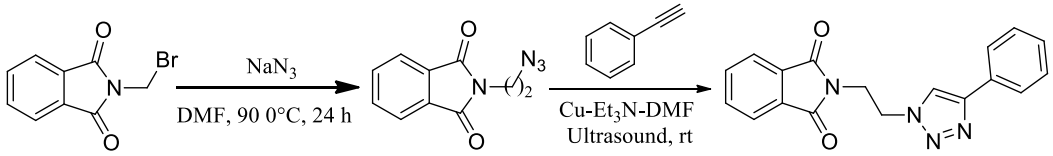

(2.13)

Reddyrajula et al.[35] (2020) had reported pyrazinamide linked 1,2,3-triazoles **(2.14)** as antimycobacterial agents. Three sets of pyrazine fused 1,2,3-triazoles **(3a-o, 5a-o and, 9a-l)** were screened against *M. tuberculosis* H37Rv. Among 42 derivatives, the 7 analogs exhibited better anti-mycobacterial property (1.56 µg/mL [Microgram/ Milliliter]), than reference drug pyrazinamide.

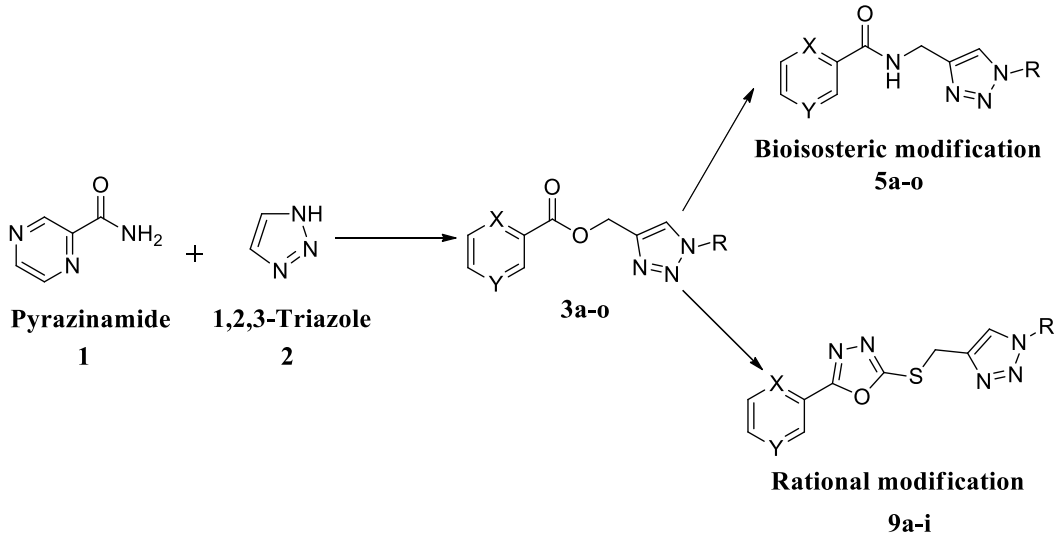

(2.14)

(Where, R= Substituted benzyl, X=-N, -CH, Y=-N, -CH)

Gao et al.[36] (2019) had reported a series of moxifloxacin-triazole-isatin hybrids **(2.15)** as antibacterial agent. The MIC value of **7e** (MIC: 0.0125-8 µg/mL, and **7g** (0.06-16 µg/mL) was found to be better than moxifloxacin (0.03-8 µg/mL).

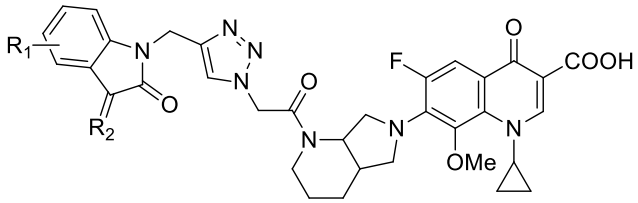

(7e= R_1=H, R_2 = N-OCH_3, 7g = R_1= 5-CH_3, R_2=N-OCH_3, 7j= R_1= F, R_2= N-OC_2H_5)

(2.15)

Khan et al.[37] (2019) had reported 1,2,3-triazole-linked diphenyl-1*H*-pyrazole acrylates **(2.16)** as cytotoxic and anti-inflammatory agents. *In-vitro* cytotoxicity screening was performed by sulforhodamine B assay against A549, MCF-7, H-29,

and HCT-116 cells. Compound **6f** was found to be most active in the series with IC_{50} of 1.962 (A549), 3.597 (HCT-116), 1.764 (MCF-7) and 4.496 (HT-29) µM. Camptothecin and, Combretastatin A4 were used as reference.

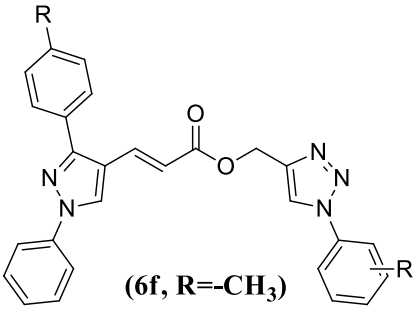

(6f, R=-CH_3)

(2.16)

Nalawade et al.[38] (2019) had reported synthesis and antimicrobial properties of some thiazolyl-pyrazolyl-1,2,3-triazole hybrid scaffolds. Series of molecules **(2.17)** were synthesized and screened *in-vitro* against *P. mirabilis (Proteus mirabilis)* NCIM 2388 (National collection of industrial microorganism), *E. coli* (*Escherichia coli*) NCIM 2574, *S. albus (Staphylococcus albus)* NCIM 2178, *A. niger* (*Aspergillus niger*) ATCC 504, *C. albicans* (*Candida albicans*) NCIM 3100, and, *R. glutinis (Rhodotorula glutinis)* NCIM 3168. Mild antifungal property was exhibited by majority of derivatives against *A. niger* (MIC 31.5 mg/mL).

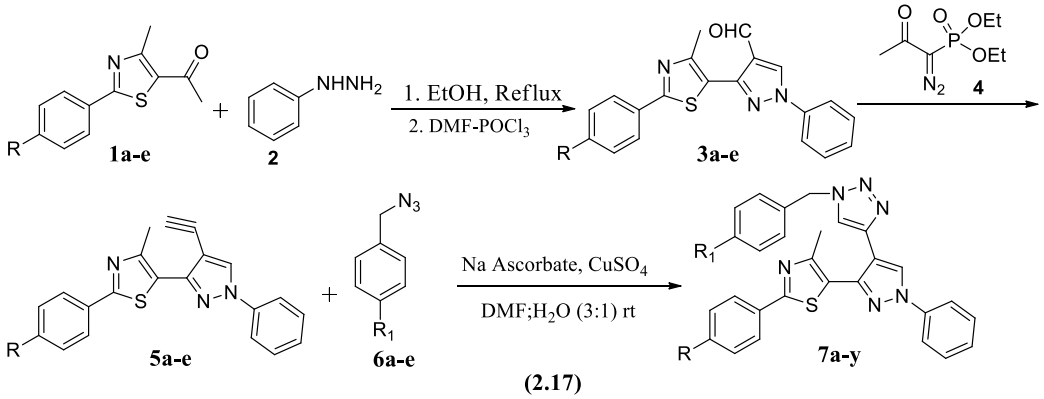

(2.17)

(R= H, F, Cl, Br & R_1= H, F, Cl, Br, -CH_3)

(2.17)

Hussain et al.[39] (2019) had reported synthesis, molecular docking and, antibacterial property of vanillin linked 1,2,3-triazoles, **3a-k (2.18).** Among tested derivatives, molecules **3b** (MIC: 5 µg/mL) and, **3g** (MIC: 10 µg/mL) and, and were most active. The molecular docking was performed on receptor 4GQQ and showed coherence with *in-vitro* study result.

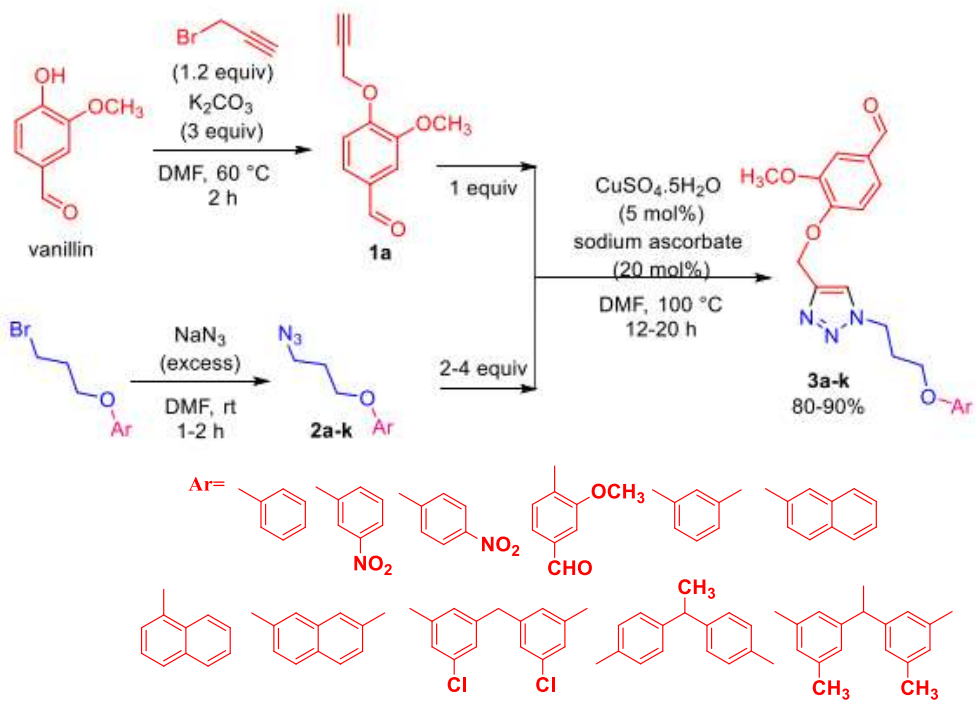

(2.18)

Kumar et al.[40] (2019) had reported antimitotic property of bergenin linked 1,2,3-triazoles **(2.19)** against HeLa (Henrietta Lacks) and A-549 cells. Among tested molecules, **3j** exhibited cytotoxicity at IC_{50}: 1.33 and 1.86 µM against HeLa and A-549 cells and, equal to doxorubicin. Cell division blockade and tubulin disruption observed by **3j.**

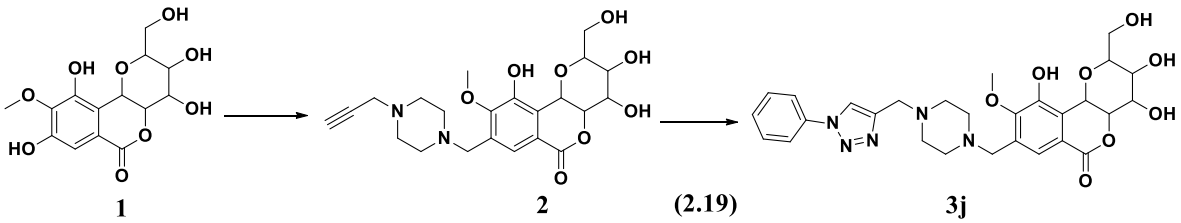

Raju et al.[41] (2019) had reported pyrrolo[2,3-*d*]pyrimidine linked 1,2,3-triazoles **(2.20)** as novel anti-tubercular agents against H37Rv strain of *M. tuberculosis (Mycobacterium tuberculosis).* Molecule **4q** and **4r** were found to be active at 0.78 µg/mL.

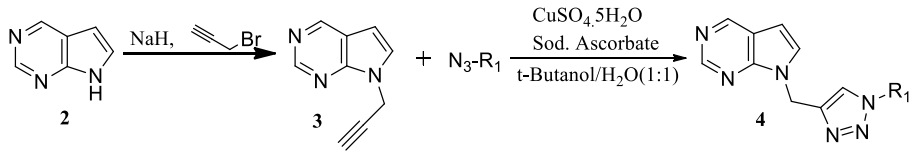

(R_1=Benzyl azide, aliphatic azides, phenyl azides, heteroaryl azides).

(2.20)

Queiroz et al.[42] (2019) had reported β-keto ana1ogs of 1,2,3-triazoles linked ethinyl estradiol **(2.21).** The derivatives were screened against hepatocellular carcinoma (HepG2) and, breast adenocarcinoma (MCF-7) cells. Moderate cytotoxicity was exhibited by **3a-f** against HepG2 cells (IC_{50}: 16.4-29.7 µM).

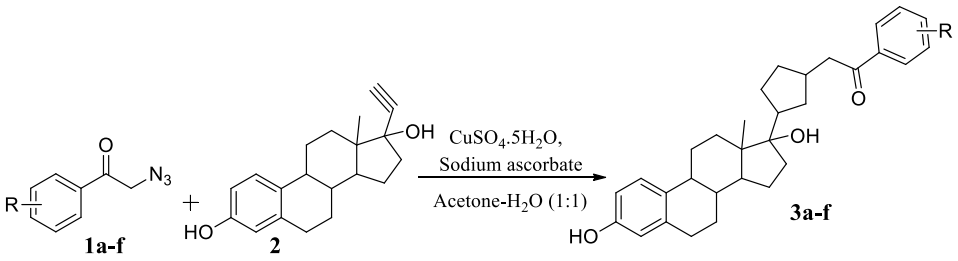

(2.21) R=H (3a), R=p-OMe (3b)
R=p-Cl (3c), R= p-Br (3d)
R= p-F (3e), R=m-F (3f)

Baharloui et al.[43] (2019) had reported a series of triazole-peptide hybrids **(2.22)** and screened against colon cancer (HT-29), breast cancer (MCF-7 and, MDA-MB-231) and, fibroblast cells. Synthesized derivatives were found to be more effective against fibroblast cells (IC_{50}:3.11±1.19 to 5.97±1.62 µM) compared to colon cancer cells HT-29 (IC_{50}: 91.87±0.39 to 93.06±1.01 µM) and breast cancer cells MCF-7 (IC_{50}: 50.11±2.09 to 83.39±0.84 µM) and, MDA-MB-231 cells (IC_{50}:78.70±1.60 to 81.22±0.30 µM).

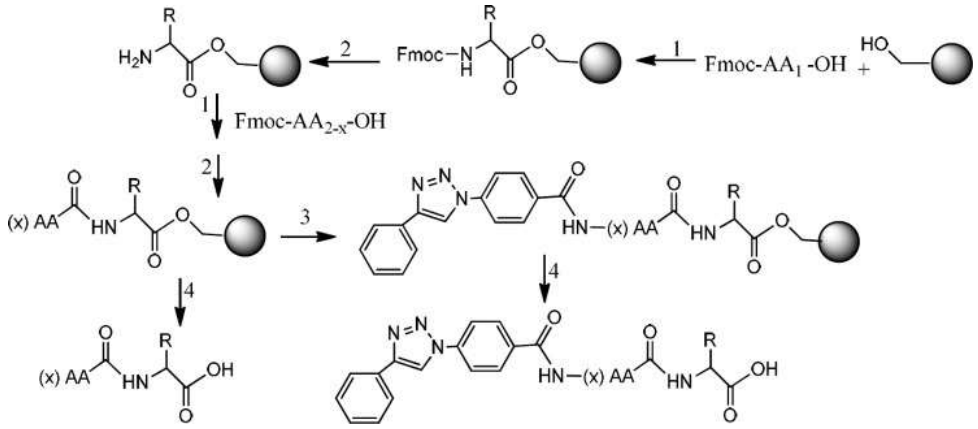

(2.22)

Srivastava et al.[44] (2018) had reported significant mycobactericidal property of 1,2,3-triazole linked β-D-ribofuranosyl-coumarin conjugates **(2.23)** by Cu-catalyzed cycloaddition reaction.

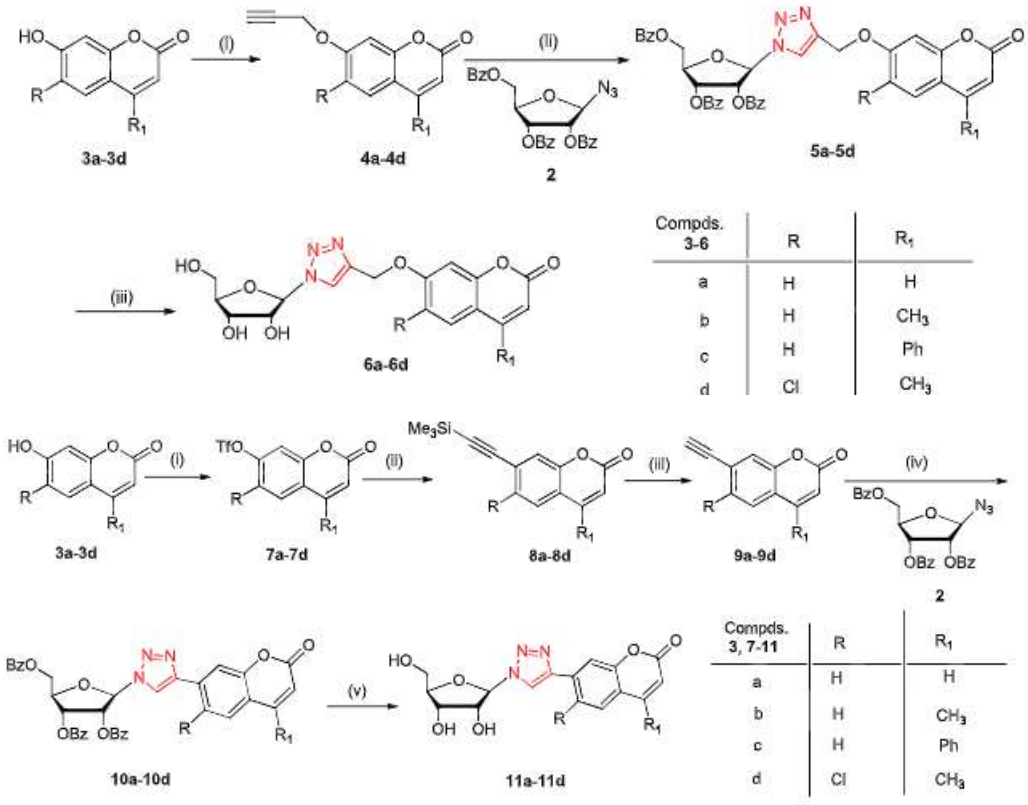

(2.23)

Lal et al.[45] (2018) had reported 1,2,3-triazole hybrid chalcones as antibacterial agents against *C. albicans, E. coli, S. epidermidis (Staphlococcus epidermidis), B. subtilis (Bacillus subtilis),* and *P. aeruginosa* (*Pseudomonas aeruginosa)* and, *A. niger*. Better

antimicrobial property was exhibited by most of the derivatives, compared to the DHA (Docosahexanoic acid). Synergism was observed with DHA, chalcone and triazole conjugates. The molecular docking performed for **5j** on topoisomerase II DNA gyrase B *(E. coli).*

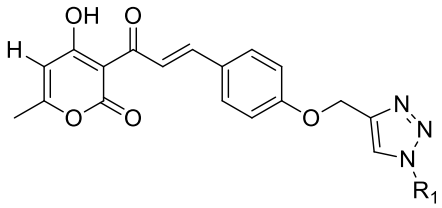

(Where R_1=Substituted benzyl (H, -NO_2,F, Br,-OCH_3)

(2.24)

Sayeed et al.[46] (2018) have reported tubulin inhibitory property of imidazopyridine linked triazoles **(8a-r)** against A-549, DU-145, HCT-116 and, MDA-MB 231 cells. These conjugates exhibited good to moderate activity. Two of the conjugates **8j** (IC_{50}: 0.63 μM), **8g** (IC_{50}: 0.51 μM) and showed significant anti-tumor activity against A549.

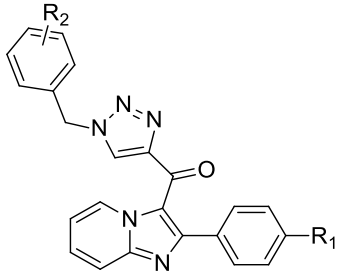

(2.25)

Where, R_1= -OCH_3, H,-Cl,. R_2= 3,4,5-$(OCH_3)_3$, 3,5-$(OCH_3)_2$, --OCH_3, 4-F,4-Cl, 4-Br.

Yadav et al.[47] (2018) have evaluated fluorinated chalcone-1,2,3-triazole conjugates against *E.coli* **(2.26).** Docking simulation study on topoisomerase II DNA Gyrase B were performed.

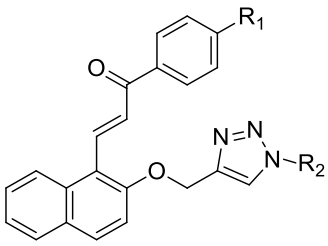

(Where R_1= Br, -OCH_3, -NO_2. R_2= Substituted benzylhalides)

(2.26)

Sakly et al.[48] (2018) had reported novel spirooxindolo conjugates of 1,2,3-triazole **(2.27)** with mild antibacterial and antifungal properties.

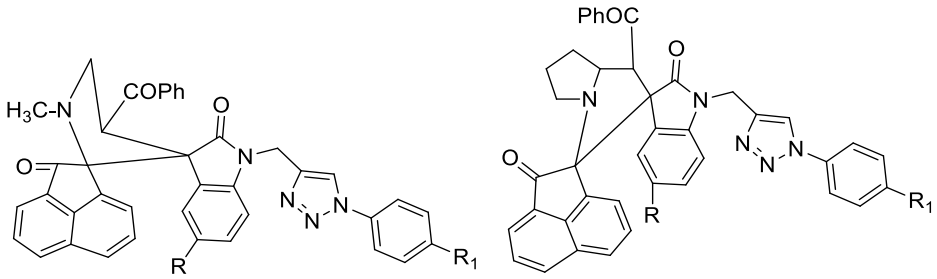

(Where, R= H, OCH_3, -CH_3, -Cl, -NO_2. R_1=H, -Br)

(2.27)

Tokala et al.[49] (2018) had reported cytotoxic property of urea/thiourea linked triazoles. *In-vitro* cytotoxicity were performed against MCF-7, MDA-MB231, A549, DU145 and, B16-F10 cell lines. Molecule **5t (2.28)** exhibited promising cytotoxicity against MCF-7 cells (IC_{50}:7.22 ± 0.47 µM). G0/G1 stage arrest was observed by **5t,** as appeared in flow cytometric study. No toxicity was seen against L-132 (normal cell).

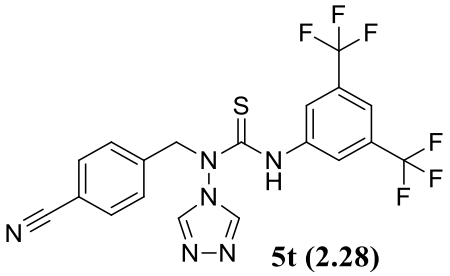

5t (2.28)

3.0 MATERIALS AND METHODS

3.1 Chemistry:

Solvents and reagents were confirmed for purity before use **(Table 3.1). Schemes 1-7** explain the synthetic routes adopted for the preparation of 1,2,3-triazole derivatives **(AD 1-48). Tables 3.2-3.7** represent the corresponding R and R_1, while the structure and physicochemical properties of final derivatives and, the intermediates are summarized in **Tables 4.1-4.12.** The m.p (melting point) values were reported uncorrected. The R_f values were determined using pre-coated Aluchrosep 60/UV254 (Ultra-violet 254) chromatographic sheets (Sd Fine-Chem Ltd.). FTIR (Fourier-transform infrared-red) spectral data were recorded in KBr (Potassium bromide) IR grade on JASCO 460+. The ^{1}H &^{13}C spectra recorded in $CDCl_3$ (Deuterated-chloroform) and DMSO-d6 (Deuterated-dimethyl sulfoxide) at 400/500 MHz (Mega-Hertz) on Bruker Ultraspec AMX-400/JEOL RESONANCE. The Chemical shift values (δ) were expressed in ppm taking TMS (Tetramethyl silane) as the reference standard. LCMS (Liquid chromatography-mass spectrometry) data for **AD 1-24** were obtained on triple quadrupole LCMS 6410 from Agilent technology. The C,H,N (carbon, hydrogen, nitrogen) analyses for **AD 25-48** were performed on thermoorganic elemental analyzer scientific flash 2000. All analytical data were summarized in **Tables 4.13-4.20.** Spectra of **AD 18** and **AD 30** were added for reference **(Figures 4.11-4.14).**

Table 3.1: List of chemicals.

Sl.No.	Name	Source
1	4-Chlorobenzyl bromide	Sigma-Aldrich
2	4-Chlorobenzyl chloride	Sigma-Aldrich
3	4-Fluorobenzyl chloride	Sigma-Aldrich
4	4-Hydroxybenzaldehyde	Sigma-Aldrich
5	4-Methoxy benzyl chloride	Sigma-Aldrich
6	4-Methyl benzyl bromide	Sigma-Aldrich
7	4-Methyl benzyl chloride	Sigma-Aldrich
8	4-Nitrobenzyl bromide	Sigma-Aldrich
9	4-Nitrobenzyl chloride	Sigma-Aldrich
10	5-Bromo isatin	Spectrochem
11	5-Chloro isatin	Spectrochem
12	5-Methyl isatin	Spectrochem
13	6-Chloro isatin	Spectrochem
14	7-Chloroisatin	S D Fine-Chem Ltd
15	Acetone	S D Fine-Chem Ltd
16	Acetonitrile	S D Fine-Chem Ltd
17	Anhyd. Potassium carbonate	S D Fine-Chem Ltd
18	Anhydrous methanol	S D Fine-Chem Ltd
19	Anhydrous sodium sulphate	S D Fine-Chem Ltd
20	Benzyl bromide	Sigma-Aldrich
22	Benzyl chloride	Sigma-Aldrich
23	Chloroform	S D Fine-Chem Ltd
24	Dichloromethane	S D Fine-Chem Ltd
25	Dimethylformamide	S D Fine-Chem Ltd
26	Dry benzene	Spectrochem
27	Ethyl acetate	Spectrochem
28	Glacial acetic acid	Spectrochem
29	Hydrazine hydrate (85%)	Spectrochem

30	Hydrochloric acid (concentrated)	S D Fine-Chem Ltd
31	Isatin	S D Fine-Chem Ltd
32	Piperidine	S D Fine-Chem Ltd
33	Propargyl bromide	Sigma-Aldrich
34	Sodium ascorbate	S D Fine-Chem Ltd
35	Sodium azide	S D Fine-Chem Ltd
36	Sodium hydride	S D Fine-Chem Ltd
37	Tertiary butanol	S D Fine-Chem Ltd
38	Triphenyl phosphine	Sigma-Aldrich

Methods:

Schemes

1. Synthesis of 4-(prop-2-yn-1-yloxy)benzaldehyde (3)

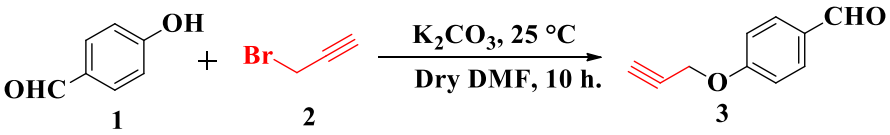

2. Synthesis of benzyl azide (6a-d)

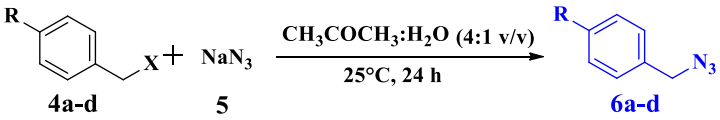

(R= H, Cl, -CH_3, NO_2)

[Table 3.2]

3. Synthesis of 4-((1-benzyl-1*H*-1,2,3-triazol-4-yl)methoxy)benzaldehyde (7a-d)

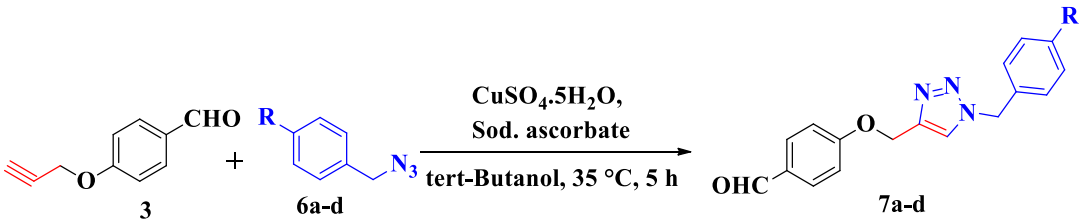

(R=H, Cl, -CH_3, NO_2)

[Table 3.3]

4. Synthesis of benzyltriphenylphosphonium halide (10a-f)

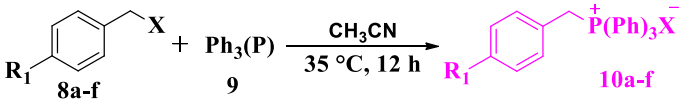

(R_1= H, F, Cl, CH_3, OCH_3, NO_2; X=Cl, Br)

[Table 3.4]

5. Synthesis of 2-oxindole (13a-f)

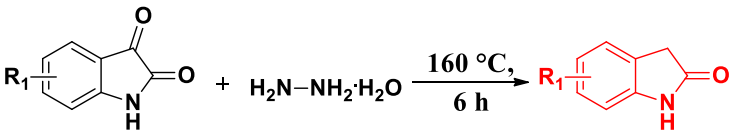

11a-f 12 13a-f

(R= H, 5-Cl, 5-Br, 5-CH_3, 6-Cl, 7-Cl)

[Table 3.5]

6. Synthesis of 1-benzyl-4-((4-styrylphenoxy)methyl)-1*H*-1,2,3-triazole (AD 01-24)

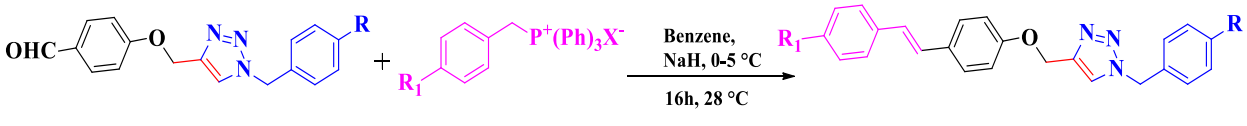

7a-d 10a-f AD 01-24

(R= H, -Cl, -CH_3, -NO_2, R_1 =H, -F, -Cl, -CH_3, -OCH_3, -NO_2).

[Table 3.6]

7. Synthesis of 3-(4-((1-benzyl-1*H*-1,2,3-triazol-4yl)methoxybenzylidene)indolin-2-one (AD 25-48)

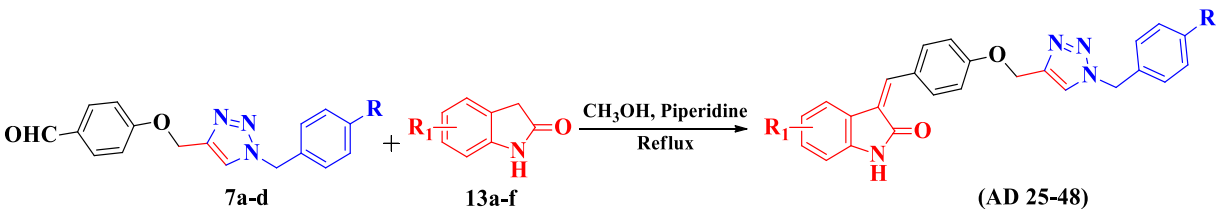

7a-d 13a-f (AD 25-48)

(R= H, -Cl, -CH_3, -NO_2; R_1 = H, 5-Cl, 5-Br, 5-CH_3, 6-Cl, 7-Cl)

[Table 3.7]

Table 3.2: R of benzylazide.

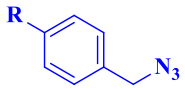

(6a-d)

Code	R	Code	R
6a	H	**6c**	CH_3
6b	Cl	**6d**	NO_2

Table 3.3: R of (4-((1-benzyl-1*H*-1,2,3-triazol-4-yl) methoxy)benzaldehyde

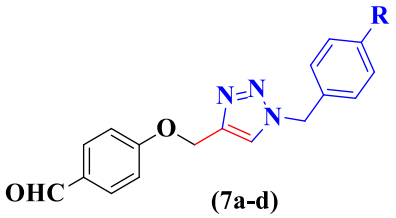

(7a-d)

Code	R	Code	R
7a	H	**7c**	CH_3
7b	Cl	**7d**	NO_2

Table 3.4: R of triphenylphosphonium benzylhalide.

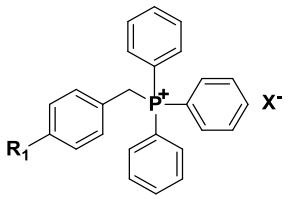

(10a-f)

Code	R_1	X	Code	R_1	X
10a	H	Cl	**10d**	CH_3	Cl
10b	F	Cl	**10e**	OCH_3	Cl
10c	Cl	Cl	**10f**	NO_2	Br

Table 3.5: R of indolin-2-one (2-Oxindole).

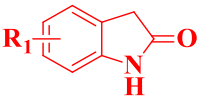

13a-f

Code	R_1	Code	R_1
13a	H	**13d**	5-CH_3
13b	5-Cl	**13e**	6-Cl
13c	5-Br	**13f**	7-Cl

Table 3.6: R and R_1 of 1-benzyl-4-((4-styrylphenoxy)methyl)-1*H*-1,2,3-triazole.

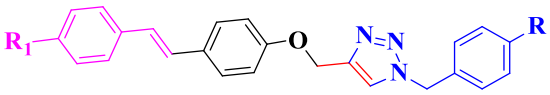

(AD 01-24)

Code	R_1	R	Code	R_1	R
AD-1	H	H	**AD-13**	H	CH_3
AD-2	F	H	**AD-14**	F	CH_3
AD-3	Cl	H	**AD-15**	Cl	CH_3
AD-4	CH_3	H	**AD-16**	CH_3	CH_3
AD-5	OCH_3	H	**AD-17**	OCH_3	CH_3
AD-6	NO_2	H	**AD-18**	NO_2	CH_3
AD-7	H	NO_2	**AD-19**	H	Cl
AD-8	F	NO_2	**AD-20**	F	Cl
AD-9	Cl	NO_2	**AD-21**	Cl	Cl
AD-10	CH_3	NO_2	**AD-22**	CH_3	Cl
AD-11	OCH_3	NO_2	**AD-23**	OCH_3	Cl
AD-12	NO_2	NO_2	**AD-24**	NO_2	Cl

Table 3.7: R and R_1 of 3-(4-((1-benzyl-1*H*-1,2,3-triazol-4yl)methoxybenzylidene) indolin-2-one.

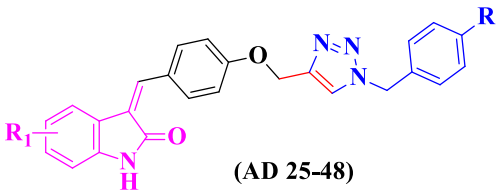

(AD 25-48)

Code	R_1	R	Code	R_1	R
AD-25	H	H	**AD-37**	H	CH_3
AD-26	5-Cl	H	**AD-38**	5-Cl	CH_3
AD-27	6-Cl	H	**AD-39**	6-Cl	CH_3
AD-28	7-Cl	H	**AD-40**	7-Cl	CH_3
AD-29	5-Br	H	**AD-41**	5-Br	CH_3
AD-30	5-CH_3	H	**AD-42**	5-CH_3	CH_3
AD-31	H	NO_2	**AD-43**	H	Cl
AD-32	5-Cl	NO_2	**AD-44**	5-Cl	Cl
AD-33	6-Cl	NO_2	**AD-45**	6-Cl	Cl
AD-34	7-Cl	NO_2	**AD-46**	7-Cl	Cl
AD-35	5-Br	NO_2	**AD-47**	5-Br	Cl
AD-36	5-CH_3	NO_2	**AD-48**	5-CH_3	Cl

Procedure[50-54]

1. 4-(Prop-benzyloxy)benzaldehyde **(3)**.

2. Benzylazide **(6a-d).**

3. 4-((1-Substituted benzyl-1*H*-1,2,3-triazol-4-yl) methoxy)benzaldehyde **(7a-d).**

4. Benzyltriphenylphosphonium halide **(10a-f).**

6. 2-Oxindole **(13a-f).**

5. 1-Benzyl-4-((4-styrylphenoxy)methyl)-1*H*-1,2,3-triazole **(AD 1-24).**

7. 3-(4-((1-Benzyl-1*H*-1,2,3-triazol-4-yl)methoxybenzylidene)indolin-2-one **(AD 25-48).**

1. General procedure for the synthesis of 4-(prop-benzyloxy)benzaldehyde[13] (3)

Propargyl bromide **2** (2.38 g, 20 mM) was added in drop to suspension of 4-hydroxyl benzaldehyde **1** (2.56 g, 21 mM) and K_2CO_3 (Potassium carbonate anhydrous) 2.76 g, 20 mM in 30 mL DMF (Dimethyl formamide) and stirred for 10 h (hours) at 25 °C (Degree Celsius). To the reaction mixture, 50 mL cold water was added followed by extraction with 3 x 50 mL $CHCl_3$ (Chloroform). The organic solvent was combined, dried over $MgSO_4$ anhydrous (magnesium sulfate) and, removed under vacuum. The solid mass of was recrystallized from EtOH (ethanol) to get white crystals of **3**. R_f (Retardation/Retention factor) 0.56, Yield 70%,110-112 °C.

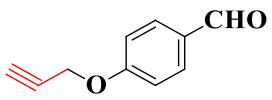

3

2. General procedure for the synthesis of benzyl azide[50] (6a-d)

15.0 mM (0.98 g) NaN_3 (sodium azide) **5** was stirred at 25 °C for 24 h in a solution of 10.0 mM aralkyl halide (chloride/bromide) **4** in 80 mL 4:1 v/v dimethyl ketone-water mixture. The resulting solution was extracted with 3 × 50 mL $CHCl_3$ and, dried over MgSO4 (anhydrous) and, reduced under vacuum to get respective aralkyl azides (benzyl azides) **6a-d** as colorless to pale yellow oils.

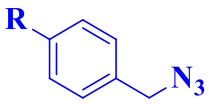

6a-d

[Table 4.1 & 4.2]

3. General procedure for synthesis of 4-((1-substituted benzyl-1*H*-1,2,3-triazol-4-yl) methoxy)benzaldehyde[13] (7a-d)

To the solution of 12 mM of 4-OH-benzaldehyde **3** and respective azides **6a-d** in 20 mL *t*-C_4H_9OH (tertiary butanol), the 1.24 mM of sodium ascorbate and 0.62 mM of

$CuSO_4.5H_2O$ (Copper sulphate pentahydrate) in 20 mL distilled water were added and stirred for 5 h at 35 °C. Reaction was confirmed by change in R_f value. The reaction the mixture was extracted in $CHCl_3$ and dried over anhydrous $MgSO_4$ to get crude triazole-benzldehyde **7a-d**. The solid mass was recrystallized from EtOH.

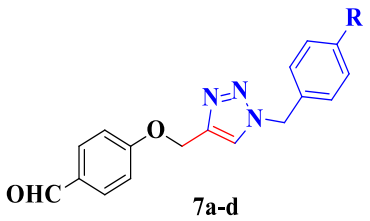

7a-d

[Table 4.3 & 4.4]

4. General procedure for the synthesis of benzyltriphenylphosphonium halide[51] (10a-f)

31.7 mM benzyl halide (chloride/bromide) **8a-f** and 32.7 mM (8.57 g,) triphenylphosphine $P(Ph)_3$ **9** were refluxed for 12 h in 20 mL acetonitrile. The solvent was distilled-out to get crude benzyl triphenylphosphonium halide. The resulting compounds **10a-f** were re-crystallized from EtOH.

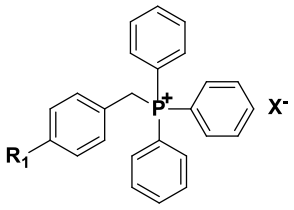

(10a-f)

[Table 4.5 & 4.6]

5. General procedure for the synthesis of 2-oxindole[53] (13a-f)

0.05 M of 1*H*-indole 2,3-dione **11a-f** was suspended in 80 mL of 85% $NH_2.NH_2.H_2O$ (hydrazine hydrate) **12** and refluxed at 160 °C for 6 h. Resulting solution was allowed to stand for 40 minutes in 100 mL of cold water. Filtered the precipitated solid residue and acidified the filtrate with 0.1N HCl (Hydrochloric acid)). Crystals of respective 2-oxindoles **13a-f** were obtained after 24 h of acid treatment.

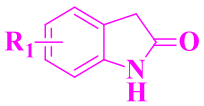

13a-f

[Table 4.7 & 4.8]

6. General procedure for the synthesis of 1-benzyl-4-((4-styrylphenoxy)methyl) -1*H*-1,2,3-triazoles[52] (AD 1-24).

0.478 g (20 mM) of NaH (sodium hydride) was added to an equi-molar suspension of benzyl triphenylphosphonium halides **10a-f** and triazole-aldehydes **7a-d** at 0-5 °C in benzene (dry) with stirring. The reaction was continued at 28 °C for 16 h. Unreacted NaH was quenched with 10 mL MeOH (Methanol) and extracted with $CHCl_3$-H_2O mixture. The $CHCl_3$ portion was collected, dried over anhydrous $MgSO_4$ and reduced under vacuum. The solid mass of, **AD 1-24** were recrystallized from EtOH.

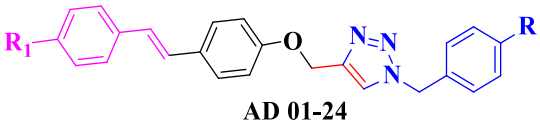

AD 01-24

[Table 4.9 & 4.10].

7. General procedure for synthesis of 3-(4-((1-Benzyl-1*H*-1,2,3-triazol-4yl)methoxy benzylidene)indolin-2-ones[16, 54] (AD 25-48).

1.0 mM of 1*H*-1,2,3-triazole-benzaldehydes, respective 2-oxindoles and, 0.5 mL of piperidine were refluxed in 30 mL of anhydrous MeOH to get precipitate of **AD 25-48.** The reaction mixture was cooled and the crude mass of **AD 25-48** was re-crystallized from the DMF-MeOH mixture in an appropriate ratio.

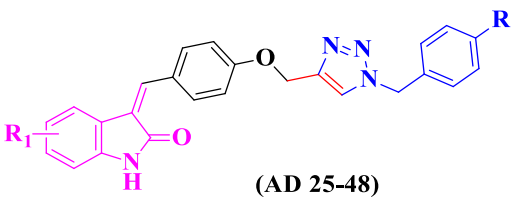

(AD 25-48)

[Table 4.11 & 4.12]

3.2 Biology:

1-Benzyl-4-((4-styrylphenoxy)methyl)-1*H*-1,2,3-triazoles[55-59] (AD 1-24)

Cell lines are,

Capan-1 (Pancreatic adeno-carcinoma)

HCT-116 (Colorectal carcinoma)

NCI-H460 (Lung carcinoma).

DND-41 (Acute lymphoblastic leukemia)

K-562 (Chronic myeloid leukemia)

Z-138 (Non-Hodgkin lymphoma)

Cell culture condition

DND-41 cells obtained from the DSMZ (Deutsche Sammlung von Mikroorganismen und Zellkulturen Leibniz-Institut), Germany, while the rest of the cells were obtained from the ATCC Manassas, United States of America (USA) and cultured according to the suppliers' instructions. Culture media were obtained from GIBCO Life Technologies, USA, and 10% fetal bovine serum was obtained from GE Healthcare Life Sciences, USA.

***In-vitro* cytotoxicity assay of AD 1-24**

Capan-1, NCI-H460 and 500-5000 HCT-116 cells per well seeded in Greiner's 384-well culture plates and treated with seven different concentration of **AD 1-24** (100 to 6.4 × 10-3 µM). The Z-138, DND-41 and K-562 cells seeded in 384-well (2500 to 5000 cells/well) culture plate, treated with seven concentrations of **AD 1-24** (100 to 6.4 × 10-3 µM) and, incubated for 72h in IncuCyte® at 37 °C from Essen BioScience Inc., USA **(Table 4.21).** The real time images (X10) were taken at 3h interval and, cell growth was quantified in triplicate (IC_{50} inµM) based on cellular confluence (in %) analyzed by the IncuCyte® taking Docetaxel and Staurosporine as references.

In-silico studies[60-68]

All 3D (Three dimensional) structures were prepared on Avogadro v1.2.0 and energy minimization done with MMFF94s (Merck molecular force field 9s). The drug-likeness and pharmacokinetic parameters were predicted using SwissADME. Molecular simulations (dynamics) performed on tubulin receptor **1TUB**. Ligands and the target preparations done using PyRx while AutoDock Vina with LGA (Lamarckian genetic algorithm) was used for docking. Discovery studio was used to visualize the docking **(Table 4.22).**

3-(4-((1-benzyl-1*H*-1,2,3-triazol-4yl)methoxybenzylidene)indolin-2-ones[58, 59, 69, 70] (25-48)

Cell lines

HeLa (Human cervix carcinoma cells).

HL-60 (Human acute promyelocytic cells).

CEM (Human T-lymphocyte cells).

L1210 (Murine leukemia cells).

Jurkat cells (Human T lymphocyte cells)

In-vitro cytotoxic activity of AD 25-48

The cytotoxicity of 1,2,3-triazole analogs **(AD 25-48)** were investigated against HeLa, CEM and L1210 cell lines according to the literature. The IC_{50} were calculated and expressed in µM **(Table 4.23).** All experiments were performed in triplicate. Further, the cytotoxic activity of compound **AD-27** was analyzed using Guava Via Count Reagent (Merck Millipore, Burlington, USA). In brief, after 24 and 48 h treatment with **AD-27,** cells were diluted with 7-AAD (7-Aminoactinomycin D) containing reagent. Flow cytometric analyses were performed after 5 minutes incubation at 37 °C.

Cell cultures and treatments

Jurkat, CEM, and HL-60 cells were obtained from LGC, UK. The RPMI (Rosewell Park Memorial Institute) 1640 medium with 10% heat-inactivated bovine serum, 1% penicillin/streptomycin, and 1% l-glutamine (Sigma Aldrich) were used to culture Jurkat and CEM cells while, the HL-60 cells were cultured in RPMI 1640 with 20% inactive bovine serum keeping other adjuvants in same concentration. Cells were stored at 37°C in 5% CO_2 and treated with 1,2,3-triazole analog **(AD-27)**. Etoposide 10µg/mL, Camptothecin 2 µM, and H_2O_2 0.5/1 mM (Sigma Aldrich) were used as positive controls.

The cell death pathways were predicted by pre-treating cells for 1h with reference inhibitors followed by 24h treatment with **AD-27** (8 µM). For this purpose 75 µM Z-VAD-75 FMK (carbobenzoxy valyl-alanyl-aspartyl-[*O*-methyl]-fluoromethylketone) Biovision, CA USA), 5 µM Ola (olaparib) Selleckem, USA, 75 µM Nec-1s (necrostatin-1s), 1 µM Ferr-1(Ferrostatin-1)Sigma-Aldrich, India, 10 µM DFO (deferoxamine mesylate) Across Organics, USA, and 100 µM Vit E (Vitamin. E), Sigma Aldrich, India to inhibit apoptosis, parthanatos, necroptosis and ferroptosis, respectively

Analysis of cell death mechanisms

Guava Nexin Reagent containing 7-AAD and annexin V-phycoerythrin (Merck Millipore) used to differentiate apoptosis with necrosis. Cells were exposed for 24h to **AD-27,** and then diluted in Guava Nexin Reagent.

Non-apoptotic cell death and viability were assessed using SYTOX™ Green Nucleic Acid Stain (Thermo Fisher Scientific) according to the manufacturer's protocol.

SYTOX™ Green Nucleic Acid Stain is a fluorescent and cell membrane impermeable dye that could easily penetrate only compromised membranes of dead cells, where it

binds DNA, thus increasing its fluorescence. Briefly, after pre-treatment of 1 h with the different chemical inhibitors and treatment of 24 and 48 h with **AD-27** cells were supplemented with SYTOX™ Green Nucleic Acid Stain 10 Nm. Flow cytometric analyses were performed after 20 minutes incubation.

Measurement of mitochondrial potential

The MitoProbeTM DilC1 (5) assay kit from Thermo Fisher Scientific was used to assess mitochondrial membrane potential. The active potential is represented by the high intensity of accumulated DilC1 (5) [1,1′,3,3,3′,3′-hexamethylindo dicarbocyanine iodide] in the mitochondrial membrane. Reverse is the case when the membrane potential is altered. Briefly, after 24h of treatment with **AD-30,** cells (10^6) were washed and suspended in 50 nM DilC1 (5) at 37°C for 20 minutes in 5% CO_2 followed by washing and resuspension in PBS 1X. Flow cytometric analysis was performed taking 50 µM CCCP (Cyclic citrullinated peptide) as positive control. The % of treated cells with reduced mitochondrial potential was measured compared to untreated cells.

Evaluation of caspase-8 and caspase-3 activity

Colorimetric protease assay Kit from Thermo-Fisher Scientific was used to assess caspase activity. In brief, the cells were treated with PBS 1X, centrifuged and collected. Bradford assay was performed to normalize the protein concentration.

Cell lysates were incubated at 37°C for 2 h in 2X reaction buffer with 10 mM DTT (Dithiothreitol) and 200 µM p-nitroanilide conjugated caspase substrate, the caspase-selective tripeptide Ile-Glu-Thr-Asp (Isoleucine-Glutamine-Threonine-Aspartate) and Asp-Glu-Val-Asp-8 and 3 respectively. The pNA (Peptide nucleic acid) was used as chromophore in the process. The absorbance is measured for pNA in activated caspase sample at 405 nm, on Victor X3 Perkin Elmer microplate reader. An increase in number of treated cells compared to untreated one was taken as the measure of caspase activity.

Measurement of ROS generation

H2DCFDA (2′,7′-dichlorodihydrofluoresceine) Sigma-Aldrich probe was used to assess the ROS formation. H2DCFDA is a non-fluorescent and cell-permeable probe which is hydrolyzed by intracellular esterase of viable cells into H2DCF. In turn, H2DCF is oxidized in presence of ROS into DCF (2′,7′-dichlorofluorescein), which is highly fluorescent. In brief, 20 minutes before the different time end points (1, 3 or 6 h of treatment with **AD-30**) H2DCFDA 10 μM was added in each well. Then, cells were incubated for 20 minutes at 37 °C in CO_2 5%, centrifuged (1×10^6 cells) and re-suspended in PBS 1X (Phosphate buffer saline) for flow cytometry analysis. Intracellular ROS levels were expressed as an increase in a number of treated cells compared the untreated one.

Cell-cycle and cell-cycle-related proteins expression analysis

Cells were treated with **AD-30** for 6 and 24 h, followed by fixation in 70% ethanol (ice-cold). After washing, 200 μL suspension of treated cells was prepared in propidium-iodide rich Guava Cell Cycle Reagent. Flow cytometric analysis was performed after 30 minutes incubation at room temperature. % cell was quantified (G0/G1, S, and G2/M phases) analyzing DNA content based on the use of Guava Cell Cycle Reagent. In order to analyze the expression of cyclin A, cyclin B1 and CDK1 (Cyclin-dependent kinase-1), after treatment for 24 h, cells were fixed by 70% cold ethanol and permeabilized using 0.25% cold Triton X-100 in Wash Buffer (WB; PBS 1X + 1% bovine serum albumin). Then, samples were washed and incubated for 30 minutes with the corresponding primary 1:50 part antibody anti-cyclin A and, anti-cyclin B1, and 1:200 anti-CDK1 (Invitrogen, Thermo Fisher Scientific). The cells were rinsed with WB and stained using secondary antibody (1:200 anti-mouse and anti-rabbit 1:200 for another 30 minutes. The flow cytometric analyses were-performed and MFI (Mean fluorescence

intensity) was measured. Cyclin A, Cyclin B1, and CDK1 expression were indicated as increase in number of treated vs untreated cells.

Analysis of DNA damage

The genotoxic potential of **AD-30** was assessed evaluating phosphorylation of histone γ-H2A.X. The 5 h was treated with increasing concentrations of **AD-30,** and, incubated for 30 minutes with γ-H2A.X-Alexa Fluor® antibody. Then, samples were analyzed via flow cytometry. Phosphorylation of histone γ-H2A.X was expressed as an increase in treated cells compared to untreated cells. Etoposide 10μg/mL was used as the positive control during the study. Flowcytometric analyses performed on Easy-Cyte Flow-cytometer from Millipore, Hayward, USA.

ADME (Absorption, Distribution, Metabolism and Excretion) evaluation

The 3D structures of AD **25-48** were drawn using Avogadro v1.2.0 and optimized using the MMFF94s force field. Swiss-ADME webserver was used to evaluate ADME, pharmacokinetics, and drug-likeness of **AD 25-48 (Table-4.24).**

In-silico studies:

Molecular docking simulations

EGFR **(Pdb ID: 6P8Q)** was used as a target and, 10-benzyl-2-fluoro-5,10-dihydro-11*H*-dibenzo[*b,e*][1,4]diazepin-11-one as co-ligand during the study. The ligand and 6P8Q were prepared using PyRx. Docking studies were performed on Auto-DockVina software with LGA. Discovery studio-Biovia 2017 was used for the visualization of docking results.

Statistical analysis[58, 59]

Results were expressed as mean ± SEM (Standard error of mean) and performed in triplicate. Statistical analyses were performed by repeated-measures ANOVA (Analysis of variance) using GraphPad InStat 6.0 (San Diego, USA). $p < 0.05$ were considered

significant and represented as **** $p < 0.0001$, *** $p < 0.001$, ** $p < 0.01$, and * $p < 0.05$.

In-vitro Anti-Mycobacterial Activity:[71-76]

Mycobacterium tuberculosis H37Rv

The anti-mycobacterial assay is performed on H37Rv strain (fluorescent). The potency is expressed in terms of OD (optical density) and fluorescence. Two readouts were taken to minimize auto-fluorescence problem due to sample precipitation. A linear relationship between OD and fluorescence readout was established to justify fluorescence as a measure of mycobacterial growth. MICs values were calculated. The strain used was equivalent to the parental strain in terms of phenotypes and virulence. Results were summarized in **Table 3.8 & 4.25.**

Table-3.8: List of reagents/solvents used for *in-vitro* Anti-Mycobacterial Activity (*M. tuberculosis* H37Rv).

Reagent	**Supplier**	**Catalog Number**	**Lot Number**
DMSO	Fisher	NC0539145	DN490
Middlebrook 7H9 Base	VWR	271310-500G	5173939
Middlebrook OADC Supplement	VWR	211866	6336518
Tween 80	Fisher	BP338-500	136611
Rifampicin	Sigma-Aldrich	R3501	SLBD2314V
Solution	**Recipe**		
7H9-Tw-OADC	4.7 g/L 7H9 base broth, 0.05% w/v Tween 80,10% v/v OADC (Oleic acid albumin-dextrose catalase) supplement		

The MIC of the tested compounds was calculated by measuring 5 days of bacterial growth. 10-point 2-fold serial dilutions made in DMSO and diluted with 7H9-Tw-OADC medium. The concentration of DMSO should not be higher than 2%. Growth

rate was measured using a BioTek™ Synergy H4 plate reader as OD590 and fluorescence at Em 590 (Emission-590) and Ex 560 (Extinction-600), respectively. The dose response curve was plotted as % growth by GraphPad Prism 6. The MIC was calculated from the inflection point of the fitted curve to the lower asymptote **(Figure 3.1 A).** IC_{50} and IC_{90} values were calculated. **(Figure 3.1 B).**

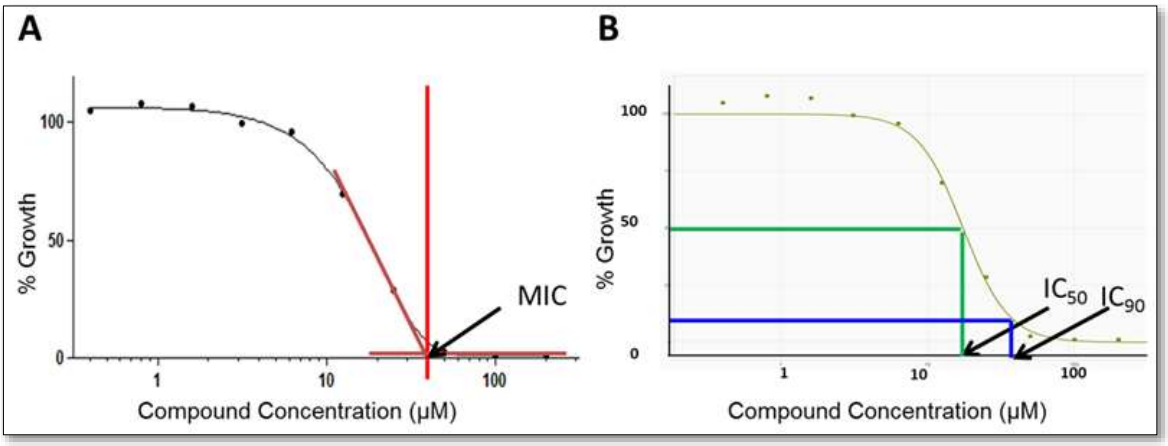

Figure-3.1: MIC, IC_{50}, and, IC_{90} calculation from dose response cureve.

The MIC was reported as > maximum concentration tested when less than 75% inhibition was observed during the study.

For other Mycobacterial species such as *Mycobacterium abscessus* subsp. *bollettii* 103 and *M. avium* (*Mycobactrium avium)* subsp. *avium* 2285 (S) the experiment is performed in aerobic conditions. MIC values were determined based on optical density and metabolic activity values using Amalar blue reagent similar to *M. tuberculosis.*

Table-3.9: List of reagents/solvents used for In-vitro Anti-Mycobacterial Activity (*M. abscessus* [*Mycobacterium abscessus*] & *M. avium*).

Reagent	Supplier	Catalog Number	Lot Number
DMSO	Fisher	NC0539145	DN490
Middlebrook 7H9 base broth	VWR	271310	5173939
Middlebrook OADC supplement	VWR	211866	6336518
Tween 80	Fisher	BP-338-500	136611
Rifampicin	Sigma-Aldrich	R3501	SLBD2314V
Alamar blue	BioRad	BUF012B	160728A
Solution	**Recipe**		
7H9-Tw-OADC	4.7 g/L 7H9 base broth, 0.05% w/v Tween 80, 10% v/v OADC supplement		

M. abscessus

Plates inoculated with *M. abscessus* strain and incubated at 37˚C for 3 days. The bacterial growth was measured as change in OD_{590} using BioTek™ Synergy H4 plate reader. The dose response curve was plotted as % growth GraphPad Prism 6. The MIC was calculated from the inflection point of the fitted curve to the lower asymptote. The dose response curves plotted using the Levenberg-Marquardt algorithm. IC_{50} and IC_{90} vales were calculated. Rifampicin was used as reference during the study. The MIC was reported as > maximum concentration tested when less than 75% inhibition was observed during the study. Results were summarized in **Table 3.9 & 4.26.**

M. avium

M. avium inoculated plates were incubated at 37 ˚C for 5 days. 10 µL of Alamar blue was added to 100 µL of culture in each well. Incubation was done at 37˚C for 24 h. The

colors of each plate were recorded. The blue coloured wells represent no metabolic changes in mycobacterial cell. Results were summarized in **Table 3.9 & 4.27.**

4.0 EXPERIMENTAL RESULTS

4.1 Chemistry:

Table-4.1: Structure and IUPAC name of benzyl azide (6a-d).

Code	Structure and IUPAC name	Code	Structure and IUPAC name
6a	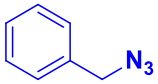 **Azidomethylbenzene**	**6b**	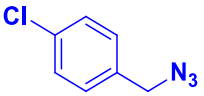 **1-Azidomethyl-4-chlorobenzene**
6c	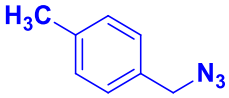 **1-Azidomethyl-4-methylbenzene**	**6d**	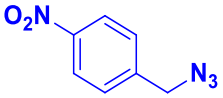 **1-Azidomethyl-4-nitrobenzene**

Table-4.2: Physicochemical properties of benzylazide (6a-d).

Code	Appearance	M.F	M.W	R_f Value*		Yield (%)
				Benzyl azide	Benzyl bromide	
6a	Colourless liquid	$C_7H_7N_3$	133.15	0.58	0.70	55
6b	Colourless liquid	$C_6H_6ClN_3$	167.6	0.64	0.75	60
6c	Light yellow liquid	$C_8H_9N_3$	147.18	0.54	0.66	65
6d	Colourless liquid	$C_7H_6N_4O_2$	178.15	0.48	0.60	60

*** Ethyl acetate-Hexane (60:40)**

Table-4.3: Structure and IUPAC name of 4-(prop-benzyloxy)benzaldehyde. (7a-d)

Code	Structure and IUPAC name	Code	Structure and IUPAC name
7a	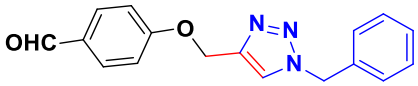 **4-((1-Benzyl-1H-1,2,3-triazol-4-yl) methoxy)benzaldehyde**	**7b**	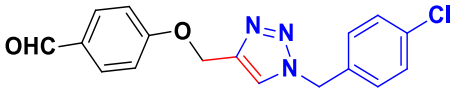 **4-((1-(4-Chlorobenzyl)-1*H*-1,2,3-triazol-4-yl) methoxy)benzaldehyde**
7c	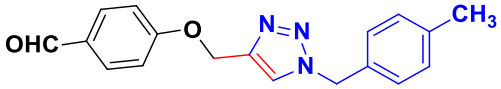 **4-((1-(4-Methylbenzyl)-1H-1,2,3-triazol-4-yl) methoxy)benzaldehyde**	**7d**	 **4-((1-(4-Nitrobenzyl)-1H-1,2,3-triazol-4-yl) methoxy)benzaldehyde**

Table-4.4: Physicochemical properties of 4-((1-benzyl-1*H*-1,2,3-triazol-4-yl) methoxy)benzaldehyde (7a-d).

Code	Appearance	M.F	M.W	Yield (%)	M.P (°C)		R_f Value*	
					5a-d	3**	5a-d	3**
7a	Buff white solid	$C_{19}H_{17}N_3O_2$	319.36	55	130-32	**110-12**	0.70	**0.56**
7b	White solid	$C_{19}H_{16}ClN_3O_2$	353.80	60	110-13		0.65	
7c	Light brown solid	$C_{20}H_{19}N_3O_2$	333.38	65	156-58		0.50	
7d	Light yellow solid	$C_{19}H_{16}N_4O_4$	364.35	60	207-08		0.40	

*** Ethyl acetate/n-Hexane (5:5).**

3 4-(prop-2-yn-1-yloxy)benzaldehyde.**

Table-4.5: Structure & IUPAC name of benyzyltrriphenylphosphonium chloride (10a-f).

Code	Structure and IUPAC name	Code	Structure and IUPAC name
10a	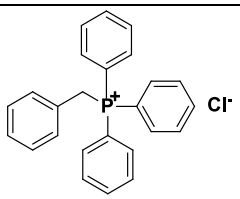 **Benzyltriphenylphosphonium chloride**	**10d**	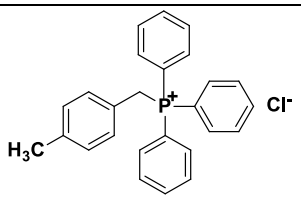 **(4-Methylbenzyl)triphenylphosphonium chloride**
10b	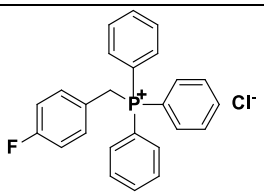 **(4-Fluorobenzyl)triphenylphosphonium chloride**	**10e**	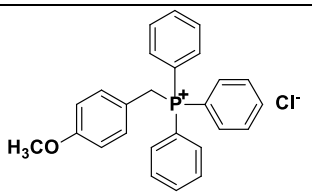 **(4-Methoxybenzyl)triphenylphosphonium chloride**
10c	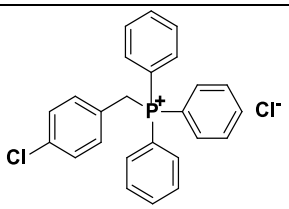 **(4-Chlorobenzyl)triphenylphosphonium chloride**	**10f**	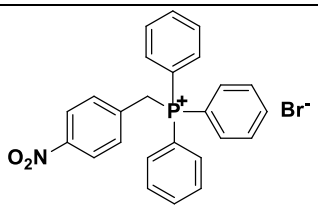 **(4-Nitrobenzyl)triphenylphosphonium bromide**

Table-4.6.: Physicochemical property of benzyl triphenylphosphonium chloride (10a-f).

Sl. No.	M.F	M.W	M.P (°C)		Yield (%)
			Obs.	Commercial grade*	
10a	$C_{25}H_{22}ClP$	388.87	335-38	337	75
10b	$C_{25}H_{21}ClFP$	406.87	308-10	310-12	65
10c	$C_{25}H_{21}Cl2P$	423.32	288-91	286-91	78
10d	$C_{26}H_{24}ClP$	402.91	258-60	260-62	80
10e	$C_{26}H_{24}ClOP$	418.90	235-37	235-39	60
10f	$C_{25}H_{21}BrNO_2P$	478.33	272-74	275	50

*** Sigma-Aldrich.**

Table-4.7: Structure & IUPAC name of indoline-2-one (2-oxindole) (13a-f).

Code	Structure and IUPAC name	Code	Structure and IUPAC name
13a	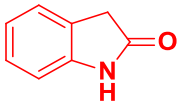 **Indolin-2-one**	**13b**	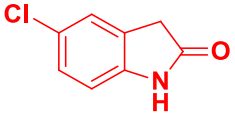 **5-Chloroindolin-2-one**
13c	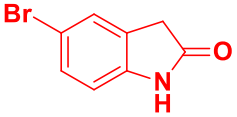 **5-Bromoindolin-2-one**	**13d**	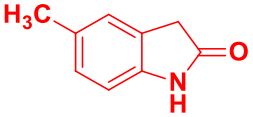 **5-Methylindolin-2-one**
13e	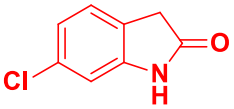 **6-Chloroindolin-2-one**	**13f**	 **6-Chloroindolin-2-one**

Table-4.8: Physicochemical properties of indoline-2-one (2-oxindole) (13a-f).

Code	M.F	M.W	M.P (°C)		Yield (%)
			Obs.	Commercial grade*	
13a	C_8H_7NO	133.15	125-28	123-28	45
13b	C_8H_6ClNO	167.59	196-98	194-97	45
13c	C_8H_6BrNO	212.04	88-90	90-92	50
13d	C_9H_9NO	147.17	170-71	168[53]	42
13e	C_8H_6ClNO	167.59	193-95	195-99	35
13f	C_8H_6ClNO	167.59	119-220	221-22	30

*** Sigma-Aldrich**

Table-4.9: Structure and IUPAC name of -1-benzyl-4-((4-styrylphenoxy) methyl)-1*H*-1,2,3-triazoles (AD 1-24).

Code	Structure and IUPAC name	Code	Structure and IUPAC name
AD-1	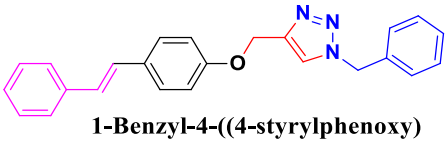 1-Benzyl-4-((4-styrylphenoxy) methyl)-1*H*-1,2,3-triazole	AD-2	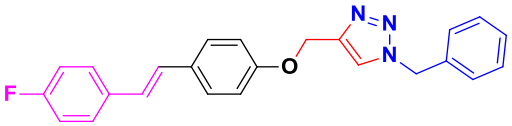 1-Benzyl-4-((4-(4-fluorostyryl)phenoxy) methyl)-1*H*-1,2,3-triazole.
AD-3	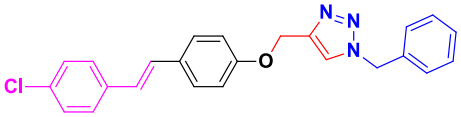 1-Benzyl-4-((4-(4-chlorostyryl)phenoxy) methyl)-1*H*-1,2,3-triazole	AD-4	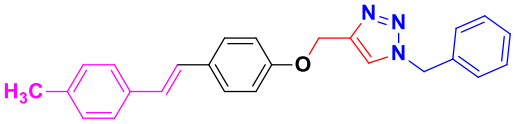 1-Benzyl-4-((4-(4-methylstyryl)phenoxy) methyl)-1*H*-1,2,3-triazole
AD-5	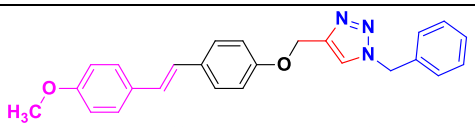 1-Benzyl-4-((4-(4-methoxystyryl)phenoxy) methyl)-1*H*-1,2,3-triazole	AD-6	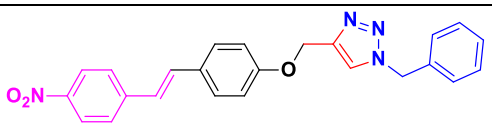 1-Benzyl-4-((4-(4-methoxystyryl)phenoxy) methyl)-1*H*-1,2,3-triazole
AD-7	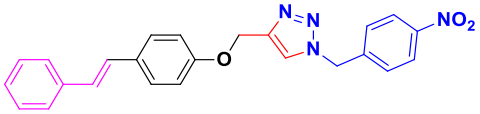 1-(4-Nitrobenzyl)-4-((4-styrylphenoxy) methyl)-1*H*-1,2,3-triazole	AD-8	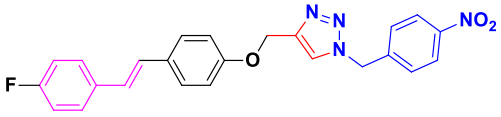 (*E*)-4-((4-(4-Fluorostyryl)phenoxy)methyl) -1-(4-nitrobenzyl)-1*H*-1,2,3-triazole
AD-9	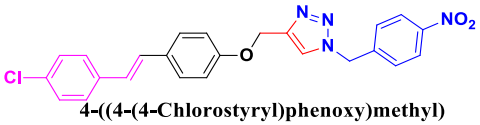 4-((4-(4-Chlorostyryl)phenoxy)methyl) -1-(4-nitrobenzyl)-1*H*-1,2,3-triazole	AD-10	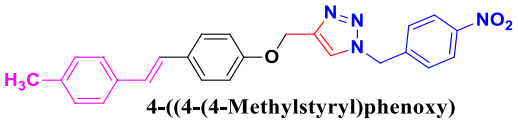 4-((4-(4-Methylstyryl)phenoxy) methyl)-1-(4-nitrobenzyl)-1*H*-1,2,3-triazole
AD-11	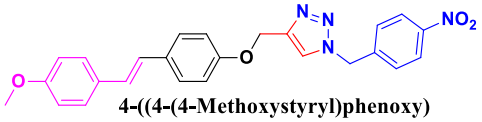 4-((4-(4-Methoxystyryl)phenoxy) methyl)-1-(4-nitrobenzyl)-1*H*-1,2,3-triazole	AD-12	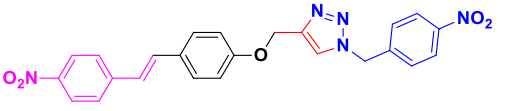 1-(4-Nitrobenzyl)-4-((4-(4-nitrostyryl)phenoxy) methyl)-1*H*-1,2,3-triazole
AD-13	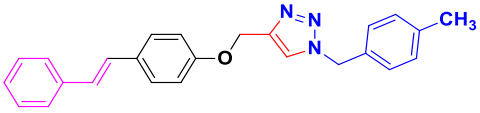 (1-(4-Methylbenzyl)-4-((4-styrylphenoxy) methyl)-1*H*-1,2,3-triazole	AD-14	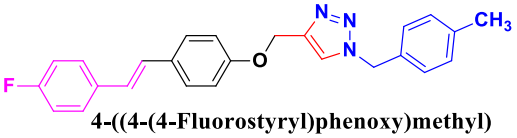 4-((4-(4-Fluorostyryl)phenoxy)methyl) -1-(4-methylbenzyl)-1*H*-1,2,3-triazole
AD-15	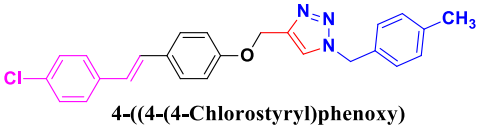 4-((4-(4-Chlorostyryl)phenoxy) methyl)-1-(4-methylbenzyl)-1*H*-1,2,3-triazole	AD-16	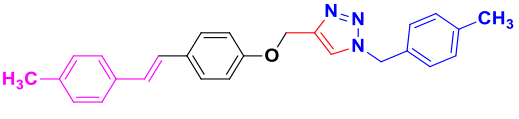 1-(4-Methylbenzyl)-4-((4-(4-methylstyryl) phenoxy)methyl)-1*H*-1,2,3-triazole

AD-17	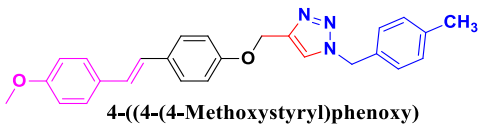 4-((4-(4-Methoxystyryl)phenoxy) methyl)-1-(4-methylbenzyl)-1*H*-1,2,3-triazole	**AD-18**	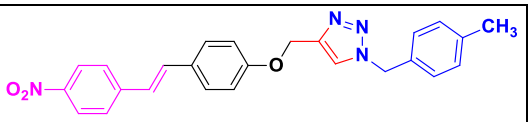 1-(4-Methylbenzyl)-4-((4-(4-nitrostyryl) phenoxy)methyl)-1*H*-1,2,3-triazole
AD-19	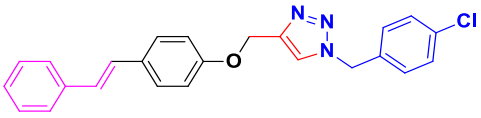 1-(4-Chlorobenzyl)-4-((4-styrylphenoxy) methyl)-1*H*-1,2,3-triazole	**AD-20**	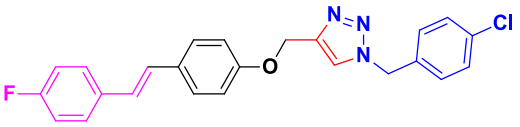 1-(4-Chlorobenzyl)-4-((4-(4-fluorostyryl) phenoxy)methyl)-1*H*-1,2,3-triazole
AD-21	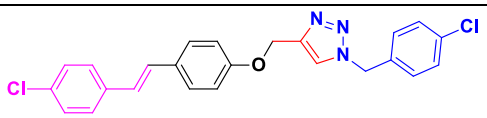 1-(4-Chlorobenzyl)-4-((4-(4-chlorostyryl) phenoxy)methyl)-1*H*-1,2,3-triazole	**AD-22**	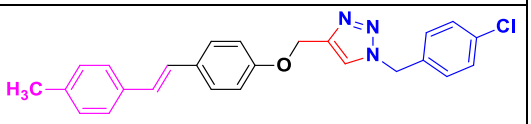 1-(4-Chlorobenzyl)-4-((4-(4-methylstyryl) phenoxy)methyl)-1*H*-1,2,3-triazole
AD-23	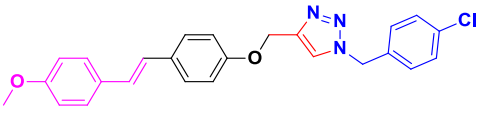 1-(4-Chlorobenzyl)-4-((4-(4-methoxystyryl) phenoxy)methyl)-1*H*-1,2,3-triazole	**AD-24**	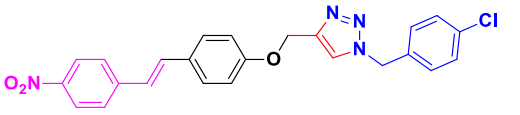 1-(4-Chlorobenzyl)-4-((4-(4-nitrostyryl)phenoxy) methyl)-1*H*-1,2,3-triazole

Table 4.10: Physicochemical properties of 1-benzyl-4-((4-styrylphenoxy) methyl)-1*H*-1,2,3-triazoles (AD 1-24).

Compound	Appearance	M.F	M.W	M.P (°C)	Yield (%)	R_f *
AD-1	White fluffy mass	$C_{24}H_{21}N_3O$	367.44	202-04	35	0.65
AD-2	White fluffy mass	$C_{24}H_{20}FN_3O$	385.43	180-82	45	0.70
AD-3	Colourless crystals	$C_{24}H_{20}ClN_3O$	401.89	229-30	39	0.55
AD-4	Colourless crystals	$C_{25}H_{23}N_3O$	381.47	102-04	28	0.50
AD-5	White fluffy mass	$C_{24}H_{23}N_3O_2$	397.47	190-92	39	0.60
AD-6	Light yellow crystals	$C_{24}H_{20}N_4O_3$	412.44	176-77	36	0.72
AD-7	Light yellow amorphous powder	$C_{24}H_{20}N_4O_3$	412.44	145-47	45	0.80
AD-8	Light yellow crystals	$C_{24}H_{19}FN_4O_3$	430.43	182-84	32	0.65
AD-9	Yellow fluffy mass	$C_{24}H_{19}ClN_4O_3$	446.89	190-92	28	0.55
AD-10	Yellow crystals	$C_{25}H_{22}N_4O_3$	426.47	208-11	42	0.56
AD-11	Yellow amorphous powder	$C_{25}H_{22}N_4O_4$	442.47	207-09	28	0.72
AD-12	Yellow fluffy mass	$C_{24}H_{19}N_5O_5$	457.44	207-08	33	0.66
AD-13	White crystals	$C_{24}H_{19}N_5O_5$	457.44	174-76	33	0.48

AD 14	White fluffy powder	$C_{25}H_{23}N_3O$	381.47	204-06	32	0.65
AD 15	White amorphous powder	$C_{25}H_{22}FN_3O$	399.46	187-90	42	0.55
AD 16	White crystals	$C_{25}H_{22}ClN_3O$	415.91	200-02	42	0.40
AD 17	Whit fluffy mass	$C_{26}H_{25}N_3O$	395.50	166-68	35	0.50
AD 18	White crystals	$C26H_{25}N_3O_2$	426.47	148-50	42	0.80
AD 19	White crystals	$C_{25}H_{22}N_4O3$	401.89	170-71	34	0.70
AD 20	White crystals	$C_{24}H_{20}ClN_3O$	401.89	170-72	42	0.52
AD 21	White crystals	$C_{24}H_{19}ClFN_3O$	436.33	128-30	36	0.63
AD 22	White crystals	$C_{24}H_{19}Cl_2N_3O$	415.91	165-66	35	0.48
AD 23	White amorphous powder	$C_{25}H_{22}ClN_3O_2$	431.91	192-94	35	0.55
AD 24	Yellow crystals	$C_{24}H_{19}ClN_4O_3$	446.89	174-76	39	0.65

*** Mobile Phase: Ethylacetate: Hexane (8:2)**

Table 4.11: Structure and IUPAC name of -3-(4-((1-benzyl-1*H*-1,2,3 triazol-4yl) methoxybenzylidene)indolin-2-ones (AD 25-48)

Code	Structure &IUPAC Name	Code	Structure & IUPAC Name
AD-25	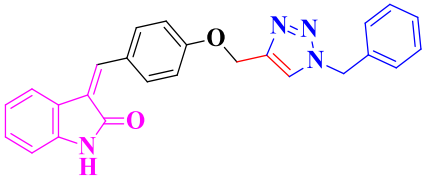 3-(4-((1-Benzyl-1*H*-1,2,3-triazol-4-yl)methoxy) benzylidene)indolin-2-one	AD-26	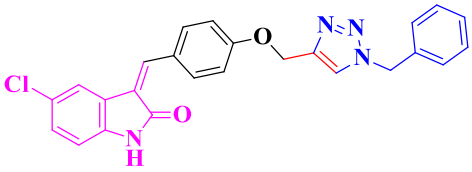 3-(4-((1-Benzyl-1*H*-1,2,3-triazol-4-yl)methoxy) benzylidene)-5-chloroindolin-2-one
AD-27	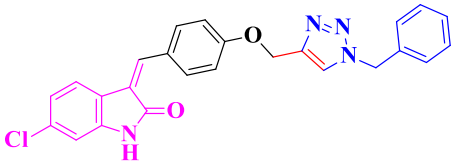 3-(4-((1-Benzyl-1*H*-1,2,3-triazol-4-yl)methoxy) benzylidene)-6-chloroindolin-2-one	AD-28	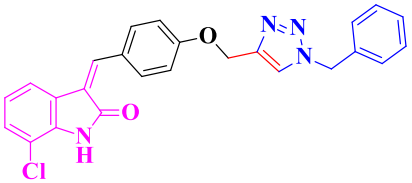 3-(4-((1-Benzyl-1*H*-1,2,3-triazol-4-yl)methoxy) benzylidene)-7-chloroindolin-2-one
AD-29	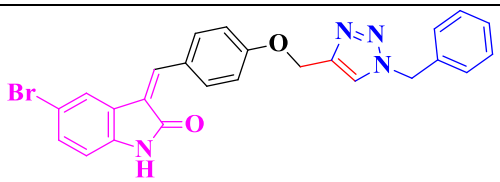 3-(4-((1-Benzyl-1*H*-1,2,3-triazol-4-yl)methoxy) benzylidene)-5-bromoindolin-2-one	AD-30	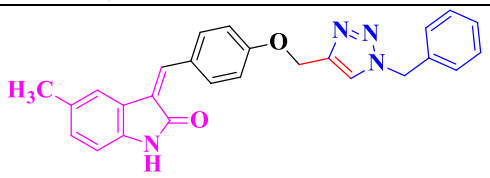 3-(4-((1-Benzyl-1*H*-1,2,3-triazol-4-yl)methoxy) benzylidene)-5-methylindolin-2-one
AD-31	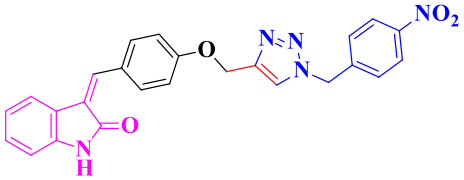 3-(4-((1-(4-Nitrobenzyl)-1*H*-1,2,3-triazol-4-yl) methoxy)benzylidene)indolin-2-one	AD-32	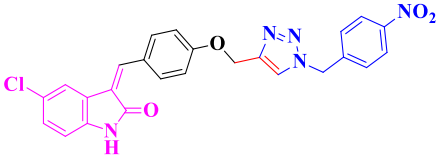 5-Chloro-3-(4-((1-(4-nitrobenzyl)-1*H*-1,2,3-triazol-4-yl) methoxy)benzylidene)indolin-2-one
AD-33	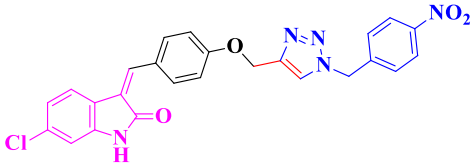 6-Chloro-3-(4-((1-(4-nitrobenzyl)-1*H*-1,2,3-triazol-4-yl) methoxy)benzylidene)indolin-2-one	AD-34	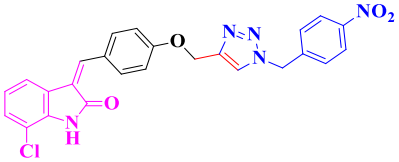 7-Chloro-3-(4-((1-(4-nitrobenzyl)-1*H*-1,2,3-triazol-4-yl) methoxy)benzylidene)indolin-2-one
AD-35	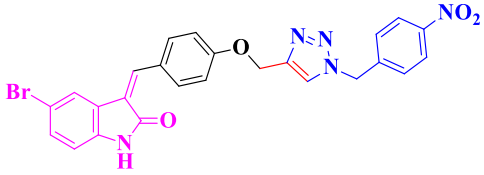 5-Bromo-3-(4-((1-(4-nitrobenzyl)-1*H*-1,2,3-triazol-4-yl) methoxy)benzylidene)indolin-2-one	AD-36	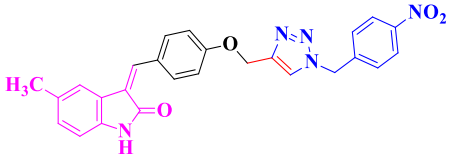 5-Methyl-3-(4-((1-(4-nitrobenzyl)-1*H*-1,2,3-triazol-4-yl) methoxy)benzylidene)indolin-2-one

AD-37	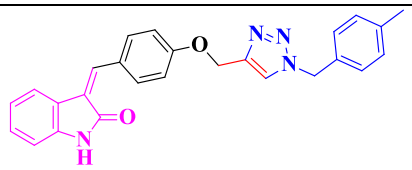 3-(4-((1-(4-Methylbenzyl)-1*H*-1,2,3-triazol-4-yl) methoxy)benzylidene)indolin-2-one	**AD-38**	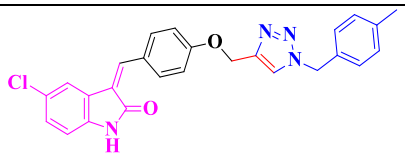 5-Chloro-3-(4-((1-(4-methylbenzyl)-1*H*-1,2,3-triazol-4-yl) methoxy)benzylidene)indolin-2-one
AD-39	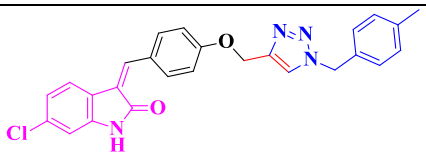 6-Chloro-3-(4-((1-(4-methylbenzyl)-1*H*-1,2,3-triazol-4-yl) methoxy)benzylidene)indolin-2-one	**AD-40**	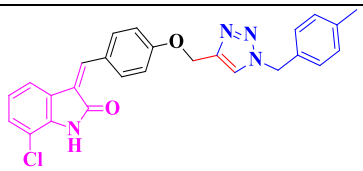 7-Chloro-3-(4-((1-(4-methylbenzyl)-1*H*-1,2,3-triazol-4-yl) methoxy)benzylidene)indolin-2-one
AD-41	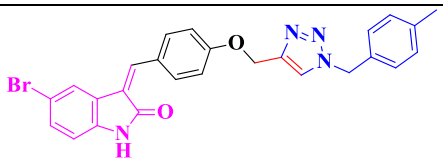 5-Bromo-3-(4-((1-(4-methylbenzyl)-1*H*-1,2,3-triazol-4-yl) methoxy)benzylidene)indolin-2-one	**AD-42**	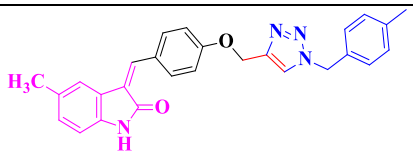 5-Methyl-3-(4-((1-(4-methylbenzyl)-1*H*-1,2,3-triazol-4-yl) methoxy)benzylidene)indolin-2-one
AD-43	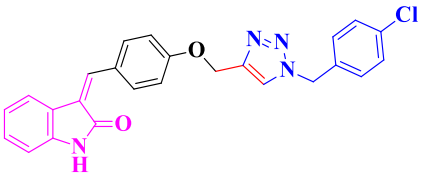 3-(4-((1-(4-Chlorobenzyl)-1*H*-1,2,3-triazol-4-yl) methoxy)benzylidene)indolin-2-one	**AD-44**	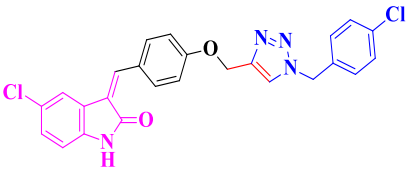 5-Chloro-3-(4-((1-(4-chlorobenzyl)-1*H*-1,2,3-triazol-4-yl) methoxy)benzylidene)indolin-2-one
AD-45	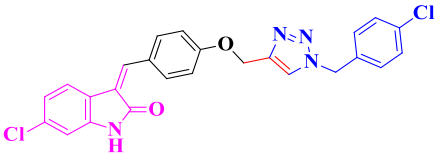 6-Chloro-3-(4-((1-(4-chlorobenzyl)-1*H*-1,2,3-triazol-4-yl) methoxy)benzylidene)indolin-2-one	**AD-46**	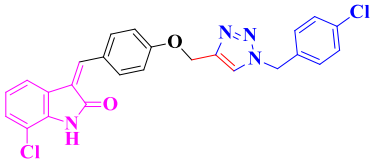 7-Chloro-3-(4-((1-(4-chlorobenzyl)-1*H*-1,2,3-triazol-4-yl) methoxy)benzylidene)indolin-2-one
AD-47	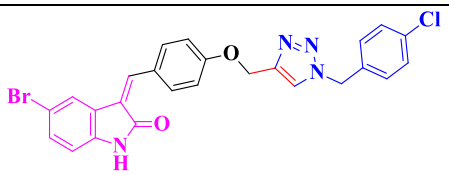 5-Bromo-3-(4-((1-(4-chlorobenzyl)-1*H*-1,2,3-triazol-4-yl) methoxy)benzylidene)indolin-2-one	**AD-48**	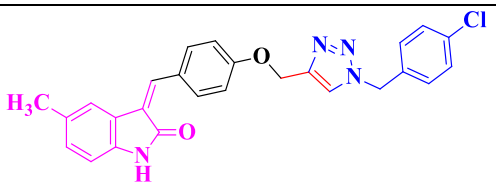 3-(4-((1-(4-Chlorobenzyl)-1*H*-1,2,3-triazol-4-yl) methoxy)benzylidene)-5-methylindolin-2-one

Table 4.12: Physicochemical properties of 3-(4-((1-benzyl-1*H*-1,2,3-triazol-4yl) methoxybenzylidene)indolin-2-ones (AD 25-48).

Compound	Physical Appearance	M.F	M.W	M.P (°C)	Yield (%)	R_f *
AD 25	Yellow amorphous powder	$C_{25}H_{20}N_4O_2$	408.45	170-72	55	0.50
AD 26	Orange amorphous mass	$C_{25}H_{19}ClN_4O_2$	442.90	260-62	58	0.45
AD-27	Yellow amorphous powder	$C_{25}H_{19}ClN_4O_2$	442.90	181-83	65	0.50
AD 28	Yellow amorphous powder	$C_{25}H_{19}ClN_4O_2$	442.90	214-16	73	0.55
AD 29	Orange amorphous powder	$C_{25}H_{19}BrN_4O_2$	487.35	238-40	62	0.45
AD 30	Orange amorphous powder	$C_{26}H_{22}N_4O_2$	422.48	220-22	55	0.50
AD 31	Orange amorphous powder	$C_{25}H_{19}N_5O_4$	453.45	214-15	63	0.65
AD 32	Yellow amorphous powder	$C_{25}H_{18}ClN_5O_4$	487.89	220-22	55	0.60
AD 33	Yellow amorphous powder	$C_{25}H_{18}ClN_5O_4$	487.89	178-80	54	0.45

AD 34	Yellow amorphous powder	$C_{25}H_{18}ClN_5O_4$	487.89	210-13	58	0.40
AD 35	Yellow amorphous powder	$C_{25}H_{18}BrN_5O_4$	532.35	210-12	65	0.48
AD 36	Orange amorphous powder	$C_{26}H_{21}N_5O_4$	467.48	216-18	55	0.56
AD 37	Yellow amorphous powder	$C_{26}H_{22}N_4O_2$	422.28	200-01	70	0.38
AD 38	Yellow fluffy mass	$C_{26}H_{21}ClN_4O_2$	456.92	242-44	48	0.62
AD 39	Yellow amorphous powder	$C_{26}H_{21}ClN_4O_2$	456.92	189-90	56	0.53
AD 40	Orange fluffy mass	$C_{26}H_{21}ClN_4O_2$	456.92	212-14	55	0.47
AD 41	Orange fluffy mass	$C_{26}H_{21}BrN_4O_2$	501.37	238-40	46	0.56
AD 42	Yellow amorphous powder	$C_{27}H_{24}N_4O_2$	436.57	208-10	60	0.44
AD 43	Orange amorphous powder	$C_{25}H_{19}ClN_4O_2$	442.90	184-86	65	0.45
AD 44	Yellow amorphous powder	$C_{25}H_{18}Cl_2N_4O_2$	477.34	242-44	52	0.57
AD 45	Yellow amorphous powder	$C_{25}H_{18}Cl_2N_4O_2$	477.34	242-46	68	0.55

AD46	Yellow fluffy mass	$C_{25}H_{18}Cl_2N_4O_2$	477.34	250-52	62	0.50
AD 47	Yellow amorphous powder	$C_{25}H_{18}BrClN_4O_2$	521.79	242-43	67	0.48
AD 48	Yellow amorphous powder	$C_{26}H_{21}ClN_4O_2$	456.92	220-21	56	0.62

*** Mobile Phase: Chloroform:Ethanol (8:2)**

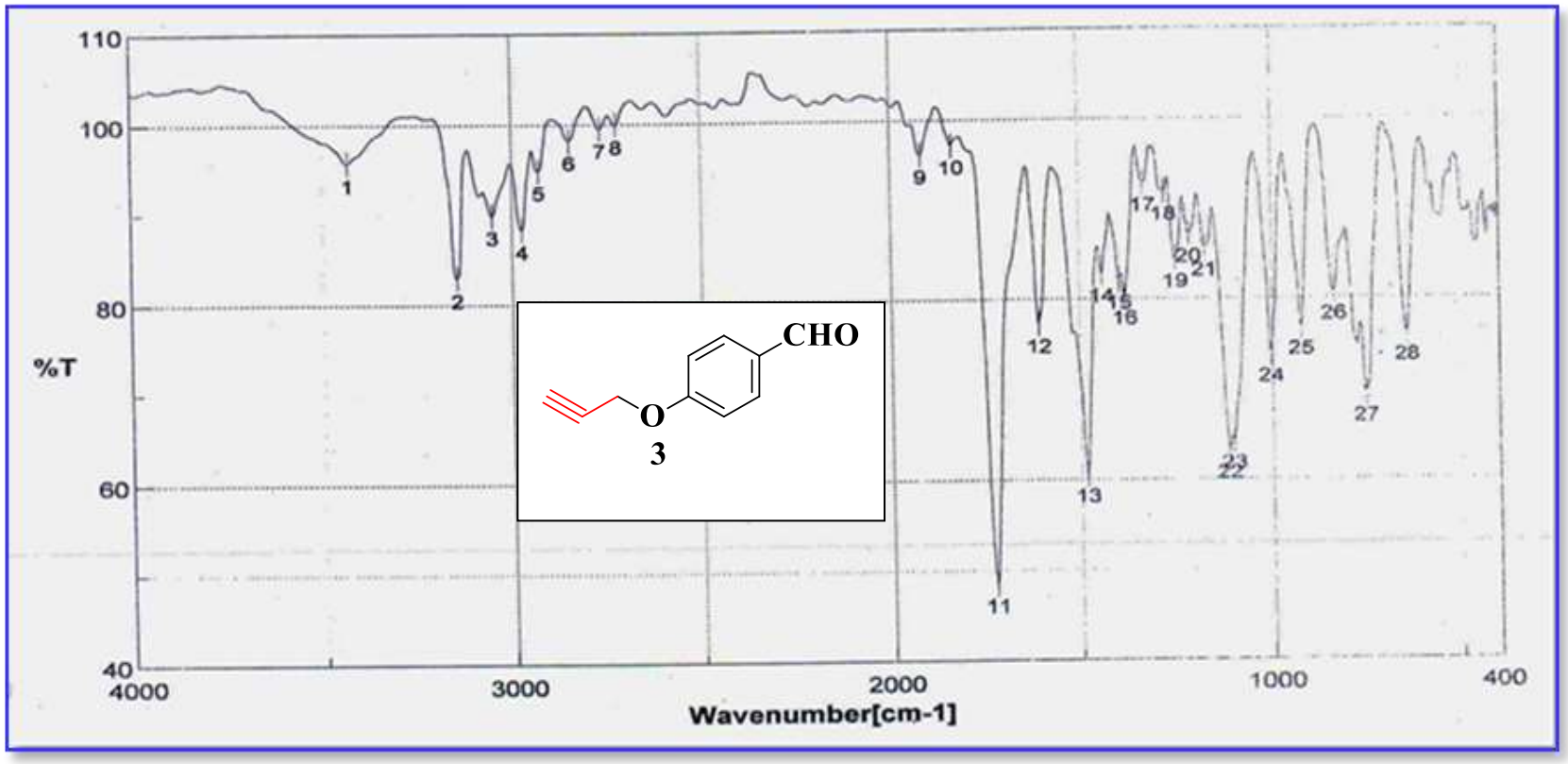

Figure 4.1: FTIR Spectrum of 4-(prop-2-yn-1-yloxy)benzaldehyde. (3)

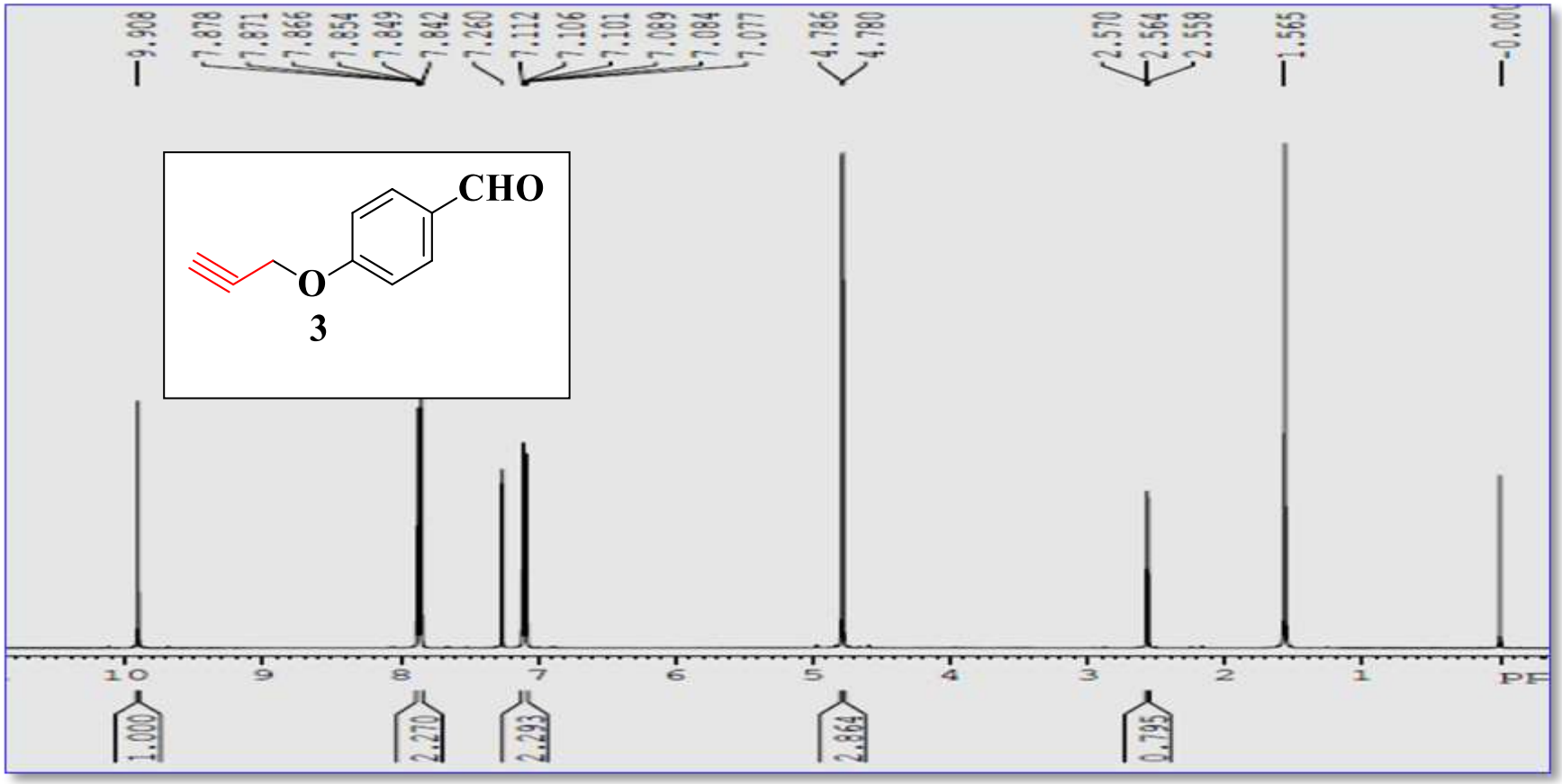

Figure. 4.2: ^{1}H-NMR Spectrum of 4-(prop-2-yn-1-yloxy)benzaldehyde. (3)

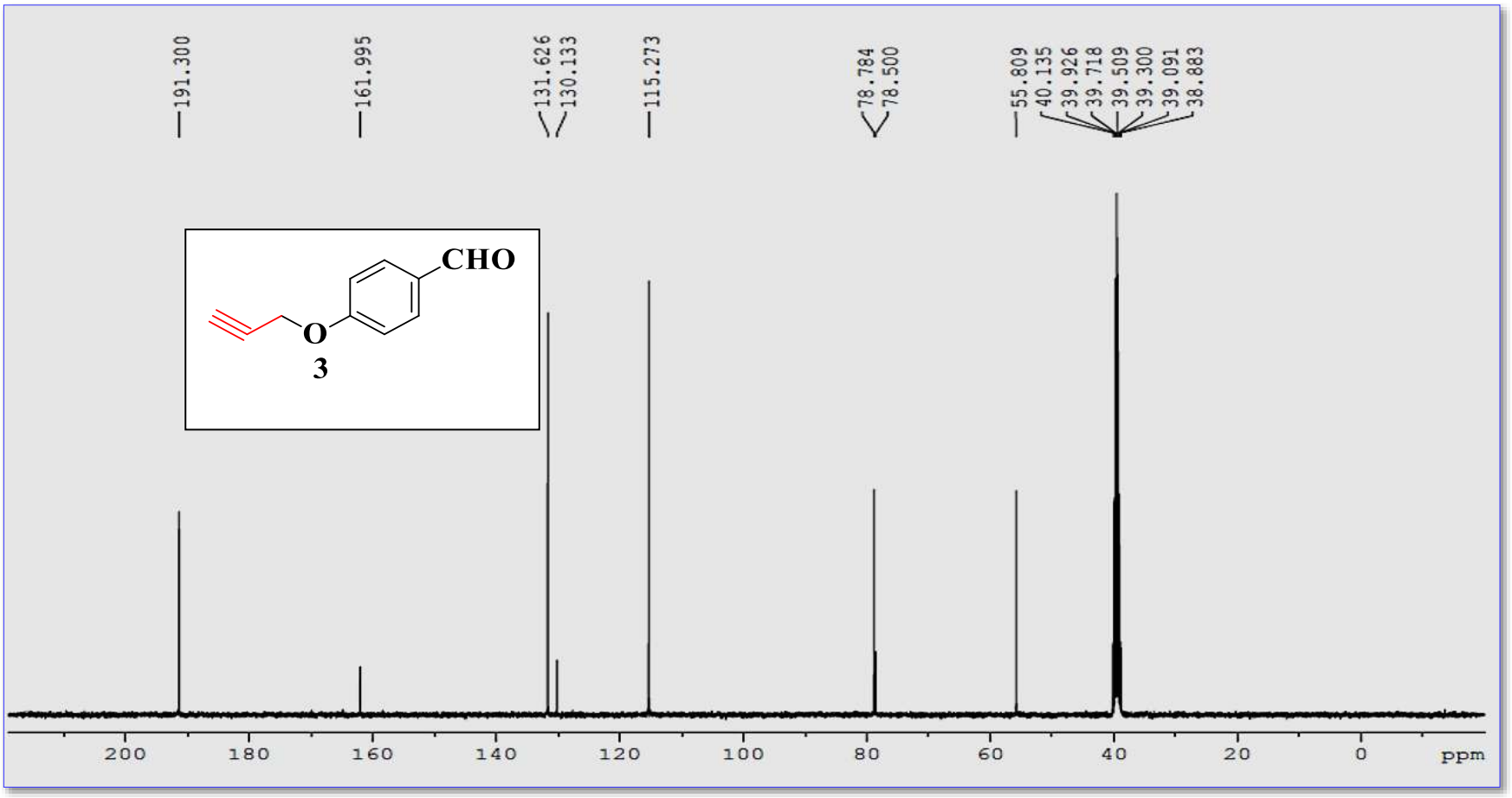

Figure. 4.3: ^{13}C-NMR Spectrum of 4-(prop-2-yn-1-yloxy)benzaldehyde. (3)

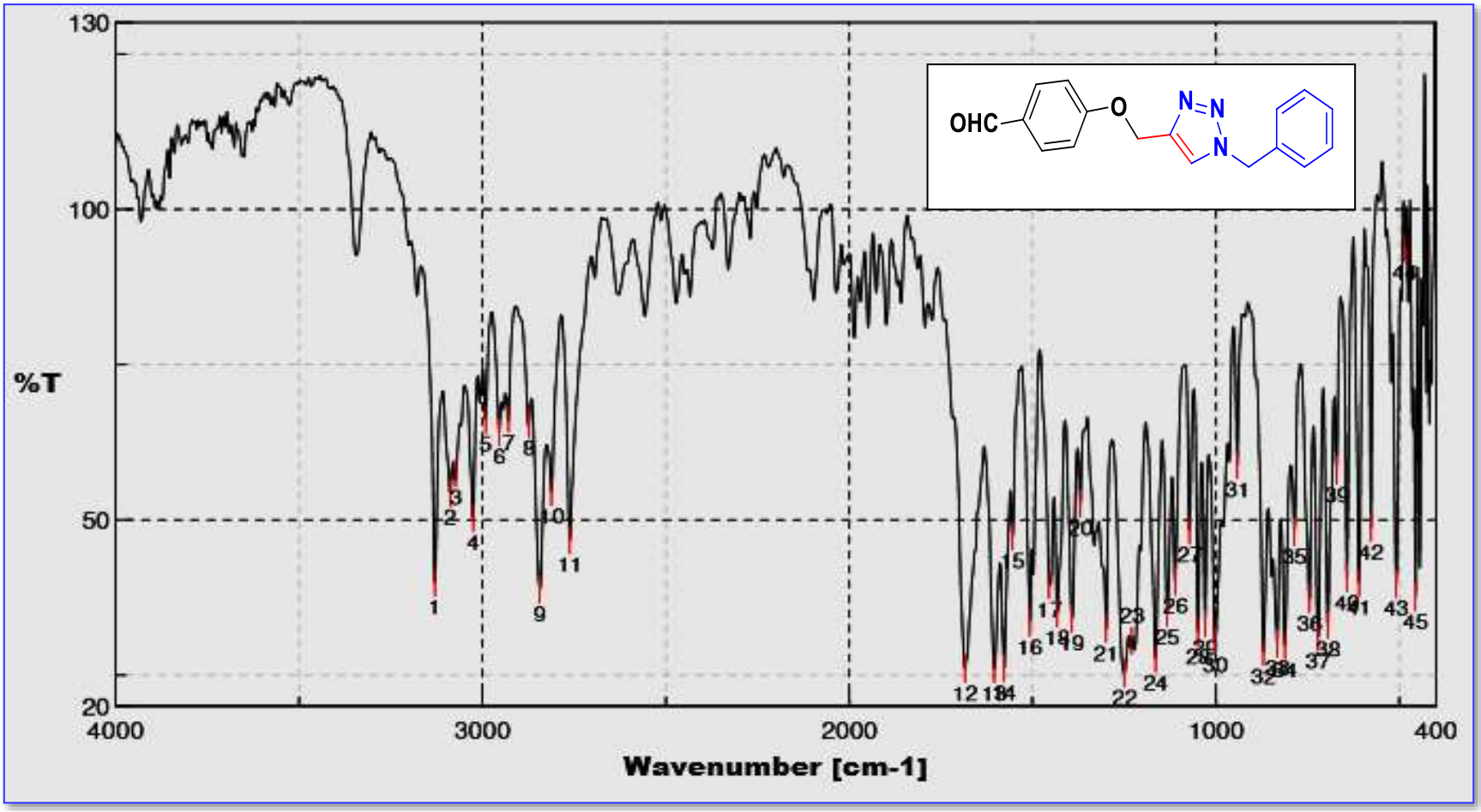

Figure. 4.4: FTIR Spectrum of 4-((1-Benzyl-1*H*-1,2,3-triazol-4-yl)methoxy)benzaldehyde. (7a)

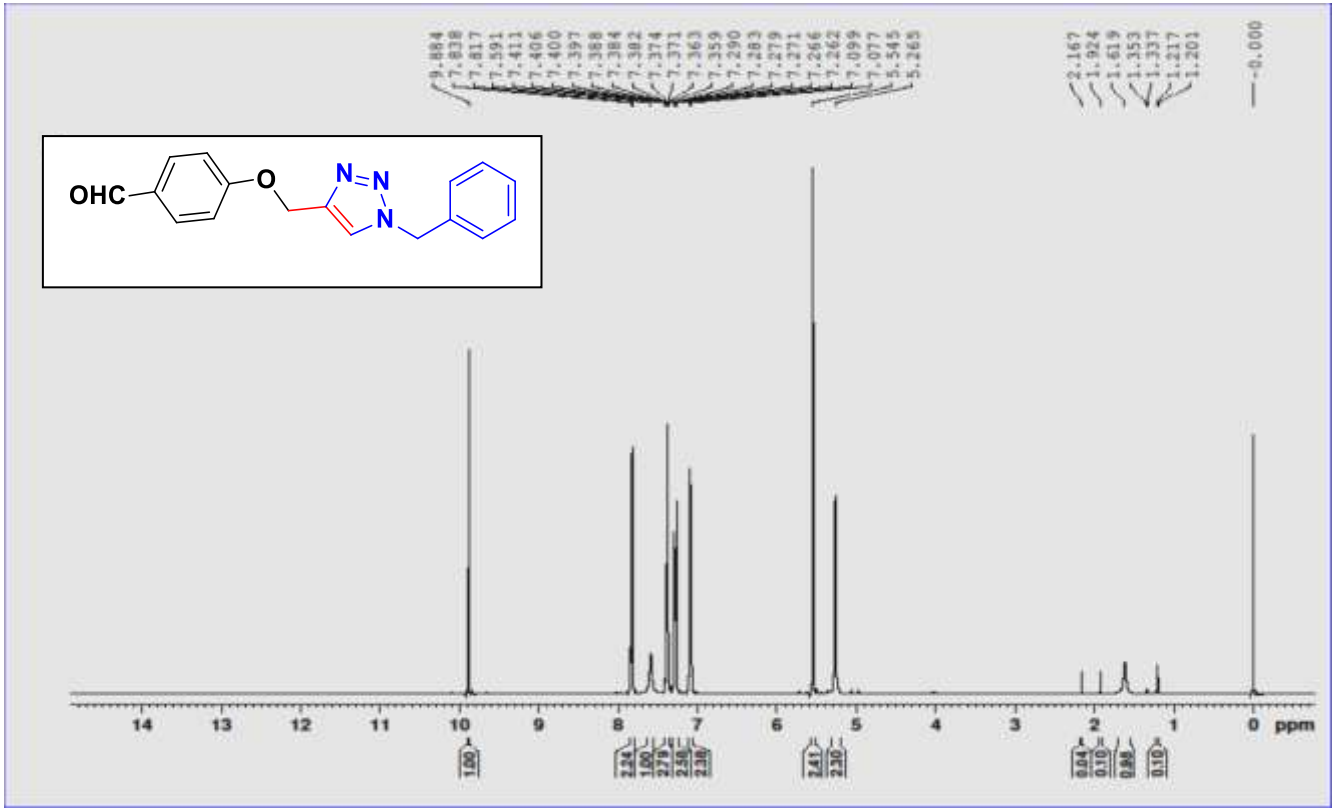

NMR (400 MHz, DMSO-d_6): 5.27 (s, 2H, -OCH_2-), 5.55 (s, 2H, -NCH_2-), 7.10 (2H, d, *j*=8.4 Ar-H.) 7.29-7.26 (m, 2H, ar.), 7.40-7.36 (m, 3H, ar.), 7.59 (s, 1H, triazole-H), 7.84 (2H, d, *j*=8.8 Ar-H.), 9.88 (s, 1H, -CHO) ppm.

Figure. 4.5: ^{1}H NMR spectrum of 4-((1-Benzyl-1*H*-1,2,3-triazol-4-yl)methoxy)benzaldehyde. (7a)

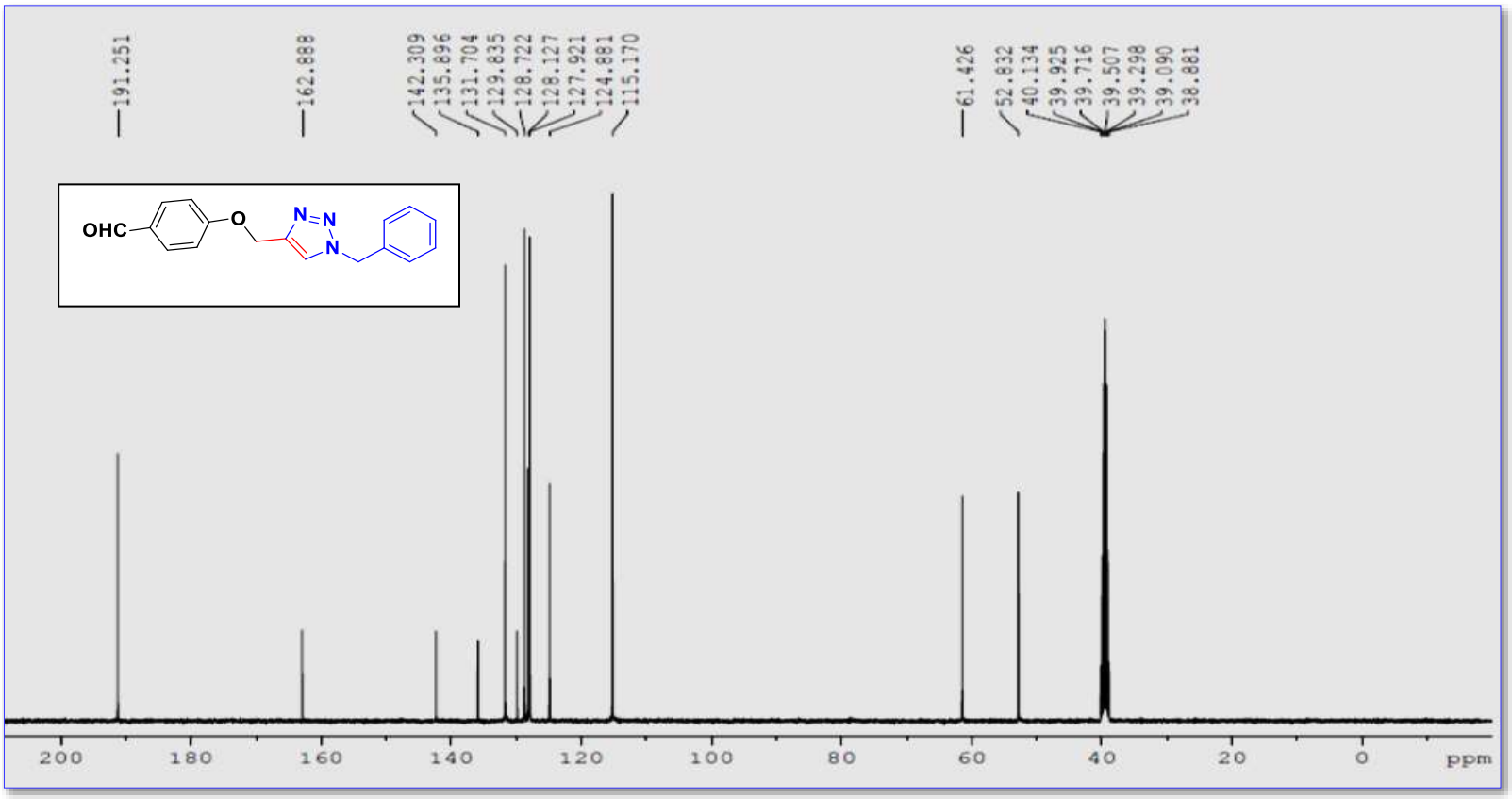

NMR (400 MHz, DMSO-d$_6$): 38.88, 39.09, 39.29, 39.50, 39.71, 39.92, 40.13, 52.83, 61.42, 115.17, 124.88, 127.92, 128.12, 128.72, 129.83, 131.70, 135.89, 142.30, 162.88, 191.25 δ ppm.

Figure. 4.6: ^{13}C-NMR spectrum of 4-((1-Benzyl-1*H*-1,2,3-triazol-4-yl)methoxy)benzaldehyde. (7a)

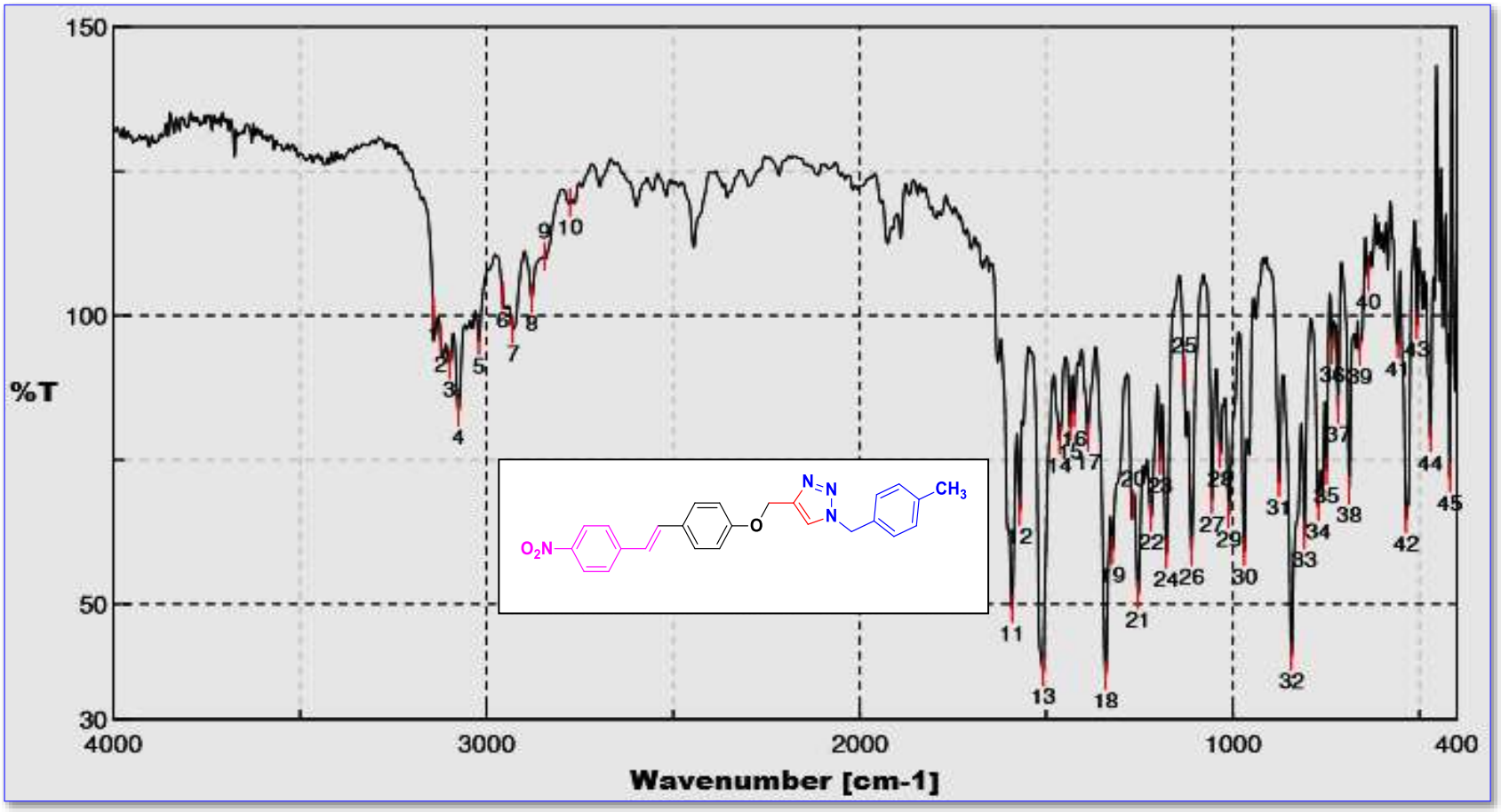

Figure. 4.7: FTIR spectrum of 1-(4-methylbenzyl)-4-((4-(4-nitrostyryl)phenoxy)methyl)-1*H*-1,2,3-triazole. (AD 18)

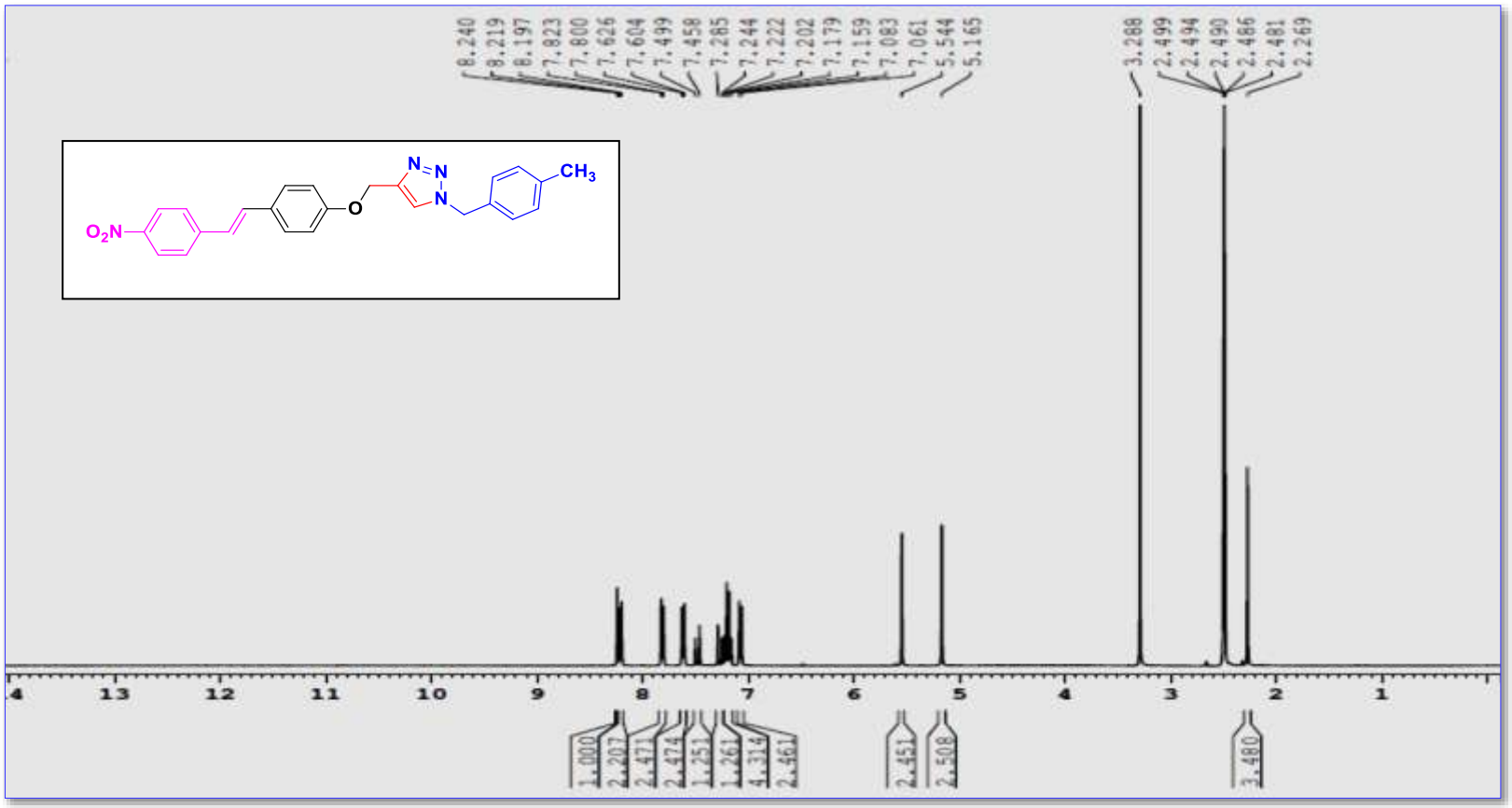

Figure. 4.8: ^{1}H-NMR Spectrum of 1-(4-methylbenzyl)-4-((4-(4-nitrostyryl) phenoxy)methyl)-1*H*-1,2,3-triazole. (AD 18)

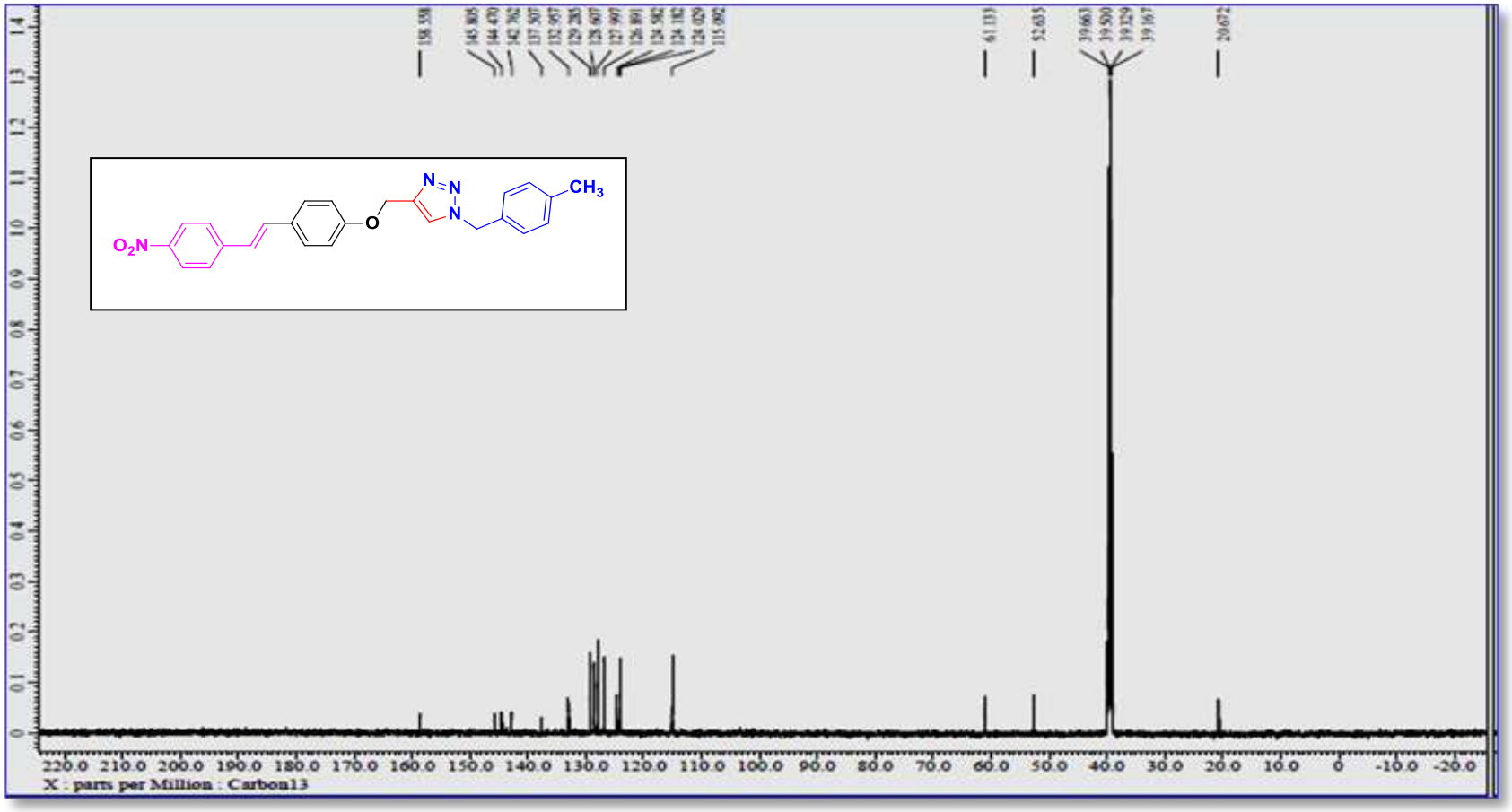

Figure. 4.9: ^{13}C-NMR spectrum of 1-(4-methylbenzyl)-4-((4-(4-nitrostyryl) phenoxy)methyl)-1*H*-1,2,3-triazole. (AD 18)

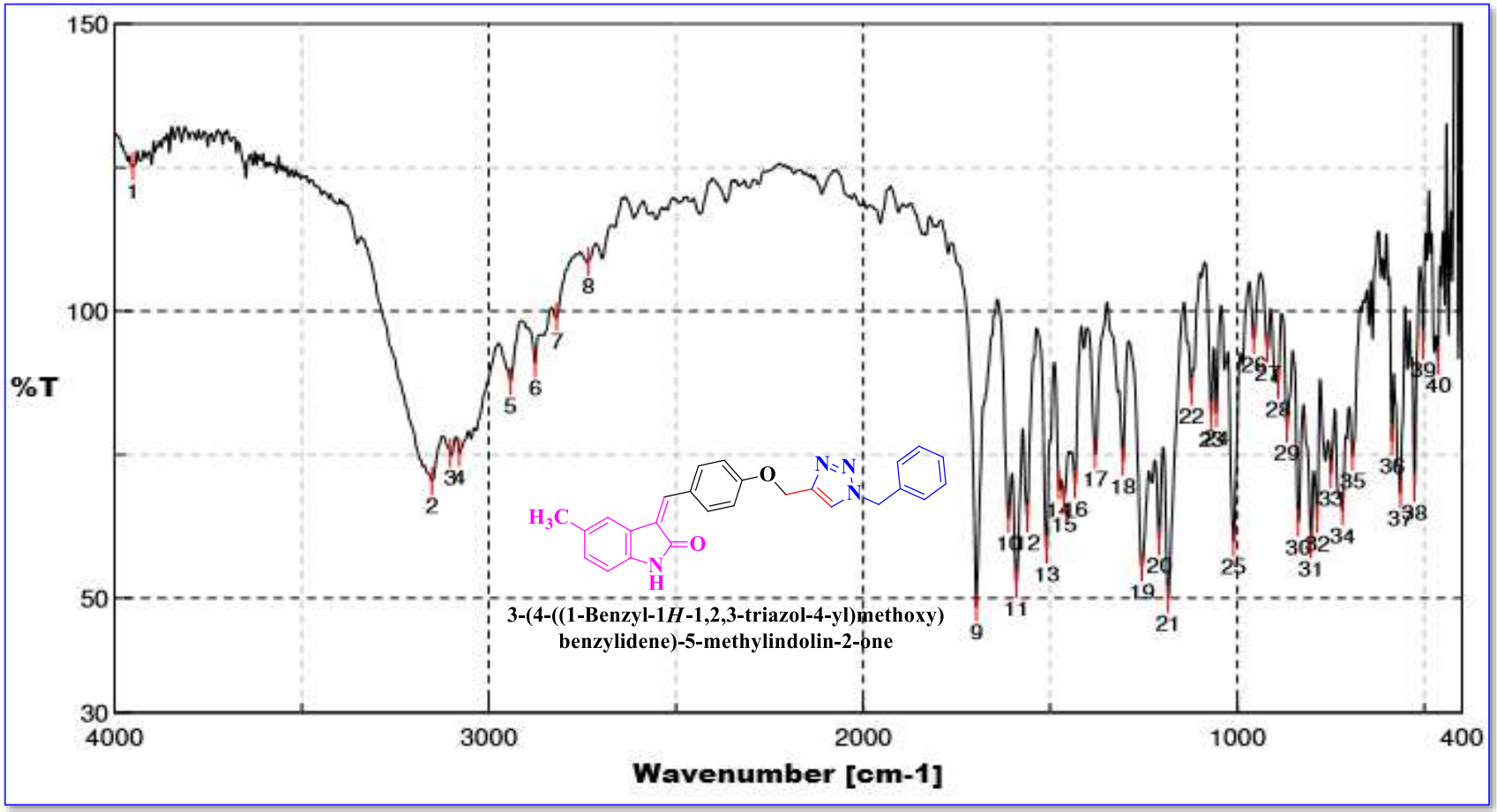

Figure. 4.10: FTIR Spectrum of 3-(4-((1-benzyl-1*H*-1,2,3-triazol-4-yl)methoxy)benzylidene)-5-methylindolin-2-one. (AD-30)

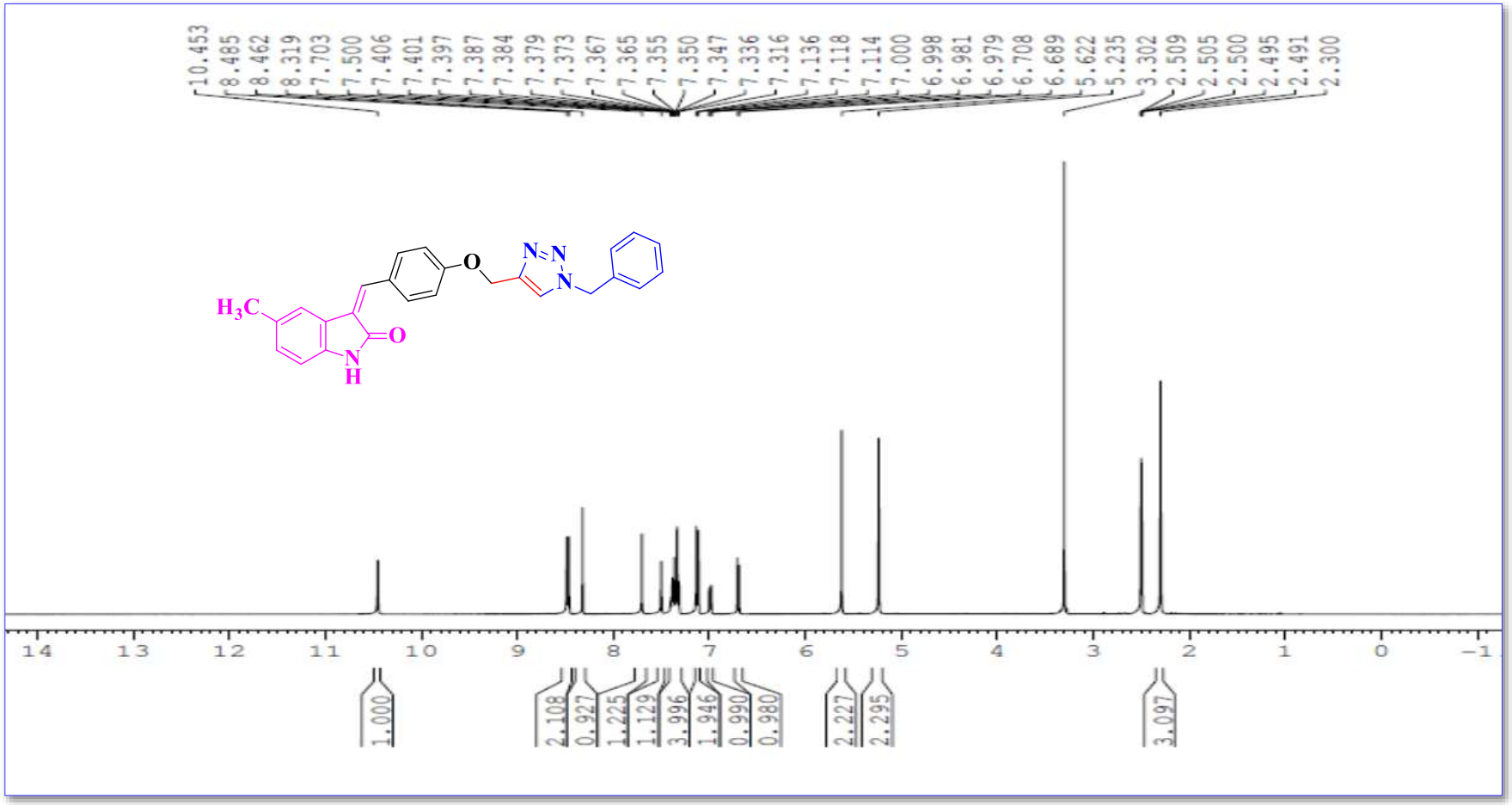

Figure. 4.11: ^{1}H-NMR Spectrum of 3-(4-((1-benzyl-1*H*-1,2,3-triazol-4-yl)methoxy)benzylidene)-5-methylindolin-2-one. (AD-30)

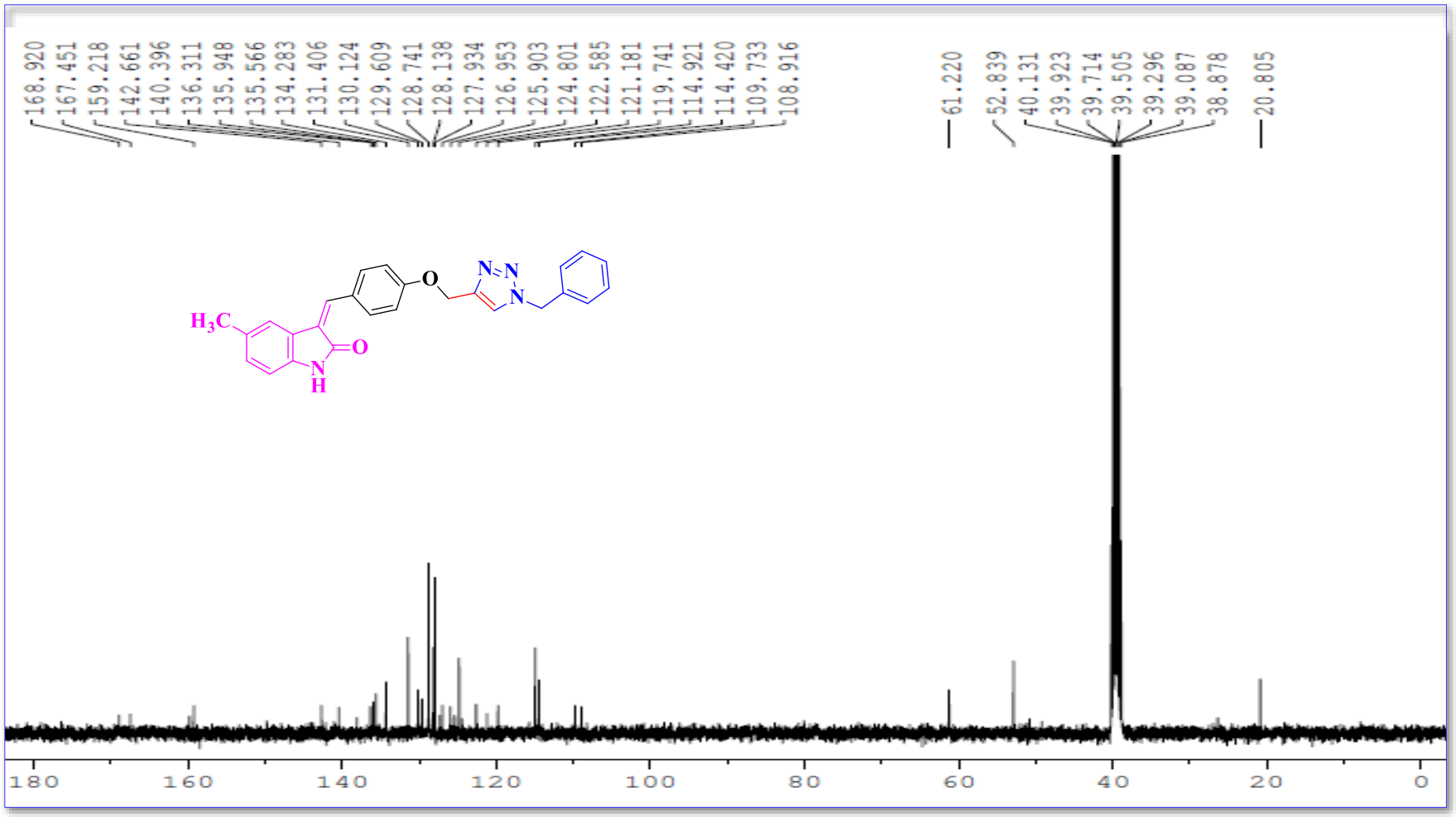

Figure. 4.12: ^{13}C-NMR Spectrum of 3-(4-((1-benzyl-1*H*-1,2,3-triazol-4-yl)methoxy)benzylidene)-5-methylindolin-2-one. (AD-30)

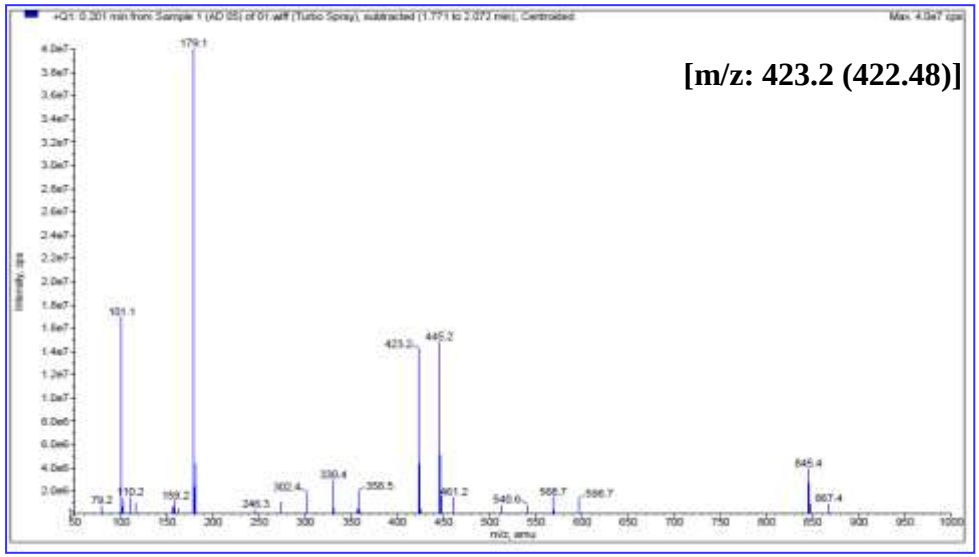

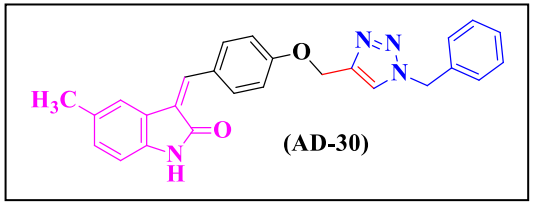

Figure. 4.13: LCMS of 3-(4-((1-benzyl-1*H*-1,2,3-triazol-4-yl)methoxy) benzylidene)-5-methylindolin-2-one. (AD-30)

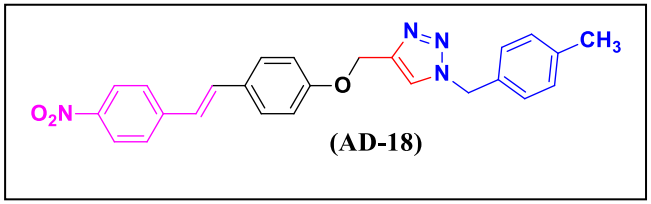

Figure. 4.14: LCMS of 1-(4-methylbenzyl)-4-((4-(4-nitrostyryl)phenoxy)methyl)-1*H*-1,2,3-triazole. (AD-18).

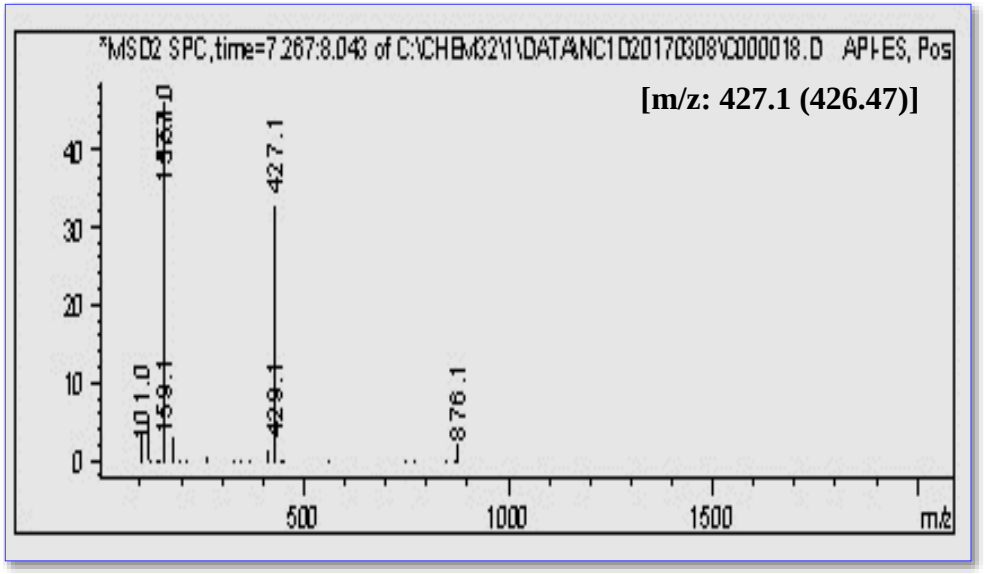

Table-4.13: FTIR spectral data of 1-benzyl-4-((4-styrylphenoxy)methyl)-1*H*-1,2,3-triazoles. (AD 1-24)

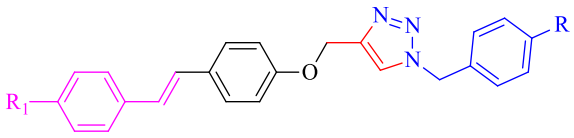

Code	Transmittance peaks (cm^{-1})
AD-1	3010-3005 (-CH, Ar.), 2873-2750 (-CH, Ali.), 1602 (>C=C<), 1455 ($-CH_2$), 1243 (-O-).
AD-2	3074-3050 (-CH, Ar.), 2860-2790 (-CH, Ali.), 1605 (>C=C<), 1455 ($-CH_2$), 1266 (-O-).
AD-3	3033-3000 (-CH, Ar.), 2918-2780 (-CH, Ali.), 1603 (>C=C<), 1467 ($-CH_2$), 1249 (-O-).
AD-4	3070-3050 (-CH, Ar.), 2964-2778 (-CH, Ali.), 1603 (>C=C<), 1467 ($-CH_2$), 1378 ($-CH_3$), 1244 (-O-).
AD-5	3034-3002 (-CH, Ar.), 2837-2780 (-CH, Ali.), 1606 (>C=C<), 1467 ($-CH_2$), 1384 ($-CH_3$), 1253 (-O-).
AD-6	3101-3050 (-CH, Ar.), 2838-2750 (-CH, Ali.), 1591(>C=C<), 1513 ($-NO_2$), 1453 ($-NO_2$), 1178 (-O-).
AD-7	3087-3030 (-CH, Ar.), 2872-2768 (-CH, Ali.), 1606 (>C=C<), 1515 ($-NO_2$), 1447 ($-NO_2$), 1210 (-O-).
AD-8	3098-3055 (-CH, Ar.), 2874-2850 (-CH, Ali), 1607 (>C=C<), 1517 ($-NO_2$), 1458 ($-NO_2$), 1217 (-O-).
AD-9	3084-3058 (-CH, Ar.), 2781-2854 (-CH, Ali.), 1604 (>C=C<), 1514 ($-NO_2$), 1457 ($-NO_2$), 1256 (-O-).
AD-10	3087-3048 (-CH, Ar.), 2912-2854 (-CH, Ali.), 1604 (>C=C<), 1515 ($-NO_2$), 1453 ($-NO_2$), 1349 ($-CH_3$), 1255 (-O-).
AD-11	3087-3039 (-CH, Ar.), 2836-2750 (-CH, Ali.), 1607 (>C=C<), 1516 ($-NO_2$), 1462 ($-NO_2$), 1349 ($-CH_3$), 1254 (-O-).
AD-12	3050-3001 (-CH, Ar.), 2936-2850 (-CH, Ali.), 1516 ($-NO_2$), 1507 ($-NO_2$), 1176 (-O-).
AD-13	3027-3002 (-CH, Ar.), 2872-2786 (-CH, Ali,), 1602 (>C=C<) 1462 ($-CH_2$), 1380 ($-CH_3$), 1243 (-O-).
AD-14	3077-3060 (-CH, Ar.), 2872-2860 (-CH, Ali.), 1605 (>C=<), 1454 ($-CH_2$), 1213 (-O-).
AD-15	3077-3030 (-CH, Ar.), 2877-2748 (-CH, Ali), 1605 (> C=C<), 1457 ($-CH_2$), 1177(-O-).
AD-16	3050-3023 (-CH, Ar.), 2843-2734 (-CH. Ali), 1602 (>C=C<), 1455, ($-CH_2$), 1388 ($-CH_3$), 1240 (-O-).

AD-17	3079-3001 (-CH, Ar.), 2840-2780 (-CH, Ali.), 1605 (.C=C<), 1395 (-CH_3), 1249 (-O-).
AD-18	3075-3065 (-CH, Ar.), 2926-2800 (-CH, Ali.), 1592 (-NO_2), 1509 (-NO_2), 1465 (-CH_2), 1388 (-CH_3), 1219 (-O-).
AD-19	3050-3023 (-CH, Ar.), 2823-2791 (-CH, Ali.), 1606 (>C=C<), 1459 (-CH_2), 1394 (-CH_3), 1258 (-O-).
AD-20	3064-3010 (-CH, Ar.), 2850-2790 (-CH, Ali.), 1607 (>C=C<), 1459 (-CH_2), 1380 (-CH_3), 1216 (-O-).
AD-21	3059-3008 (-CH, Ar.), 2937-2801 (-CH, Ali.), 1606 (>C=C<), 1492 (-CH_2), 1368 (-CH_3), 1258 (-O-).
AD-22	3087-3040 (-CH, Ar.), 2921-2801 (-CH, Ali.), 1604 (>C=C<), 1459 (-CH_2), 1336 (-CH_3), 1253 (-O-).
AD-23	3077-3055 (-CH, Ar.), 2841-2781 (-CH, Ali.), 1606 (>C=C<), 1388 (-CH_3), 1251 (-O-).
AD-24	3089-3052 (-CH, Ar.), 2826-2744 (-CH, Ali.), 1634 (>C=C<), 1587 (-NO_2), 1509 (-NO_2), 1427 (-CH_2), 1217 (-O-).

Table 4.14: ^{1}H-NMR data of -1-benzyl-4-((4-styrylphenoxy)methyl)-1*H*-1,2,3-triazoles. (AD 1-24).

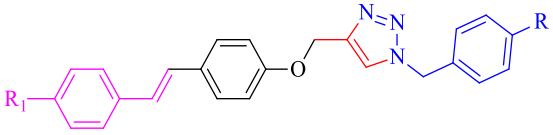

Code	Chemical shift values (δ ppm)
AD-1	5.15 (2H, s, -CH_2-), 5.61 (2H, s, -OCH_2-), 7.04 (2H, d, J = 8.8 Hz, Ar-H), 7.11 (1H, d, J = 16.4 Hz, styryl -CH=C-), 7.17-7.25 (2H, md, J = 16.4 Hz, styryl -C=CH-), 7.30-7.39 (7H, m, Ar-H), 7.54 (4H, m, Ar-H), 8.27 (1H, s, Triazole-H).
AD-2	5.15 (2H, s, -CH_2-), 5.60 (2H, s, -OCH_2-), 7.04 (2H, d, J = 11.6 Hz, Ar-H), 7.12 (2H, d, J = 6.8 Hz, Ar-H), 7.16-7.20 (2H, m, Ar-H), 7.30-7.39 (5H, m, Ar-H), 7.53 (2H, d, J = 11.2 Hz, Ar-H), 7.58-7.61 (2H, m, Ar-H), 8.27 (1H, s, Triazole-H).
AD-3	5.15 (2H, s, -CH_2-), 5.60 (2H, s, -OCH_2-), 7.03 (2H, d, J = 8.4 Hz, Ar-H), 7.11 (1H, d, J = 16.8 Hz, styryl -CH=C-), 7.23 (1H, d, J = 16.8 Hz, styryl -C=CH-), 7.29-7.38 (3H, m, Ar-H), 7.45 (2H, d, J = 8.8 Hz, Ar-H), 7.55 (2H, d, J = 8.8 Hz, Ar-H), 7.54 (2H, d, J = 8.8 Hz, Ar-H), 8.27 (1H, s, Triazole-H).
AD-4	2.29 (3H, s, -CH_3), 5.14 (2H, s, -CH_2-), 5.60 (2H, s, 2H, -OCH_2-), 7.03 (2H, d, J = 8.8 Hz, Ar-H), 7.06 (1H, d, J = 16.8 Hz, styryl -CH=C-), 7.10 (1H, d, J = 16.8 Hz, styryl -C=CH-), 7.17 (2H, d, J = 8 Hz, Ar-H), 7.29-7.39 (4H, m, Ar-H), 7.45 (2H, d, J = 8 Hz, Ar-H), 7.52 (2H, d, J = 8.8 Hz, Ar-H), 8.27 (1H, s, Triazole-H).
AD-5	3.76 (3H, s, -OCH_3), 5.14 (2H, s, -CH_2-), 5.60 (2H, s, -OCH_2-), 6.93 (2H, d, J = 8.8 Hz, Ar-H), 6.99-7.03 (4H, m, Ar-H,), 7.30-7.39 (5H, m, Ar-H), 7.49 (4H, d, J = 8 Hz, Ar-H), 8.27 (1H, s, Triazole-H).
AD-6	5.18 (2H, s, -CH_2-), 5.61 (2H, s, -OCH_2-), 7.09 (2H, d, J = 8.8 Hz, Ar-H), 7.29 (1H, d, J = 16.4 Hz, styryl -CH=C-), 7.30-7.39 (5H, m, Ar-H), 7.50 (1H, d, J = 16.4 Hz, styryl -C=CH-), 7.63 (2H, d, J = 8.8 Hz, Ar-H), 7.82 (2H, d, J = 8.8 Hz, Ar-H), 8.22 (2H, d, J = 8.8 Hz, Ar-H), 8.28 (1H, s, Triazole-H).
AD-7	5.18 (2H, s, -CH_2-), 5.80 (2H, s,-OCH_2-), 7.05 (2H, d, J = 8.8 Hz, Ar-H), 7.11 (1H, d, J = 16.4 Hz, styryl -CH=C-), 7.21 (1H, d, J = 16.8 Hz, styryl -C=CH-), 7.25 (1H, d, J = 7.2 Hz, Ar-H), 7.35 (2H, t, J = 15.6 Hz, Ar-H), 7.51-7.56 (5H, m, Ar-H), 8.25 (2H, d, J = 8.0 Hz, Ar-H), 8.38 (1H, s, Triazole-H).
AD-8	5.18 (2H, s, -CH_2-), 5.80 (2H, s, -OCH_2-), 7.05 (d, 2H, J = 9.2, Hz Ar-H), 7.12 (2H, d, J = 6.4 Hz, Ar-H), 7.16-7.20 (2H, m, Ar-H), 7.51-7.54 (4H, m, Ar-H), 7.57-7.61 (2H, m, Ar-H), 8.24 (2H, d, J = 8.8 Hz, Ar-H), 8.35 (1H, s, Triazole-H).
AD-9	5.18 (2H, s, -CH_2-), 5.80 (2H, s, -OCH_2-), 7.05 (2H, d, J = 8.8 Hz, Ar-H), 7.11 (1H, d, J = 16.8 Hz, styryl -CH=C-), 7.24 (1H, d, J = 16.8 Hz, styryl -C=CH-), 7.41 (2H, d, J = 8.8 Hz, Ar-H), 7.51-7.55 (4H, m, Ar-H), 7.58 (2H, d, J = 8.4 Hz, Ar-H), 8.24 (2H, d, J = 8.8 Hz, Ar-H), 8.35 (1H, s, Triazole-H).

AD-10	2.29 (3H, s, -CH_3), 5.17 (2H, s, -CH_2-), 5.80 (2H, s, -OCH_2-), 7.04 (2H, d, J = 8.8 Hz, Ar-H), 7.06 (1H, s, J = 16 Hz, styryl -CH=C-), 7.10 (1H, s, J = 16 Hz, styryl -C=CH-), 7.17 (2H, d, J = 8.0 Hz, Ar-H), 7.45 (2H, d, J = 8.0 Hz, Ar-H), 7.50-7.54 (4H, dd, Ar-H), 8.24 (2H, d, J = 8.8 Hz, Ar-H), 8.35 (1H, s, Triazole-H).
AD-11	3.76 (3H, s, -OCH_3), 5.17 (2H, s, -CH_2-), 5.79 (2H, s, -OCH_2-), 6.93 (2H, d, J = 8 Hz, Ar-H), 7.00-7.03 (4H, m, Ar-H), 7.49 (4H, d, J =. 8.4 Hz, Ar-H), 7.53 (2H, d, J = 9 Hz, Ar-H), 8.24 (2H, d, J = 8.8 Hz, Ar-H), 8.34 (1H, s, Triazole-H).
AD-12	5.20 (2H, s, -CH_2-), 5.80 (2H, s, -OCH_2-), 7.09 (2H, d, J = 8.8 Hz, Ar-H), 7.29 (1H, d, J = 16.4 Hz, styryl -CH=C-), 7.50 (1H, d, J = 16.4 Hz, styryl -C=CH-), 7.54 (2H, d, J = 8.4 Hz, Ar-H), 7.63 (2H, d, J = 8.8 Hz, Ar-H), 7.82 (2H, d, J = 8.8 Hz, Ar-H),), 8.22 (2H, d, J = 9.2 Hz, Ar-H), 8.25 (2H, d, J = 8.8 Hz, Ar-H), 8.36 (1H, s, Triazole-H).
AD-13	2.27 (3H, s, -CH_3), 5.14 (2H, s, -CH_2-), 5.54 (2H, s, -OCH_2-), 7.04 (2H, d, J = 8.8 Hz, Ar-H), 7.07 (1H, d, J = 16.4 Hz, styryl -CH=C-), 7.16-7.25 (6H, m, Ar-H), 7.35 (2H, t, J = 16.0 Hz, Ar-H), 7.55 (4H, t, J = 16.8 Hz, Ar-H), 8.23 (1H, s, Triazole-H).
AD-14	2.27 (3H, s, -CH_3), 5.14 (2H, s, -CH_2-), 5.54 (2H, s, -OCH_2-), 7.04 (2H, d, J = 8.8 Hz, Ar-H), 7.12 (2H, d, J = 6.8 Hz, Ar-H), 7.16-7.22 (6H, m, Ar-H), 7.52 (2H, d, J = 8.4 Hz, Ar-H), 7.57-7.61 (2H, m, Ar-H), 8.23 (1H, s, Triazole-H).
AD-15	2.27 (3H, s, -CH_3), 5.14 (2H, s, -CH_2-), 5.54 (2H, s, -OCH_2-), 7.04 (2H, d, J = 8.8 Hz, Ar-H), 7.11 (1H, d, J = 16.4 Hz, styryl -CH=C-), 7.16-7.23 (5H, m, Ar-H), 7.40 (2H, d, J = 8.8 Hz, Ar-H), 7.54 (2H, d, J = 8.8 Hz, Ar-H), 7.59 (2H, d, J = 8.8 Hz, Ar-H), 8.23 (1H, s, Triazole-H).
AD-16	2.27 (3H, s, -CH_3), 2.29 (3H, s, -CH_3-), 5.13 (2H, s, -CH_2-), 5.40 (2H, s,-OCH_2-), 7.02 (2H, d, J = 8.8 Hz, Ar-H), 7.06 (1H, s, J = 16.8 Hz, styryl -CH=C-), 7.10 (1H, s, J = 16.8 Hz, styryl -C=CH-), 7.15-7.22 (6H, m, Ar-H), 7.45 (2H, d, J = 8.0 Hz, Ar-H), 7.51 (2H, d, J = 8.8 Hz, Ar-H), 8.23 (1H, s, Triazole-H).
AD-17	2.27 (3H, s, -CH_3), 3.76 (3H, s, 3H, -OCH_3), 5.13 (2H, s, -CH_2-), 5.54 (2H, s, -OCH_2-), 6.93 (2H, d, J = 8.8 Hz, Ar-H), 6.99-7.02 (4H, m, Ar-H), 7.16-7.22 (4H, m, Ar-H), 7.47-7.50 (4H, m, Ar-H), 8.23 (1H, s, Triazole-H).
AD-18	2.27 (3H, s, -CH_3), 5.17 (2H, s, -CH_2-), 5.54 (2H, s, -OCH_2-), 7.08 (2H, d, J = 8.4 Hz, Ar-H), 7.18 (2H, d, J = 8 Hz, Ar-H), 7.22 (2H, d, J = 8 Hz, Ar-H), 7.29 (1H, d, J = 16.4 Hz, styryl -CH=C-), 7.50 (1H, d, J = 16.4 styryl -C=CH-), 7.63 (2H, d, J = 8.8 Hz, Ar-H), 7.82 (2H, d, J = 9.2 Hz, Ar-H), 8.22 (2H, d, J = 8.8 Hz, Ar-H), 8.24 (1H, s, Triazole-H).
AD-19	5.15 (2H, s, -CH_2-), 5.61 (2H, s, -OCH_2-), 7.04 (2H, d, J = 8.8 Hz, Ar-H), 7.11 (1H, d, J = 16.4 Hz, styryl -CH=C-), 7.21 (1H, d, J = 16.4 Hz, styryl -C=CH-), 7.25 (1H, d, J = 7.2 Hz, Ar-H), 7.32-7.37 (4H, m, Ar-H), 7.45 (2H, d, J = 8.4 Hz, Ar-H), 7.56 (4H, t, J = 15.2 Hz, Ar-H), 8.28 (1H, s, Triazole-H).
AD-20	5.15 (3H, s, -CH_2), 5.61 (2H, s, -OCH_2-), 7.04 (2H, d, J = 8.8 Hz, Ar-H), 7.12 (2H, d, J = 6.4 Hz, Ar-H), 7.16-7.20 (2H, m, Ar-H), 7.34 (2H, d, J = 10.8 Hz , Ar-H), 7.45 (2H, d, J = 8.4 Hz, Ar-H), 7.53 (2H, d, J = 11.6 Hz, Ar-H), 7.58-7.61 (2H, m, Ar-H), 8.28 (1H, s, Triazole-H).

AD-21	5.15 (2H, s, -CH_2-), 5.61 (2H, s, -OCH_2-), 7.05 (2H, d, J = 8.8 Hz, Ar-H), 7.11 (1H, d, J = 16.8 Hz, styryl -CH=C-), 7.24 (1H, d, J = 16.8 Hz, styryl -C=CH-), 7.34 (2H, d, J = 8.4 Hz, Ar-H), 7.38-7.46 (4H, dd, J = 8.8, 8.8 Hz, Ar-H), 7.52-7.59 (4H, dd, J = 8.4, 8.8 Hz, Ar-H), 8.20 (1H, s, Triazole-H).
AD-22	2.29 (3H, s, -CH_3), 5.15 (2H, s, -CH_2-), 5.61 (2H, s, -OCH_2-), 7.02 (2H, d, J = 8.8 Hz, Ar-H), 7.06 (1H, d, J = 16 Hz, styryl -CH=C-), 7.10 (1H, d, J = 16 Hz, styryl -C=CH-), 7.17 (2H, d, J = 7.6 Hz, Ar-H), 7.36 (2H, d, J = 8.4 Hz, Ar-H), 7.45 (4H, d, J = 8.4 Hz, Ar-H), 7.51 (2H, d, J = 8.8 Hz, Ar-H), 8.27 (1H, s, Triazole-H).
AD-23	3.76 (3H, s, -OCH_3), 5.14 (2H, s, -CH_2-), 5.61 (2H, s, -OCH_2-), 6.93 (2H, d, J = 8.8 Hz, Ar-H), 7.00-7.03 (4H, m, Ar-H), 7.34 (2H, d, J = 8.4 Hz, Ar-H), 7.45 (2H, d, J = 8.4 Hz, Ar-H), 7.50 (4H, d, J = 8.8 Hz, Ar-H), 8.28 (1H, s, Triazole-H).
AD-24	5.18 (2H, s, -CH_2-), 5.62 (2H, s, -OCH_2-), 7.09 (2H, d, J = 8.8 Hz, Ar-H), 7.29 (1H, d, J = 16.4 Hz, styryl -CH=C-), 7.35 (2H, d, J = 8.4 Hz, Ar-H), 7.45 (2H, d, J = 8.4 Hz, Ar-H), 7.50 (1H, d, J = 16.4 Hz, styryl -C=CH-), 7.63 (2H, d, J = 8.8 Hz, Ar-H), 7.83 (2H, d, J = 8.8 Hz, Ar-H), 8.22 (2H, d, J = 8.8 Hz, Ar-H), 8.29 (1H, s, Triazole-H).

Table 4.15: ^{13}C-NMR data of 1-benzyl-4-((4-styrylphenoxy)methyl)-1*H*-1,2,3-triazoles. (AD 1-24).

Code	Chemical shift values (δ ppm)
AD-1	52.82, 61.12, 114.97, 124.66, 126.16, 126.30, 127.06, 127.19, 127.75, 127.93, 128.13, 128.63, 128.74, 157.72
AD-2	52.84, 61.11, 114.97, 115.43, 115.60, 124.72, 125.15, 127.73, 127.91, 127.96, 128.01, 128.17, 128.78, 129.95, 133.97, 136.02, 142.94, 157.73, 160.43, 162.37.
AD-3	53.37, 61.66, 115.53, 125.25, 125.51, 128.35, 128.44, 128.49, 128.70, 129.17, 129.31, 129.42, 130.30, 131.94, 136.55, 136.90, 139.73, 143.44, 158.43.
AD-4	20.78, 52.81, 61.10, 124.65, 126.08, 126.23, 126.39, 127.57, 127.92, 128.12, 128.73, 129.23, 130.13, 134.53, 135.98, 136.50, 143.05, 157.59, 178.69
AD-5	52.82, 55.11, 61.11, 114.11, 114.93, 124.65, 125.69, 125.95, 127.37, 127.42, 127.93, 128.13, 128.74, 129.97, 130.36, 135.99, 142.96, 157.38, 158.65.
AD-6	53.40, 61.70, 115.65, 124.61, 124.75, 125.32, 127.47, 128.52, 128.73, 129.18, 129.33, 129.81, 133.52, 136.56, 143.37, 145.04, 146.37, 159.13
AD-7	51.92, 61.10, 114.99, 123.95, 125.16, 126.19, 126.34, 127.23, 127.79, 127.95, 128.67, 129.05, 130.05, 137.33, 143.12, 143.42, 147.25, 157.69
AD-8	51.92, 61.11, 115.00, 115.19, 115.39, 115.56, 123.90, 125.10, 125.17, 127.71, 127.87, 127.92, 127.99, 129.01, 129.98, 131.75, 133.91, 143.12, 143.36, 147.24, 157.67, 160.41, 162.35
AD-9	51.94, 61.11, 115.04, 123.96, 125.01, 125.18, 127.83, 127.94, 128.65, 128.87, 129.06, 129.82, 131.44, 136.37, 143.11, 143.42
AD-10	20.80, 51.91, 61.08, 114.97, 123.92, 125.13, 126.27, 126.92, 127.61, 129.03, 129.25, 130.19, 134.53, 136.53, 143.13, 143.39, 147.24, 157.52
AD-11	51.91, 55.11, 61.08, 114.11, 114.96, 123.92, 125.11, 125.07, 126.02, 127.43, 129.03, 129.96, 130.41, 143.15, 143.39, 147.24, 157.34, 158.65.

AD-12	51.93, 61.14, 115.13, 123.92, 124.03, 124.23, 125.16, 126.90, 128.62, 129.04, 129.29, 132.93, 143.00, 143.37, 144.46, 145.82, 158.52
AD-13	20.67, 52.63, 61.11, 114.96, 124.54, 126.16, 126.29, 127.20, 127.76, 127.99, 128.65, 129.28, 129.98, 132.99, 137.33, 137.49, 142.88, 157.72
AD-14	20.63, 52.60, 61.10, 114.95, 115.34, 115.55, 124.47, 125.11, 127.67, 127.88, 127.95, 129.24, 129.91, 132.95, 133.93, 137.45, 142.85, 157.68
AD-15	20.67, 52.62, 61.09, 114.95, 115.41, 115.58, 124.54, 125.13, 127.70, 127.93, 127.99, 129.28, 129.92, 132.99, 133.93, 137.50, 142.87, 157.70, 160.41, 162.32.
AD-16	20.65, 20.78, 52.61, 61.1.0, 113.70, 114.94, 124.49, 126.08, 126.22, 126.93, 127.57, 127.97, 129.22, 129.26, 130.25, 133.01, 134.50, 136.49, 137.59, 142.89, 157.55.
AD-17	20.66, 52.62, 55.11, 61.10, 114.11, 114.93, 124.49, 125.69, 125.98, 127.37, 127.41, 127.97, 129.27, 129.97, 130.35, 132.99, 137.48, 142.92, 157.37, 158.64.
AD-18	20.67, 52.64, 61.13, 115.09, 124.03, 124.18, 124.58, 126.89, 127.99, 128.61, 129.29, 132.96, 137.51, 142.76, 144.47, 145.81, 158.56.
AD-19	51.01, 61.11, 114.97, 115.19, 124.73, 126.16, 126.31, 127.19, 127.76, 127.95, 128.63, 128.75, 129.89, 130.01, 131.75, 132.87, 134.98, 137.32, 142.99, 157.70, 191.38.
AD-20	52.0, 61.10, 114.97, 115.40, 115.57, 124.73, 125.15, 127.70, 127.88, 127.92, 127.99, 128.75, 129.89, 129.95, 132.86, 133.92, 134.98, 142.98, 157.69, 160.41, 162.34.
AD-21	52.01, 61.11, 124.74, 124.97, 127.78, 127.88, 128.61, 128.75, 128.86, 129.77, 129.89, 131.39, 132.86, 134.98, 136.34, 142.95, 157.86.
AD-22	20.78, 51.99, 61.10, 114.95, 124.71, 126.09, 126.25, 126.93, 127.85, 128.74, 129.23, 129.88, 130.16, 132.85, 134.53, 134.97, 136.51, 143.0, 157.54.
AD-23	51.99, 55.10, 61.10, 114.10, 114.94, 124.68, 125.68, 125.99, 127.36, 128.74, 129.88, 129.96, 130.37, 132.85, 134.97, 143.02, 157.35, 158.64.
AD-24	52.02, 61.14, 115.11, 124.23, 124.83, 126.92, 128.63, 128.79, 129.27, 129.93, 132.96, 134.35, 135.01, 142.88, 144.49, 145.82, 158.56.

Table 4.16: LCMS data of 1-benzyl-4-((4-styrylphenoxy)methyl)-1H-1,2,3-triazoles. (AD: 1-24).

Code	Obs. Mass & Mode of Ionization	Cal. Mass
AD-1	+MS (ESI) m/z: 369.1	368.4
AD-2	+MS (ESI) m/z: 386.1	386.4
AD-3	+MS (ESI) m/z: 402.1	402.9
AD-4	+MS (ESI) m/z: 382.1	382.5
AD-5	+MS (ESI) m/z: 398.1	398.5
AD-6	+MS (ESI) m/z: 413.1	413.4
AD-7	+MS (ESI) m/z: 414.1	413.4
AD-8	+MS (ESI) m/z: 431.1	431.4
AD-9	+MS (ESI) m/z: 448.0	447.9
AD-10	+MS (ESI) m/z: 427.1	427.5
AD-11	+MS (ESI) m/z: 444.1	443.5
AD-12	+MS (ESI) m/z: 458.0	458.4
AD-13	+MS (ESI) m/z: 382.0	382.5
AD-14	+MS (ESI) m/z: 400.1	400.5
AD-15	+MS (ESI) m/z: 416.1	416.9
AD-16	+MS (ESI) m/z: 396.1	396.5
AD-17	+MS (ESI) m/z: 412.1	412.5
AD-18	+MS (ESI) m/z: 427.1	427.5
AD-19	+MS (ESI) m/z: 402.1	402.9
AD-20	+MS (ESI) m/z: 420.0	420.9
AD-21	+MS (ESI) m/z: 437.0	437.3
AD-22	+MS (ESI) m/z: 432.1	416.9
AD-23	+MS (ESI) m/z: 432.1	432.9
AD-24	+MS (ESI) m/z: 447.1	447.9

Table-4.17: FTIR spectral data of 3-(4-((1-benzyl-1*H*-1,2,3-triazol-4yl)methoxy benzylidene)indolin-2-ones (AD 25-48).

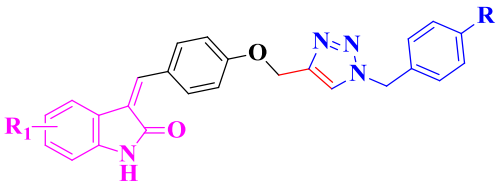

Code	Transmittance peaks (cm^{-1})
AD-26	3204 (-NH), 3050-3033 (-CH, Ar.), 2945-2850 (-CH, Ali.), 1697 (>C=O), 1590 (>C=C<), 1464 (-CH_2), 1185 (-O-).
AD-27	3198 (-NH), 3030 (-CH, Ar.), 2845-2823 (-CH, Ali.), 1698 (>C=O), 1604 (>C=C<), 1476 (-CH2), 1338 (-CH3), 1184 (-O-).
AD-28	3151(-NH), 3050-3040 (-CH, Ar.), 2925-2802 (-CH, Ali.), 1700 (>C=O), 1592 (>C=C<), 1449 (-CH2), 1226 (-O-).
AD-29	3154 (-NH), 3038-3010 (-CH, Ar.), 2941-2789 (-CH, Ali.) 1697 (>C=O), 1591 (>C=C<), 1471 (-CH2), 1186 (-O-).
AD-30	3198 (NH)-, 3066-3049 (-CH, Ar.), 2876-2079 (-CH, Ali.), 1698 (>C=O), 1601 (>C=C<), 1482 (-CH_2), 1201 (-O-).
AD-31	3185 (-NH), 3059 (-CH, Ar.), 2919-2801 (-CH, Ali.), 1695 (>C=O), 1610 (>C=C<), 1514 (-NO2), 1449 (-NO2), 1481 (-CH2), 1174 (-O-).
AD-32	3201 (-NH), 3060-3050 (-CH, Ar.), 2890-2820 (-CH, Ali.), 1701 (>C=O), 1599 (>C=C<), 1560 (-NO_2), 1512 (-NO_2), 1483 (-CH_2), 1192 (-O-).
AD-33	3201 (-NH), 3090-3058 (-CH, Ar.), 2864-2763(-CH, Ali.), 1695 (>C=O), 1616 (C=C<), 1528 (-NO2), 1499 (-NO2), 1472 (-CH2), 1185 (-O-).
AD-34	3210 (-NH), 3066-3055 (-CH, Ar.), 2950-2865 (-CH, Ali.), 1695 (>C=O), 1610 (>C=C<), 1514 (-NO2), 1481 (-NO2), 1432 (-CH2), 1174 (-O-).
AD-35	3157 (-NH), 3078-3050 (-CH, Ar.), 2856-2766 (-CH, Ali.), 1698 (>C=O), 1589 (-NO_2), 1477 (-CH_2), 1190 (-O-).
AD-36	3169 (-NH), 3010 (-CH, Ar.), 2826-2780 (-CH, Ali.), 1672 (>C=O), 1602 (>C=C<), 1594 (-NO_2), 1503 (-NO_2), 1489 (-CH_2), 1376 (-CH_3), 1189 (-O-).
AD-37	3229 (-NH), 3010-3002 (-CH, Ar.), 2811-2790 (-CH, Ali.), 1692 (>C=O), 1594 (>C=<), 1476 (-CH_2), 1386 (-CH_3), 1167 (-O-).
AD-38	3158 (-NH), 3059 (-CH, Ar.), 2890-2805 (-CH, Ali.), 1699 (>C=O), 1590 (>C=C<), 1465 (-CH2), 1381(-CH3), 1187 (-O-).
AD-39	3203 (-NH), 3023-3010 (-CH, Ar.), 2838-2785 (-CH, Ali.), 1692 (>C=O), 1586 (>C=C<), 1448 (-CH_2), 1389 (-CH_3), 1175 (-O-).

AD-40	3201 (-NH), 3023-3002 (-CH, Ar.), 2804-2802 (-CH, Ali.), 1698 (>C=O), 1612 (>C=C<), 1486 (-CH2), 1379 (-CH3), 1198 (-O-).
AD-41	3158 (-NH), 3043 (-CH, Ar.), 2859-2812 (-CH, Ali.), 1698 (>C=O), 1611 (>C=C<), 1462 (-CH2), 1381 (-CH3), 1187 (-O-).
AD-42	3198 (-NH), 3043-3023 (-CH, Ar.), 2821-2765 (-CH, Ali.), 1695 (>C=O), 1602 (>C=C<), 1489 ($-CH_2$), 1378 ($-CH_3$), 1184 (-O-).
AD-44	3201 (-NH), 3051-3012 (-CH, Ar.), 2862-2754 (-CH, Ali.), 1701 (>C=O), 1486 ($-CH_2$), 1201 (-O-).
AD-45	3142 (-NH), 3042-3010 (-CH, Ali.), 2828-2786 (>C=C<), 1700 (>C=O), 1613 (>C=C<), 1476 (-CH2), 1176 (-O-).
AD-46	3201 (-NH), 3015 (-CH, Ar.), 2811-2788 (-CH, Ali.), 1699 (>C=O), 1604 (>C=C<), 1486 (-CH2), 1388 (-CH3), 1201 (-O-).
AD-47	3204 (-NH), 3013-3005 (-CH, Ar.), 2798 (-CH, Ali.), 1695 (>C=O), 1613 (>C=C<), 1486 ($-CH_2$), 1198 (-O-).
AD-48	3141 (-NH), 3030-3010 (-CH, Ar.), 2911-2865 (-CH, Ali.), 1682 (>C=O), 1582 (>C=C<), 1482 ($-CH_2$), 1173 (-O-).

Table 4.18: ^{1}H NMR data of 3-(4-((1-benzyl-1*H*-1,2,3-triazol-4yl)methoxy benzylidene)indolin-2-ones. (AD 25-48)

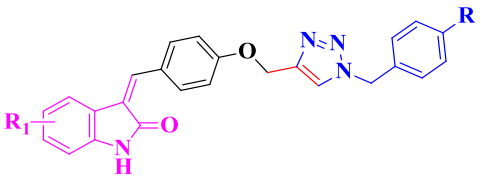

Code	^{1}H-NMR (400/500 MHz, DMSO-d$_6$, δ/ppm)
AD-26	5.24 (s, 2H, -NCH$_2$-), 5.61 (s, 2H, -OCH$_2$-), 6.81 (d, 1H, J=6.4 Hz), 7.15 (d, 2H, J=7.2 Hz), 7.21-7.19 (m, 1H, ar.), 7.34-7.31 (m, 3H, ar.), 7.39-7.36 (m, 2H, ar.), 7.81-7.80 (d, 1H, J=2.0 Hz), 7.88 (s, 1H, benzylidene-H), 8.32 (s, 1H, triazole-H), 8.50 (d, 2H, J=7.2 Hz), 10.71 (s, 1H, -NH).
AD-27	5.24 (s, 2H, -NCH$_2$-), 5.61 (s, 2H, -OCH$_2$-), 6.81 (d, 1H, J=6.8 Hz), 7.01 (d, 1H, J=7.2 Hz), 7.12 (d, 2H, J=7.2 Hz), 7.19 (t, 1H, J=12.8 Hz), 7.34-7.31(m, 3H, ar.), 7.39-7.36 (m, 2H, ar.), 8.32-8.29 (m, 3H, ar.), 8.41 (s, 1H, triazole-H), 10.86 (s, 1H, -NH).
AD-28	5.24 (s, 2H, -NCH$_2$-), 5.61 (s, 2H, -OCH$_2$-), 7.00 (t, 1H, J=15.6 Hz), 7.16 (d, 2H, J=8.8 Hz), 7.25 (d, 1H, J=8.8 Hz), 7.40-7.28 (m, 5H, ar.), 7.67 (d, 1H, J=7.2 Hz), 7.83 (s, 1H, benzylidene-H), 8.31 (s, 1H, triazole-H), 8.49 (d, 2H, J=9.2 Hz), 10.99 (s, 1H, -NH).
AD-29	5.24 (s, 2H, -NCH$_2$-), 5.61 (s, 2H, -OCH$_2$-), 6.84-6.75 (m, 1H, ar.), 7.22-7.13 (m, 2H, ar.), 7.40-7.31 (m, 5H, ar.), 7.70-7.65 (m, 1H, ar.), 7.89 (s, 1H, benzylidene-H), 7.93 (s, 1H, ar.), 8.32 (s, 1H, triazole-H), 8.50 (d, 2H, J=6.8 Hz), 10.72 (s, 1H, -NH).
AD-30	2.29 (s, 3H, -CH$_3$), 5.23 (s, 2H, -NCH$_2$-), 5.61 (s, 2H,-OCH$_2$-), 6.70 (d, 1H, J=7.6 Hz), 6.99 (d, 1H, J=8.4 Hz), 7.13 (d, 2H, J=8.8 Hz), 7.40-7.31 (m, 5H, ar.), 7.49 (s, 1H, ar.), 7.69 (s, 1H, benzylidene-H), 8.37 (s, 1H, triazole-H), 8.47 (d, 2H, J=9.2 Hz), 10.44 (s, 1H,-NH).
AD-31	5.26 (s, 2H, -NCH$_2$-), 5.80 (s, 2H, -OCH$_2$-), 6.81 (d, 1H, J=8.0 Hz), 6.96 (t, 1H, J=16 Hz), 7.23-7.12 (td, 3H, J=15.6 Hz, 8.4 Hz), 7.94-7.52 (sdd, 4H, J=8.8 Hz, 8.8 Hz), 8.23 (d, 2H, J=8.8 Hz), 8.38 (s, 1H, triazole-H), 8.48 (d, 2H, J=8.8 Hz), 10.56 (s, 1H, -NH).
AD-32	5.27 (s, 2H, -NCH$_2$-), 5.80 (s, 2H, -OCH$_2$-), 6.82 (d, 1H, J=8.0 Hz), 7.15 (d, 2H, J=8.8 Hz), 7.21-7.18 (m, 1H, ar.), 7.55 (d, 2H, J=8.8 Hz), 7.80-7.79 (m, 1H, ar.), 7.88 (s, 1H, benzylidene-H),), 8.25 (d, 2H, J=8.8 Hz), 8.39 (s, 1H, triazole-H, 8.50 (d, 2H, J=8.8 Hz), 10.69 (s, 1H, -NH).

AD-33	5.26 (s, 2H, -NCH_2-), 5.81 (s, 2H, -OCH_2-), 6.81 (d, 1H, J=6.8 Hz), 7.01 (d, 1H, J=6.8 Hz), 7.12 (d, 2H, J=7.2 Hz), 7.19 (t, 1H, J=12.8 Hz), 7.54 (d, 2H, J=7.2 Hz), 8.25-8.21 (m, 2H, ar.), 8.32 (d, 2H, J=6.8 Hz), 8.41 (d, 2H, J=6.0 Hz), 10.86 (s, 1H, -NH).
AD-34	5.27 (s, 2H, -NCH_2-), 5.81 (s, 2H, -OCH_2-), 6.99 (t, 1H, J=15.6 Hz), 7.17 (d, 2H, J=8.8 Hz), 7.23 (d, 1H, J=8.8 Hz), 7.55-7.52 (d, 2H, J=8.8 Hz), 7.67 (d, 1H, J=7.6 Hz), 7.84 (s, 1H, benzylidene-H), 8.25-8.22 (d, 2H, J=8.8 Hz), 8.39 (s, 1H, triazole-H), 8.50 (d, 2H, J=9.2 Hz), 11.00 (s, 1H, -NH).
AD-35	5.27 (s, 2H, -NCH_2-), 5.80 (s, 2H, -OCH_2-), 6.77 (d, 1H, J=8.4 Hz), 7.16 (d, 2H, J=9.2 Hz), 7.34-7.31 (m, 1H, ar.), 7.54 (d, 2H, J=8.8 Hz), 7.92 (m, 2H, ar.), 8.25 (d ,2H, J=8.8 Hz), 8.39 (s, 1H, triazole-H), 8.50 (d, 2H, J=9.2 Hz), 10.70 (s, 1H, -NH).
AD-36	2.17 (s, 3H, -CH_3), 5.29 (s, 2H, -NCH_2-), 5.81 (s, 2H,-OCH_2-), 6.76 (d, 1H, J=8.0 Hz), 7.03 (d, 1H, J=7.2 Hz), 7.20 (d, 2H, J=8.8 Hz), 7.44 (s, 1H, ar.), 7.55-7.52 (m, 3H, ar.), 7.71 (d, 2H, J=8.8 Hz), 8.24 (d, 2H, J=8.8 Hz), 8.39 (s, 1H, triazole-H), 10.41 (s, 1H, -NH).
AD-37	2.67 (s, 3H, -CH_3), 5.22 (s, 2H -NCH_2-), 5.55 (s, 2H, -OCH_2-), 6.81 (d, 1H, J=6.0 Hz), 6.97 (t, 1H, J=13.2 Hz), 7.13 (d, 2H, J=7.2 Hz), 7.22 (m, 2H, ar.), 7.18 (m, 3H, ar.), 7.67 (d, 1H, J=6.0 Hz), 7.74 (s, 1H, benzylidene-H), 8.28 (s, 1H, triazole-H), 8.47 (d, 2H, J=7.2 Hz), 10.58 (s, 1H,-NH).
AD-38	2.26 (s, 3H, -CH_3), 5.23 (s, 2H, -NCH_2-), 5.55 (s, 2H, -OCH_2-), 6.77 (d, 1H, J=8.4 Hz), 7.23-7.12 (m, 7H, ar.), 7.88-7.80 (m, 2H, ar.), 8.27 (s, 1H, triazole-H), 8.49 (d, 2H, J=8.8 Hz), 10.69 (s, 1H,-NH).
AD-39	2.27 (s, 3H, -CH_3), 5.22 (s, 2H, -NCH_2-), 5.55 (s, 2H, -OCH_2-), 6.81 (d, 1H, J=7.2 Hz), 7.01 (d, 1H, J=7.2 Hz), 7.11 (d, 2H, J=7.2 Hz), 7.19-7.16 (m, 3H, ar.), 7.22-7.20 (m, 2H, ar.), 8.27 (s, 1H, triazole-H), 8.32 (d, 2H, J=7.2 Hz), 8.40 (s, 1H, ar.), 10.86 (s, 1H, -NH).
AD-40	2.27 (s, 3H, -CH_3), 5.23 (s, 2H, -NCH_2-), 5.50 (s, 2H, -OCH_2-), 6.99 (t, 1H, J=15.6 Hz), 7.25-7.13 (m, 7H, ar.), 7.67 (d, 1H, J=7.2 Hz), 7.84 (s, 1H, benzylidene-H), 8.27 (s, 1H, triazole-H), 8.49 (d, 2H, J=8.8 Hz), 11.00 (s, 1H, -NH).
AD-41	2.27 (s, 3H, -CH_3), 5.23 (s, 2H, -NCH_2-), 5.55 (s, 2H, -OCH_2-), 6.77 (d, 1H, J=8.0 Hz), 7.23-7.12 (m, 6H, ar.), 7.34-7.31 (dd, 1H, J=8.4, ind6), 7.88 (s, 1H, benzylidene-H), 7.92 (d, 1H, J=2.0, ind4), 8.27 (s, 1H, triazole H), 8.50 (d, 2H, J=9.2 Hz), 10.70 (s, 1H,-NH).
AD-42	2.18 (s, 3H, -CH_3), 2.27 (s, 3H, -CH_3), 5.22 (s, 2H, -NCH_2-), 5.55 (s, 2H, -OCH_2-), 6.76 (d, 1H, J=8.0 Hz), 7.04 (d, 1H, J=8.0 Hz), 7.23-7.16 (m, 6H, ar.), 7.45 (s, 1H, ar), 7.53 (s, 1H, benzylidene-H), 7.70 (d, 2H, J=8.8 Hz), 8.27 (s, 1H, triazole-H), 10.41 (s, 1H, -NH)

AD-44	5.26 (s, 2H, -NCH_2-), 5.63 (s, 2H, -OCH_2-), 6.82 (d, 1H, J=8.8 Hz), 7.18 (d, 2H, J=8.8 Hz), 7.26-7.22 (m, 1H, ar.), 7.38 (d, 2H, J=8.2 Hz), 7.43 (d, 2H, J=8.2 Hz), 7.82 (m, 1H, ar.), 7.92 (s, 1H, benzylidene-H), 8.32 (s, 1H, triazole-H), 8.55 (d, 2H, J=8.8), 10.77 (s, 1H, -NH).
AD-45	5.23 (s, 2H, -NCH_2-), 5.62 (s, 2H, -OCH_2-), 6.82 (d, 1H, J=8.0 Hz), 7.14 (d, 2H, J=8.0 Hz), 7.35 (d, 2H, J=8.0 Hz), 7.45 (d, 2H, J=8.0 Hz), 7.70 (d, 2H, J=8.0 Hz), 7.80 (s, 1H, benzylidene-H), 8.33 (s, 1H, triazole-H), 8.47 (d, 2H, J=8.0), 10.75 (s, 1H, -NH).
AD-46	5.24 (s, 2H, -NCH_2-), 5.62 (s, 2H, -OCH_2-), 7.00 (t, 1H, J=16.0 Hz), 7.16 (d, 2H, J=8.0 Hz), 7.23 (m, 1H, ar), 7.35 (d, 2H, J=8.0 Hz), 7.45 (d, 2H, J=8.0 Hz), 7.68 (s, 1H, ar.), 7.85 (s, 1H, benzylidene-H), 8.33 (s, 1H, triazole-H), 8.50 (d, 2H, J=8.0 Hz), 10.04 (s, 1H, -NH).
AD-47	5.24 (s, 2H, -NCH_2-),5.62 (s, 2H, -OCH_2-), 6.77 (d, 1H, J=8.0 Hz), 7.15 (d, 2H, J=8.0 Hz), 7.35-7.31 (m, 3 H, ar.), 7.45 (d, 2H, J=8.0 Hz), 7.89 (s, 1H, ar.), 7.93 (s, 1H, benzylidene-H), 8.33 (s, 1H, triazole-H), 8.50 (d, 2H, J=8.8 Hz), 10.73 (s, 1H, -NH).
AD-48	2.29 (s, 3H, -CH_3), 5.22 (s, 2H, -NCH_2-), 5.62 (s, 2H, -OCH_2-), 6.68 (d, 1H, J=8.0 Hz), 6.97 (d, 1H, J=8.2 Hz), 7.11 (d, 2H, J=8.2 Hz), 7.35 (d, 2H, J=8.0 Hz), 7.45 (d, 2H, J=8.0 Hz), 7.70 (s, 1H, benzylidene-H), 7.49 (s, 1H, ar.), 8.34 (s, 1H, triazole-H), 8.46 (d, 2H, J=8.0), 10.48 (s, 1H,-NH).

Table 4.19: ^{13}C-NMR data of 3-(4-((1-benzyl-1*H*-1,2,3-triazol-4yl)methoxy benzylidene)indolin-2-one, (AD 25-48).

Code	^{13}C-NMR (100 MHz, DMSO-d$_6$, δ/ppm)
AD-26	52.82, 61.20, 110.49, 114.53, 119.28, 123.03, 124.82, 125.24, 127.06, 127.27, 127.55, 127.92, 128.12, 128.73, 134.70, 135.93, 138.68, 138.84, 142.54, 160.27, 167.09.
AD-27	52.82, 61.20, 110.48, 114.52, 119.28, 123.03, 124.82, 125.24, 127.06, 127.26, 127.54, 127.92, 128.12, 128.72, 134.70, 135.93, 138.68, 138.84, 142.54, 160.27, 167.09.
AD-28	52.82, 52.84, 61.22, 113.54, 114.55, 117.85, 122.06, 123.49, 124.84, 126.99, 127.19, 127.71, 127.94, 128.14, 128.75, 134.69, 135.49, 137.49, 138.75, 142.56, 160.31, 167.22. 167.22.
AD-30	52.84, 61.22, 108.91, 109.73, 114.42, 114.92, 119.74, 122.59, 124.80, 125.90, 126.95, 127.93, 128.14, 128.74, 129.61, 130.12, 131.41, 134.28, 135.57, 135.95, 136.31, 140.40, 142.66, 159.22, 167.45.
AD-31	51.92, 61.15, 109.15, 114.44, 119.23, 120.85, 123.88, 124.33, 125.23, 125.27, 127.28, 128.23, 129.01, 134.31, 136.61, 140.25, 142.81, 143.31, 147.23, 159.81, 167.32.
AD-32	51.95, 61.20, 110.52, 114.59, 119.31, 123.11, 123.90, 125.28, 127.13, 127.28, 127.59, 129.04, 134.72, 138.66, 138.87, 143.32, 147.25, 142.76, 160.24, 167.12.
AD-33	51.92, 61.13, 109.92, 114.53, 115.09, 120.03, 120.73, 123.24, 123.88, 125.24, 126.70, 129.00, 131.60, 134.51, 136.74, 143.31, 159.41, 167.19.
AD-34	51.94, 61.20, 113.55, 114.58, 117.86, 122.06, 123.53, 125.285, 127.03, 127.19, 127.72, 129.04, 134.69, 137.50, 138.71, 142.75, 143.32, 147.25, 160.26, 167.22.
AD-35	51.93, 61.19, 111.02, 112.94, 114.57, 122.03, 122.94, 123.89, 125.27, 127.13, 127.70, 129.03, 130.37, 134.72, 138.68, 139.22, 142.75, 160.23, 166.98.

AD-36	20.79, 51.92, 61.21, 109.71, 114.94, 121.16, 122.56, 123.88, 125.21, 125.93, 127.00, 129.56, 130.11, 131.39, 134.27, 135.51, 140.40, 142.84, 143.31, 147.22, 159.16, 168.90.
AD-37	20.64, 52.64, 61.81, 109.16, 114.44, 119.24, 120.87, 124.18, 124.65, 125.29, 127.25, 127.98, 128.24, 129.27, 132.94, 134.32, 136.67, 137.49, 140.24, 142.58, 159.87, 167.33.
AD-38	20.63, 52.63, 61.20, 110.48, 114.53, 119.27, 123.03, 124.66, 125.24, 127.06, 127.27, 127.54, 127.96, 129.23, 131.52, 132.92, 134.70, 137.47, 138.68, 138.84, 142.50, 160.27, 167.09.
AD-39	20.64, 52.64, 61.20, 109.12, 114.51, 120.64, 120.67, 122.98, 124.29, 124.66, 127.08, 127.98, 129.26, 132.24, 132.93, 134.52, 137.49, 137.82, 141.31, 142.53, 160.13, 167.20.
AD-40	20.64, 52.65, 61.22, 113.54, 114.55, 117.84, 122.05, 123.48, 124.68, 126.99, 127.19, 127.70, 127.98, 129.26, 132.93, 134.69, 137.49, 138.74, 142.52, 160.30, 167.22.
AD-41	20.63, 52.63, 61.20, 111.00, 112.93, 114.53, 122.01, 122.88, 124.66, 127.07, 127.70, 127.97, 129.25, 130.34, 132.92, 134.71, 137.47, 138.71, 139.20, 142.50, 160.28, 166.96.
AD-42	20.78, 52.82, 61.16, 108.90, 114.41, 119.73, 124.38, 124.79, 125.34, 127.31, 127.92, 128.12, 128.66, 128.73, 129.60, 134.27, 135.94, 136.30, 138.02, 142.62, 159.79, 167.44.
AD-44	52.00, 61.19, 110.49, 114.54, 119.28, 123.05, 124.87, 125.24, 127.08, 127.26, 127.55, 128.73, 129.87, 134.70, 134.92, 138.67, 138.84, 142.60, 160.24, 167.09.
AD-45	52.03, 61.24, 109.94, 115.07, 120.05, 120.77, 123.26, 124.59, 124.87, 126.68, 128.74, 129.89, 131.58, 132.88, 133.61, 134.93, 136.79, 142.67, 143.97, 159.45, 168.80.
AD-46	52.03, 61.21, 113.54, 114.54, 115.04, 117.83, 122.03, 123.50, 124.88, 127.00, 127.18, 127.69, 128.73, 129.88, 131.68, 132.88, 134.68, 134.91, 137.49, 138.70, 1421.60, 160.27, 167.21.
AD-47	52.04, 61.21, 111.04, 112.96, 114.57, 122.03, 122.92, 124.90, 127.11, 127.71, 128.76, 129.90, 130.38, 132.88, 134.74, 134.93, 138.72, 139.22, 142.63, 160.27, 166.99.

AD-48	20.78, 52.01, 61.15, 108.90, 114.42, 119.73, 124.40, 124.85, 125.33, 126.97, 127.33, 128.73, 129.88, 131.40, 134.27, 134.92, 136.28, 138.03, 142.69, 159.77, 167.44.

Table 4.20: Elemental (C, H, N) analytical data of 3-(4-((1-benzyl-1*H*-1,2,3-triazol-4yl) methoxy benzylidene)indolin-2-one. (AD 25-48)

Elements (%)	Mol. Formula	C		H		N	
		Obs.	Calc.	Obs.	Calc.	Obs.	Calc.
AD-26	$C_{25}H_{19}ClN_4O_2$	67.80	67.67	4.32	4.25	12.6	12.69
AD-27	$C_{25}H_{19}ClN_4O_2$	67.80	4.32	4.32	4.29	12.6	12.69
AD-28	$C_{25}H_{19}ClN_4O_2$	67.80	67.71	4.32	4.35	12.6	12.66
AD-29	$C_{25}H_{19}BrN_4O_2$	61.61	61.53	3.93	3.95	11.5	11.53
AD-30	$C_{25}H_{22}N_4O_2$	73.92	73.81	5.25	5.21	13.2	13.23
AD-31	$C_{25}H_{19}N_5O_4$	66.22	66.15	4.22	4.16	15.4	15.49
AD-32	$C_{25}H_{18}ClN_5O_4$	61.54	61.45	3.72	3.67	14.3	14.39
AD-33	$C_{25}H_{18}ClN_5O_4$	61.54	61.49	3.72	3.65	14.3	14.41
AD-34	$C_{25}H_{18}ClN_5O_4$	61.54	61.42	3.72	3.61	14.3	14.41
AD-35	$C_{25}H_{18}BrN_5O_4$:	56.41	56.37	3.41	3.35	13.1	13.20
AD-36	$C_{26}H_{21}N_5O_4$	66.80	66.59	4.53	4.48	14.9	15.01
AD-37	$C_{25}H_{22}N_4O_2$	73.92	73.81	5.25	5.21	13.2	13.32
AD-38	$C_{26}H_{21}ClN_4O_2$	68.34	68.27	4.63	4.53	12.2	12.23
AD-39	$C_{26}H_{21}ClN_4O_2$	68.34	68.25	4.63	4.57	12.2	12.31
AD-40	$C_{26}H_{21}ClN_4O_2$	68.34	68.24	4.63	4.57	12.2	12.32
AD-41	$C_{26}H_{21}BrN_4O_2$	62.28	62.16	4.22	4.17	11.1	11.21
AD-42	$C_{27}H_{24}N_4O_2$	74.29	74.15	5.54	5.47	12.8	12.91
AD-44	$C_{25}H_{18}Cl_2N_4O_2$	62.91	63.01	3.80	3.71	11.7	11.79
AD-45	$C_{25}H_{18}Cl_2N_4O_2$	62.91	62.83	3.80	3.69	11.7	11.83
AD-46	$C_{25}H_{18}Cl_2N_4O_2$	62.91	62.83	3.80	3.74	11.7	11.81
AD-47	$C_{25}H_{18}BrClN_4O_2$	57.55	57.48	3.48	3.45	10.7	10.82
AD-48	$C_{26}H_{21}ClN_4O_2$	68.34	68.25	4.63	4.55	12.2	12.36

4.2 Biology:

1-Benzyl-4-((4-styrylphenoxy)methyl)-1*H*-1,2,3-triazoles (AD: 1-24)

***In-vitro* cellular cytotoxicity**

In vitro cytotoxicity evaluations of **AD 1-24** were performed using six different human cancer cell lines (DND-41, NCI-H460, Z-138, Capan-1, HCT-116, and K-562) and summarized as 50% inhibitory concentrations (IC_{50}) in **Table-4.21.**

Table 4.21: *In-vitro* cytotoxicity data of 1-benzyl-4-((4-styrylphenoxy) methyl)-1*H*-1,2,3-triazoles

(AD: 1-24).

Compound	Capan-1	HCT-116	NCI-H460	DND-41	K-562	Z-138
	Pancreatic adeno-carcinoma	Colorectal carcinoma	Lung carcinoma	Acute lymphoblastic leukemia	Chronic myeloid leukemia	Non-Hodgkin lymphoma
AD-1	46.7	29.1	34.3	61.4	39.9	>100
AD-2	30.7	46.7	31.7	>100	>100	>100
AD-3	96.4	36.1	>100	>100	19.3	>100
AD-4	>100	>100	81.7	>100	>100	60.3
AD-5	55.3	13.5	35.1	>100	>100	>100
AD-6	45.3	62.4	40.7	>100	>100	>100
AD-7	>100	26.1	78.5	82.1	>100	>100
AD-8	40.2	12.2	11.6	>100	>100	>100
AD-9	62.3	21.3	31.3	>100	>100	>100
AD-10	62.3	>100	98.3	>100	>100	>100
AD-11	50.2	12.6	95.4	>100	>100	>100

AD-12	70.3	76.7	44.3	>100	>100	>100
AD-13	45.9	>100	41.7	>100	>100	>100
AD-14	73.4	>100	>100	>100	>100	>100
AD-15	51.8	>100	47.3	81.2	>100	>100
AD-16	52.4	87.4	60.8	>100	>100	>100
AD-17	34.6	30.5	37.1	>100	>100	>100
AD-18	39.5	21.3	16.2	>100	>100	>100
AD-19	80.6	33	61.1	>100	>100	>100
AD-20	67.3	71.5	91.9	>100	>100	>100
AD-21	41.3	36.5	33.8	>100	>100	>100
AD-22	>100	57.3	>100	>100	>100	>100
AD-23	48.9	36	12.4	>100	>100	>100
AD-24	>100	55.8	72.5	>100	>100	>100
Docetaxel	0.0063	0.0008	0.0001	0.0019	0.0034	0.0019
STS*	0.0046	0.0003	0.0032	0.0064	0.0298	0.0003

*** STS: Staurosporine**

***In-silico* analyses:**[77-81]

The physicochemical properties and drug-likeness violation by **AD 1-24** was summarized in **Table-4.22. Figures 4-7** explain the receptor (1TUB) interactions and the forces involved in it.

Table 4.22: Physicochemical and pharmacokinetic properties (*in-silico*) of 1-benzyl-4-((4-s tyrylphenoxy)methyl)-1*H*-1,2,3-triazoles. (AD 1-24)

		Physicochemical Properties							Lipophilicity						Drug-likeness					Water Solubility		Pharmacokinetics	
Comp.	Binding Affinity	MW (g/mol)	Fsp^3	RB	HBA	HBD	MR	tPSA	ilogP	XlogP3	WlogP	MlogP	SILICOS-IT	Consensus logP	Lipinski	Ghose	Veber	Egan	Muegge	ESOL	Class	Log K_p (cm/s)	F
AD-1	-10.3	367.44	0.08	7	3	0	112.12	39.94	3.83	5.05	4.71	4.01	4.86	4.49	0	0	0	0	1	-5.45	Moderately	-4.96	0.55
AD-2	-9.9	385.43	0.08	7	4	0	112.08	39.94	3.84	5.15	5.27	4.38	5.27	4.78	1	0	0	0	1	-5.60	Moderately	-4.99	0.55
AD-3	-10.6	401.89	0.08	7	3	0	117.13	39.94	4.18	5.68	5.36	4.49	5.49	5.04	1	0	0	0	1	-6.04	Poorly	-4.72	0.55
AD-4	-10.4	381.47	0.12	7	3	0	117.09	39.94	4.03	5.42	5.01	4.22	5.38	4.81	1	0	0	0	1	-5.74	Moderately	-4.78	0.55
AD-5	-10.3	397.47	0.12	8	4	0	118.61	49.17	4.23	5.03	4.71	3.66	4.91	4.51	0	0	0	0	1	-5.51	Moderately	-5.15	0.55
AD-6	-10.1	412.44	0.08	8	5	0	120.94	85.76	3.50	4.88	4.61	3.86	2.68	3.91	0	0	0	0	0	-5.49	Moderately	-5.35	0.55
AD-7	-9.7	412.44	0.08	8	5	0	120.94	85.76	3.53	4.88	4.61	3.86	2.68	3.91	0	0	0	0	0	-5.49	Moderately	-5.35	0.55
AD-8	-11.2	430.43	0.08	8	6	0	120.90	85.76	3.55	4.98	5.17	4.24	3.10	4.21	1	0	0	0	0	-5.65	Moderately	-5.39	0.55
AD-9	-10.2	446.89	0.08	8	5	0	125.95	85.76	3.74	5.51	5.27	4.34	3.32	4.44	1	0	0	0	1	-6.09	Poorly	-5.11	0.55
AD-10	-10.5	426.47	0.12	8	5	0	125.91	85.76	3.84	5.25	4.92	3.26	3.21	4.10	0	0	0	0	1	-5.80	Moderately	-5.17	0.55
AD-11	-10.3	442.47	0.12	9	6	0	127.43	94.99	3.72	4.85	4.62	2.74	2.75	3.74	0	0	0	0	0	-5.56	Moderately	-5.56	0.55
AD-12	-10.1	457.44	0.08	9	7	0	129.76	131.58	3.29	4.71	4.52	3.01	0.53	3.21	0	0	0	0	0	-5.55	Moderately	-5.75	0.55
AD-13	-9.6	381.47	0.12	7	3	0	117.09	39.94	4.09	5.42	5.01	4.22	5.38	4.83	1	0	0	0	1	-5.74	Moderately	-4.78	0.55
AD-14	-10.2	399.49	0.12	7	4	0	117.04	39.94	4.28	5.52	5.57	4.59	5.80	5.15	1	0	0	0	1	-5.90	Moderately	-4.82	0.55
AD-15	-10.2	415.91	0.12	7	3	0	122.10	39.94	4.42	6.05	5.67	4.69	6.02	5.37	1	1	0	0	1	-6.34	Poorly	-4.54	0.55
AD-16	-10.5	395.50	0.15	7	3	0	122.05	39.94	4.27	5.78	5.32	4.42	5.91	5.14	1	0	0	0	1	-6.04	Poorly	-4.61	0.55
AD-17	-10.5	411.50	0.15	8	4	0	123.58	49.17	4.54	5.39	5.02	3.86	5.44	4.85	0	0	0	0	1	-5.81	Moderately	-4.98	0.55
AD-18	-10.9	426.47	0.12	8	5	0	125.91	85.76	3.87	5.25	4.92	3.26	3.21	4.10	0	0	0	0	1	-5.80	Moderately	-5.17	0.55
AD-19	-9.3	401.89	0.08	7	3	0	117.13	39.94	4.14	5.68	5.36	4.49	5.49	5.03	1	0	0	0	1	-6.04	Poorly	-4.72	0.55
AD-20	-9.7	419.88	0.08	7	4	0	117.09	39.94	4.21	5.78	5.92	4.86	5.91	5.33	1	1	0	1	1	-6.19	Poorly	-4.76	0.55
AD-21	-10.0	436.33	0.08	7	3	0	122.14	39.94	4.34	6.31	6.01	4.96	6.13	5.55	1	1	0	1	1	-6.63	Poorly	-4.48	0.55
AD-22	-10.2	415.91	0.12	7	3	0	122.10	39.94	4.27	6.05	5.67	4.69	6.02	5.34	1	1	0	0	1	-6.34	Poorly	-4.54	0.55

AD-23	-10.4	431.91	0.12	8	4	0	123.62	49.17	4.44	5.65	5.37	4.13	5.55	5.03	0	0	0	0	1	-6.10	Poorly	-4.92	0.55
AD-24	-10.5	446.89	0.08	8	5	0	125.95	85.76	3.73	5.51	5.27	4.34	3.32	4.43	1	0	0	0	1	-6.09	Poorly	-5.11	0.55
Docetaxel	-9.4	807.88	0.56	14	14	5	205.25	224.45	4.30	2.81	2.94	1.06	3.51	2.92	2	3	2	1	3	-5.85	Moderately	-9.23	0.17
STS	-10.8	466.53	0.32	2	4	2	139.39	69.45	3.19	3.24	3.39	2.60	3.02	3.09	0	1	0	0	1	-5.06	Moderately	-6.85	0.55

(M.W:Molecular weight, tPSA:topological polar surface area, MR: Molar refractivity, Fsp3: Fraction of sp3 carbon atoms, HBD: hydrogen bonds donor, HBA: hydrogen bond acceptor, RB: rotatable bonds, LogP values: indicator of Lipophilicity, ESOL: aqueous solubility parameter, Log Kp: skin permeation, F: Bioavailability Score)

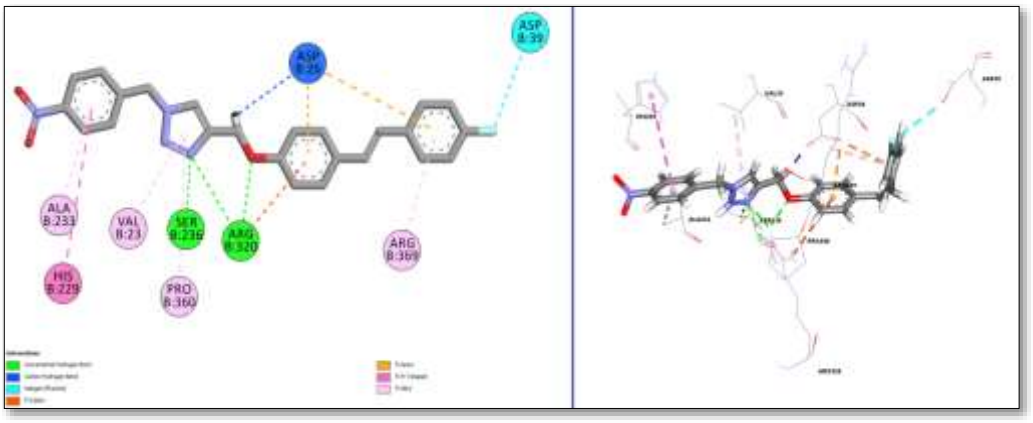

Figure 4.15: The 2D and 3D representations of interactions between compound AD-08 and 1TUB receptor.

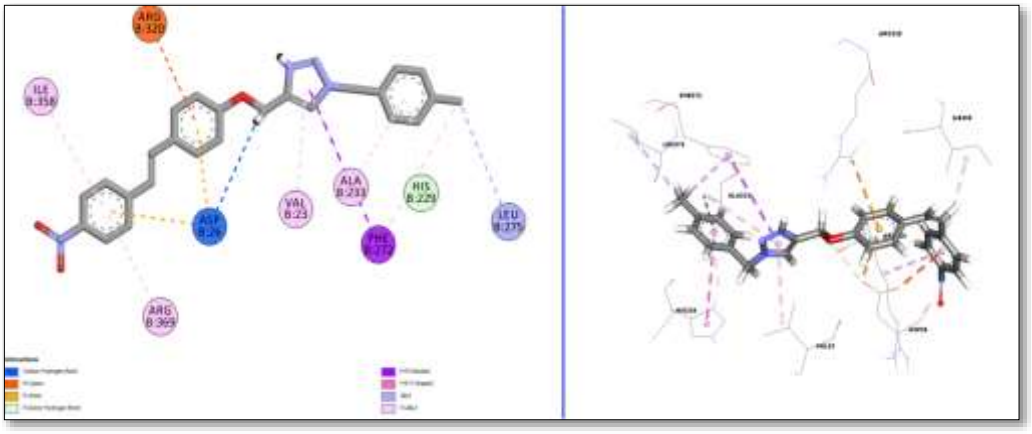

Figure 4.16: The 2D and 3D representations of interactions between compound AD-18 and 1TUB receptor.

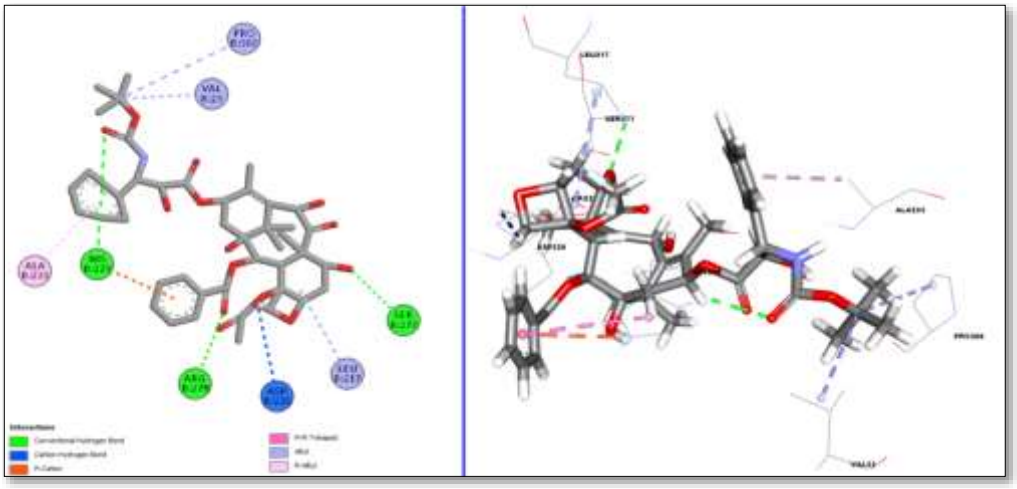

Figure 4.17. The 2D and 3D representations of interactions between Docetaxel (co-ligand) and 1TUB receptor.

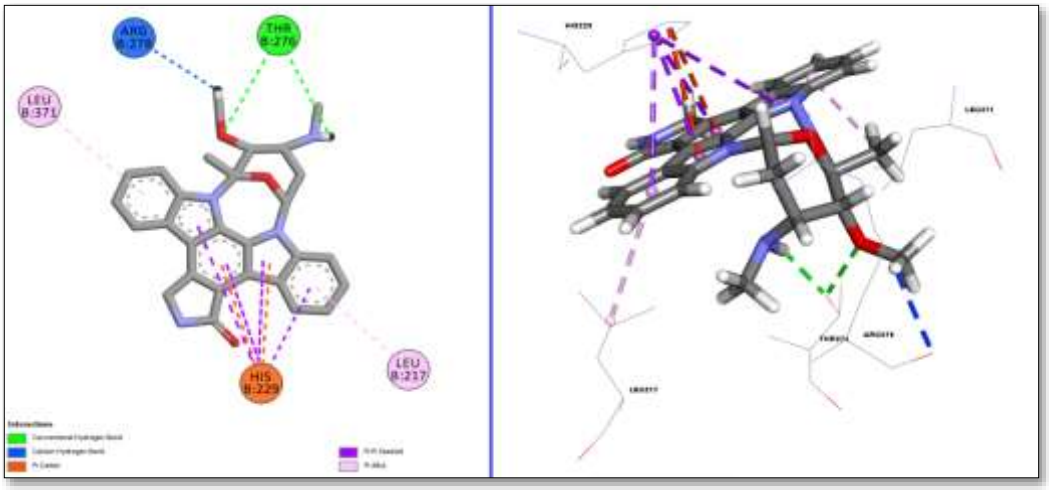

Figure 4.18. The 2D and 3D representations of interactions between STS and 1TUB receptor.

3-(4-((1-benzyl-1*H*-1,2,3-triazol-4-yl)methoxybenzylidene)indolin-2-ones (AD 25-48)

***In-vitro* cytotoxicity evaluation.**

All analogs (**AD 25-48**) were preliminarily screened against murine L1210, CEM, and HeLa cells. The results are summarized in **Table 4.23.** HeLa and CEM cells were selected to ascertain triazoles (**AD 25-48**) toxicity against human cells.

Table 4.23: *In-vitro* cytotoxicity data of 3-(4-((1-benzyl-1*H*-1,2,3-triazol-4-yl) methoxybenzylidene)indolin-2-ones (AD 25-48).

Compound	IC_{50} (µM)		
	L1210	**CEM**	**HeLa**
AD-25/7a*	8.1 ± 2.2	3.6 ± 2.5	4.6 ± 0.0
AD-26/7b	>250	33 ± 3.4	133 ± 18
AD-27/7f	44 ± 4.0	18 ± 4.0	66 ± 3.4
AD-28/7e	29 ± 1.0	7.3 ± 1.9	38 ± 3
AD-29/7d	150 ± 14	6.7 ± 1.9	36 ± 0.6
AD-30/7c	3.0 ± 0.9	1.5 ± 0.6	3.4 ± 0.6
AD-31/7k	34 ± 2.0	3.9 ± 0.8	11 ± 3.0
AD-32/7g	32 ± 1.0	5.0 ± 0.7	7.8 ± 2.9
AD-33/7i	19 ± 2.0	11 ± 6.0	20 ± 1.0
AD-34/7j	17 ± 9.0	67 ± 2.5	7.1 ± 4.4
AD-35/7h	32 ± 1.5	6.0 ± 1.1	9.2 ± 1.7
AD-36/7l	30 ± 4.0	4.6 ± 0.4	12 ± 3.0
AD-37/7m	19 ± 4.0	4.4 ± 0.6	4.8 ± 0.1
AD-38/7q	24 ± 6	5.7 ± 1.0	15 ± 1.0
AD-39/7n	31 ± 4.0	33 ± 3.0	70 ± 3.5
AD-40/7r	100 ± 13	18 ± 17	31 ± 3.9
AD-41/7p	38 ± 2.5	7.4 ± 1.7	16 ± 1.0
AD-42/7o	5.3 ± 0.5	3.8 ± 0.8	4.4 ± 0.6

AD-43/7s	12 ± 0.9	3.8 ± 1.7	3.7 ± 0.1
AD-44/7t	20 ± 4.0	5.3 ± 1.4	13 ± 1.0
AD-45/7w	14 ± 1.1	1.7 ± 0.8	3.9 ± 0.4
AD-46/7x	17 ± 3.0	6.8 ± 0.7	8.1 ± 1.9
AD-47/7u	20 ± 6.0	5.5 ± 0.1	12 ± 6.0
AD-48/7v	4.8 ± 1.1	4.0 ± 0.6	3.7 ± 0.4
Melphalan	**2.13 ± 0.02**	**1.4 ± 0.4**	**NT**

***Biological study code**

NT: Not tested

Caspase inhibition and induction of apoptosis

The molecular mechanism of cytotoxicity was established by flow cytometry. In order to analyze triggers of apoptosis or necrosis an annexin V/7-AAD assay was performed **(Figure 4.19).**

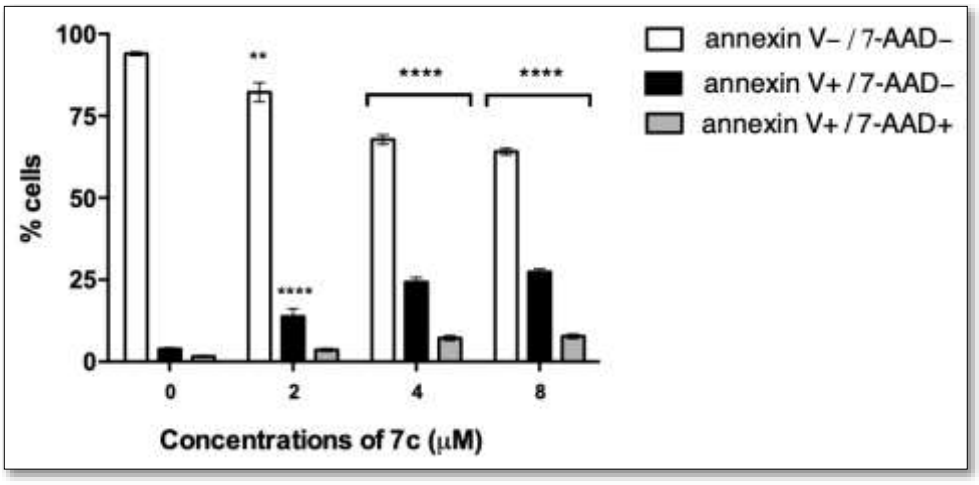

Figure 4.19. Percentage (%) of viable (annexin V-/7-AAD), early apoptotic (annexin V+/7-AAD-), and late apoptotic or necrotic (annexin V+/ 7-AAD+) cells (A) and cell cycle distribution (B) following 6 h treatment of Jurkat cells with 7c/AD-30. ** p< 0.01; **** p< 0.0001 versus untreated cells.

The **7c/AD-30** induced extrinsic apoptotic pathway was assessed by analyzingcaspase-8 activity. Change in mitochondrial potential was taken as measure of apoptosis during the study. To assess the involvement of the intrinsic apoptotic pathway, change in mitochondrial transmembrane potential was measured **(Figure 4.20).**

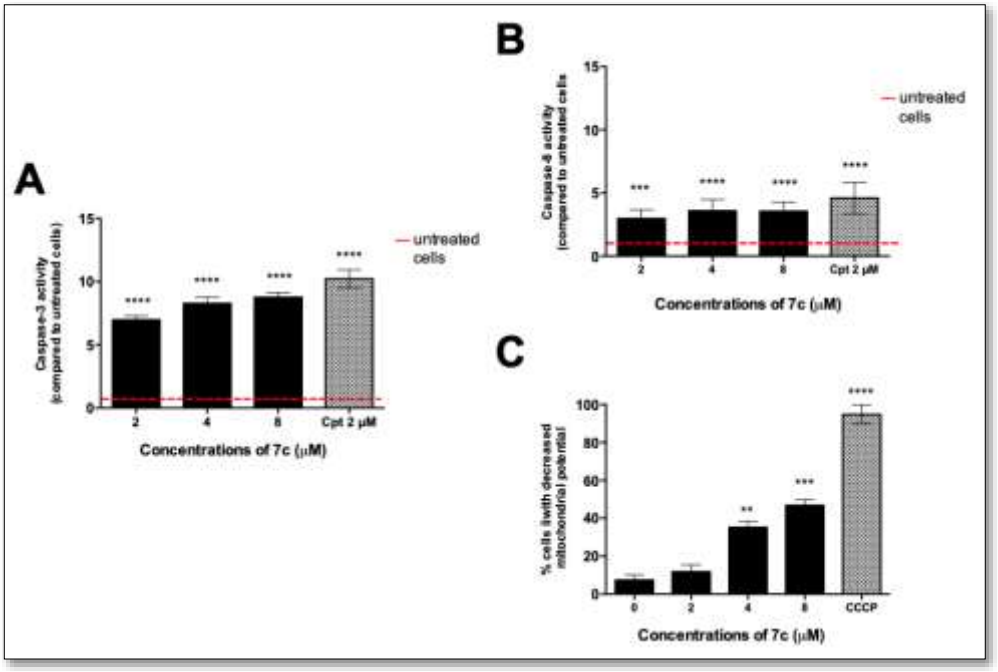

NT: Not tested

Figure 4.20. Activity of caspase-3 (A) and caspase-8 (B) and percentage (%) of cells with decreased mitochondrial potential (C) after 24h treatment of Jurkat cells with increasing concentrations of 7c/AD-30. Cpt (camptothecin) and CCCP (carbonyl cyanide 3-chlorophenylhydrazone) were used as positive controls. **p< 0.01; ***p<0.001; ****p< 0.0001 versus untreated cells.

To determine whether **7c/AD-30** could activate non-canonical cell death programs, Jurkat cells were pre-treated for 1h with different chemical inhibitors[*i.e.* Z-VAD-FMK, Ola, Nec-1s, Ferr-1, DFO, and Vit. E] in order to inhibit apoptosis, parthanatos, necroptosis and ferroptosis, respectively and the cell viability was analyzed by flow cytometry **(Figure-4.21).**

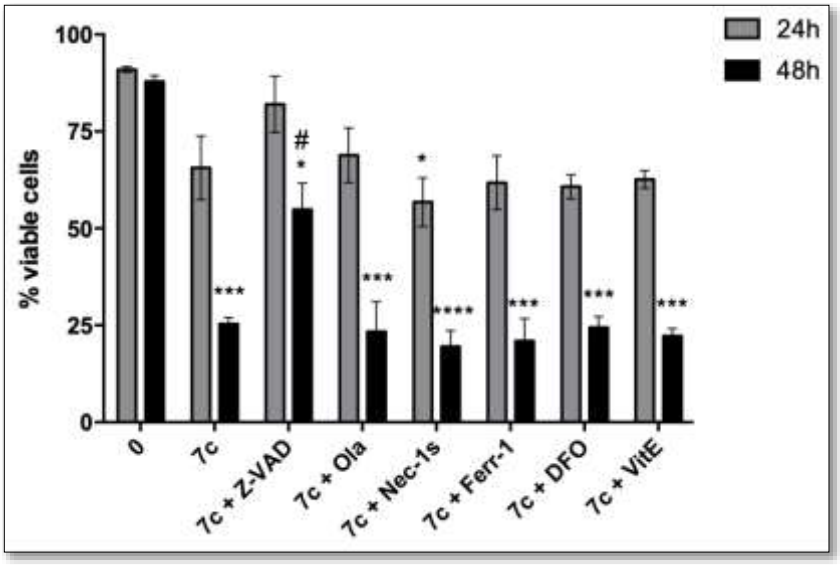

Figure 4.21. Percentage (%) of viable cells after pre-treatment for 1h with Z-VAD-FMK (Z-VAD), Ola, Nec-1s, Ferr-1, DFO, or Vit-E following 24h and 48h treatment with 7c/AD-30 8µM. *p< 0.05; ***p< 0.001; ****p< 0.0001 versus untreated cells. # p< 0.05 versus 7c-treated cells.

ROS production

The intracellular ROS level was measured after different treatment times with **AD-30**.

No modulation of ROS levels was observed after **AD-30** treatment **(Figure 4.22).**

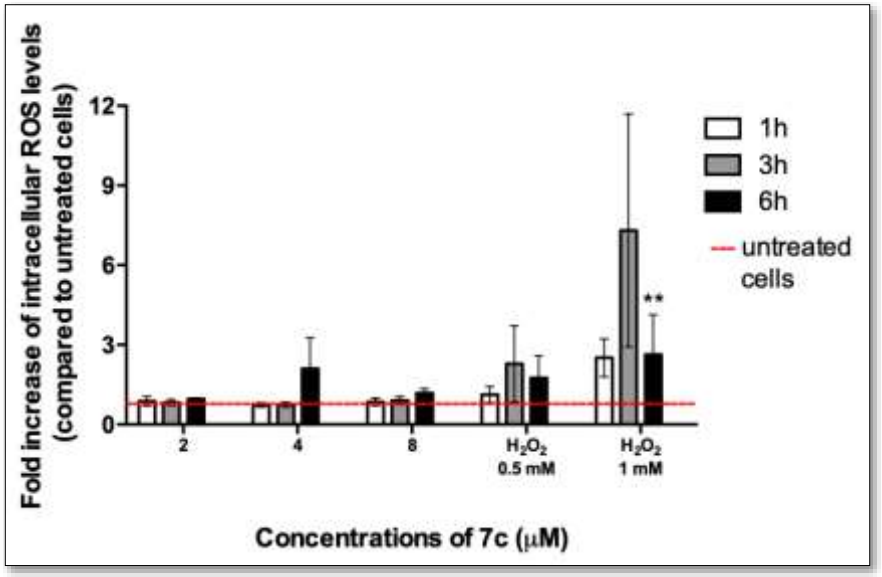

Figure 4.22. Intracellular ROS levels, expressed as fold increase versus untreated cells, of Jurkat cells treated with 7c/AD-30. H2O2 0.5 and 1mM were used as positive control. **p< 0.01versus untreated cells.

Cell-cycle perturbations

Cell cycle is a sequence of closely coordinated molecular processes that control DNA replication and chromosome division, ultimately leading to cell division and transfer of genetic material. To explore the cytostatic potential of **7c/AD-30** the cell-cycle progression of **7c/AD-30** treated cells together with the expression of some cyclins and CDKs were analysed **(Figures 4.23-4.25).**

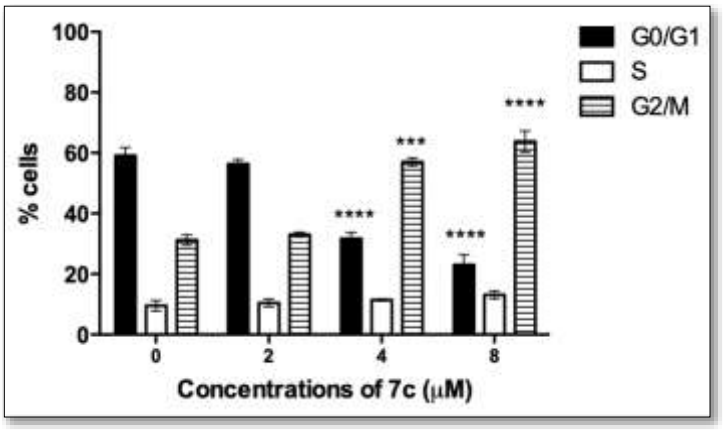

Figure 4.23. Cell-cycle distribution after Jurkat treatment with AD-30 for 24h. ***p< 0.001; ****p< 0.0001 versus untreated cells.

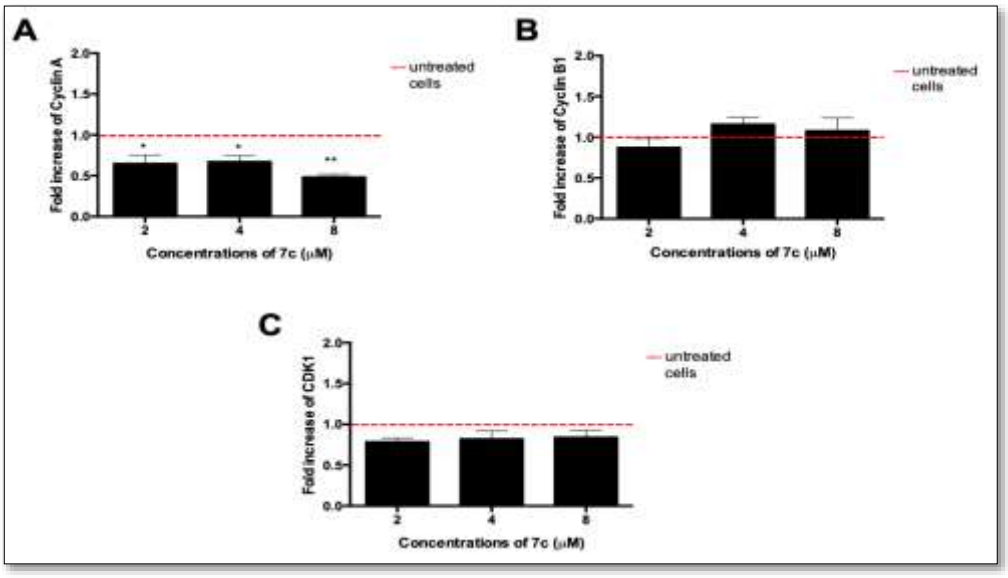

Figure 4.24. Expression of cyclin A (A), cyclin B1 (B), and CDK1 (C), indicated as fold increase versus untreated cells, following 24h treatment of Jurkat cells with 7c/AD-30. *p< 0.05; **p< 0.01 versus untreated cells.

Pro-apoptotic & cytostatic activity

The pro-apoptotic and cytostatic activities of **7c/AD-30** were analyzed to assess whether the two events were related or independent from each other **(Figure 4.25).**

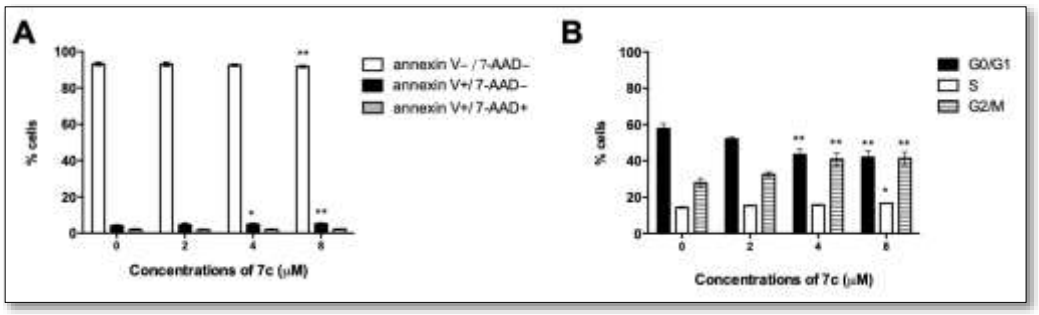

Figure 4.25. Percentage (%) of viable (annexin V-/7-AAD), early apoptotic (annexin V+/7-AAD-), and late apoptotic or necrotic (annexin V+/ 7-AAD+) cells (A) and cell cycle distribution (B) following 6 h treatment of of Jurkat cells with 7c/AD-30. ** p< 0.01; **** p< 0.0001 versus untreated cells.

Genotoxicity evaluation

A toxicological profile was performed by analyzing the genotoxicity of **7c/AD-30** by analyzing the phosphorylation of H2A.X (P-H2A.X) at Serine-139. Following 5h treatment of Jurkat cells with **7c/AD-30**, no major change in H2A.X phosphorylation seen. **(Figure 4.26).**

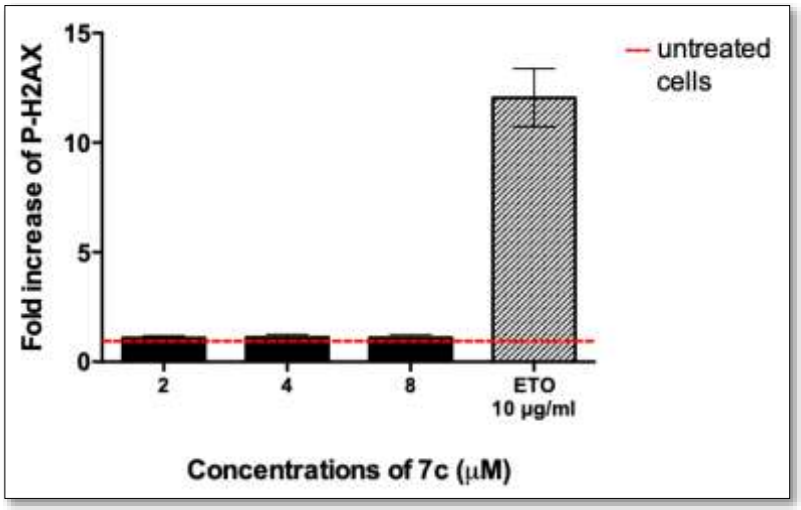

Figure 4.26. Relative expression of P-H2AX following 5h treatment of Jurkat cells with increasing concentrations of 7c/AD-30. ETO (Etoposide) 10μg/mL was used as positive control. **p< 0.01 versus untreated cells.

Physicochemical properties and ADME parameters

The physicochemical parameters and drug-likeness violation by **AD 25-48** predicted by Swiss-ADME web-server and, summarized in **Table 4.24**.

Table 4.24. Physicochemical and drug likeness properties (*in-silico*).

		Code							Lipophilicity						Water solubility		Violation of drug-likeness filters						
Comp.	Binding Affinity	MW (g/mol)	Fsp^3	RB	HBA	HBD	MR	tPSA	iLogP	XLogP	WLogP	MLogP	SILICOS-IT	Consensus LogP	ESOL	Class	Lipinski	Ghose	Veber	Egan	Muegge	Bioavailability Score	Log K_p (cm/s)
AD-25/7a*	-10.9	408.45	0.08	6	4	1	122.45	69.04	3.36	3.76	3.57	3.18	4.18	3.61	-4.89	Moderately	0	0	0	0	0	0.55	-6.12
AD-26/7b	-10.7	442.90	0.08	6	4	1	127.46	69.04	3.67	4.39	4.22	3.65	4.82	4.15	-5.49	Moderately	0	0	0	0	0	0.55	-5.88
AD-27/7f	-10.7	442.90	0.08	6	4	1	127.46	69.04	3.61	4.39	4.22	3.65	4.82	4.14	-5.49	Moderately	0	0	0	0	0	0.55	-5.88
AD-28/7e	-11.0	442.90	0.08	6	4	1	127.46	69.04	3.71	4.39	4.22	3.65	4.82	4.16	-5.49	Moderately	0	0	0	0	0	0.55	-5.88
AD-29/7e	-10.3	487.35	0.06	6	4	1	130.15	69.04	3.65	4.45	4.33	3.75	4.86	4.21	-5.80	Moderately	0	2	0	0	0	0.55	-6.11
AD-30/7c	-11.1	422.48	0.12	6	4	1	127.41	69.04	3.54	4.12	3.87	3.38	4.71	3.93	-5.19	Moderately	0	0	0	0	0	0.55	-5.95
AD-31/7k	-10.6	453.45	0.08	7	6	1	131.27	114.86	3.08	3.59	3.47	3.11	2.01	3.05	-4.95	Moderately	0	1	0	0	0	0.55	-6.52
AD-32/7g	-10.9	487.89	0.08	7	6	1	136.28	114.86	3.35	4.22	4.13	3.58	2.65	3.59	-5.55	Moderately	0	2	0	0	0	0.55	-6.28
AD-33/7i	-10.8	487.89	0.08	7	6	1	136.28	114.86	3.16	4.22	4.13	3.58	2.65	3.55	-5.55	Moderately	0	2	0	0	0	0.55	-6.28
AD-34/7j	-10.7	487.89	0.08	7	6	1	136.28	114.86	3.14	4.22	4.13	3.58	2.65	3.54	-5.55	Moderately	0	2	0	0	0	0.55	-6.28
AD-35/7k	-10.5	532.35	0.08	7	6	1	138.97	114.86	3.44	4.28	4.24	3.69	2.69	3.67	-5.86	Moderately	1	2	0	0	0	0.55	-6.51
AD-36/7l	-10.8	467.48	0.12	7	6	1	136.23	114.86	3.35	3.95	3.78	2.50	2.54	3.23	-5.25	Moderately	0	1	0	0	0	0.55	-6.35
AD-37/7m	-10.9	422.48	0.12	6	4	1	127.41	69.04	3.60	4.12	3.87	3.38	4.71	3.94	-5.19	Moderately	0	0	0	0	0	0.55	-5.95
AD-38/7q	-10.9	456.92	0.12	6	4	1	132.42	69.04	3.92	4.75	4.53	3.85	5.34	4.48	-5.79	Moderately	0	1	0	0	0	0.55	-5.71
AD-39/7n	-10.6	456.92	0.12	6	4	1	132.42	69.04	3.80	4.75	4.53	3.85	5.34	4.45	-5.79	Moderately	0	1	0	0	0	0.55	-5.71
AD-40/7r	-10.4	456.92	0.12	6	4	1	132.42	69.04	3.90	4.75	4.53	3.85	5.34	4.48	-5.79	Moderately	0	1	0	0	0	0.55	-5.71
AD-41/7p	-10.8	501.37	0.12	6	4	1	135.11	69.04	3.86	4.81	4.64	3.95	5.38	4.53	-6.10	Moderately	1	2	0	0	0	0.55	-5.94

AD-42/7o	**-11.5**	**436.51**	**0.15**	**6**	**4**	**1**	**132.38**	**69.04**	**3.70**	**4.49**	**4.18**	**3.59**	**5.23**	**4.24**	**-5.49**	**Moderately**	**0**	**1**	**0**	**0**	**0**	**0.55**	**-5.77**
AD-43/7s	**-10.7**	**442.90**	**0.08**	**6**	**4**	**1**	**127.46**	**69.04**	**3.62**	**4.39**	**4.22**	**3.65**	**4.82**	**4.14**	**-5.49**	**Moderately**	**0**	**0**	**0**	**0**	**0**	**0.55**	**-5.88**
AD-44/7t	**-10.9**	**477.34**	**0.08**	**6**	**4**	**1**	**132.47**	**69.04**	**3.76**	**5.01**	**4.87**	**4.12**	**5.46**	**4.64**	**-6.08**	**Moderately**	**0**	**1**	**0**	**0**	**1**	**0.55**	**-5.65**
AD-45/7w	**-11.0**	**477.34**	**0.08**	**6**	**4**	**1**	**132.47**	**69.04**	**3.81**	**5.01**	**4.87**	**4.12**	**5.46**	**4.65**	**-6.08**	**Moderately**	**0**	**1**	**0**	**0**	**1**	**0.55**	**-5.65**
AD-46/7x	**-10.8**	**477.34**	**0.08**	**6**	**4**	**1**	**132.47**	**69.04**	**3.94**	**5.01**	**4.87**	**4.12**	**5.46**	**4.68**	**-6.08**	**Moderately**	**0**	**1**	**0**	**0**	**1**	**0.55**	**-5.65**
AD-47/7u	**-10.8**	**521.79**	**0.08**	**6**	**4**	**1**	**135.16**	**69.04**	**3.88**	**5.08**	**4.98**	**4.22**	**5.49**	**4.73**	**-6.40**	**Moderately**	**2**	**2**	**0**	**0**	**1**	**0.17**	**-5.88**
AD-48/7v	**-11.3**	**456.92**	**0.12**	**6**	**4**	**1**	**132.42**	**69.04**	**3.78**	**4.75**	**4.53**	**3.85**	**5.34**	**4.45**	**-5.79**	**Moderately**	**0**	**1**	**0**	**0**	**0**	**0.55**	**-5.71**
Melphalan	**-8.0**	**313.26**	**1.00**	**8**	**4**	**3**	**80.01**	**69.72**	**2.79**	**1.25**	**1.35**	**1.56**	**1.72**	**1.73**	**-2.04**	**Soluble**	**0**	**0**	**0**	**0**	**0**	**0.55**	**-7.32**
Co-ligand	**-8.1**	**364.55**	**1.00**	**2**	**4**	**2**	**99.73**	**35.50**	**0.00**	**4.01**	**2.95**	**3.49**	**1.02**	**2.29**	**-4.49**	**Moderately**	**0**	**0**	**0**	**0**	**0**	**0.55**	**-5.68**

***In-silico* study code**

Bioavailability Radar Scheme

The bioavailabity radar was predicted using Swiss-ADME webserver. It allows a rapid and clear assessment of drug similarity of compounds and their oral bioavailability. In the radar scheme, the red-colored zone shows preferred physicochemical space for oral bioavailability of molecules considering flexibility, lipophilicity, saturation, size, polarity, and solubility **(Figure 4.27).**

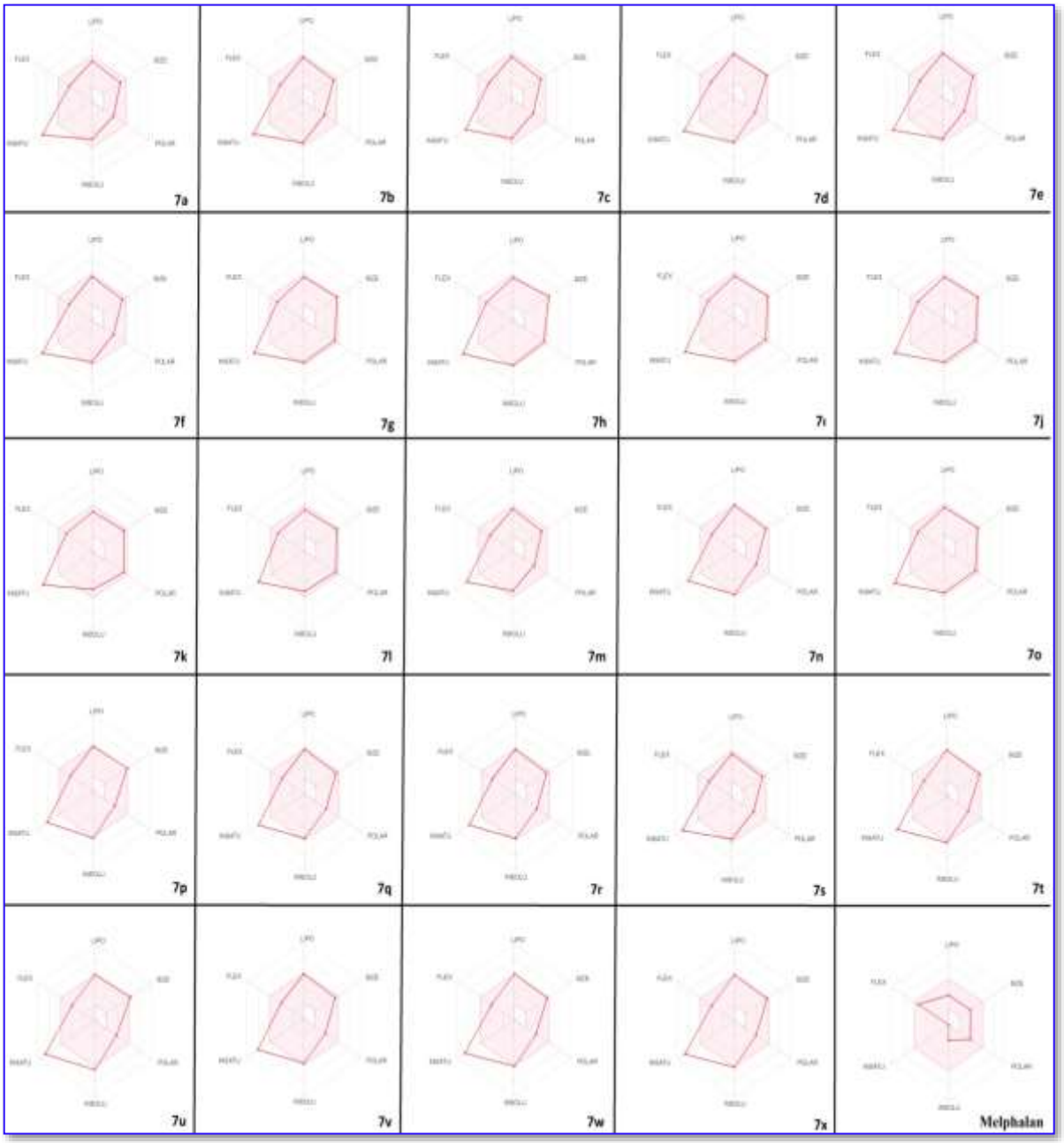

Figure 4.27. Bioavailability radar schemes of all synthesized compounds.

Molecular docking

Molecular docking was performed to identify the possible binding sites on **6P8Q EGFR** receptor. **Table 4.24** represents the physicochemical and drug-likeness properties of the synthesized derivatives while, **Figures 4.28** and **4.29** show the 2D and 3D interactions with **6P8Q EGFR** receptor.

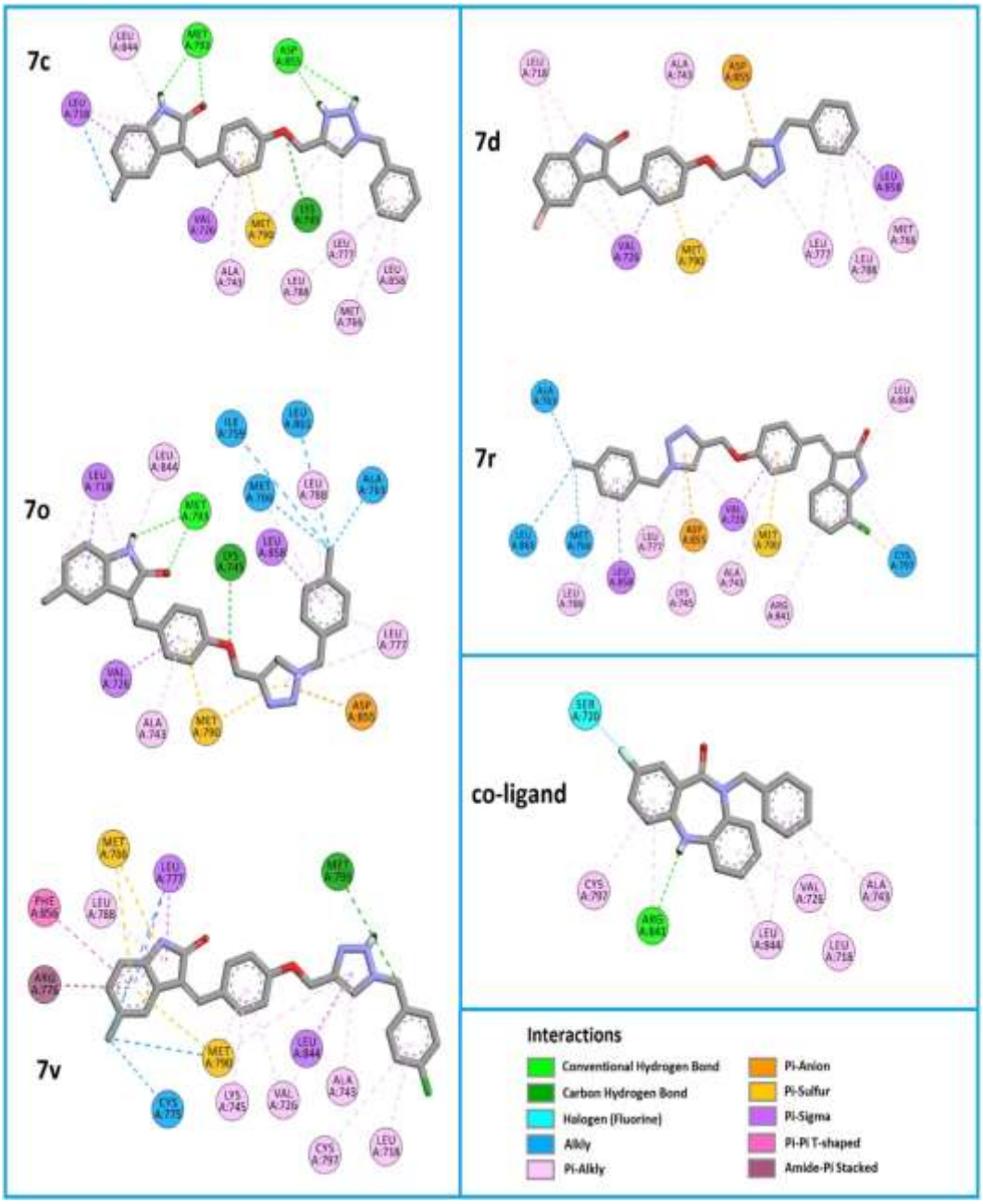

Figure 4.28. 2D Interaction diagram between 6P8Q receptor and compounds 7c/AD-30, 7d/AD-29, 7o/AD-42, 7r/AD-40, 7v/AD-48, and co-ligand.

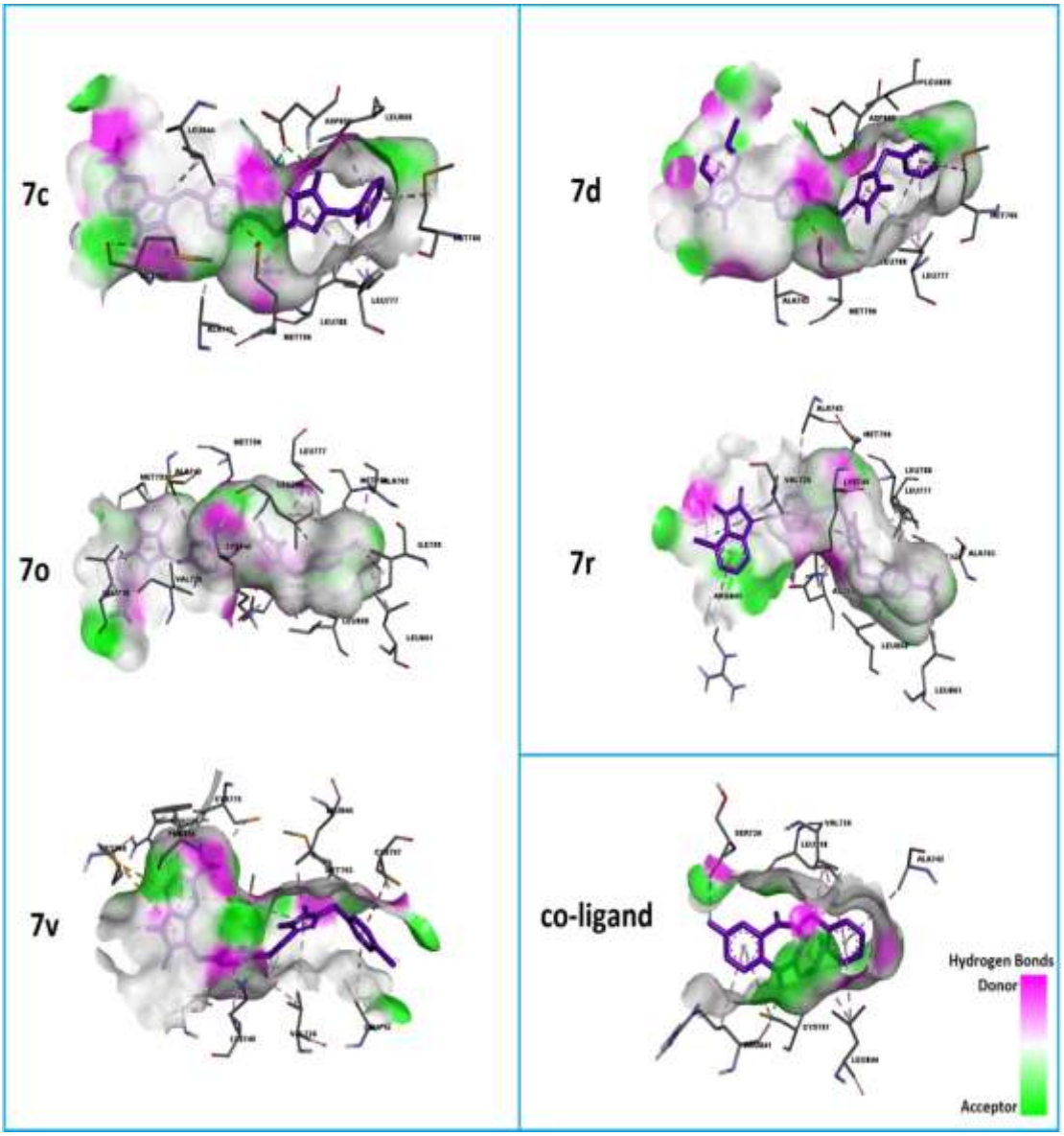

Figure 4.29. 3D Interactions on the Hydrogen Bond surface between 6P8Q receptor and compounds 7c/AD-30, 7d/AD-29, 7o/AD-42, 7r/AD-40, 7v/AD-48, and co-ligand.

In-vitro Antimycobacterial activity:

Anti-mycobacterial properties were evaluated against *M. tuberculosis, M. abscessus,* and, *M. avium* as per NCI standard protocol. DMSO was used as solvent and Rifampicin as a reference standard during the study. MIC, IC_{50}, and IC_{90} values were calculated. A dose-response curve was plotted for the tested molecules. Results were summarized in **Tables 4.25-4.27,** and, **Figures 4.30-4.32**

Table 4.25: MIC of tested compounds against *M. tuberculosis* H37Rv

NCI ID	Submitter ID	Strain ID	MIC (µM)	IC_{50} (µM)	IC_{90} (µM)
NCI-0003562	**AD 28**	H37Rv	> 20	> 20	> 20
NCI-0003563	**AD 30**	H37Rv	> 200	> 200	> 200
NCI-0003564	**AD 31**	H37Rv	> 200	> 200	> 200
NCI-0003565	**AD 39**	H37Rv	> 200	> 200	> 200
NCI-0003566	**AD 40**	H37Rv	> 200	> 200	> 200
NCI-0003567	**AD 41**	H37Rv	> 200	> 200	> 200
NCI-0003568	**AD 42**	H37Rv	> 200	> 200	> 200
NCI-0003569	**AD 43**	H37Rv	> 200	> 200	> 200
NCI-0003570	**AD 44**	H37Rv	> 100	> 100	> 100
NCI-0003571	**AD 45**	H37Rv	> 200	> 200	> 200
NCI-0003572	**AD 46**	H37Rv	> 200	> 200	> 200
NCI-0003573	**AD 47**	H37Rv	> 200	> 200	> 200
NCI-0003574	**AD 48**	H37Rv	> 200	> 200	> 200
NCI-0000017	**Rifampicin**	**H37RV**	**0.0073**	**0.00047**	**0.0079**

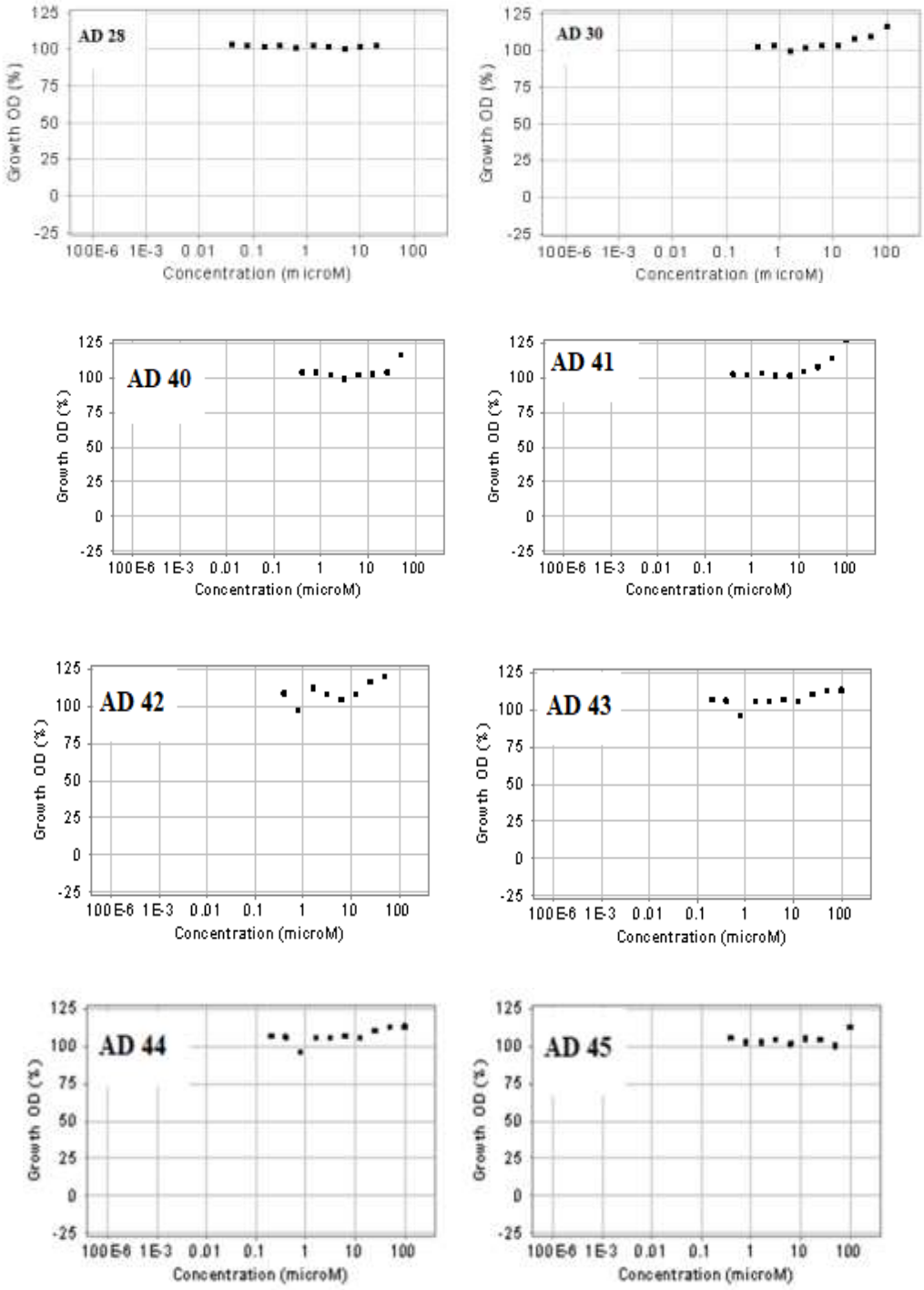

Figure 4.30 (A): Dose response curve of tested molecules against *M. tuberculosis*.

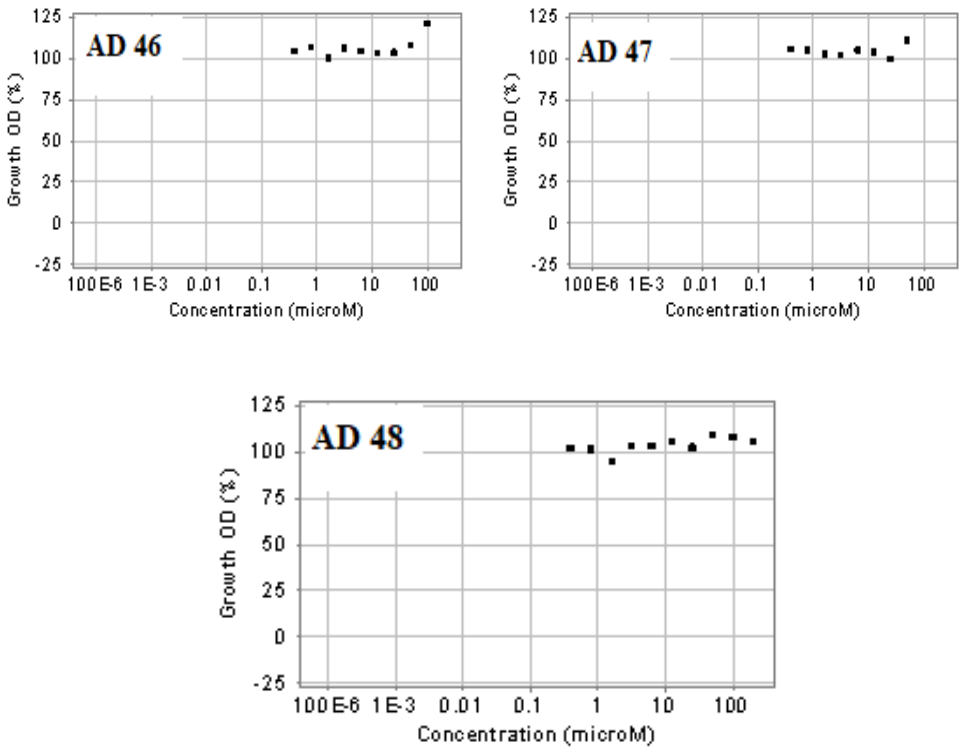

Figure 4.30 (B): Dose response curve of tested molecules against *M. tuberculosis*.

Table 4.26: MIC of tested compounds against *M. abscessus* (bollettii 103).

NCI ID	Submitter ID	Species	MIC (µM)	IC_{50} (µM)	IC_{90} (µM)
NCI-0003562	**AD 28**	*M. abscessus*	> 20	> 20	> 20
NCI-0003563	**AD 30**	*M. abscessus*	> 200	> 200	> 200
NCI-0003564	**AD 31**	*M. abscessus*	> 200	> 200	> 200
NCI-0003565	**AD 39**	*M. abscessus*	> 200	> 200	> 200
NCI-0003566	**AD 40**	*M. abscessus*	> 200	> 200	> 200
NCI-0003567	**AD 41**	*M. abscessus*	> 200	> 200	> 200
NCI-0003568	**AD 42**	*M. abscessus*	> 200	> 200	> 200
NCI-0003569	**AD 43**	*M. abscessus*	> 200	> 200	> 200
NCI-0003570	**AD 44**	*M. abscessus*	> 100	> 100	> 100
NCI-0003571	**AD 45**	*M. abscessus*	> 200	> 200	> 200
NCI-0003572	**AD 46**	*M. abscessus*	> 200	> 200	> 200
NCI-0003573	**AD 47**	*M. abscessus*	> 200	> 200	> 200
NCI-0003574	**AD 48**	*M. abscessus*	> 200	> 200	> 200
NCI-0000017	**Rifampicin**	*M. abscessus*	**3.7**	**2.2**	**3.6**

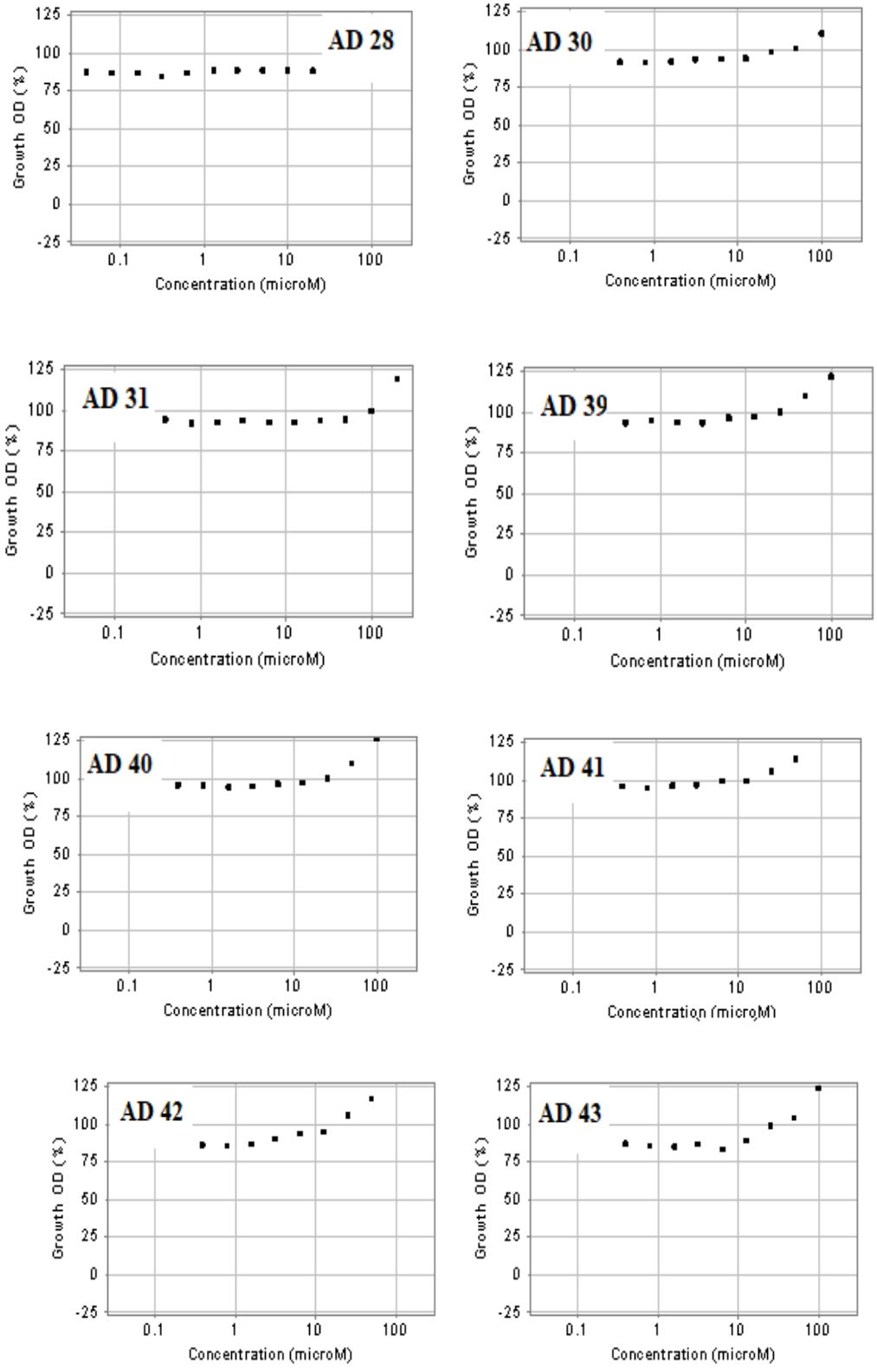

Figure 4.31 (A): Dose response curve of tested molecules against *M. abscessus*

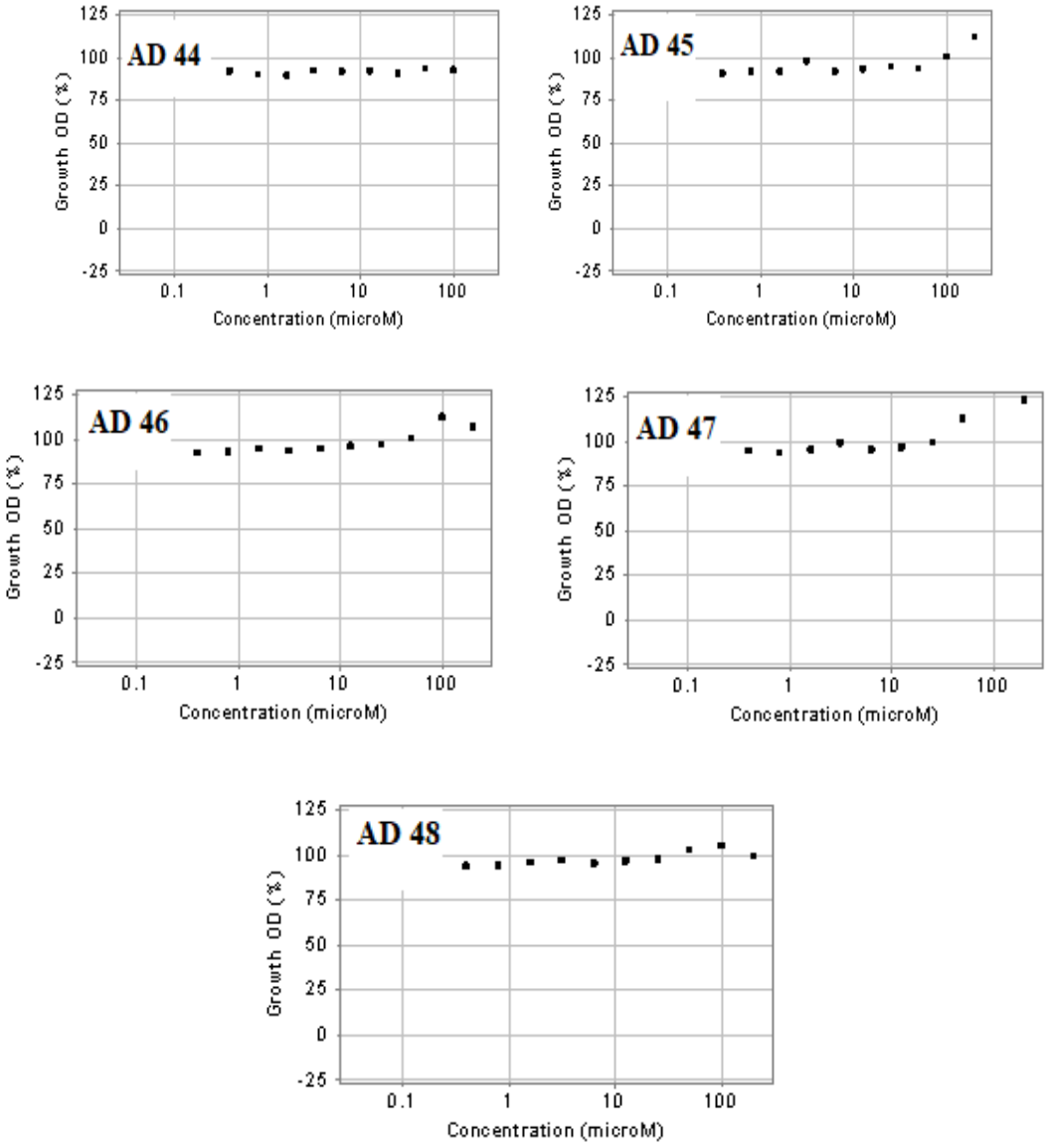

Figure 4.31 (B): Dose response curve of tested molecules against *M. abscessus*

Table 4.27: MIC of tested compounds against *M. avium*. (*avium* 2285)

NCI ID	Submitter ID	Species	MIC (µM)
NCI-0003562	**AD 28**	*M. avium*	> 20
NCI-0003563	**AD 30**	*M. avium*	> 200
NCI-0003564	**AD 31**	*M. avium*	> 200
NCI-0003565	**AD 39**	*M. avium*	> 200
NCI-0003566	**AD 40**	*M. avium*	> 200
NCI-0003567	**AD 41**	*M. avium*	> 200
NCI-0003568	**AD 42**	*M. avium*	> 200
NCI-0003569	**AD 43**	*M. avium*	> 200
NCI-0003570	**AD 44**	*M. avium*	> 200
NCI-0003571	**AD 45**	*M. avium*	> 200
NCI-0003572	**AD 46**	*M. avium*	> 200
NCI-0003573	**AD 47**	*M. avium*	> 200
NCI-0003574	**AD 48**	*M. avium*	> 200
NCI-0000017	**Rifampicin**	***M. avium***	**0.078**

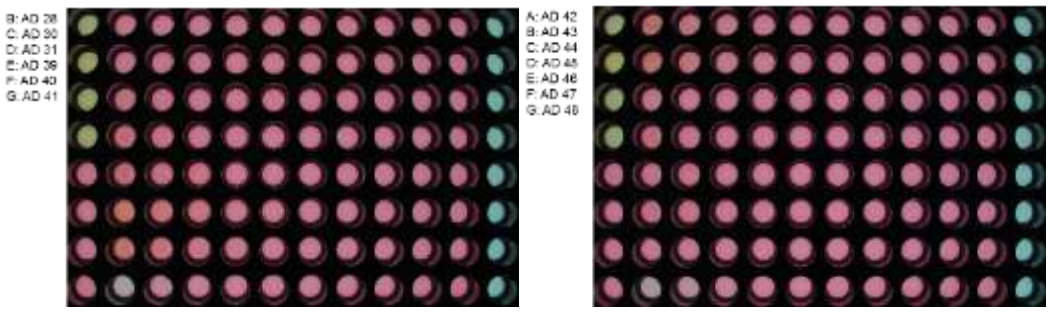

Figure 4.32: Plate image of tested compounds against *M. avium*.

5.0 DISCUSSION

5.1 Chemistry:

1-Benzyl-4-((4-styrylphenoxy)methyl)-1*H*-1,2,3-triazoles[82-84] (AD 1-24)

Twenty-four stilbene-linked 1*H*-1,2,3-triazoles **(AD 1-24)** were obtained by reacting triazole-benzaldehydes **(7a-d)** with aralkyl triphenylphosphonium halides **(10a-f).** The **7a-d** were organized in regioselective copper (Cu)-catalyzed dipolar cycloaddition (1, 3) of 4-(prop-2-benzyloxy)benzaldehyde **(3)** with aryl azides **(6a-d).** Compound **3** was obtained in a reaction between *p*-OH-benzaldehyde **(1)** and 3-bromoprop-1-yne **(2).** Reactions were summarized in schemes **1-6.** The structures of synthesized derivatives **AD 1-24** were summarized in **Table 4.9**. The FTIR, NMR (^{1}H &^{13}C) and, LCMS analytical data have been included in tables **4.13-4.16.** The mechanism of synthesis follows Wittig reaction.[85] **(Figure 5.1)**

The peaks between 3098-3001 (-CH, ar.), 2964-2734 (-CH, ali.), 1634-1591 (>C=C<), 1492-1437 (-CH_2), and, 1266 cm-^{1} (-O-) in FTIR spectra of **AD 1-24** represent the groups in parentheses. The -CH_2 bending appeared between,1492-1427 cm-^{1}. The -CH_3 bending for **AD-4, AD-5, AD-10, AD-11, AD 13-18, AD-22,** and **AD-23** appeared between 1395-1336 cm^{-1}, and, the -NO_2 stretching of **AD 6-12, AD-18,** and **AD-24** were seen between 1587-1440 cm^{-1}.

In ^{1}H-NMR spectra the singlet triazole-H appeared between 8.38-8.20 δ ppm. Peaks between 8.25-6.93 δ ppm represent aromatic-H while, the two doublet peaks between 7.50-7.06 δ ppm represent ***E***-CH=CH (*styryl* moiety). The -NCH_2- and -OCH_2- protons appeared in the range of 5.80-5.40 and 5.20-5.13 δ ppm respectively. The -CH_3 protons of **AD-4, AD-9, AD 13-18,** and **AD-22** appeared between 2.29-2.27 δ ppm and -OCH_3 protons of **AD-5, AD-11, AD-17,** and **AD-23** appeared at 3.76 δ ppm. The ^{13}C NMR spectra displayed peaks between 162.37-111.53 δ ppm for the

aromatic carbons, 61.70-61.08 δ ppm for -OCH_2 and, 55.11-51.01 δ ppm for -NCH_2-. The -CH_3 carbon of **AD-4, AD-10, AD 13-18,** and **AD-20** appeared between 20.80-20.63 δ ppm. The -NCH_2 protons appeared at 5.52 δ ppm along with, singlet triazole-H at 7.59 δ ppm in **7a. Table 4.10** contains the physicochemical properties of **AD 1-24.**

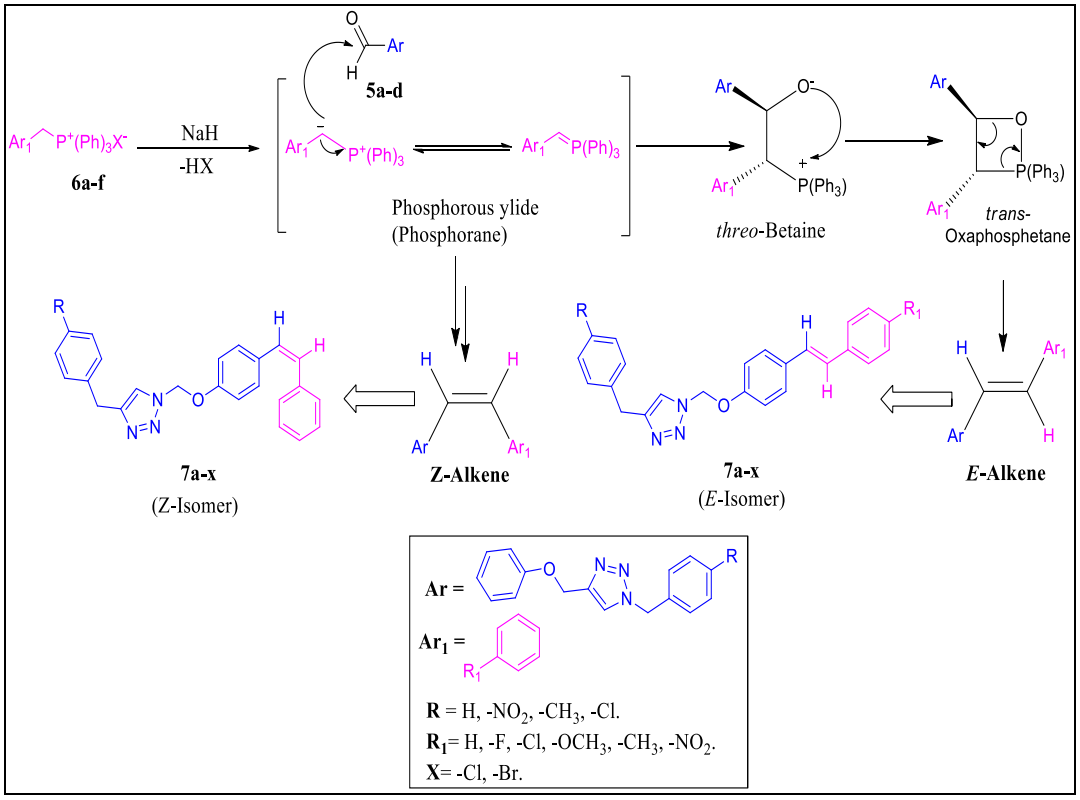

Figure 5.1: Benzyl-4-((4-styrylphenoxy)methyl)-1*H*-1,2,3-triazoles[85] (AD 1- 24)

3-(4-((1-Benzyl-1*H*-1,2,3-triazol-4-yl)methoxybenzylidene)indolin-2-ones (AD 25-48)

A series of twenty-four indoline-2-one linked 1,2,3-triazoles **(AD 25-48)** were prepared by refluxing triazole-benzaldehyde **(7a-d)** and indolin-2-one **(13a-f)** in methanol using piperidine as a catalyst, **Scheme 7**.

The mechanism of synthesis (**Figure 5.2**) follows Knoevenagel condensation.[86] An *enol* intermediate formed initially by reacting triazole-benzalaldehyde **(7a-d)** and,

indolin-2-one **(13a-f)** undergoes Aldol condensation. The subsequent base-induced elimination of H_2O from Aldol lead to the formation of **AD 25-48.**

The new molecules **(AD 25-48)** were characterized by their FTIR, NMR ($^1H/^{13}C$) data. Further, the purity of synthesized derivatives ascertained by single spot on TLC plates. The FTIR spectra showed stretching transmittance peaks between 3141-3229 (N-H), 3090-3010 (C-H, ar.), 2950-2754 (C-H, ali.), 1701-1672 (>C=O), 1616-1582 (>C=C<) and 1226-1167 (-O-) cm^{-1} for the peaks in parentheses. The methylene ($-CH_2$) bending peaks were observed between 1489-1448 cm^{-1}. The bending peaks for methyl group ($-CH_3$) in **AD-30, AD 36-42,** and **AD-48** appeared in the range of 1389-1338 cm^{-1}. The nitro ($-NO_2$) stretching in **AD 32-36** was observed between 1594-1449 cm^{-1} **(Table-4.17).** In ^{1}H-NMR spectra, the singlet -NH proton was observed between 11.00-10.04 δ ppm whereas, triazole ring proton appeared in the range of 8.41-8.27 δ ppm. The prominent signals between 8.55-6.68 δ ppm represent aromatic protons and, the signals between 7.93-7.53 δ ppm appeared for benzylidene-CH**.** The $O-CH_2-$ was confirmed by a singlet peak between 5.81-5.50 δ ppm and the $-N-CH_2$ protons appeared between 5.29-5.22 δ ppm. Methyl protons of **AD-30, AD 36-42** and **AD-48** were seen in the range of 2.67-2.17 δ ppm **(Table 4.18).** The ^{13}C NMR spectra displayed the peaks between 168.80-166.99 δ ppm for >C=O of 2-oxindole, 160.30-108.70 δ ppm for the aromatic carbons, 61.81-61.13 δ ppm for $-OCH_2$ and, 55.84-51.92 δ ppm for $-NCH_2-$. The $-CH_3$ carbon of **AD-30, AD 36-42,** and **AD-48** appeared between 20.79-20.63 δ ppm **(Table 4.19).** The C, H, N elemental data summarized in **Table 4.20** further supports the purity of **AD 25-48. Table 4.10** contains the physicochemical properties of **AD 25-48.**

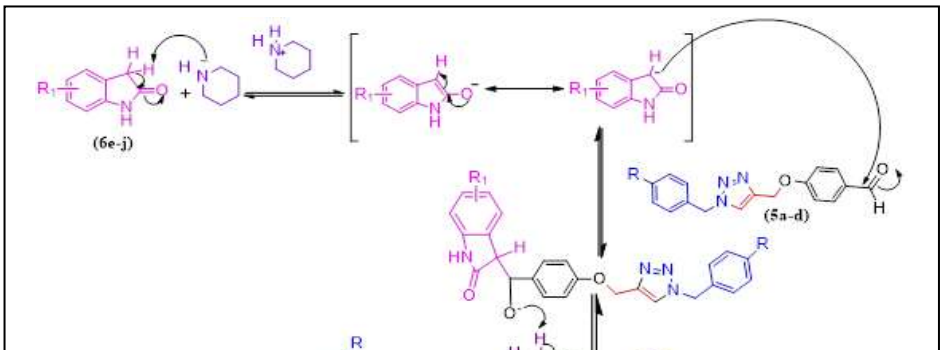

Figure 5.2: Reaction mechanism for synthesis of 3-(4-((1-benzyl-1H-1,2,3-triazol-4yl)methoxybenzylidene)indolin-2-ones86 (AD 25-48).

5.2 Biology:

1-Benzyl-4-((4-styrylphenoxy)methyl)-1*H*-1,2,3-triazoles (AD 1-24)

Irrespective of aromatic ring substitution, **AD 1-24** were found poor cytotoxic toward DND-41, K-562 and Z-138 cells. Moderate cytotoxicity was observed against Capan-1, HCT-116 and, NCI-H460 cells. Except for **AD-04, AD-07, AD-22** and, **AD-24** majority have displayed cytotoxicity between 31-96 μM against Capan-1 cells. The cytotoxicity against HCT-116 cells was observed between 12-87 μM. Molecule **AD-05, AD-08** and **AD-11** were most potent (IC_{50}:12-13 μM), while **AD-01, AD-07, AD-09, AD-17** and **AD-18** exerted moderate cytotoxicity (IC_{50}: 20-30 μM) against HCT-116 cells. The **AD-08, AD-18** and **AD-23,** were cytotoxic at 12-16 μM against NCI-H460 cells. Except **AD-07, AD-22** and **AD-24** rest of the molecules were cytotoxic at >30 μM against HCT-116. In case of acute DND-41, only **AD-01, AD-07** and **AD-15** cytotoxicity (60-80 μM). Against K-562 cells only **AD-01** and **AD-03** were active at 40 and 19 μM respectively. Similarly, for Z-138, only **AD-04** was cytotoxic (IC_{50}: 60 μM). In general, results summarized in **Table 4.21** suggest most of the compounds to

be cytotoxic against carcinoma cells but not towards leukemia and lymphoma cells. None of the compounds was as potent as the reference standards used in the study.

The ADME properties and drug-likeness violations of **AD 1-24** were calculated. Lipinski, Ghose, Veber, Ega, and, Muegge[87] filters were used to calculate ADME properties and the drug-likeness of **AD 1-24.** Not more than one violation is expected for an orally active drug. Data in **Table 4.22** show **AD 1-24** and STS meet these criteria. However, docetaxel violated all filters more than once (except the Muegge filter).

Fsp^3 is used to interpret the drug-likeness properties of a molecule[88]. The Fsp^3 values of **AD 1-24** were lower than docetaxel and STS. The ESOL values suggest moderate water solubility for all derivatives. Molecule **AD-03, AD-10, AD-15, AD-16, AD-19, AD-20, AD-21, AD-22, AD-23,** and **AD-24** are poorly water soluble (ESOL>-6). Log *Kp* represents the skin permeability of a molecule. The lower negative log *Kp* value suggests higher skin permeation. Results suggest high skin-permeability for all derivatives[89]. The F score/bioavailability[90] of synthesized derivatives and STS were found higher than docetaxel **(Table 4.22).**

The docking study for **AD 1-24** was performed on tubulin-docetaxel complex 1TUB. The **AD-08** and **AD-18** showed good *in-vitro* cytotoxicity and higher receptor affinity than the reference molecule docetaxel. The 2D and 3D interaction diagram shows the binding regions of **AD-08, AD-18,** STS and docetaxel with 1TUB receptor. STS had exhibited highest receptor affinity among all.

Compound **AD-08** has 3 coHB (conventional hydrogen bonds) and 1 caHB (carbon-hydrogen bond). Three electrostatic, 2 PA (pi-anion), 1 PC (pi-cation), 5 hydrophobic 1PT (pi-pi T-shaped), 3 PAI (pi-alkyl), and 1 halogen interaction was observed for

AD-08. On the other hand, compound **AD-18** has 1 coHB, 1 pdHB (pi-donor hydrogen bond), 1 PC, 2 PA, and 2 PT, 6 PAl, 1 Alkyl interaction.

The docetaxel has 3 coHB, 1 caHB, 1 PC, 1 PT, 2 PAl, 5 Al interactions, while, STS has 3 coHB, 1 caHB, 1 PC, 2 PAl, and, 4 PSt interactions **(Figures 4.15-4.18).**

3-(4-((1-benzyl-1*H*-1,2,3-triazol-4yl)methoxybenzylidene)indolin-2-ones (AD 25-48)

All synthesized derivatives **AD 25-48** were preliminarily screened against L1210, CEM, and HeLa cells. Compound, **7c/AD-30,** and **7w/AD-45** were found to be equipotent whereas **7b/AD-26, 7j/AD-34** and **7n/AD-39** exhibited poor cytotoxicity in comparison to melphalan. Against HeLa cells **7a/AD-25, 7c/AD-30, 7m/AD-37, 7o/AD-42, 7s/AD-43, 7v/AD-48** and **7w/AD-45** showed good cytotoxicity, whereas **7g/AD-32, 7h/AD-35, 7j/34, 7k/31, 7l/36, 7t/AD-44, 7u/AD-47** and **7x/AD-46** exhibited moderate cytotoxic activity. Moderate/poor cytotoxicity exhibited against L1210 cells by majority of molecules, except **7c/AD-30, 7o/AD-42** and **7v/AD-48.** A mechanism of action was established taking the most potent compound from the series **(7c/AD-30).** Drug likeness was predicted using the SwissADME webserver. Results were summarized in **Tables 4.23 and 4.24** and **Figures 4.19-4.29.**

Structure Activity Relationship (SAR): AD 25-48

Compounds **7a-x/AD 25-48** were less effective against L1210 cells in comparison to standard melphalan (2.13 µM). However, the introduction of a methyl group at position 5 of indolin-2-one, led to the most effective compounds, namely **7c/AD-27, 7o/AD-39,** and **7v/AD-46,** with IC_{50} 3.0, 5.3, and 4.8 µM respectively, against L1210 cells. Substituents different from the methyl group on indolin-2-one and benzyl group did not improve cytotoxicity against L1210 cells. Substitutions made at position 5, 6, or 7 on indolin-2-one and at position 4 on benzyl group (compounds **7c/AD-30, 7w/AD-45)** retained the cytotoxicity against CEM cells, except for **7b/AD-26, 7f/AD-**

27, 7j/AD-33, and **7r/AD-40.** In general, the replacement of hydrogen with -CH_3, -Cl, or -NO_2 at position 4 of the benzyl group, as well as a substitution at position 5, 6, or 7 on indolin-2-one, increased the cytotoxicity against HeLa cells.

Since **7c/AD-30** was found to be most potent against CEM leukemic cells, the preliminary cytotoxicity of **7c/AD-30** against different leukemic cells (HL-60, CEM, and Jurkat) was performed using a cytofluorimetric technique. Among all, Jurkat cells were found to be the most sensitive to **7c/AD-30** (data not shown) hence chosen further investigate its anticancer potential **(Table 4.23).**

Different cell-death modalities such as apoptosis (intrinsic & extrinsic), autophagy, and necrosis were defined based on morphological changes associated with specific mechanisms. Among all types, apoptosis is the most studied and known mechanism of cell demise. The extrinsic apoptotic pathway led to the activation of pro-caspase-8/10 while the intrinsic pathway led to irreversible and diffused mitochondrial outer membrane permeability causing the collapse of mitochondrial membrane potential and cell death.[91, 92]

In order to analyze if **7c/AD-30** triggers apoptotic or necrotic cell death, the annexin V/7-AAD assay was performed. After 24 h of treatment with **7c/AD-30** dose-dependent response was observed with increased the number of apoptotic cells. Apoptotic cells % started to increase from 2 μM (14% versus 3.9% in untreated cells), and further increased up to the highest tested concentration, where they reached about 27%. Alongside the increase in apoptotic cells, the percentage of necrotic cells remained constant between 3% and 7% at all tested concentrations[93] **(Figure 4.19).**

Caspase-3 is activation was observed following 7h treatment involving intrinsic and extrinsic pathway of apoptosis. Its activity markedly increased after treatment with **7c/AD-30,** up to about 8 times at 4 and 8 μM confirming apoptosis induction by

7c/AD-30. Involvement of extrinsic apoptotic process in pro-apoptotic property of **7c/AD-30,** activity of caspase-8 was evaluated and found to increase up to about 4 times at concentrations 4 and 8 µM after the treatment. To assess the involvement of the intrinsic apoptotic pathway, the decrease in mitochondrial transmembrane potential was measured. A significant increase in cells with reduced potential was recorded starting from concentration 4 µM, and the percentage further increased to about 46% at 8 µM. On the whole, our results indicate that **7c/AD-30** activates both apoptotic pathways **(Figure 4.20).** The ability of **7c/AD-30** to activate both apoptotic pathways is noteworthy and it could be a future lead against cancer.[94, 95]

In recent years, accumulating evidence increasingly pointed out that various non-apoptotic cell deaths process. Jurkat cells were treated with Z-VAD-FMK, ola, Nec-1s, Ferr-1, DFO, and Vit-E for 1 h to inhibit apoptosis, parthanatos, necroptosis and ferroptosis respectively to confirm canonical cell death. Then, after pre-treatment, cells were treated with **7c/AD-30** 8 µM for 24 h and 48 h and cell viability was analyzed by flow cytometry. Among all the pharmacological inhibitors, only Z-VAD-FMK increased Jurkat cell viability, just partially after 24 h and significantly after 48 h. The recorded cell viability of Z-VAD-FMK pre-treated cells was 82% at 24 h (versus 65% of **7c/AD-30** treated cells) and 55% at 48 h (versus 25% of **7c/AD-30** treated cells). Results indicate that **7c/AD-30** does not induce non-canonical cell death as ferroptosis, necroptosis, or parthanatos, but exclusively caspase-dependent apoptosis[96, 97] **(Figure 4.21).**

ROS plays a central role in cell signaling and represents one of many stimuli that leads to apoptotic cell death. Hence, intracellular ROS levels were measured after treatment with **7c/AD-30**. No significant modulation of ROS levels was observed

(Figure 4.22) indicating non-involvement of ROS in cytotoxic response of **7c/AD-30.**

Cell cycle is a coordinated molecular processes that control DNA replication and chromosome division via G1, S, G2, and M (Mitosis) phases. All phases of cell cycles were strictly controlled by cyclins and cyclin-dependent kinases. Since the G1/S and G2/M checkpoints finely control cell proliferation, cell-cycle arrest is considered one of the most common events triggering the inhibition of cell proliferation. Hence, to explore the cytostatic potential of **7c/AD-30** cell-cycle progression of **7c/AD-30** treated cells together with the expression of some cyclins and CDKs were analyzed. The treatment with increasing concentrations of **7c/AD-30** induced a significant accumulation of cells in G2/M stage. At 4 µM concentration cells accumulation was observed in G2/M stage of cell cycle while, decrease in G0/G1 cell population observed at 8 µM.

Further, after 24h of treatment, **7c/AD-30** did not modulate the expression of cyclin B1 and CDK1; however, a slight downregulation of cyclin A was observed **(Figure 4.23-25).** A decrease in cyclin A expression, but not a modulation of cyclin B and CDK1 was observed with **7c/AD-30** treatment suggesting blockade of cell-cycle progression during the transition from the G2 to the M phase, where cyclin A starts to be degraded prior to the entry of cells in mitosis[98] **(Figure 4.23-4.25).**

The pro-apoptotic and cytostatic activities of **7c/AD-30** were analyzed after 6 h of treatment to assess whether both events were related or independent from each other. At 6 h of treatment, no cell death was observed, while a substantial block of the cell cycle was reported suggesting **7c/AD-30** induced apoptosis as a secondary effect, related to its cytostatic activity.

Considering the potential anticancer activities of **7c/AD-27**, a preliminary assessment of its toxicological profile was performed. The genotoxicity of **7c/AD-30** was verified by analyzing the phosphorylation of H2A.X (P-H2A.X) at Serine 139. P-H2A.X is considered an early cellular response to DNA double-strand breaks. Following 5 h treatment of Jurkat cells with **7c/AD-30,** the increase in H2A.X phosphorylation was not seen, confirming no genotoxicity from **7c/AD-30**[99, 100] **(Figure 4.26).**

***In-silico study*:**

The MW, tPSA, MR, Fsp3, and hydrogen bonding properties of **7c/AD-30** were evaluated. tPSA is the sum of surface areas of polar atoms in a molecule and, is used to estimate the drug transport properties across the membrane. Lower tPSA values indicate a higher tendency for transport. The tPSA values obtained for all compounds were within the range recommended by various drug-likeness filters. Fsp3 values represent drug-likeness properties of molecules. Lower Fsp3 values observed for all derivatives. MR is defined as a measure of the overall polarity of a molecule and is found to be in the range of (40 to 130). LogP values are the most widely used measure of lipophilicity and represent an indicator of drug permeability to reach the target tissue in the body. The LogP values used by the different drug-likeness filters MLogP, WLogP, and XLogP. It is observed that the compounds **7t/AD-44** (XLogP=5.01), **7u/AD-47** (XLogP=5.08), **7w/AD-45** (XLogP=5.01), and **7x/AD-46** (XLogP=5.01) slightly exceed the acceptability limit (XLogP< 5) while other LogP values meet general standards. ESOL is an aqueous solubility parameter and is considered one of the key physical properties in drug discovery.[102] Moderate water solubility observed for all derivatives. To predict the drug-likeness properties of a molecule Lipinski, Ghose, Egan, Muegge, and, Veber (GSK) filters were used. Except **7 u/AD-47,** the

remaining molecules are following the rules of drug-likeness. The bioavailability score value of **7u/AD-47** was found to be 0.17 while, for other synthesized compounds, co-ligand and melphalan it was in the range of 0.55. The Log Kp are the skin permeation parameter. The higher negative LogKp value of the molecule indicates less skin penetration. Accordingly, all the synthesized derivatives had higher skin permeability than melphalan **(Table 4.24)**

Further, the bioavailability radar scheme predicted using the SwissADME web server allows a rapid and clearer assessment of drug similarity of compounds. In the radar scheme, the red-colored zone shows suitable physicochemical space for oral bioavailability of molecules by taking into criteria such as flexibility, lipophilicity, saturation, size, polarity, and solubility. According to the radar scheme, it is observed that all criteria except *In-situ* remain within the red-colored region **(Figure 4.27).**

Further, the molecular docking simulation was performed to evaluate the binding affinity of **AD 25-48** with the EGFR receptor. It was observed that all compounds had higher docking scores than co-ligand (10-benzyl-2-fluoro-5,10-dihydro-11*H*-dibenzo[b,e][1,4]diazepin-11-one), an inhibitor of the **6P8Q EGFR** receptor. Therefore, it can be inferred that these compounds could act as EGFR inhibitors.[103] When the values are examined, we also observe that docking affinity values are in good agreement with in vitro cytotoxicity results. The three compounds with the highest binding affinity are **7c/AD-30** (-11.1 kcal/mol), **7o/AD-42** (-11.5 kcal/mol), and **7v/AD-48** (-11.3 kcal/mol) while the two compounds with the lowest binding affinity are compounds **7d/AD-29** (-10.3 kcal/mol) and **7r/AD-40** (-10.4 kcal/mol). Considering both these results and in vitro cytotoxicity results, we displayed the 2D interaction of these compounds and co-ligand with the 6P8Q EGFR receptor. It is seen in the diagram that all of the compounds **7c/AD-30, 7o/AD-42,** and **7v/AD-48** have, in

common, hydrogen bonds with MET793 (Methionine-793), Pi-Sulfur with MET790, and Pi-Alkyl type interactions with LEU788, ALA743. These residues actively participate in binding. On the other hand, compounds **7p/AD-41** and **7r/AD-40** with the lowest binding affinity have common eight interactions with the 6P8Q receptor. These interactions are Pi-Sigma with ALA726 and LEU 858, Ala743, LEU777, LEU788, Pi-Alky with MET790, Pi-Anion with ASP855, and Pi-Sulfur with MET790. These common interactions could be an important finding for low binding affinity **(Figure 4.28)**

Due to the importance of hydrogen bonds in terms of the pharmacological properties of molecules, we also demonstrated the 3D interactions of the above-mentioned compounds and the co-ligand along with a hydrogen bond surface. From the figure, acceptor and donor surface areas can be seen easily **(Figure 4.29).**

Further, results summarized in **Tables 4.25-4.27** and **Figures 4.30-4.32** found none of the tested derivatives as anti-tubercular in nature. The MIC, IC_{50} and, IC_{90} values of tested derivatives were found to be >200 µM compared to reference rifampicin (0.00047-3.7 µM) against *M. tuberculosis, M. abscessus* and, *M. avium.*

6.0 SUMMARY

- A total of, forty-eight 1,2,3-triazole derivatives **(AD 1-48)** were synthesized.
- The triazole-benzaldehydes **(7a-d)** were reacted with triphenylphosphonium halide **(6a-f)** to get 1-benzyl-4-((4-styrylphenoxy)methyl)-1*H*-1,2,3-triazoles **(AD 1-24).**
- The triazole-indolin-2-one analogs **(AD 25-48)** were obtained by reacting **7a-d)** and 2-oxindole **(13a-f).**
- Structure and purity of synthesized derivatives were confirmed by TLC, FTIR, NMR (^{1}H &^{13}C), and LCMS data.
- *In-vitro* cytostatic assays were performed against human and murine cancerous cells.
- Selective toxicity and mechanism of action were predicted by taking active molecules from the series **(AD-8, 18 & AD-30).**
- To understand the molecular basis of action, *In-silico* studies were performed on tubulin heterodimer **(1TUB)** and EGFR receptor **(6P8Q).**
- Results suggest **AD-8, 18** & **AD-30** as a potential lead against cancer. However, none of these were similar in potency to standard melphalan, STS, and docetaxel in potency. Hence, further study is required in this aspect.
- None of the tested derivatives were anti-tubercular in nature.

7.0 CONCLUSION

A total of, twenty-four resveratrol-linked 1,2,3-triazoles **(AD 1-24)** were synthesized, characterized, and, screened for *in-vitro* cytotoxicity. The compounds were selective towards carcinoma cells. Docking simulations were performed with the 1TUB receptor. Molecules **AD-08** and **AD-18** showed good *in-vitro* cytotoxicity and better 1TUB affinity. The four H-bonding, three electrostatic, five hydrophobic, and one halogen interactions were observed with **AD-08** while, two H-bondings, three electrostatic, and nine hydrophobic interactions were involved in **AD-18-1TUB** interactions. Even though the molecules exhibited promising cytotoxic properties structural optimization is needed for better results.

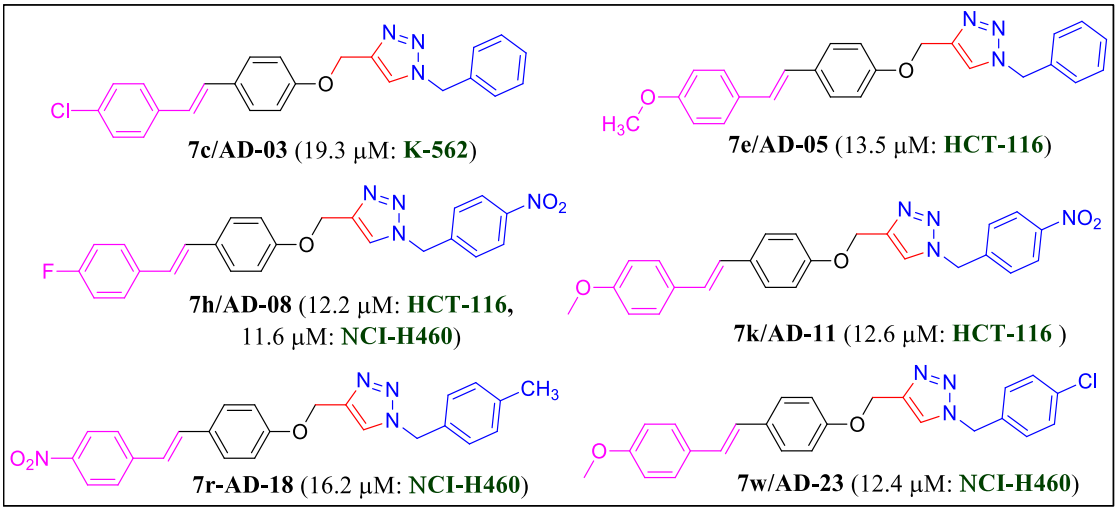

A series of indolin-2-one (2-oxindole) fused 1,2,3-triazoles **(AD 25-48)** were obtained in good yield and evaluated for their cytotoxicity after due characterization. Most of the compounds were active against CEM and HeLa cells (IC_{50}: 1.5-67 µM & 3.4-133 µM respectively, whereas, **7a/AD-25, 7c/AD-30, 7o/AD-42,** and **7v/AD-48** showed cytotoxicity between 3-8.1 µM against L1210 cells. Compound **7c/AD-30**(IC_{50}: 1.5µM) was found to be equipotent with standard melphalan (IC_{50}: 1.4 µM), hence, selected for further studies. A study on Jurkat cells revealed that **7c/AD-30** induced apoptosis by activating intrinsic and extrinsic pathways. **7c/AD-30** was found

to block cancer cell proliferation. No genotoxicity was observed by **7c/AD-30**. Further, a good coherence was observed between docking simulation and *in-vitro* cytotoxicity results. All compounds were found to have higher docking scores than the co-ligand. *In-silico* study showed that MET793, MET790, LEU788, and ALA743 residue of the **6P8Q EGFR** receptor involved in interactions with **7c/AD-30, 7o/AD-**39, and **7v/AD-48.** Structure-activity relationship study found the presence of the -CH_3 group is preferred at position 5 of indolin-2-one against murine L1210 cells and, the substitution on positions 5, 6, or 7 of indoline-2-one increases cytotoxicity against HeLa cells.

Based on biological data it was found that molecule **7c/AD-30** & **7w/AD-45** have the potential to become a lead against cancer (CEM cell lines). Further study is warranted to establish it. However, the synthesized derivatives fail to exert anti-mycobacterial properties during the study.

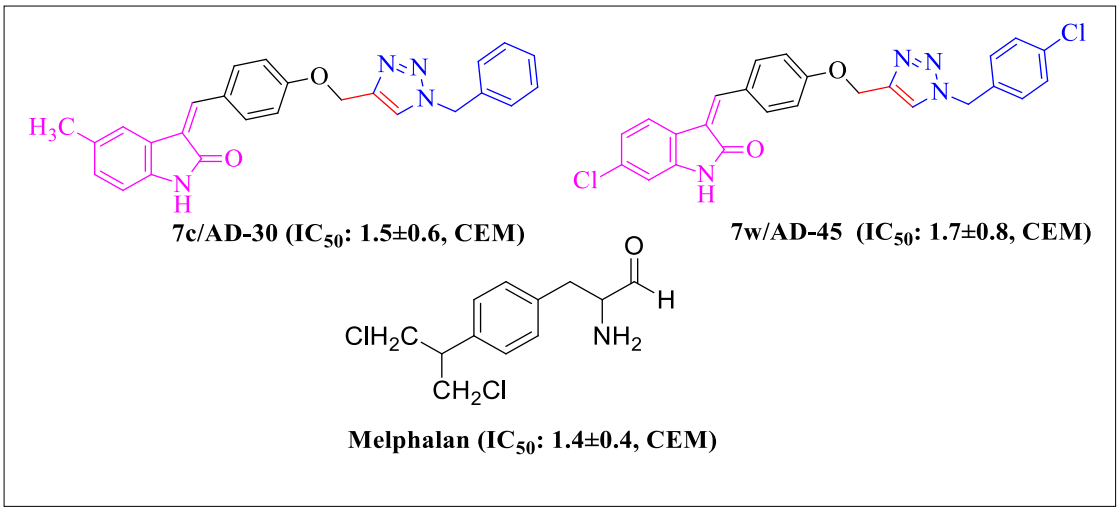

8.0 REFERENCES

1. World Health Organization. Cancer. Overview. Accessed on December 24, 2022. https://www.who.int/health-topics/cancer.
2. Anand P, Kunnumakara AB, Sundaram C, et al. Cancer is a preventable disease that requires major lifestyle changes. *Pharm Res.* 2008;25:2097-2116. doi.10.1007/s11095-008-9661-9.
3. Varghese C. 50 Years of cancer control in India. Cancer prevention and control in India. Accessed on December 24, 2022. https://main.mohfw.gov. in/sites/default/files/Cancer.
4. Sathishkumar K, Chaturvedi M, Das P et al. Cancer incidence estimates for 2022 & projection for 2025: Result from National Cancer Registry Programme, India. *Indian J Med Res.* 2022. doi/10.4103/ijmr.ijmr_1821_22.
5. Cancer Treatment Centers of America. What is cancer? Accessed on December 24, 2022.https://www.cancercenter.com/what-is-cancer.
6. Richard AH. Lippincott's Illustrated Reviews: Pharmacology. 5th ed. Wolter-Kluwer;2012.
7. Calabresi P, Chabner BA. Chemotherapy of neoplastic diseases. In: Hardman J, Limbird LE, Gilman AG, ed. Goodman and Gilman's, The Pharmacologic Basis of Therapeutics. 10th ed. McGraw-Hill Medical Publishing Division; 2001:1381-8.
8. World Health Organization. Tuberculosis. Updated October 27, 2022. Accessed December 24, 2022. https://www.who.int/news-room/fact-sheets/detail/ tuberculosis.
9. Chandna H. TB cases down but India still has 27% of all global patients, tops WHO list. ThePrint. October 18, 2019. Accessed January 12, 2020. https://theprint.in/health/tb-cases-down-india-27-global-who-list/307755.

10. Bill and Melinda Gates Foundation. India announces plan to end tuberculosis by 2025. Accessed December 24, 2022. https://www.gatesfoundation.org/ideas/articles/india-announces-plan-to-end-tuberculosis-by-2025.
11. Martins P, Jesus J, Santos S, et al. Heterocyclic anticancer compounds: recent advances and the paradigm shift towards the use of nanomedicine's tool box. *Molecules* 2015;20:16852-91. doi.org/10.3390/molecules200916852.
12. Bozorov K, Zhao J, Aisa HA. 1,2,3-Triazole-containing hybrids as leads in medicinal chemistry: A recent overview. *Bioorg Med Chem.* 2019;27:3511-31. doi.org/10.1016/j.bmc.2019.07.005.
13. Kumar D, Beena, Khare G, et al. Synthesis of novel 1,2,3-triazole derivatives of isoniazid and their *in-vitro* and *in-vivo* antimycobacterial activity evaluation. *Eur J Med Chem.* 2014;23:301-13. doi:10.1016/j.ejmech.2014.05.005.
14. Bonandi E, Christodoulou MS, Fumagalli G, et al. The 1,2,3-triazole ring as a bioisostere in medicinal chemistry. *Drug Discov Today.* 2017;22:1572-81. doi:10.1016/j.drudis.2017.05.014.
15. Kaushik NK, Kaushik N, Attri P, et al. Biomedical Importance of Indoles. *Molecules* 2013;18:6620-62. doi:10.3390/molecules18066620.
16. Iyer D, Vartak SV, Mishra A. Identification of a novel BCL2-specific inhibitor that binds predominantly to the BH1 domain. *FEBS J.* 2016;283:3408-37. doi.org/10.1111/ febs.13815K.
17. Koushki M, Dashatan AN, Ahmadi N, et al. Resveratrol: A miraculous natural compound for diseases treatment. *Food Sci Nutr*. 2018;6:2473-90.doi.org/10.1002/fsn3.855.

18. Loureiro JA, Andrade S, Duarte A, et al. Resveratrol and grape extract-loaded solid lipid nanoparticles for the treatment of Alzheimer's disease. *Molecules* 2017;22:277. doi.org/10.3390/molecules22020277.
19. Salehi B, Mishra AP, Nigam M, et al. Resveratrol: A double-edged sword in health benefits. *Biomedicines.* 2018;6:91. doi.org/10.3390/biomedicines6030091.
20. Ahmed NS, Samec M, Liskova A et al. Tamoxifen and oxidative stress: an overlooked connection. *Discov Oncol*. 2021;12:17. doi.org/10.1007/s12672-021-00411-y.
21. Othman EM, Fayed EA, Husseiny EM, et al. The effect of novel synthetic semicarbazone- and thiosemicarbazone-linked 1,2,3-triazoles on the apoptotic markers, VEGFR-2, and cell cycle of myeloid leukemia. *Bioorg Chem.* 2022; 127:105968. doi.org/10.1016/j.bioorg.2022.105968.
22. Aouad MR, Almehmadi MA, Albelwi FF, et al. Targeting the interplay between MMP-2, CA II and VEGFR-2 via new sulfonamide-tethered isomeric triazole hybrids; Microwave-assisted synthesis, computational studies and evaluation. *Bioorg Chem.* 2022;124:105816. doi.org/101016/j.bioorg.2022.105816.
23. Tan A. Synthesis, spectroscopic characterization of novel phthalimides derivatives bearing 1,2,3-triazole unit and examination as potential SARS-CoV-2 inhibitors via *in-silico* studies. *J Mol Struct*. 2022;1261:132915. doi.org/10.1016/j.molstruc. 2022.132915.
24. Mlaki´c M, Faraho I, Odak I, et al. Synthesis, photochemistry and computational study of novel 1,2,3-triazole hetero stilbenes: Expressed biological activity of their electrocyclization photoproducts. *Bioorg Chem.* 2022;121:105701. doi.org/10. 1016/j.bioorg.2022.105701.

25. Narul Y, Acar I, Yetkin D, et al. Synthesis of novel immunomodulatory 1,4-disubstituted bis-1,2,3-triazoles by using click chemistry and their intracellular mechanism of action. *Bioorg Med Chem Lett*. 2022;69:128800. doi.org/10.1016/j.bmcl.2022.128800.
26. Oubellaa A, Mansouri E, Fawzi M, et al. Thiazolidinone-linked1,2,3-triazoles with monoterpenic skeleton as new potential anticancer agents: Design, synthesis and molecular docking studies. *Bioorg Chem.* 2021;115:105184. doi.org/10.1016/j.bioorg.2021.105184.
27. Abbouchi EA, Brahmi EN, Hiebel MA et al. Synthesis and evaluation of a novel class of ethacrynic acid derivatives containing triazoles as potent anticancer agents. *Bioorg Chem.* 2021;115:105293. doi.org/10.1016/j.bioorg.2021.105293.
28. Kumar CBP, Prathibha BS, Prasad KNN, et al. Click synthesis of 1,2,3-triazole based imidazoles: Antitubercular evaluation, molecular docking and HSA binding studies. *Bioorg Med Chem Lett*. 2021;36:127810. doi.org/10.1016/j.bmcl.2021.127810.
29. Oliveira VNM, Moura CFA, Peixoto AS, et al. Synthesis of alkynylated 1,2,4-oxadiazole/1,2,3-1*H*-triazole glycoconjugates: Discovering new compounds for use in chemotherapy against lung carcinoma and Mycobacterium tuberculosis. *Eur J Med Chem.* 2021;220:113472. doi.org/10.1016/j.ejmech.2021.113472.
30. Ashour HF, Abou-Zeid LA, El-Sayed MAA et al. 1,2,3-Triazole-Chalcone hybrids: Synthesis, in vitro cytotoxic activity and mechanistic investigation of apoptosis induction in multiple myeloma RPMI-8226. *Eur J Med Chem.* 2020;189:112062. doi.org/10.1016/j.ejmech.2020.112062.
31. Kaur R, Singh R, Kumar A, et al. *Heliyon* 1,2,3-Triazole β-lactam conjugates as antimicrobial agents. 2020;6:e04241. doi.org/10.1016/j.heliyon.2020.e04241.

32. Pasupuleti BG, Khongsti K, Das B, et al. 1,2,3-Triazole tethered 1,2,4-trioxanes: Studies on their synthesis and effect on osteopontin expression in MDA-MB-435 breast cancer cells. *Eur J Med Chem,* 2020;186:111908. doi.org/10.1016/j.ejmech. 2019.111908.
33. Pinheiro S, Pessôa JC, Pinheiro EMC, et al. 2*H*-1,2,3-Triazole-chalcones as novel cytotoxic agents against prostate cancer. *Bioorg Med Chem Lett*. 2020;30:127454. doi.org/10.1016/j.bmcl.2020.127454.
34. Holanda VN, da Silva WV, do Nascimento PH, et al. Antileishmanial activity of 4-phenyl-1-[2-(phthalimido-2-yl)ethyl]-1H-1,2,3-triazole (PT4) derivative on *Leishmania amazonensis* and *Leishmani abraziliensis*: *In silico* ADMET, *in vitro* activity, docking and molecular dynamic simulations. *Bioorg Chem*. 2020;105:104437. doi.org/10.1016/j.bioorg.2020.104437.
35. Reddyrajula R, Dalimba U. The bioisosteric modification of pyrazin amide derivatives led to potent antitubercular agents: Synthesis via click approach and molecular docking of pyrazine-1,2,3-triazoles. *Bioorg Med Chem Lett*. 2020;30:126846. doi.org/10.1016/j.bmcl.2019.126846.
36. Gao F, Ye L, Kong F, et al. Design, synthesis and antibacterial activity evaluation of moxifloxacin amide-1,2,3-triazole-isatinhybrids. *Bioorg Chem.* 2019;91:103162. doi.org/10.1016/j.bioorg.2019.103162.
37. Khan MF, Anwer T, Bakht A, et al. Unveiling novel diphenyl-1*H*-pyrazole based acrylates tethered to 1,2,3-triazoleas promising apoptosis inducing cytotoxic and anti-inflammatory agents. *Bioorg Chem.* 2019;87:667-78. doi.org/10.1016/j. bioorg.2019.03.071.

38. Nalawade J, Shinde A, Chavan A, et al. Synthesis of new thiazolyl-pyrazolyl-1,2,3-triazole derivatives as potential antimicrobial agents. *Eur J Med Chem.* 2019;197:649-59. doi.org/10.1016/j.ejmech.2019.06.074.
39. Hussain M, Qadri T, Hussain Z, et al. Synthesis, antibacterial activity and molecular docking study of vanillin derived 1,4-disubstituted 1,2,3-triazoles as inhibitors of bacterial DNA synthesis. *Heliyon.* 2019;5:e02812. doi.org/10.1016/j. heliyon.2019.e02812.
40. Kumar PP, Siva B, Rao BV, et al. Synthesis and biological evaluation of bergenin-1,2,3-triazolehybrids as novel class of anti-mitotic agents. *Bioorg Chem.* 2019;91:103161. doi.org/10.1016/j.bioorg.2019.103161.
41. Raju KS, Reddy SA, Sabitha G, et al. Synthesis and biological evaluation of 1*H*-pyrrolo[2,3-d]pyrimidine-1,2,3-triazole derivatives as novel anti-tubercular agents. *Bioorg Med Chem Lett.* 2019;29:284-90. doi.org/10.1016/j.bmcl.2018.11.036.
42. Queiroz TM, Orozco EVM, Silva VR, et al. Semi-synthesis of β-keto-1,2,3-triazole derivatives from ethinylestradiol and evaluation of the cytotoxic activity. *Heliyon.* 2019;5:e02408.doi.org/10.1016/j.heliyon.2019.e024 08.
43. Baharloui M, Mirshokraee SA, Monfared A, et al. Design and synthesis of novel triazole-based peptide analogues as anticancer agents. *Iran J Pharm Res*. 2019;18:e126183. doi.10.22037/ijpr.2019.111722.13320.
44. Srivastava S, Bimal D, Bohra K, et al. Synthesis and antimycobacterial activity of 1-(β-d-ribofuranosyl)-4-coumarinyloxymethyl-/-coumarinyl-1,2,3-triazole. *Eur J Med Chem*. 2018;150:268-81.doi.org/10.1016/j.ejmech.2018.02.067.
45. Lal K, Yadav P, Kumar A, et al. Design, synthesis, characterization, antimicrobial evaluation and molecular modeling studies of some dehydro acetic acid-chalcone-

1,2,3-triazole hybrids. *Bioorg Chem.* 2018;77:236-44. doi.org/10.1016/j.bioorg. 2018.01.016.

46. Sayeed IB, Vishnuvardhan MVPS, Nagarajan A, et al. Imidazopyridine linked triazoles as tubulin inhibitors, effectively triggering apoptosis in lung cancer cell line. *Bioorg Chem.* 2018;80:714-20. doi.org/10.1016/j.bioorg.2018.07.026.
47. Yadav P, Lal K, Kumar L, et al. Synthesis, crystal structure and antimicrobial potential of some fluorinated chalcone-1,2,3-triazole conjugates. *Eur J Med Chem.* 2018;155:263-74. doi.org/10.1016/j.ejmech.2018.05.055.
48. Sakly R, Edziri H,Askri M, et al. One-pot four-component domino strategy for the synthesis of novel spirooxindole-pyrrolidine/pyrrolizidine-linked 1,2,3-triazole conjugates via stereo- and regioselective [3+2] cycloaddition reactions: In vitro antibacterial and antifungal studies. *Comptes Rendus Chimie* 2018;21:41-53. doi.org/10.1016/j.crci.2017.11.009.
49. Tokala R, Bale S, Janrao IP, et al. Synthesis of 1,2,4-triazole-linked urea/thiourea conjugates as cytotoxic and apoptosis inducing agents. *Bioorg Med Chem Lett*. 2018;28:1919-24. doi.org10.1016/j.bioorg.2018.01.016.
50. Hong L, Lin W, Zhang F, et al. Ln[N(SiMe3)2]3-catalyzed cycloaddition of terminal alkynes to azides leading to 1,5-disubstituted 1,2,3- triazoles: new mechanistic features. *Chem Commun*. 2013; 49:5589-91. doi.org/10.1039/ C3CC42534G.
51. Karki SS, Bhutle SR, Pedgaonkar GS, et al. Synthesis and biological evaluation of some stilbene-based analogues. *Med Chem Res.* 2011;20:1158-63. doi.org/10.1007/s00044-010-9450-y.

52. Karki SS, Bhutle SR, Sahoo S, et al. Synthesis and biological evaluation of some stilbene derivatives. *Med Chem Res*. 2011;20:1349-56. doi.org/10.1007/s00044-010-9484-1.

53. Soriano DS. Example of the Wolff-Kishner reduction procedure suitable for an undergraduate organic lab experiment: Preparation of oxindole. *J Chem Educ.* 1993;70:332. doi.org/10.1021/ed070p332.

54. Atulya, N, Guntuku L, Guggilapu SD, et al. Synthesis and apoptosis inducing studies of triazole linked 3-benzylidene isatin derivatives. *Eur J Med Chem.* 2016;124:782-93. doi.org/10.1016/j.ejmech.2016.09.009.

55. Pavić K, Perković I, Gilja P, et al. Design, synthesis and biological evaluation of novel primaquine-cinnamic acid conjugates of the amide and acylsemicarbazide type. *Molecules*. 2016;21:1629. doi.org/10.3390/molecules21121629.

56. Montero AMD, Fossell FMD, Hortobagyi MD et al. Docetaxel for treatment of solid tumours: a systematic review of clinical data. *Lancet Oncol*. 2005;6:229-39. doi.org/10.1016/S1470-2045(05)70094-2.

57. Gescher A. Analogs of staurosporine: potential anticancer drugs? *Gen Pharmacol-Vasc S.* 1998;31:721-28. doi.org/10.1016/S0306-3623(98)00069-X.

58. Kumar S, Hegde M, Gopalakrishnan V, et al. 2-(4-Chlorobenzyl)-6-aryl imidazo[2,1-b][1,3,4]thiadiazoles: Synthesis, cytotoxic activity and mechanism of action. *Eur J Med Chem.* 2014;84,687-97. doi.org/10.1016/j.ejmech.2014.07.054.

59. Kumar S, Hegde M, Gopalakrishnan V, et al. Synthesis and antiproliferative activity of imidazo[2,1-b][1,3,4]thiadiazole derivatives. *Bioorg Med Chem Lett.* 2014;24:4682-88. doi.org/10.1016/j.bmcl.2014.08.032.

60. Daina A, Michielin O, Zoete V. iLOGP: a simple, robust, and efficient description of n-octanol/water partition coefficient for drug design using the GB/SA approach. *J Chem Inf Model.* 2014;54:3284-301. doi.org/10.1021/ci500467k.
61. Daina A, Michielin O, Zoete V. SwissADME: a free web tool to evaluate pharmacokinetics, drug-likeness and medicinal chemistry friendliness of small molecules. *Sci Rep.* 2017;7:42717. doi.org/10.1038/srep42717.
62. Hanwell MD, Curtis DE, Lonie DC, et al. Avogadro: an advanced semantic chemical editor, visualization, and analysis platform. *J Cheminform.* 2012;4:17. doi.org/10.1186/1758-2946-4-17.
63. Nicholls A. What do we know and when do we know it? *J Comput Aided Mol Des*. 2008; 22:239-55. doi.org/10.1007/s10822-008-9170-2.
64. Trott O, Olson AJ. AutoDock Vina: improving the speed and accuracy of docking with a new scoring function, efficient optimization, and multithreading. *J Comput Chem*. 2010;31:455-61. doi.org/10.1002/jcc.21334.
65. Solis FJ, Wets RJB. Minimization by random search techniques. *Math Oper Res*. 1981;6:19-30. doi.org/10.1287/moor.6.1.19.
66. Huey R, Morris GM, Olson AJ, et al. A semiempirical free energy force field with charge-based desolvation. *J Comput Chem* 2007;28:1145-52. doi.org/10.1002/jcc. 20634.
67. Dassault Systèmes. Biovia Discovery Studio: comprehensive predictive science for the life sciences. Accessed on August 20, 2018. https://www.3ds.com/products-services/biovia/products/molecular-modeling-simulation.
68. Nogales E, Wolf SG, Downing KH. Erratum: structure of the αβ tubulin dimer by electron crystallography. *Nature.* 1998;391:199-203.

69. Baraldi PG, Nunez C, Tabrizi M, et al. Design, synthesis, and biological evaluation of hybrid molecules containing α-methylene-γ-butyrolactones and polypyrrole minor groove binders. *J Med Chem.* 2004;47:2877-86. doi.org/10.1021/jm 031104y.

70. Bradford MM. A rapid and sensitive method for the quantitation of microgram quantities of protein utilizing the principle of protein-dye binding. *Anal Biochem.* 1976;72:248-54. doi.org/10.1016/0003-2697(76)90527-3.

71. Bevan CD, Lloyd RS. A high-throughput screening method for the determination of aqueous drug solubility using laser nephelometry in microtiter plates. *Anal Chem*. 2000;72:1781-7. doi.org/10.1021/ac9912247.

72. Ollinger J, Bailey MA, Moraski GC, et al. A dual read-out assay to evaluate the potency of compounds active against *Mycobacterium tuberculosis*. *PLOS One*. 2013:8:e60531. doi.org/10.1371/journal.pone.0060531.

73. Lambert RJ, Pearson J. Susceptibility testing: accurate and reproducible minimum inhibitory concentration (MIC) and non-inhibitory concentration (NIC) values. *J Appl Microbiol.* 2000;88:788-90. doi.org/10.1046/j.1365-2672.2000.01017.x.

74. Franzblau SG, Witzig RS, McLaughlin JC, et al. P. Rapid, low-technology MIC determination with clinical *Mycobacterium tuberculosis* isolates by using the microplate Alamar Blue Assay. *J Clin Microbiol*. 1998;36:362-6. doi.org/10.1128/JCM.36.2.362-366.1998.

75. Simeonov A, Jadhav A, Thomas CJ, et al. Fluorescence spectroscopic profiling of compound libraries. *J Med Chem.* 2008;51:2363-71. doi.org/10.1021/jm701301m.

76. Zelmer A, Carroll P, Andreu N, et al. A new in vivo model to test anti-tuberculosis drugs using fluorescent imaging. *J Antimicrob Chemother*. 2012. 67:1948-60. doi.org/10.1093/jac/dks161.

77. Carroll P, Schreuder LJ, Karugaba JM, et al. Sensitive detection of gene expression in mycobacteria under replicating and non-replicating conditions using optimized far-red reporters. *PLoS One*. 2010. 5(3):e9823. doi.org/10.1371/journal.pone. 0009823.

78. Lipinski CA, Lombardo F, Dominy BW, et al. Experimental and computational approaches to estimate solubility and permeability in drug discovery and development settings. *Adv Drug Deliv Rev.*1997;23:3-25. doi.org/10.1016/S0169-409X(96)00 423-1.

79. Ghose AK, Viswanadhan VN, Wendoloski JJ. A knowledge-based approach in designing combinatorial or medicinal chemistry libraries for drug discovery. 1. A qualitative and quantitative characterization of known drug databases. *J Comb Chem.* 1999;1:55-68. doi.org/10.1021/cc9800071.

80. Veber DF, Johnson SR, Cheng HY, et al. Molecular properties that influence the oral bioavailability of drug candidates. *J Med Chem*. 2002;45:2615-23. doi.org/10.1021/jm020017n.

81. Egan WJ, Merz KM, Baldwin JJ. Prediction of drug absorption using multivariate statistics. *J Med Chem*. 2000;43:3867-77. doi.org/10.1021/jm 000292e.

82. Srivastava V, Lee H. Synthesis and bio-evaluation of novel quinolino-stilbene derivatives as potential anticancer agents. *Bioorg Med Chem Lett*. 2015;23:7629-40. doi.org/10.1016/j.bmc.2015.11.007.

83. Duan YC, Guan YY, Zhai XY, et al. Discovery of resveratrol derivatives as novel LSD1 inhibitors: design, synthesis and their biological evaluation. *Eur J Med Chem*. 2017;126:246-58. doi.org/10.1016/j.ejmech.2016.11.035.

84. Pavia DL, Lampman GM, Kriz GS. Introduction to spectroscopy: A guide for students of organic chemistry. 3rd ed. Thomson Learning;2001.

85. Maryanoff BE, Reitz AB, Mutter MS, et al. Stereochemistry and mechanism of the Wittig reaction. Diasteromeric reaction intermediates and analysis of the reaction course. *J Am Chem Soc*. 1986;108:7664-78. doi.org/10.1021/ja00284a034.

86. Dalessandro EV, Collin H, Guimaraes LGL, et al. Mechanism of the piperidine-catalyzed Knoevenagel condensation. Reaction in methanol: the role of iminium and enolate ions. *J Phys Chem*. 2017;121:5300-07. doi.org/10.1021/acs.jpcb.7b 03191.

87. Muegge I, Heald SL, Brittelli D. Simple selection criteria for drug-like chemical matter. *J Med Chem.* 2001;44:1841-6. doi.org/10.1021/jm015507e.

88. Lovering F, Bikker J, Humblet C. Escape from flatland colon increasing saturation as an approach to improving clinical success. *J Med Chem*. 2009;52:6752-6. doi.org/10.1021/jm901241e.

89. Potts RO, Guy RH. Predicting skin permeability. *Pharm Res*. 1992;9:663-9. doi.org/10.1023/a:1015810312465.

90. Martin YC. A bioavailability score. *J Med Chem.* 2005;48:3164-70. doi.org/10.1021/jm0492002.

91. Galluzzi L, Vitale I, Aaronson SA, et al. Molecular mechanisms of cell death: recommendations of the nomenclature committee on cell death. *Cell Death Differ*. 2018;25:486-541. doi.org/10.1038/s41418-017-0012-4.

92. Greco G, Catanzaro E, Fimognari C. Natural products as inducers of non-canonical cell death: a weapon against cancer. *Cancers.* 2021;13:1-64. doi.org/10.3390/ cancers13020304.

93. D'Arcy MS. Cell death: a review of the major forms of apoptosis, necrosis and autophagy. *Cell Biol Int.* 2019;43:582-92. doi.org/10.1002/cbin.11137.

94. Mohammad RM, Muqbil I, Lowe L, et al. Broad targeting of resistance to apoptosis in cancer. *Semin. Cancer Biol*. 2015;35:S78-103. doi.org/10.1016/j.sem cancer.2015.03.001.

95. Fulda S. Tumor resistance to apoptosis. *Int J Cancer*. 2009;124:511-15. doi.org/ 10.1002/ijc.24064.

96. Zimmermann M, Meyer N. Annexin V/7-AAD staining in keratinocytes. In: Stoddart MJ (Ed). Mammalian cell viability: methods and protocols. Humana Press;2011:57-63. doi.org/10.1007/978-1-61779-108-6_8.

97. Nagata S. Apoptosis and clearance of apoptotic cells. *Annu Rev Immunol.* 2018;36:489-517. doi.org/10.1146/annurev-immunol-042617-053010.

98. Hochegger H, Takeda S, Hunt T. Cyclin-dependent kinases and cell-cycle transitions: does one fit all? *Nat Rev Mol Cell Biol*. 2008;9:910-16. doi.org/10.1038/nrm2510.

99. Mah LJ, El-Osta A, Karagiannis TC. γH2AX: A sensitive molecular marker of DNA damage and repair. *Leukemia.* 2010;24:679-86. doi.org/10.1038/leu.2010.6.

100. Nohmi T. Thresholds of genotoxic and non-genotoxic carcinogens. *Toxicol Res.* 2018;34:281-90. doi.org/10.5487/TR.2018.34.4.281.

101. Cornwell BS, Bandaru SSM, Napierkowski M, et al. Pentathiepins: A novel class of glutathione peroxidase 1 inhibitors that induce oxidative stress, loss of mitochondrial membrane potential and apoptosis in human cancer cells. *Chem Med Chem.* 2020;15:1515-28. doi.org/10.1002/cmdc.202000160.

102. Delaney JS. ESOL: Estimating aqueous solubility directly from molecular structure. *J Chem Inf*. 2004;44:1000-05. doi.org/10.1021/ci034243x.

103. Wykosky J, Fenton T, Furnari F, et al. Therapeutic targeting of epidermal growth factor receptor in human cancer: successes and limitations. *Chin J Cancer*. 2011;30:5-12. doi.org/10.5732/cjc.010.10542.

9.0 ANNEXURE

- **List of Publications:**

1. Das A, Greco G, **Kumar S,** Catanzaro E, Morigi R, Locatelli A, Schols D, Alici H, Tahtaci H, Ravindran F, Fimognari C, Karki S.S. Synthesis, *in-vitro* cytotoxicity, molecular docking and ADME study of some indolin-2-one linked 1,2,3-triazole derivatives. *Computational Biology and Chemistry.* 2022;97:107641. https://doi.org/10.1016/j.compbiolchem.2022.107641. **(Q2, I.F: 3.737)**

2. Das A, Kumar S, Persoons L, Daelemans D, Schols D, Alici H, Tahtaci H, Karki, S.S. Synthesis, *in-silico* ADME, molecular docking and in vitro cytotoxicity evaluation of stilbene linked 1,2,3-triazoles. *Heliyon*. 2021;7:e05893. doi.org/10.1016/j.heliyon.2020.e05893. **(Q1, I.F: 3.776)**

Computational Biology and Chemistry 97 (2022) 107641

Contents lists available at ScienceDirect

Computational Biology and Chemistry

journal homepage: www.elsevier.com/locate/cbac

Synthesis, *in vitro* cytotoxicity, molecular docking and ADME study of some indolin-2-one linked 1,2,3-triazole derivatives

Arnika Das [a,1], Giulia Greco [b,1], Sujeet Kumar [a], Elena Catanzaro [b], Rita Morigi [d], Alessandra Locatelli [d], Dominique Schols [c], Hakan Alici [e], Hakan Tahtaci [f], Febina Ravindran [g], Carmela Fimognari [b,*], Subhas S. Karki [a,*]

[a] *Department of Pharmaceutical Chemistry, Dr.Prabhakar B Kore Basic Science Research Centre, Off-Campus, KLECollege of Pharmacy, (A Constituent unit of KAHER-Belagavi), Bengaluru 560010, Karnataka, India*
[b] *Department for Life Quality Studies, Alma Mater Studiorum – Università di Bologna, Rimini, Italy*
[c] *Rega Institute for Medical Research, Department of Microbiology, Immunology and Transplantation, Laboratory of Virology and Chemotherapy, KU Leuven, B-3000 Leuven, Belgium*
[d] *Department of Pharmacy and Biotechnology, Alma Mater Studiorum-Università di Bologna, Italy*
[e] *Department of Physics,Faculty of Arts and Sciences, Zonguldak Bulent Ecevit University, 67100 Zonguldak, Turkey*
[f] *Department of Chemistry, Faculty of Science, Karabuk University, 78050 Karabuk, Turkey*
[g] *Institute of Bioinformatics and Applied Biotechnology, Electronic city phase 1, Bangalore 560100, Karnataka, India*

ARTICLE INFO

Key words:
Indolin-2-one
Cytotoxicity
Apoptosis
Cell cycle
Molecular docking
EGFR
1,2,3-Triazole

ABSTRACT

In pursuit of an anticancer lead, a library of 1,2,3-triazole derivatives (**7a-x)** was prepared, characterized and screened for *in vitro* cytotoxicity in different cell lines. Most of the compounds proved to be cytotoxic with IC_{50} values in the low micromolar range. Further studies showed that the most active compound **7c** induces caspase-dependent apoptosis in Jurkat cells by activating both the intrinsic and the extrinsic apoptotic pathways and perturbs cell-cycle progression. Moreover, **7c** did not show any genotoxic activity. Molecular docking simulations were performed against epidermal growth factor receptor (EGFR). Docking experiments showed that, compounds **7c**, **7o** and **7 v** bind within active sites of epidermal growth factor receptor EGFR (Pdb ID: 6P8Q) by strong hydrogen bonds with residue *MET793*, Pi-Sulfur with residue *MET790* and Pi-Alkyl type interactions with residues *LEU788*, *ALA743*. The SwissADME webserver investigation suggested that most of the synthesized compounds follow the rules of drug-likeness.

1. Introduction

Resistance to chemotherapy is a main obstacle in cancer treatment. Despite the advances in molecular biology and availability of drug discovery tools, getting a promising anticancer *lead* still seems to be an uphill task. In search of a *lead* with possible anticancer property, the heterocyclic skeletons were explored extensively. Better chemical reactivity, greater receptor affinity, rapid body clearance and low toxicity make heterocyclic moieties the first choice synthon in drug discovery process (Pearce, 2017), triazole is an example of it. Further, the development of Disarib (Fig. 1) as a potent BCL2-inhibitor (Iyer et al., 2016) paved the idea of synthesizing some indole based triazole analogs with potential anticancer activity. Among heterocycles, indole is one of the most promising moieties. Thanks to its physicochemical properties, indole ring is considered a golden scaffold to design new antitumoral agents (Wan et al., 2019). Indeed, several indole derivatives were reported as anticancer compounds (Wan et al., 2019; Jia et al., 2020), such as Sunitinib, Osimertinib and Nintedanib (Fig. 1). 1,2,3-Triazole is a well-known scaffold with substantial biological activities. In fact, 1,2,3-triazole derivatives have been reported as anticancer (Atulya et al., 2016; Chen et al., 2008; Narsimha et al., 2016; Carroux et al., 2013; Duan et al., 2013; Yan et al., 2010, Sztanke al, 2008), cytotoxic (Das et al., 2021), antioxidant (Mady et al., 2014), anti-HIV (Velázquez et al., 1998; Johns etal, 2009), anti-tubercular (Kumar et al., 2014; Yempala et al., 2014; Patpi et al., 2012), antimicrobial (Hussain et al., 2019; Behbehani et al., 2011; Holla et al., 2005; Chen et al., 2000),

* Corresponding authors.
E-mail addresses: carmela.fimognari@unibo.it (C. Fimognari), subhasskarki@gmail.com (S.S. Karki).
[1] These authors contributed equally to this work.

https://doi.org/10.1016/j.compbiolchem.2022.107641
Received 20 July 2021; Received in revised form 19 January 2022; Accepted 7 February 2022
Available online 9 February 2022

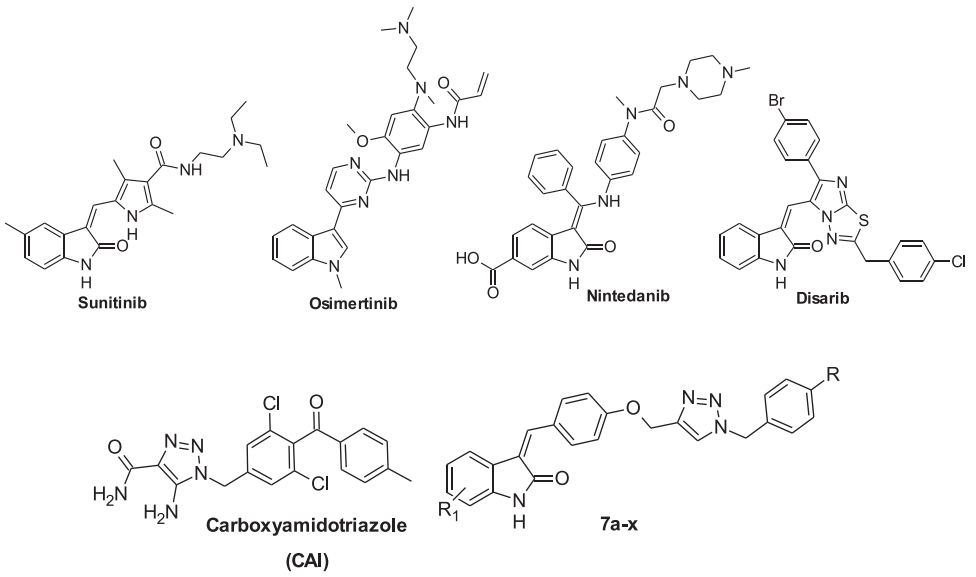

Fig. 1. Structures of indole containing drugs (Sunitinib, Osimertinib, Nintedanib and Disarib) in clinical and preclinical stages, triazole containing drug (CAI) and synthesized derivatives **7a–x**.

antifungal (Sheehan et al., 1999), anti-inflammatory (Hafez et al., 2008; Rao etal, 2014), antimalarial (Gujjar et al., 2009), and anticonvulsant (Ulloora et al., 2013; Erol et al., 1995) agents. Apart from being a versatile synthon, the triazole moiety is used as bioisostere to modify biological and physicochemical properties of a *lead* in drug discovery process (Bonandi et al., 2017). The most common method used to synthesize 1,2,3-triazole nucleus is 1,3-dipolar cycloaddition of azide with alkyne (Kumar et al., 2014), and the same has been adopted for the proposed work, which deals with synthesis and *in vitro* cytotoxicity investigation of newly synthesized 1,2,3-triazole derivatives (**7a-x**). Moreover, the most active compound **7c** was deeper investigated in order to understand the molecular mechanisms responsible for its cytotoxic activity.

Further, the pharmacokinetic properties and ADME parameters of the synthesized compounds were also investigated.

Epidermal Growth Factor Receptor (EGFR) is a transmembrane protein regulating development and homeostasis; besides, it also plays a key role in cancer development (Sigismund et al., 2018). Indeed, its improper activation, due to gene amplification, mutations or over expression, has been observed in different cancer types, including lung (Mitsudomi et al., 2010), glioblastoma (Verhaak et al., 2010; Mellinghoff et al., 2005), head-neck (Grandis et al., 1998, Kalyankrishna et al., 2006), anal (Walker et al., 2009), and ovarian cancers (Nielsen et al., 2004; Morrison et al., 2012). Therefore, this receptor is assumed to be one of the most important target structures for the development of new anticancer agents (Jain et al., 2018; De Clercq et al., 2019; To et al., 2019). In this context, the crystal structure of EGFR (PDB ID: 6P8Q) was considered as the target structure and the inhibition effect of the synthesized compounds on this receptor was investigated by molecular docking simulations. Here, the calculations were performed with AutoDockVina (Trott et al., 2010) using Lamarckian genetic algorithm (Solis et al., 1981, Huey et al., 2007) and great agreement with *in vitro* results was observed. In addition, the possible binding sites of some high-scoring compounds to EFGR were determined.

2. Experimental section

2.1. Chemistry

Reagents and solvents were assured for purity before use. Progress of reactions was confirmed by thin layer chromatography (TLC) on a pre-coated Aluchrosep silica gel 60/UV254 plates (Sd Fine-Chem Ltd.). Melting point (m.p.) was measured by open capillary tube method in liquid paraffin (heavy), and reported uncorrected. Fourier transformer infrared (FTIR) spectra were recorded using infrared (IR) grade potassium bromide (KBr) by diffuse reflectance technique on JASCO 460^{+}. The ^{1}H/^{13}C NMR spectra were recorded in deuterated dimethyl sulphoxide (DMSO-d_6) and chloroform ($CDCl_3$) between 400 and 500/100 MHz on Bruker (Ultraspec AMX 400) and JEOL RESONANCE. Chemical shift (δ) values were expressed in ppm using tetramethylsilane (TMS) as reference. CHN analysis was done on Thermo scientific Flash 2000 organic elemental analyzer. Mass spectra of (Z)− 3-(4-((1-arylmethyl-1 H-1,2,3-triazol-4-yl)methoxybenzylidene)indolin-2-ones (**7a-d, 7o** and **7 v**) were recorded on triple-quadrupole liquid chromatography mass spectrometry (LC-MS) 6410 from Agilent Technologies. Compounds 4-(prop-2-ynyloxy)benzaldehyde **(3)** and 4-((1-arylmethyl-1*H*-1,2,3-triazol-4-yl)methoxy)benzaldehydes **(5A-D)** were synthesized according to literature (Kumar et al., 2013). Various arylazides **(4A-D)** were prepared as per the literature (Hong et al., 2013). Various indolin-2-ones (6E-J) were prepared according to literature (Soriano al, 1993). Compounds **7a** and **7 s** were prepared as per the literature (Atulya et al., 2016).

2.2. General procedure for the synthesis of (Z)-3-(4-((1-benzyl-1 H-1,2,3-triazol-4 yl)methoxy benzylidene)indolin-2-ones (7b-x)

The appropriate aldehyde **5** (1 mmol) was dissolved in anhydrous methanol (30 mL) and treated with the equivalent of respective 2-oxindole **6** and piperidine (0.5 mL). The reaction mixture was refluxed and the precipitate formed on cooling was collected by filtration and recrystallized from DMF/methanol mixture in various proportions.

2.2.1. (Z)-3-(4-((1-benzyl-1 H-1,2,3-triazol-4-yl)methoxy)benzylidene)-5-chloroindolin-2-one (7b)

Yield 58%; m.p.260–262 °C; IR (KBr) ν_{max}/cm^{-1}: 3204, 3050, 2945, 1697, 1590, 1511, 1464, 1185;^{1}H NMR (400 MHz, DMSO-d_6, δ/ppm): 10.71 (s, 1 H, -NH), 8.50 (d, 2 H, *J*=7.2 Hz), 8.32 (s, 1 H, triazole-H), 7.88 (s, 1 H, benzylidene-H), 7.81–7.80 (d, 1 H, *J*=2.0 Hz), 7.39–7.36 (m, 2 H, ar.), 7.34–7.31 (m, 3 H, ar.), 7.21–7.19 (m, 1 H, ar.), 7.15 (d, 2 H, *J*=7.2 Hz), 6.81 (d, 1 H, *J*=6.4 Hz), 5.61 (s, 2 H, -OCH_2-), 5.24 (s, 2 H, -NCH_2-). ^{13}C NMR (100 MHz, DMSO-d_6, δ/ppm): 167.09, 160.27, 142.54, 138.84, 138.68, 135.93, 134.70, 128.73, 128.12, 127.92,

127.55, 127.27, 127.06, 125.24, 124.82, 123.03, 119.28, 114.53, 110.49, 61.20, 52.82. Anal. Calcd. for $C_{25}H_{19}ClN_4O_2$: C, 67.80; H, 4.32; N, 12.65: Found C, 67.67; H, 4.25; N, 12.69%. +MS (ESI) *m/z*: 443.20 (442.90).

2.2.2. (Z)-3-(4-((1-benzyl-1 H-1,2,3-triazol-4-yl)methoxy)benzylidene)-5-methylindolin-2-one (7c)

Yield 55%; m.p.220–222 °C; IR (KBr) ν_{max}/cm^{-1}:3198, 3049, 2876, 1698, 1601, 1543, 1482, 1379, 1201; ^{1}H NMR (400 MHz, DMSO-d_6, δ/ppm)**:** 10.44 (s, 1 H,-NH), 8.47 (d, 2 H, *J*=9.2 Hz), 8.37 (s, 1 H, triazole-H), 7.69 (s, 1 H, benzylidene-H),7.49 (s, 1 H, ar.), 7.40–7.31 (m, 5 H, ar.), 7.13 (d, 2 H, *J*=8.8 Hz), 6.99 (d, 1 H, *J*=8.4 Hz), 6.70 (d, 1 H, *J*=7.6 Hz), 5.61 (s, 2 H,-OCH_2-), 5.23 (s, 2 H, -NCH_2-), 2.29 (s, 3 H, -CH_3). ^{13}C NMR (100 MHz, DMSO-d_6, δ/ppm): 167.45, 159.22, 142.66, 140.40, 136.31, 135.95, 135.57, 134.28, 131.41, 130.12, 129.61, 128.74, 128.14, 127.93, 126.95, 125.90, 124.80, 122.59, 119.74, 114.92, 114.42, 109.73, 108.91, 61.22, 52.84. Anal. Calcd. for $C_{25}H_{22}N_4O_2$: C, 73.92; H, 5.25; N, 13.26: Found C, 73.81; H, 5.21; N, 13.23%. +MS (ESI) *m/z*: 423.2 (422.48).

2.2.3. (Z)-3-(4-((1-benzyl-1 H-1,2,3-triazol-4-yl)methoxy)benzylidene)-5-bromoindolin-2-one (7d)

Yield 62%; m.p.238–240 °C; IR (KBr) ν_{max}/cm^{-1}:3154, 3038, 2941 1697, 1591, 1512, 1471, 1186; ^{1}H NMR (400 MHz, DMSO-d_6, δ/ppm): 10.72 (s, 1 H, -NH), 8.50 (d, 2 H, *J*=6.8 Hz) 8.32 (s, 1 H, triazole-H), 7.93 (s, 1 H, ar.), 7.89 (s, 1 H, benzylidene-H), 7.70–7.65 (m, 1 H, ar.),7.40–7.31 (m, 5 H, ar.), 7.22–7.13 (m, 2 H, ar.), 6.84–6.75 (m, 1 H, ar.) 5.61 (s, 2 H, -OCH_2-), 5.24 (s, 2 H, -NCH_2-). Anal. Calcd. for $C_{25}H_{19}BrN_4O_2$: C, 61.61; H, 3.93; N, 11.50: Found C, 61.53; H, 3.95; N, 11.53%. -MS (ESI) *m/z*: 485.0 (487.35).

2.2.4. (Z)-3-(4-((1-benzyl-1 H-1,2,3-triazol-4-yl)methoxy)benzylidene)-7-chloroindolin-2-one (7e)

Yield 73%;m.p.214–216 °C; IR (KBr) ν_{max}/cm^{-1}:3151, 3040, 2925, 1700, 1592, 1449, 1482, 1226; ^{1}H NMR (400 MHz, DMSO-d_6, δ/ppm): 10.99 (s, 1 H, -NH), 8.49 (d, 2 H, *J*=9.2 Hz), 8.31 (s, 1 H, triazole-H), 7.83 (s, 1 H, benzylidene-H), 7.67 (d, 1 H, *J*=7.2 Hz), 7.40–7.28 (m, 5 H, ar.), 7.25 (d, 1 H, *J*=8.8 Hz), 7.16 (d, 2 H, *J*=8.8 Hz), 7.00 (t, 1 H, *J*=15.6 Hz), 5.61 (s, 2 H, -OCH_2-), 5.24 (s, 2 H, -NCH_2-).^{13}C NMR (100 MHz, DMSO-d_6, δ/ppm): 167.22, 160.31, 142.56, 138.75, 137.49, 135.94, 134.69, 128.75, 128.14, 127.94, 127.71, 127.19, 126.99, 124.84, 123.49, 122.06, 117.85, 114.55, 113.54, 61.22, 52.84. Anal. Calcd. for $C_{25}H_{19}ClN_4O_2$: C, 67.80; H, 4.32; N, 12.65: Found C, 67.71; H, 4.35; N, 12.66%.

2.2.5. (Z)-3-(4-((1-benzyl-1 H-1,2,3-triazol-4-yl)methoxy)benzylidene)-6-chloroindolin-2-one (7 f)

Yield 65%;m.p.181–183 °C; IR (KBr) ν_{max}/cm^{-1}:3198, 3030, 2845, 1698, 1604, 1543, 1476, 1184; ^{1}H NMR (500 MHz, DMSO-d_6, δ/ppm)**:** 10.86 (s, 1 H, -NH), 8.41 (s, 1 H, triazole-H), 8.32–8.29 (m, 3 H, ar.), 7.39–7.36 (m, 2 H, ar.), 7.34–7.31(m, 3 H, ar.), 7.19 (t, 1 H, *J*=12.8 Hz), 7.12 (d, 2 H, *J*=7.2 Hz), 7.01 (d, 1 H, *J*=7.2 Hz), 6.81 (d, 1 H, *J*=6.8 Hz), 5.61 (s, 2 H, -OCH_2-), 5.24 (s, 2 H, -NCH_2-).^{13}C NMR (100 MHz, DMSO-d_6, δ/ppm): 167.09, 160.27, 142.54, 138.84, 138.68, 135.93, 134.70, 128.72, 128.12, 127.92, 127.54, 127.26, 127.06, 125.24, 124.82, 123.03, 119.28, 114.52, 110.48, 61.20, 52.82. Anal. Calcd. for $C_{25}H_{19}ClN_4O_2$: C, 67.80; H, 4.32; N, 12.65: Found C, 67.68; H, 4.29; N, 12.69%.

2.2.6. (Z)-5-chloro-3-(4-((1-(4-nitrobenzyl)1 H-1,2,3-triazol-4-yl) methoxy) benzylidene)indolin-2-one (7 g)

Yield 55%; m.p.220–222 °C; IR (KBr) ν_{max}/cm^{-1}:3201, 3060, 2890, 1701, 1599, 1560, 1512, 1483, 1192; ^{1}H NMR (400 MHz, DMSO-d_6, δ/ppm): 10.69 (s, 1 H, -NH), 8.50 (d, 2 H, *J*=8.8 Hz), 8.39 (s, 1 H, triazole-H), 8.25 (d, 2 H, *J*=8.8 Hz), 7.88 (s, 1 H, benzylidene-H), 7.80–7.79 (m, 1 H, ar.), 7.55 (d, 2 H, *J*=8.8 Hz), 7.21–7.18 (m, 1 H, ar.), 7.15 (d, 2 H, *J*=8.8 Hz), 6.82 (d, 1 H, *J*=8.0 Hz), 5.80 (s, 2 H, -OCH_2-), 5.27 (s, 2 H, -NCH_2-).^{13}C NMR (100 MHz, DMSO-d_6, δ/ppm): 167.12, 160.24, 147.25, 143.32, 142.76, 138.87, 138.66, 134.72, 129.04, 127.59, 127.28, 127.13, 125.28, 123.90, 123.11, 119.31, 114.59, 110.52, 61.20, 51.95. Anal. Calcd. for $C_{25}H_{18}ClN_5O_4$: C, 61.54; H, 3.72; N, 14.35: Found C, 61.45; H, 3.67; N, 14.39%.

2.2.7. (Z)-5-bromo-3-(4-((1-(4-nitrobenzyl)-1 H-1,2,3-triazol-4-yl) methoxy) benzylidene)indolin-2-one (7 h)

Yield 65%; m.p.210–212 °C; IR (KBr) ν_{max}/cm^{-1}:3157, 3078, 2856, 1698, 1589, 1477, 1190; ^{1}H NMR (400 MHz, DMSO-d_6, δ/ppm)**:** 10.70 (s, 1 H, -NH), 8.50 (d, 2 H, *J*=9.2 Hz), 8.39 (s, 1 H, triazole-H), 8.25 (d,2 H, *J*=8.8 Hz), 7.92 (m, 2 H, ar.), 7.54 (d, 2 H, *J*=8.8 Hz), 7.34–7.31 (m, 1 H, ar.), 7.16 (d, 2 H, *J*=9.2 Hz), 6.77 (d, 1 H, *J*=8.4 Hz), 5.80 (s, 2 H, -OCH_2-), 5.27 (s, 2 H, -NCH_2-).^{13}C NMR (100 MHz, DMSO-d_6, δ/ppm): 166.98, 160.23, 147.25, 143.32, 142.75, 139.22, 138.68, 134.72, 130.37, 129.03, 127.70, 127.13, 125.27, 123.89, 122.94, 122.03, 114.57, 112.94, 111.02, 61.19, 51.93. Anal. Calcd. for $C_{25}H_{18}BrN_5O_4$: C, 56.41; H, 3.41; N, 13.16: Found C, 56.37; H, 3.35; N, 13.20%.

2.2.8. (Z)-6-chloro-3-(4-((1-(4-nitrobenzyl)-1 H-1,2,3-triazol-4-yl) methoxy) benzylidene)indolin-2-one (7i)

Yield 54%; m.p.178–180 °C;IR (KBr) ν_{max}/cm^{-1}:3201, 3090, 2864, 1695, 1616, 1528, 1499, 1472, 1185; ^{1}H NMR (500 MHz, DMSO-d_6, δ/ppm): 10.86 (s, 1 H, -NH), 8.41 (d, 2 H, *J*=6.0 Hz), 8.32 (d, 2 H, *J*=6.8 Hz), 8.25–8.21 (m, 2 H, ar.), 7.54 (d, 2 H, *J*=7.2 Hz), 7.19 (t, 1 H, *J*=12.8 Hz), 7.12 (d, 2 H, *J*=7.2 Hz), 7.01 (d, 1 H, *J*=6.8 Hz), 6.81 (d, 1 H, *J*=6.8 Hz), 5.81 (s, 2 H, -OCH_2-), 5.26 (s, 2 H, -NCH_2-).^{13}C NMR (100 MHz, DMSO-d_6, δ/ppm): 167.19, 159.41, 143.31, 136.74, 134.51, 131.60, 129.00, 126.70, 125.24, 123.88, 123.24, 120.73, 120.03, 115.09, 114.53, 109.92, 61.13, 51.92. Anal. Calcd. for $C_{25}H_{18}ClN_5O_4$: C, 61.54; H, 3.72; N, 14.35: Found C, 61.49; H, 3.65; N, 14.41%.

2.2.9. (Z)-7-chloro-3-(4-((1-(4-nitrobenzyl)-1 H-1,2,3-triazol-4-yl) methoxy) benzylidene)indolin-2-one (7j)

Yield 58%; m.p.210–213 °C; IR (KBr) ν_{max}/cm^{-1}:3227, 3066, 2950, 1695, 1610, 1514, 1481, 1432, 1174; ^{1}H NMR (400 MHz, DMSO-d_6, δ/ppm)**:** 11.00 (s, 1 H, -NH), 8.50 (d, 2 H, *J*=9.2 Hz), 8.39 (s, 1 H, triazole-H), 8.25–8.22 (d, 2 H, *J*=8.8 Hz), 7.84 (s, 1 H, benzylidene-H), 7.67 (d, 1 H, *J*=7.6 Hz), 7.55–7.52 (d, 2 H, *J*=8.8 Hz), 7.23 (d, 1 H, *J*=8.8 Hz), 7.17 (d, 2 H, *J*=8.8 Hz), 6.99 (t, 1 H, *J*=15.6 Hz), 5.81 (s, 2 H, -OCH_2-), 5.27 (s, 2 H, -NCH_2-).^{13}C NMR (100 MHz, DMSO-d_6, δ/ppm): 167.22, 160.26, 147.25, 143.32, 142.75, 138.71, 137.50, 134.69, 129.04, 127.72, 127.19, 127.03, 125.28, 123.53, 122.06, 117.86, 114.58, 113.55, 61.20, 51.94. Anal. Calcd. for $C_{25}H_{18}ClN_5O_4$: C, 61.54; H, 3.72; N, 14.35: Found C, 61.42; H, 3.61; N, 14.44%.

2.2.10. (Z)-3-(4-((1-(4-nitrobenzyl)-1 H-1,2,3-triazol-4-yl)methoxy) benzylidene)indolin-2-one (7k)

Yield 63%; m.p.214–215 °C; IR (KBr) ν_{max}/cm^{-1}:3247, 3059, 2919, 1695, 1610, 1514, 1449, 1481, 1174; ^{1}H NMR (400 MHz, DMSO-d_6, δ/ppm)**:** 10.56 (s, 1 H, -NH), 8.48 (d, 2 H, *J*=8.8 Hz), 8.38 (s, 1 H, triazole-H), 8.23 (d, 2 H, *J*=8.8 Hz), 7.94–7.52 (sdd, 4 H, *J*=8.8 Hz, 8.8 Hz), 7.23–7.12 (td, 3 H, *J*=15.6 Hz, 8.4 Hz), 6.96 (t, 1 H, *J*=16 Hz), 6.81 (d, 1 H, *J*=8.0 Hz), 5.80 (s, 2 H, -OCH_2-) 5.26 (s, 2 H, -NCH_2-).^{13}C NMR (100 MHz, DMSO-d_6, δ/ppm): 167.32, 159.81, 147.23, 143.31, 142.81, 140.25, 136.61, 134.31, 129.01, 128.23, 127.28, 125.27, 125.23, 124.23, 123.88, 120.85, 119.23, 114.44, 109.15, 61.15, 51.92. Anal. Calcd. for $C_{25}H_{19}N_5O_4$: C, 66.22; H, 4.22; N, 15.44: Found C, 66.15; H, 4.16; N, 15.49%.

2.2.11. (Z)-5-methyl-3-(4-((1-(4-nitrobenzyl)-1 H-1,2,3-triazol-4-yl) methoxy)- benzylidene)indolin-2-one (7 l)

Yield 55%; m.p.216–218 °C; IR (KBr) ν_{max}/cm^{-1}:3169, 3010, 2826, 1672, 1602, 1594, 1503, 1489, 1376, 1189. ^{1}H NMR (400 MHz, DMSO-

d_6, δ/ppm): 10.41 (s, 1 H, -NH), 8.39 (s, 1 H, triazole-H), 8.24 (d, 2 H, *J*=8.8 Hz), 7.71 (d, 2 H, *J*=8.8 Hz), 7.55–7.52 (m, 3 H, ar.), 7.44 (s, 1 H, ar.), 7.20 (d, 2 H, *J*=8.8 Hz), 7.03 (d, 1 H, *J*=7.2 Hz), 6.76 (d, 1 H, *J*=8.0 Hz), 5.81 (s, 2 H,-OCH_2-), 5.29 (s, 2 H, -NCH_2-), 2.17 (s, 3 H, -CH_3). ^{13}C NMR (100 MHz, DMSO-d_6, δ/ppm): 168.90, 159.16, 147.22, 143.31, 142.84, 140.40, 135.51, 134.27, 131.39, 130.11, 129.56, 127.00, 125.93 (s), 125.21, 123.88, 122.56, 121.16, 114.94, 109.71, 61.21, 51.92, 20.79. Anal. Calcd. for $C_{26}H_{21}N_5O_4$: C, 66.80; H, 4.53; N, 14.98: Found C, 66.59; H, 4.48; N, 15.01%.

2.2.12. (Z)-3-(4-((1-(4-methylbenzyl)-1 H-1,2,3-triazol-4-yl)methoxy) benzylidene) indolin-2-one (7 m)

Yield 70%; m.p.200–201 °C; IR (KBr) ν_{max}/cm^{-1}:3229, 3010, 2811, 1692, 1594, 1498, 1476, 1386, 1167; ^{1}H NMR (500 MHz, DMSO-d_6, δ/ppm): 10.58 (s, 1 H,-NH), 8.47 (d, 2 H, *J*=7.2 Hz), 8.28 (s, 1 H, triazole-H), 7.74 (s, 1 H, benzylidene-H), 7.67 (d, 1 H, *J*=6.0 Hz), 7.22 (m, 2 H, ar.), 7.18 (m, 3 H, ar.), 7.13 (d, 2 H, *J*=7.2 Hz), 6.97 (t, 1 H, *J*=13.2 Hz), 6.81 (d, 1 H, *J*=6.0 Hz), 5.55 (s, 2 H, -OCH_2-), 5.22 (s, 2 H -NCH_2-), 2.67 (s, 3 H, -CH_3).^{13}C NMR (100 MHz, DMSO-d_6, δ/ppm): 167.33, 159.87, 142.58, 140.24, 137.49, 136.67, 134.32, 132.94, 129.27, 128.24, 127.98, 127.25, 125.29, 124.65, 124.18, 120.87, 119.24, 114.44, 109.16, 61.18, 52.64, 20.64. Anal. Calcd. for $C_{25}H_{22}N_4O_2$: C, 73.92; H, 5.25; N, 13.26: Found C, 73.81; H, 5.21; N, 13.32%.

2.2.13. (Z)-6-chloro-3-(4-((1-(4-methylbenzyl)-1 H-1,2,3-triazol-4-yl) methoxy) benzylidene)indolin-2-one (7 n)

Yield 56%; m.p.189–190 °C;IR (KBr) ν_{max}/cm^{-1}:3203, 3023, 2838, 1692, 1586, 1509, 1448, 1389, 1175; ^{1}H NMR (500 MHz, DMSO-d_6, δ/ppm): 10.86 (s, 1 H, -NH), 8.40 (s, 1 H, ar.), 8.32 (d, 2 H, *J*=7.2 Hz), 8.27 (s, 1 H, triazole-H), 7.22–7.20 (m, 2 H, ar.), 7.19–7.16 (m, 3 H, ar.), 7.11 (d, 2 H, *J*=7.2 Hz), 7.01 (d, 1 H, *J*=7.2 Hz), 6.81 (d, 1 H, *J*=7.2 Hz), 5.55 (s, 2 H, -OCH_2-), 5.22 (s, 2 H, -NCH_2-), 2.27 (s, 3 H, -CH_3).^{13}C NMR (100 MHz, DMSO-d_6, δ/ppm): 167.20, 160.13, 142.53, 141.31, 137.82, 137.49, 134.52, 132.93, 132.24, 129.26, 127.98, 127.08, 124.66, 124.29, 122.98, 120.67, 120.64, 114.51, 109.12, 61.20, 52.64, 20.64. Anal. Calcd. for $C_{26}H_{21}ClN_4O_2$: C, 68.34; H, 4.63; N, 12.26: Found C, 68.25; H, 4.57; N, 12.31%.

2.2.14. (Z)-5-methyl-3-(4-((1-(4-methylbenzyl)-1 H-1,2,3-triazol-4-yl) methoxy) benzylidene)indolin-2-one (7o)

Yield 60%; m.p.208–210 °C; IR (KBr) ν_{max}/cm^{-1}:3198, 3043, 2821, 1695, 1602, 1528, 1489, 1378, 1184; ^{1}H NMR (400 MHz, DMSO-d_6, δ/ppm): 10.41 (s, 1 H, -NH), 8.27 (s, 1 H, triazole-H), 7.70 (d, 2 H, *J*=8.8 Hz), 7.53 (s, 1 H, benzylidene-H), 7.45 (s, 1 H, ar), 7.23–7.16 (m, 6 H, ar.), 7.04 (d, 1 H, *J*=8.0 Hz), 6.76 (d, 1 H, *J*=8.0 Hz), 5.55 (s, 2 H, -OCH_2-), 5.22 (s, 2 H, -NCH_2-), 2.27 (s, 3 H, -CH_3), 2.18 (s, 3 H, -CH_3). + MS (ESI) *m/z*: 437.50 (436.52).^{13}C NMR (100 MHz, DMSO-d_6, /ppm): 167.44, 159.79, 142.62, 138.02, 136.30, 135.94, 134.27, 129.60, 128.73, 128.66, 128.12, 127.92, 127.31, 125.34, 124.79, 124.38, 119.73, 114.41, 108.90, 61.16, 52.82, 20.78. Anal. Calcd. for $C_{27}H_{24}N_4O_2$: C, 74.29; H, 5.54; N, 12.84: Found C, 74.15; H, 5.47; N, 12.91%.

2.2.15. (Z)-5-bromo-3-(4-((1-(4-methylbenzyl)-1 H-1,2,3-triazol-4-yl) methoxy) benzylidene)indolin-2-one (7p)

Yield 46%; m.p.238–240 °C; IR (KBr) ν_{max}/cm^{-1}:3158, 3043, 2859, 1698, 1611, 1512, 1462, 1381, 1187; ^{1}H NMR (400 MHz, DMSO-d_6, δ/ppm): 10.70 (s, 1 H,-NH), 8.50 (d, 2 H, *J*=9.2 Hz), 8.27 (s, 1 H, triazole H), 7.92 (d, 1 H, *J*=2.0, ind4), 7.88 (s, 1 H, benzylidene-H), 7.34–7.31 (dd, 1 H, *J*=8.4, ind6), 7.23–7.12 (m, 6 H, ar.), 6.77 (d, 1 H, *J*=8.0 Hz), 5.55 (s, 2 H, -OCH_2-) 5.23 (s, 2 H, -NCH_2-), 2.27 (s, 3 H, -CH_3).^{13}C NMR (100 MHz, DMSO-d_6, δ/ppm): 166.96, 160.28, 142.50, 139.20, 138.71, 137.47, 134.71, 132.92, 130.34, 129.25, 127.97, 127.70, 127.07, 124.66, 122.88, 122.01, 114.53, 112.93, 111.00, 61.20, 52.63, 20.63. Anal. Calcd. for $C_{26}H_{21}BrN_4O_2$: C, 62.28; H, 4.22; N, 11.17: Found C, 62.16; H, 4.17; N, 11.21%.

2.2.16. (Z)-5-chloro-3-(4-((1-(4-methylbenzyl)-1 H-1,2,3-triazol-4-yl) methoxy) benzylidene)indolin-2-one (7q)

Yield 48%; m.p.242–244 °C; IR (KBr) ν_{max}/cm^{-1}:3158, 3059, 2890, 1699, 1590, 1510, 1465, 1381, 1187; ^{1}H NMR (400 MHz, DMSO-d_6, δ/ppm): 10.69 (s, 1 H,-NH), 8.49 (d, 2 H, *J*=8.8 Hz), 8.27 (s, 1 H, triazole-H), 7.88–7.80 (m, 2 H, ar.), 7.23–7.12 (m, 7 H, ar.), 6.77 (d, 1 H, *J*=8.4 Hz), 5.55 (s, 2 H, -OCH_2-), 5.23 (s, 2 H, -NCH_2-), 2.26 (s, 3 H, -CH_3).^{13}C NMR (100 MHz, DMSO-d_6, δ/ppm): 167.09, 160.27, 142.50, 138.84, 138.68, 137.47, 134.70, 132.92, 131.52, 129.23, 127.96, 127.54, 127.27, 127.06, 125.24, 124.66, 123.03, 119.27, 114.53, 110.48, 61.20, 52.63, 20.63. Anal. Calcd. for $C_{26}H_{21}ClN_4O_2$: C, 68.34; H, 4.63; N, 12.26: Found C, 68.27; H, 4.53; N, 12.23%.

2.2.17. (Z)-7-chloro-3-(4-((1-(4-methylbenzyl)-1 H-1,2,3-triazol-4-yl) methoxy) benzylidene)indolin-2-one (7r)

Yield 55%; m.p.212–214 °C; IR (KBr) ν_{max}/cm^{-1}:3201, 3023, 2804, 1698, 1612, 1554, 1486, 1379, 1198; ^{1}H NMR (400 MHz, DMSO-d_6, δ/ppm): 11.00 (s, 1 H, -NH), 8.49 (d, 2 H, *J*=8.8 Hz), 8.27 (s, 1 H, triazole-H), 7.84 (s, 1 H, benzylidene-H), 7.67 (d, 1 H, *J*=7.2 Hz), 7.25–7.13 (m, 7 H, ar.), 6.99 (t, 1 H, *J*=15.6 Hz), 5.50 (s, 2 H, -OCH_2-), 5.23 (s, 2 H, -NCH_2-), 2.27 (s, 3 H, -CH_3).^{13}C NMR (100 MHz, DMSO-d_6, δ/ppm): 167.22, 160.30, 142.52, 138.74, 137.49, 134.69, 132.93, 129.26, 127.98, 127.70, 127.19, 126.99, 124.68, 123.48, 122.05, 117.84, 114.55, 113.54, 61.22, 52.65, 20.64. Anal. Calcd. for $C_{26}H_{21}ClN_4O_2$: C, 68.34; H, 4.63; N, 12.26: Found C, 68.24; H, 4.57; N, 12.32%.

2.2.18. (Z)-5-chloro-3-(4-((1-(4-chlorobenzyl)-1 H-1,2,3-triazol-4-yl) methoxy) benzylidene)indolin-2-one (7 t)

Yield 52%; m.p.242–244 °C; IR (KBr) ν_{max}/cm^{-1}:3201, 3051, 2862, 1701, 1623, 1545, 1486, 1201; ^{1}H NMR (500 MHz, DMSO-d_6, δ/ppm): 10.77 (s, 1 H, -NH), 8.55 (d, 2 H, *J*=8.8), 8.32 (s, 1 H, triazole-H), 7.92 (s, 1 H, benzylidene-H), 7.82 (m, 1 H, ar.), 7.43 (d, 2 H, *J*=8.2 Hz), 7.38 (d, 2 H, *J*=8.2 Hz), 7.26–7.22 (m, 1 H, ar.), 7.18 (d, 2 H, *J*=8.8 Hz), 6.82 (d, 1 H, *J*=8.8 Hz), 5.63 (s, 2 H, -OCH_2-), 5.26 (s, 2 H, -NCH_2-). ^{13}C NMR (100 MHz, DMSO-d_6, δ/ppm): 167.09, 160.24, 142.60, 138.84, 138.67, 134.92, 134.70, 129.87, 128.73, 127.55, 127.26, 127.08, 125.24, 124.87, 123.05, 119.28, 114.54, 110.49, 61.19, 52.00. Anal. Calcd. for $C_{25}H_{18}Cl_2N_4O_2$: C, 62.91; H, 3.80; N, 11.74: Found C, 63.01; H, 3.71; N, 11.79%.

2.2.18.1. (Z)-5-bromo-3-(4-((1-(4-chlorobenzyl)-1 H-1,2,3-triazol-4-yl) methoxy) benzylidene)indolin-2-one (7 u).

Yield 67%; m.p.242–243 °C; IR (KBr) ν_{max}/cm^{-1}:3204, 3013, 2798, 1695, 1613, 1542, 1486, 1198; ^{1}H NMR (500 MHz, DMSO-d_6, δ/ppm): 10.73 (s, 1 H, -NH), 8.50 (d, 2 H, *J*=8.8 Hz), 8.33 (s, 1 H, triazole-H), 7.93 (s, 1 H, benzylidene-H), 7.89 (s, 1 H, ar.), 7.45 (d, 2 H, *J*=8.0 Hz), 7.35–7.31 (m, 3 H, ar.), 7.15 (d, 2 H, *J*=8.0 Hz), 6.77 (d, 1 H, *J*=8.0 Hz), 5.62 (s, 2 H, -OCH_2-), 5.24 (s, 2 H, -NCH_2-).^{13}C NMR (100 MHz, DMSO-d_6, δ/ppm): 166.99, 160.27, 142.63, 139.22, 138.72, 134.93, 134.74, 132.88, 130.38, 129.90, 128.76, 127.71, 127.11, 124.90, 122.92, 122.03, 114.57, 112.96, 111.04, 61.21, 52.04. Anal. Calcd. for $C_{25}H_{18}BrClN_4O_2$: C, 57.55; H, 3.48; N, 10.74: Found C, 57.48; H, 3.45; N, 10.82%.

2.2.19. (Z)-3-(4-((1-(4-chlorobenzyl)-1 H-1,2,3-triazol-4-yl)methoxy) benzylidene)-5 methylindolin-2-one (7 v)

Yield 56%; m.p.220–221 °C; IR (KBr) ν_{max}/cm^{-1}:3141, 3030, 2911, 1682, 1582, 1520, 1482, 1380, 1173; ^{1}H NMR (500 MHz, DMSO-d_6, δ/ppm): 10.48 (s, 1 H,-NH), 8.46 (d, 2 H, *J*=8.0), 8.34 (s, 1 H, triazole-H), 7.70 (s, 1 H, benzylidene-H), 7.49 (s, 1 H, ar.), 7.45 (d, 2 H, *J*=8.0 Hz),7.35 (d, 2 H, *J*=8.0 Hz), 7.11 (d, 2 H, *J*=8.2 Hz), 6.97 (d, 1 H, *J*=8.2 Hz), 6.68 (d, 1 H, *J*=8.0 Hz), 5.62 (s, 2 H, -OCH_2-), 5.22 (s, 2 H, -NCH_2-), 2.29 (s, 3 H, -CH_3).^{13}C NMR (100 MHz, DMSO-d_6, δ/ppm):

167.44, 159.77, 142.69, 138.03, 136.28, 134.92, 134.27, 131.40, 129.88, 128.73, 127.33, 126.97, 125.33, 124.85, 124.40, 119.73, 114.42, 108.90, 61.15, 52.01, 20.78. Anal. Calcd. for $C_{26}H_{21}ClN_4O_2$: C, 68.34; H, 4.63; N, 12.26: Found C, 68.25; H, 4.55; N, 12.36%. + MS (ESI) *m/z*: 457.50 (456.93).

2.2.20. (Z)-6-chloro-3-(4-((1-(4-chlorobenzyl)-1 H-1,2,3-triazol-4-yl) methoxy) benzylidene)indolin-2-one (7w)

Yield 68%; m.p.242–246 °C; IR (KBr) ν_{max}/cm^{-1}:3142, 3042, 2828, 1700, 1613, 1511, 1476, 1176; ^{1}H NMR (500 MHz, DMSO-d_6, δ/ppm): 10.75 (s, 1 H, -NH), 8.47 (d, 2 H, *J*=8.0), 8.33 (s, 1 H, triazole-H), 7.80 (s, 1 H, benzylidene-H), 7.70 (d, 2 H, *J*=8.0 Hz), 7.45 (d, 2 H, *J*=8.0 Hz), 7.35 (d, 2 H, *J*=8.0 Hz), 7.14 (d, 2 H, *J*=8.0 Hz), 6.82 (d, 1 H, *J*=8.0 Hz), 5.62 (s, 2 H, -OCH_2-), 5.23 (s, 2 H, -NCH_2-).^{13}C NMR (100 MHz, DMSO-d_6, δ/ppm): 168.80, 159.45, 143.97, 142.67, 136.79, 134.93, 133.61, 132.88, 131.58, 129.89, 128.74, 126.68, 124.87, 124.59, 123.26, 120.77, 120.05, 115.07, 109.94, 61.24, 52.03. Anal. Calcd. for $C_{25}H_{18}Cl_2N_4O_2$: C, 62.91; H, 3.80; N, 11.74: Found C, 62.83; H, 3.69; N, 11.83%.

2.2.21. (Z)-7-chloro-3-(4-((1-(4-chlorobenzyl)-1 H-1,2,3-triazol-4-yl) methoxy) benzylidene)indolin-2-one (7x)

Yield 62%; m.p.250–252 °C; IR (KBr) ν_{max}/cm^{-1}: 3201, 3015, 2811, 1699, 1604, 1548, 1486, 1201; ^{1}H NMR (500 MHz, DMSO-d_6, δ/ppm): 11.04 (s, 1 H, -NH), 8.50 (d, 2 H, *J*=8.0 Hz), 8.33 (s, 1 H, triazole-H), 7.85 (s, 1 H, benzylidene-H), 7.68 (s, 1 H, ar.), 7.45 (d, 2 H, *J*=8.0 Hz), 7.35 (d, 2 H, *J*=8.0 Hz), 7.23 (m, 1 H, ar), 7.16 (d, 2 H, *J*=8.0 Hz), 7.00 (t, 1 H, *J*=16.0 Hz), 5.62 (s, 2 H, -OCH_2-), 5.24 (s, 2 H, -NCH_2-). ^{13}C NMR (100 MHz, DMSO-d_6, δ/ppm): 167.21, 160.27, 142.62, 138.70, 137.49, 134.91, 134.68, 132.88, 131.68, 129.88, 128.73, 127.69, 127.18, 127.00, 124.88, 123.50, 122.03, 117.83, 115.04, 114.54, 113.54, 61.21, 52.03. Anal. Calcd. for $C_{25}H_{18}Cl_2N_4O_2$: C, 62.91; H, 3.80; N, 11.74: Found C, 62.83; H, 3.74; N, 11.81%.

2.3. Cell cultures and treatments

Human T-lymphoblastic cells (Jurkat and CEM) and human acute promyelocytic cells (HL-60) were provided from LGC standards (LGC Group, Middlesex, UK). Jurkat and CEM cells were cultured in Roswell Park Memorial Institute (RPMI) 1640 medium supplemented with 10% heat-inactivated bovine serum, 1% penicillin/streptomycin solution, and 1% L-glutamine solution (all obtained from Sigma Aldrich). HL-60 cells were cultured in RPMI 1640 supplemented with 20% heat-inactivated bovine serum, 1% penicillin/streptomycin solution, and 1% L-glutamine solution (all obtained from Sigma Aldrich). 293 T (human embryonic kidney epithelial cell line was purchased from National Centre for Cell Science, Pune, India. Cells were maintained at 37 °C and 5% CO_2 in a humidified atmosphere.Cells were treated with increasing concentrations of the 1,2,3-traizole analog **(7c)** for different time points depending on the biological assay. Etoposide 10 μg/mL, camptothecin 2 μM, and H_2O_2 0.5 and 1 mM (all obtained from Sigma Aldrich) were used as positive controls.

To evaluate the induction of non-canonical cell death pathways, cells were pre-treated for 1 h with different chemical inhibitors and then treated with **7c** 8 μM for 24 or 48 h. For this purpose, the following blockers were used: the pan-caspase inhibitor carbobenzoxy-valyl-alanyl-aspartyl-[O-methyl]-fluoromethylketone (Z-VAD-FMK; BioVision, CA, USA) 75 μM; the PARP-1/− 2 inhibitor olaparib (Ola; Selleckem, Houston, TX, USA) 5 μM; the RIP1 inhibitor II 7-Cl-O-Nec-1 or necrostatin-1s (Nec-1s; Sigma Aldrich) 75 μM; the inhibitor of ROS generation and lipid peroxidation ferrostatin-1 (Ferr-1, Sigma Aldrich) 1 μM; the iron chelator deferoxamine mesylate (DFO, Across Organics, Thermofisher Scientific, MA, USA) 10 μM and the peroxyl radical scavenger vitamin E (Vit E, Sigma Aldrich) 100 μM, in order to inhibit apoptosis, parthanatos, necroptosis and ferroptosis, respectively.

Table 1
In vitro cytotoxicity data of synthesized indolin-2-one linked 1,2,3-triazole analogs (**7a–x**).

Compound	IC_{50} (μM)		
	L1210	**CEM**	**HeLa**
7a	8.1 ± 2.2	3.6 ± 2.5	4.6 ± 0.0
7b	> 250	33 ± 3.4	133 ± 18
7c	3.0 ± 0.9	1.5 ± 0.6	3.4 ± 0.6
7d	150 ± 14	6.7 ± 1.9	36 ± 0.6
7e	29 ± 1.0	7.3 ± 1.9	38 ± 3
7 f	44 ± 4.0	18 ± 4.0	66 ± 3.4
7 g	32 ± 1.0	5.0 ± 0.7	7.8 ± 2.9
7 h	32 ± 1.5	6.0 ± 1.1	9.2 ± 1.7
7i	19 ± 2.0	11 ± 6.0	20 ± 1.0
7j	17 ± 9.0	67 ± 2.5	7.1 ± 4.4
7k	34 ± 2.0	3.9 ± 0.8	11 ± 3.0
7 l	30 ± 4.0	4.6 ± 0.4	12 ± 3.0
7 m	19 ± 4.0	4.4 ± 0.6	4.8 ± 0.1
7 n	31 ± 4.0	33 ± 3.0	70 ± 3.5
7o	5.3 ± 0.5	3.8 ± 0.8	4.4 ± 0.6
7p	38 ± 2.5	7.4 ± 1.7	16 ± 1.0
7q	24 ± 6	5.7 ± 1.0	15 ± 1.0
7r	100 ± 13	18 ± 17	31 ± 3.9
7 s	12 ± 0.9	3.8 ± 1.7	3.7 ± 0.1
7 t	20 ± 4.0	5.3 ± 1.4	13 ± 1.0
7 u	20 ± 6.0	5.5 ± 0.1	12 ± 6.0
7 v	4.8 ± 1.1	4.0 ± 0.6	3.7 ± 0.4
7w	14 ± 1.1	1.7 ± 0.8	3.9 ± 0.4
7x	17 ± 3.0	6.8 ± 0.7	8.1 ± 1.9
Melphalan	2.13 ± 0.02	1.4 ± 0.4	NT

NT= Not tested.

2.4. Cytotoxic activity

The cytotoxicity of 1,2,3-traizole analogs **(7a-x)** were investigated against HeLa, CEM, L1210 and HEK293T cell lines according to the literature (Baraldi et al., 2004, Sujeet et al., 2014). The IC_{50} were calculated and expressed in μM (Table 1 and Fig. S1). All experiments were performed in triplicate.

Further, the cytotoxic activity of compound **7c** was analyzed using Guava Via Count Reagent (Merck Millipore, Burlington, MA, USA) according to manufacturer's instructions. In brief, after 24 and 48 h treatment with **7c**, cells were diluted with the reagent containing 7-AAD (7-amino actinomycin D) and then incubated at room temperature in the dark for 5 min. After incubation, cells were analyzed by flow cytometry.

2.5. Analysis of cell death mechanisms

Discrimination between apoptotic and necrotic events was performed by using Guava Nexin Reagent (Merck Millipore). This reagent, containing 7-AAD and annexin V-phycoerythrin (PE), is able to distinguish apoptotic and necrotic events. Cells were exposed to **7c** for 24 h and then diluted in Guava Nexin Reagent. After incubation of 20 min at room temperature in the dark, cells were analyzed by flow cytometry. Three cell populations can be detected: live cells (annexin− / 7-AAD−), early apoptotic cells (annexin+ / 7-AAD−), and late apoptotic or necrotic cells (annexin+ / 7-AAD+).

To evaluate the induction of non-apoptotic cell death pathways, cell viability was analyzed using SYTOX™ Green Nucleic Acid Stain (Thermo Fisher Scientific), according to manufacturer's protocol. SYTOX™ Green Nucleic Acid Stain is a fluorescent and cell membrane impermeable dye that could easily penetrate only compromised membranes of dead cells, where it binds DNA, thus increasing its fluorescence. Briefly, after pre-treatment of 1 h with the different chemical inhibitors and treatment of 24 and 48 h with **7c**, cells were supplemented with SYTOX™ Green Nucleic Acid Stain 10 nM and after incubation of 20 min at room temperature in the dark, cells were analyzed by flow cytometry.

2.6. Measurement of mitochondrial potential

Analysis of mitochondrial membrane potential was assessed using MitoProbeTM DilC1(5) Assay kit (Molecular Probes, Thermo Fisher Scientific), according to manufacturer' instructions. The dye DilC1(5) (1,1′,3,3,3′,3′-hexamethylindo dicarbo-cyanine iodide) accumulates in mitochondria with active membrane potential. The intensity of DilC1(5) staining decreases when cells are treated with agents that disrupt mitochondrial potential. Briefly, after 24 h of treatment with **7c**, 10^6 cells were washed and supplemented with 50 nM DilC1(5) for 20 min at 37 °C, 5% CO_2. Then, cells were washed and resuspended in PBS 1X for flow cytometric analysis. CCCP 50 μM was used as positive control. Results were expressed as % of cells with decreased mitochondrial potential compared to untreated cells.

2.7. Evaluation of caspase-8 and caspase-3 activity

Caspase activity was assessed using Caspase 8 Colorimetric Protease Assay Kit or Caspase 3 Colorimetric Protease Assay Kit, respectively (both purchased by Thermo Fisher Scientific), according to manufacturer's instructions. Briefly, after 24 h treatment, cells were washed in PBS 1X lysed by adding Cell Lysis Buffer on ice for 10 min. Then, cellular lysates were centrifuged and collected, and protein concentration has been normalized according to Bradford assay (Bradford, 1976). Cellular lysates were incubated for 2 h at 37 °C in the dark with 2X Reaction Buffer, containing DTT 10 mM and caspase-8 or caspase-3 substrate 200 μM. Both substrates consist of a synthetic tetrapeptide, IETD (Ile--Glu-Thr-Asp) specific for caspase-8, and DEVD (Asp-Glu-Val-Asp) specific for caspase-3, which are conjugated with the chromophore p-nitroanilide (pNA). When caspases are active, the specific substrate is cleaved from the chromophore and free pNA is used as a reporter, whose absorbance is measured at 405 nm, using the microplate reader Victor X3 (Perkin Elmer). Caspases activity was expressed as the fold increase of treated cells compared to untreated cells.

2.8. Measurement of ROS generation

Intracellular ROS generation was assessed using the probe 2′,7′–dichlorodihydrofluoresceine (H2DCFDA) (Sigma Aldrich). H2DCFDA is a non-fluorescent and cell-permeable probe which is hydrolyzed by intracellular esterases of viable cells into 2′,7′–dichlorohydrofluorescein (H2DCF). In turn, H2DCF is oxidized in presence of ROS into 2′,7′–dichlorofluorescein (DCF), which is highly fluorescent. In brief, 20 min before the different time end points (1, 3 or 6 h of treatment with **7c**) H2DCFDA 10 μM was added in each well. Then, cells were incubated for 20 min at 37 °C and 5% CO_2 and, after incubation, 1×10^6 cells were centrifuged, resuspended in PBS 1X, and analyzed by flow cytometry. Intracellular ROS levels were expressed as fold increase of treated cells compared to untreated cells.

2.9. Cell-cycle and cell-cycle-related proteins expression analysis

After treatment with **7c** for 6 and 24 h, cells were fixed with 70% ice-cold ethanol; after washing, cells were suspended in 200 μL Guava Cell Cycle Reagent (Merck Millipore), containing propidium iodide, and incubated 30 min at room temperature in the dark before analysis by flow cytometry. The percentages of cells in G0/G1, S, and G2/M phases were quantified by the analysis of DNA content based on the use of Guava Cell Cycle Reagent.

In order to analyze the expression of cyclin A, cyclin B1 and CDK1, after treatment for 24 h, cells were fixed by 70% cold ethanol and permeabilized using 0.25% cold Triton X-100 in Wash Buffer (WB; PBS 1X + 1% bovine serum albumin). Then, samples were washed and incubated with the corresponding primary antibody anti-cyclin A (1:50, Invitrogen, Thermo Fisher Scientific), anti-cyclin B1 (1:50, Invitrogen, Thermo Fisher Scientific), and anti-CDK1 (1:200, Invitrogen, Thermo Fisher Scientific) for 30 min. Next, cells were washed in WB and stained with the respective secondary antibody (anti-mouse 1:200; anti-rabbit 1:200; Invitrogen) for other 30 min. Cells were washed and then

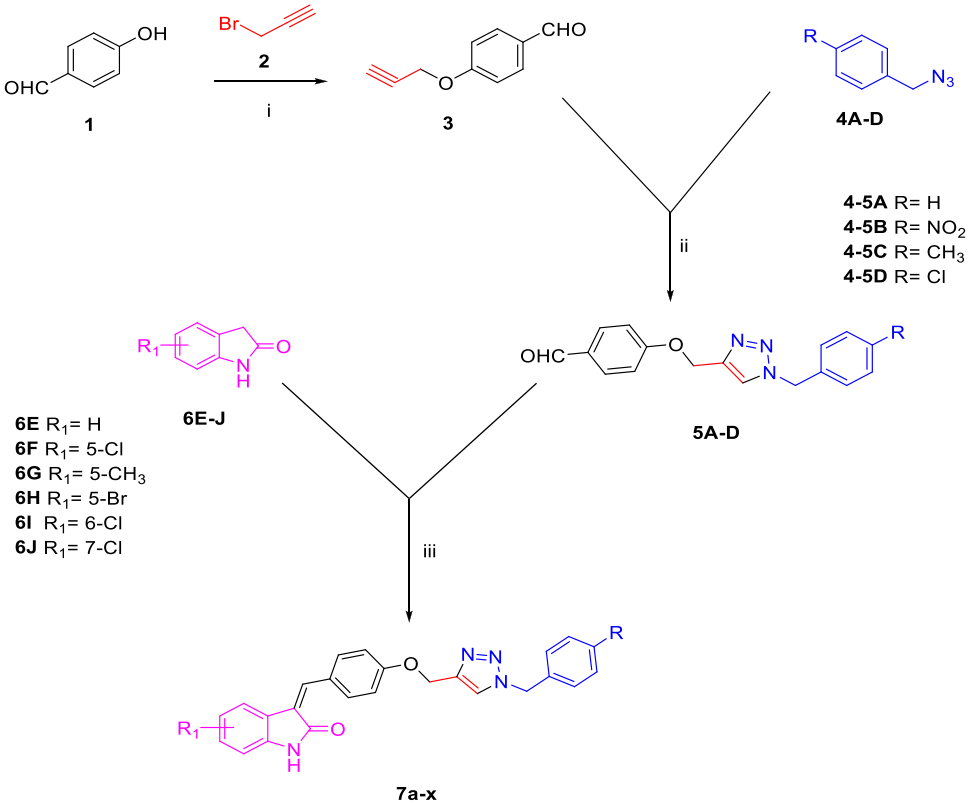

Scheme 1. Synthesis of compounds **7a-x.**

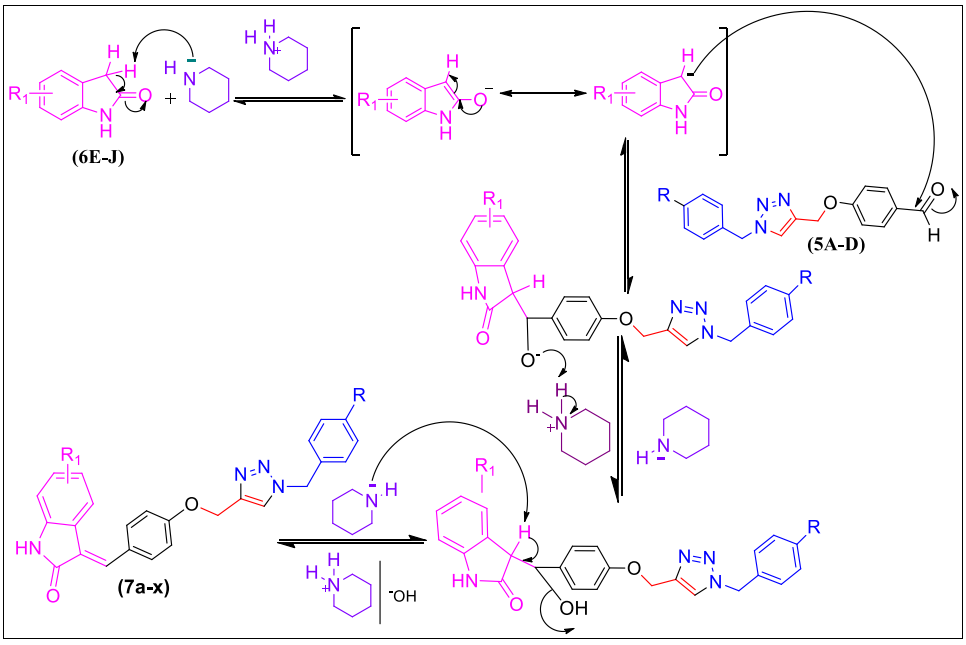

Fig. 2. Mechanism involved in the synthesis of indolin-2-one linked 1,2,3-triazole. derivatives(**7a–x**).

analyzed by flow cytometry, recording the mean fluorescence intensity (MFI) values. Expression of Cyclin A, Cyclin B1, and CDK1 were indicated as fold increase of treated cells compared to untreated cells.

2.10. Analysis of DNA damage

The genotoxic potential of **7c** was assessed evaluating the phosphorylation of histone γ-H2A.X, as marker of DNA double strand breaks. Briefly, after treatment of 5 h with increasing concentrations of **7c**, cells were fixed, permeabilized and incubated for 30 min in the dark at room temperature with an anti γ-H2A.X-Alexa Fluor® antibody (Merck Millipore, Darmstadt, Germany). Then, samples were analyzed *via* flow cytometry. Phosphorylation of histone γ-H2A.X was expressed as fold increase of treated cells compared to untreated cells. Etoposide 10 μg/mL was used as positive control.

2.11. Flow cytometry

All flow cytometric analyses were performed using an EasyCyte 5HT flow cytometer (Guava Technologies-Millipore, Hayward, CA, USA).

2.12. ADME evaluation

The 3D (three dimensional) structures of the molecules were drawn using Avogadro v1.2.0 (Hanwell et al., 2012) and the structures were optimized using MMFF94s force field. SwissADME webserver (Daina et al., 2014, 2017) were used to evaluate ADME parameters, pharmacokinetics and drug-like nature of the molecules.

2.13. Molecular docking simulations

In docking simulations, the X-ray crystal structure (Pdb ID: 6P8Q) of EGFR was used as target. The co-ligand of this structure is 10-benzyl-2-fluoro-5,10-dihydro-11*H*-dibenzo[*b,e*][1,4]diazepin-11-one. In addition, we performed all theoretical calculations for the co-ligand and melphalan, reference drug, in order to compare with the results obtained for the synthesized compounds. For docking simulations, all ligands and target were prepared by using PyRx software (Dallakyanand Olson, 2015) and subsequently the docking experiments were performed using the AutoDockVina software (Trott and Olson, 2010) with Lamarckian genetic algorithm (LGA) (Solis and Wets, 1981; Huey et al., 2007). The visualizations of docking simulations results were conducted using Discovery studio (Biovia, 2017).

2.14. Statistical analysis

All experiments are expressed as the mean ± SEM of at least three independent experiments. Statistical analyses were performed by Repeated Measures ANOVA; Tukey or Dunnett or Bonferroni were used as a post-test, using the statistical software GraphPad InStat 6.0 version (GraphPad Prism, San Diego, CA, USA). p-values below 0.05 were considered as significant and represented as * $p < 0.05$, ** $p < 0.01$, *** $p < 0.001$, and **** $p < 0.0001$.

3. Results and discussion

3.1. Chemistry

A series of twenty-four 1,2,3-triazole derivatives (**7a-x)** was prepared following Scheme 1.4-(Prop-2-ynyloxy)-benzaldehyde**(3)** was synthesized by reacting 4-hydroxybenzaldehyde (**1**) with propargyl bromide (**2**) in presence of potassium carbonate (K_2CO_3) and dry dimethylformamide (DMF), then was treated with benzyl azides (**4A-D)** in presence of sodium ascorbate and copper sulphate pentahydrate ($CuSO_4{\cdot}5\ H_2O$) to get 4-((1-benzyl-1*H*-1,2,3-triazol-4-yl)methoxy)benzaldehydes **(5A-D)** in good yield. Finally, the (Z)− 3-(4-((1-benzyl-1*H*-1,2,3-triazol-4-*yl*)methoxy)benzylidene)indolin-2-ones (**7a-x)** were obtained by refluxing triazole-aldehydes **(5A-D)** and indolin-2-one (**6E-J)** in methanol with piperidine.

The feasibility and mechanism of indolin-2-one (**6E-J**) reaction with 4-((1-arylmethyl-1*H*-1,2,3-triazol-4-yl)methoxy)benzaldehydes (**5A-D**) catalysed by piperidine follows Knoevenagel condensation (Fig. 2). An enol intermediate is formed initially between indolin-2-one **(6E-J)** and piperidine. This enol reacts with 4-((1-arylmethyl-1H–1,2,3-triazol-4-yl) methoxy)benzaldehydes (**5A-D**) and the resulting aldol undergoes subsequent base-induced elimination to form the 3-(4-((1-arylmethyl-1*H*-1,2,3-triazol-4-yl)methoxy)benzylidene)indolin-2-ones (**7a–x**).

All newly synthesized triazoles **(7a-x)** were characterized by their Fourier transform infrared (FTIR) and proton/carbon nuclear magnetic resonance ($^1H/^{13}C$ NMR) spectral data. The FTIR spectra of **7a–x**

showed stretching absorption bands between 3247 and 3141 (N-H), 3090–3010 (C-H, ar.), 2950–2798 (C-H, ali.), 1701–1672 (>C═O), 1623–1582 (>C═N-), 1554–1449 (>C═C<) and 1226–1167 (-O-) cm^{-1}. Absorption bands for -CH_2- bending were observed in the range of 1489–1448 cm^{-1}. Compound **7c**, **7l-r** and **7v** showed -CH_3 bending absorption bands appearing at 1389–1376 cm^{-1}. Absorption bands for -NO_2 stretching in **7g-l** were observed in the range of 1594–1514 cm^{-1}. In ^{1}H NMR spectra, the -NH proton as singlet was observed between δ 11.04–10.41 ppm whereas, triazole ring proton appeared in the range of δ 8.41–8.27 ppm. Prominent signals between δ 8.50–5.90 ppm represent aromatic protons and, signal between δ 7.92–7.51 ppm appeared for benzylidene -CH. Presence of -CH_2- groups was confirmed by a singlet signal between δ 5.81–5.50 (-OCH_2-) and δ 5.29–5.22 (-NCH_2-) ppm. Methyl protons of **7c, 7l-r** and **7v** were seen in the range of δ 2.67–2.17 ppm. The ^{13}C NMR spectra displayed peaks between δ 169–166 ppm for C═O of 2-oxindole, peaks between δ 159–108 ppm for aromatic carbons, peaks at δ 61 ppm for –OCH_2-, peaks between δ 51–53 ppm for triazole –NCH_2- and at δ 20–21 ppm for methyl carbon.

3.2. In vitro cytotoxicity evaluation

All 1,2,3-triazole analogs (**7a–x**) and standard Melphalan were preliminary screened against murine L1210 leukemia cells, human CEM T-lymphocytic and cervix carcinoma HeLa cells. The results are presented in Table 1. Compounds were evaluated in the HeLa and CEM bioassays to ascertain if these triazoles (**7a–x**) are toxic to human cells or not. A number of drugs used in the cancer chemotherapy are toxic to murine leukemia L1210 cells and that made us to use L1210 cell line. The alkylating agent melphalan was used as positive control. In CEM screens, most of the compounds exhibited a good cytotoxic activity either in presence or absence of substituents on 2-oxindole and benzyl group of triazole. Among the tested compounds, **7c** and **7w** proved to be as potent as melphalan, whereas only three compounds **7b, 7j** and **7n** exhibited poor activity in comparison to melphalan. In HeLa screen, the compounds **7a, 7c, 7m, 7o, 7s, 7v** and **7w** showed good cytotoxicity, whereas **7g, 7h, 7j-l, 7t, 7u** and **7x** showed moderate cytotoxic activity. In case of murine leukemia L1210, most of the compounds exhibited moderate to poor cytotoxicity except **7c, 7o** and **7v**. Moreover, the most potent cytotoxic compound **7c** was further analyzed in order to evaluate its mechanism of action and studied for drug likeliness by using SwissADME webserver.

3.3. Structure activity relationships

Compounds **7** were less effective against murine L1210 leukemia cells in comparison to standard melphalan (2.13 μM). However, the introduction of a methyl group at position 5 of indolin-2-one, led to the most effective compounds, namely **7c**, **7o** and **7 v**, with IC_{50} 3.0, 5.3 and 4.8 μM respectively, against murine L1210 cells. Substituents different from the methyl group on indolin-2-one and benzyl group did not improve cytotoxicity against murine L1210 leukemia cells. Substitutions made at position 5, 6 or 7 on indolin-2-one and at position 4 on benzyl group increased (compounds **7c**, **7w**) or maintained the cytotoxic activity against CEM cells, except for compounds **7b**, **7 f**, **7j** and **7r**. In general, replacement of hydrogen with -CH_3, -Cl or -NO_2 at position 4 of benzyl group, as well as substitution at position 5, 6 or 7 on indolin-2-one, improved cytotoxicity against HeLa cells.

3.4. Compound 7c exclusively induces caspase-dependent apoptosis in Jurkat cells and activates both intrinsic and extrinsic apoptotic pathways

We next investigated the molecular mechanisms involved in **7c**'s cytotoxicity by flow cytometry. The screening of the newly synthesized 1,2,3-triazole analogs unveiled that the most potent compound **7c** was highly cytotoxic on CEM leukemia cells. Therefore, we preliminary tested **7c** on different leukemia cell lines (*i.e.* HL-60, CEM, and Jurkat)

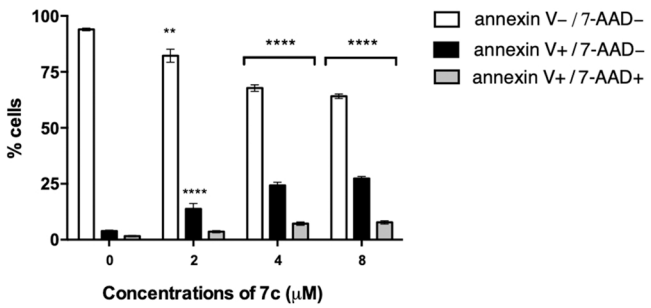

Fig. 3. Percentage (%) of viable (annexin V^-/7-AAD^-), early apoptotic (annexin V^+/7-AAD^-), and late apoptotic or necrotic (annexin V^+/ 7-AAD^+) cells after 24 h treatment of Jurkat cells with increasing concentrations of **7c**. ** $p < 0.01$; **** $p < 0.0001$ *versus* untreated cells.

using a cytofluorimetric technique, as described in materials and methods. Among all, Jurkat cells were found to be the most sensitive to **7c** cytotoxicity (data not shown) and thus were chosen to deeper investigate the anticancer potential of compound **7c**.

Different cell-death modalities were defined based on morphological alterations associated with specific mechanisms whereby dead cells are eliminated. These modalities include three types of cell demise: type I or apoptosis, type II or autophagy and type III or necrosis. Of note, apoptosis and autophagy are programmed cell death (PCD) pathways. Necrosis, instead, is a non-physiological, accidental cell death process caused by infections or trauma (Galluzzi et al., 2018, Greco et al., 2021). Among all types of PCDs, apoptosis is definitely the most studied and known mechanism of cell demise. Apoptosis is mainly mediated by two pathways: the extrinsic, or death receptor pathway, and the intrinsic, or mitochondrial pathway. The extrinsic apoptotic pathway is triggered by extracellular ligands that bind to specific transmembrane death receptors (DRs), leading to the activation of pro-caspase-8/-10. Once activation of caspase-8/-10 occurs, they cleave and activate effector caspase-3/-7, driving to apoptosis execution (Galluzzi et al., 2018). The intrinsic or mitochondrial apoptotic pathway, instead, is triggered by a wide variety of extracellular and intracellular stress stimuli that lead to the irreversible and diffuse mitochondrial outer membrane permeabilization (MOMP) (Galluzzi et al., 2018). Once the mitochondrial permeability is destroyed, the transmembrane potential collapses and multiple apoptogenic factors, as cytochrome c, are released into the cytoplasm (D'Arcy, 2019). Active caspase-9 catalyzes the proteolytic activation of executioner caspase-3 and -7, leading to apoptotic cell death (D'Arcy, 2019).

In order to analyze if **7c** triggers apoptotic or necrotic cell death, we performed the annexin V/7-AAD assay. The use of annexin V binding to phosphatidylserine *plus* 7-amino-actinomycin D (7-AAD) allows detecting apoptotic cells (annexin V^+/7-AAD^- cells) and necrotic cells (annexin V^+/ 7-AAD^+ cells) (Zimmermann and Meyer, 2011). After 24 h of treatment, **7c** increased the fraction of apoptotic cells in a dose-dependent manner. The percentage of apoptotic cells started to increase from the concentration 2 μM (14% *versus* 3.9% in untreated cells), and further increased up to the highest tested concentration, where they reached about 27%. Alongside the increase in apoptotic cells, the percentage of necrotic cells remained constant between 3% and 7% at all tested concentrations (Fig. 3).

At this point, some of the molecular pathways modulated by the newly synthesized compound **7c** have been explored. Caspase-3 is an effector caspase activated from both the intrinsic and extrinsic apoptotic pathway (Nagata et al., 2018). Its activity was markedly increased after treatment with **7c**, up to about 8 times at concentrations 4 and 8 μM (Fig. 4), confirming apoptosis induction by the indole-based derivative. Next, to investigate the involvement of the extrinsic apoptotic pathway in the pro-apoptotic activity of **7c**, we analyzed the activity of caspase-8. Its activity increased up to about 4 times at concentrations 4 and 8 μM

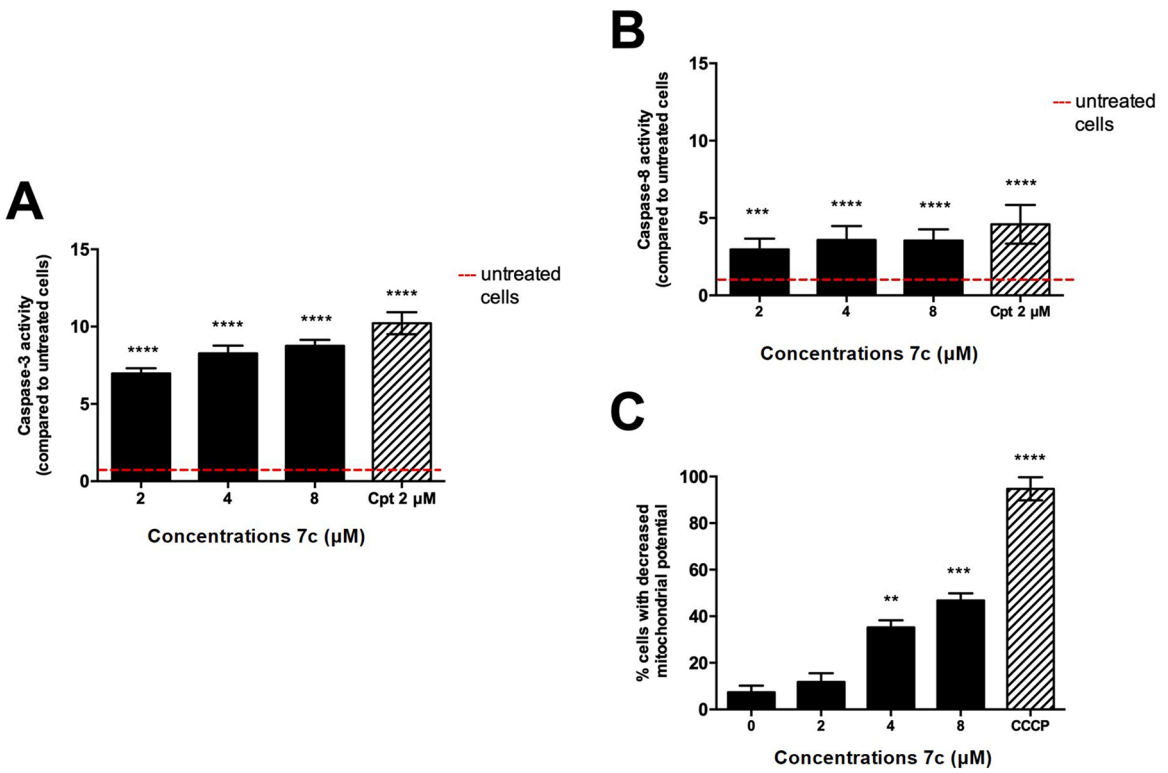

Fig. 4. Activity of caspase-3 (A) and caspase-8 (B) and percentage (%) of cells with decreased mitochondrial potential (C) after 24 h treatment of Jurkat cells with increasing concentrations of **7c**. Cpt (camptothecin) and CCCP (carbonyl cyanide 3-chlorophenylhydrazone) were used as positive controls. **p < 0.01; ***p < 0.001; ****p < 0.0001 *versus* untreated cells.

after **7c** treatment (Fig. 4). To assess the involvement of the intrinsic apoptotic pathway, we measured the decrease in mitochondrial transmembrane potential. A significant increase in cells with reduced potential was recorded starting from concentration 4 μM (35% of cells with decreased potential *versus* 7.4% in untreated cells) and the percentage further increased to about 46% at 8 μM (Fig. 4). On the whole, our results indicate that **7c** activates both apoptotic pathways.

The ability of **7c** to activate both apoptotic pathways is noteworthy. Indeed, cancer cells are characterized by high genetic and genomic instability, which can lead to the mutation of some of the molecular actors involved in a specific apoptotic pathway. As an example, overexpression of Bcl-2 (B-cell lymphoma 2) and associated anti-apoptotic proteins, impaired assembly of a functional apoptosome, inactivation of caspase-8, decreased expression or gene mutations of Fas (Fas cell surface death receptor, also called CD95) (Mohammad et al., 2015; Fulda, 2009) are just some of the multiple mechanisms involved in apoptosis resistance. The result is the development of drug resistance and the lack of efficacy of anticancer therapy (Mohammad et al., 2015). Thus, evidence that compound **7c** is able to modulate both apoptotic pathways could potentially increase its clinical potential.

In addition to apoptosis, other non-apoptotic forms of PCD have recently been discovered, which are activated regardless of apoptosis or when apoptosis is inhibited. (Greco et al., 2021) Non-apoptotic cell deaths are morphologically and biochemically different from apoptosis and comprise multiple PCD pathways (Tait et al., 2014, Greco et al., 2021), as ferroptosis, necroptosis and parthanatos. Necroptosis is a highly regulated cell death mechanism, which shares the typical morphological features of necrosis. The process of necroptosis is controlled in an apoptosis-deficient environment by receptor interacting protein RIP1 and RIP3. Together with RIP1 and 3, mixed lineage kinase domain like pseudokinase (MLKL) is also involved in necroptosis (Qin et al., 2019). Indeed, after its phosphorylation by active phosphorylated RIP3, MLKL oligomerizes and translocates to plasma membrane, which

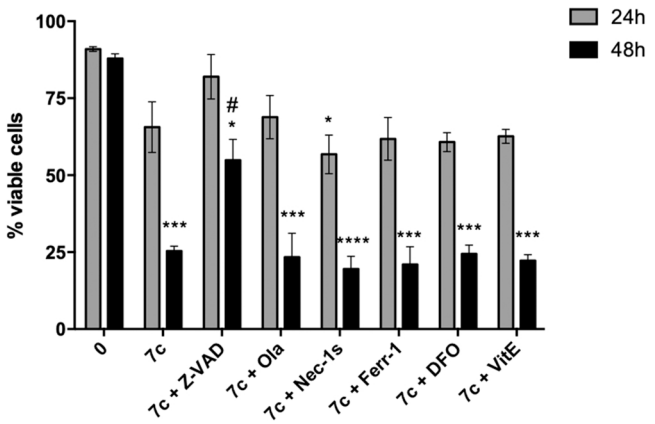

Fig. 5. Percentage (%) of viable cells after pre-treatment for 1 h with Z-VAD-FMK (Z-VAD), olaparib (Ola), necrostatin-1 s (Nec-1 s), ferrostatin-1 (Ferr-1), DFO, or vitamin E (VitE) following 24 h and 48 h treatment with **7c** 8 μM. *p < 0.05; ***p < 0.001; ****p < 0.0001 *versus* untreated cells. # p < 0.05 *versus* **7c**-treated cells.

is a crucial event for necroptosis execution (Chen et al., 2019). On the other hand, ferroptosis is a non-apoptotic form of cell death triggered by the inhibition of glutathione biosynthesis or the glutathione-dependent antioxidant enzyme GPX4 (glutathione per-oxidase 4), which leads to the accumulation of lipid reactive oxygen species (ROS) and consequently cell demise. (Cao et al., 2016). Finally, parthanatos is a peculiar form of non-canonical PCD characterized by plasma membrane rupture without the formation of apoptotic bodies and DNA fragments. Biochemically, parthanatos is a PARP-1-dependent PCD pathway, as it is mediated by the hyperactivation of PARP-1, due to a DNA-base modification (Galluzzi et al., 2018).

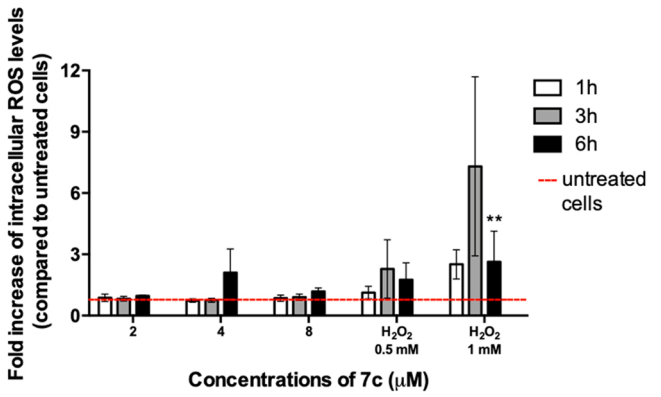

Fig. 6. Intracellular ROS levels, expressed as fold increase *versus* untreated cells, of Jurkat cells treated with increasing concentrations of **7c** for different time points. H_2O_2 0.5 and 1 mM were used as positive control. **p < 0.01*versus* untreated cells.

Hence, to determine whether **7c** could activate non-canonical cell death programs, Jurkat cells were pre-treated for 1 h with different chemical inhibitors [*i.e.* Z-VAD-FMK, olaparib, necrostatin-1s, ferrostatin-1, deferoxamine mesylate (DFO), and vitamin E] in order to inhibit apoptosis, parthanatos, necroptosis and ferroptosis, respectively. Then, after pre-treatment, cells were treated with **7c** 8 μM for 24 h and 48 h and cell viability was analyzed by flow cytometry.

Among all the pharmacological inhibitors, only the pan-caspase inhibitor Z-VAD-FMK increased Jurkat cells viability, just partially after 24 h and significantly after 48 h (Fig. 5). Recorded cell viability of Z-VAD-FMK pre-treated cells was 82% at 24 h (*versus* 65% of **7c**-treated cells) and 55% at 48 h (*versus* 25% of **7c**-treated cells). Our results indicate that **7c** does not induce non-canonical cell death as ferroptosis, necroptosis or parthanatos, but exclusively caspase-dependent apoptosis.

Regarding the ability of indoles and indole derivatives, no evidence has been found about their ability to trigger non-canonical cell death. A study conducted by Behnisch-Cornwell and colleagues, for example, investigated ferroptosis induction in human cervical cancer SISO cells by a series of newly synthesized indole-based pentathiepins, establishing that these new derivatives induce apoptosis rather than ferroptosis (Behnisch-Cornwell et al., 2020).

3.5. ROS are not involved in the pro-apoptotic activity of 7c

ROS play a central role in cell signaling and represent one of many stimuli that leads to apoptotic cell death(Galluzzi et al., 2018). We measured intracellular ROS levels after different treatment times with **7c**. **7c** did not induce any significant modulation of ROS levels (Fig. 6), thus indicating that ROS generation is not involved in the orchestration of the cytotoxic response evoked by the newly triazole derivative **7c**.

3.6. Compound 7c causes cell-cycle perturbations

Cell cycle is a sequence of closely coordinated molecular processes that control DNA replication and chromosome division, ultimately leading to cell division and transfer of genetic material. Cell cycle resides into four distinct phases: G1 (gap), S (synthesis), G2 (gap) and M (mitosis), all strictly controlled by cyclins and cyclin-dependent kinases (CDKs) (Hochegger et al., 2008). Since the G1/S and G2/M checkpoints finely control cell proliferation, cell-cycle arrest is considered one of the most common events triggering the inhibition of cell proliferation. Hence, to explore the cytostatic potential of **7c** we analyzed cell-cycle progression of **7c**-treated cells together with the expression of some cyclins and CDKs. The treatment with increasing concentrations of **7c** induced a significant accumulation of cells in the G2/M phase. Starting

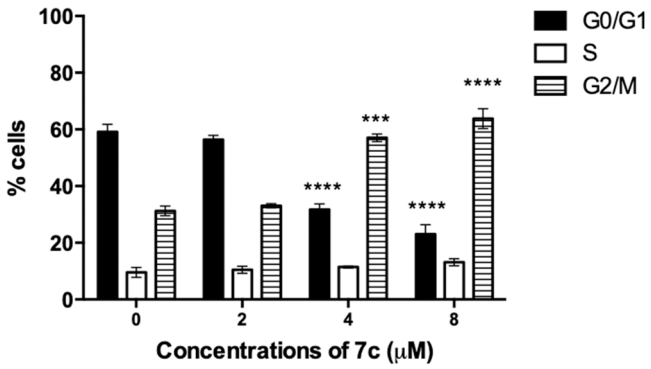

Fig. 7. Cell-cycle distribution after Jurkat cells treatment with **7c** for 24 h. ***p < 0.001; ****p < 0.0001 *versus* untreated cells.

from the concentration 4 μM the accumulation of cells in the G2/M phase appeared to be statistically significant, with 57% *versus* 31% of untreated cells; at the highest tested concentration, the percentage further increased up to 64%. This observed increase was accompanied, at all tested concentrations, by a slight compensatory decrease in cells in the G0/G1 phase, from 59% of untreated cells to 23% of cells treated with **7c** 8 μM (Fig. 7).

As mentioned before, cell cycle is tightly controlled by CDKs and cyclins. Briefly, in the G1 phase, activation of cyclin D-CDK4/6 complex leads to the phosphorylation of RB1 protein, thus promoting the expression of different genes that regulate cell-cycle progression. Then, when cells progress into the S phase, cyclin A starts to be synthesized, thus replacing cyclin D and reaching its maximal expression in the G2 phase until its degradation during the transition from the G2 to the M phase of cell cycle. Cyclin B, instead, starts to be expressed from the G2 phase and extensively accumulates prior to mitosis. Finally, CDK1 could be activated by both interphase cyclins (*i.e.*cyclins D, E, and A) and mitotic cyclin B (Hochegger et al., 2008). To explore whether **7c**-treated cells accumulate in G2 or M phase, the expression of cyclin A and B1, and CDK1 was analyzed. After 24 h of treatment, **7c** did not modulate the expression of cyclin B1 and CDK1; however, a slight downregulation of cyclin A was observed (Fig. 8). As we noticed a decrease in cyclin A expression, but not a modulation of cyclin B and CDK1, we could speculate that compound **7c** may block cell-cycle progression during the transition from the G2 to the M phase, where cyclin A starts to be degraded prior to the entry of cells in mitosis. Moreover, this hypothesis could explain why we did not observe any modulation of cyclin B1 and CDK1 expression.

3.7. The pro-apoptotic activity of 7c is linked to its cytostatic activity

Next, the pro-apoptotic and cytostatic activities of **7c** were analyzed after 6 h of treatment with **7c** to assess whether the two events were related or independent from each other. At 6 h of treatment,**7c** did not induce cell death, while a substantial block of cell cycle was already evident (Fig. 9). Thus, we can hypothesize that **7c**-induced apoptosis could be a secondary effect, related to its cytostatic activity rather than an independent event.

3.8. Compound 7c lacks genotoxic activity

Given the interesting anticancer activities observed for **7c**, a preliminary assessment of its toxicological profile was performed by analyzing its genotoxicity. The ability of a compound to cause DNA damage is a crucial factor in determining its toxicological profile, as DNA mutations are involved in the pathogenesis of several degenerative diseases, as cancer (Nohmi, 2018). Additionally, genotoxicity is a dose-independent event, which means that a range of concentrations where genotoxicity does not occur cannot be always established

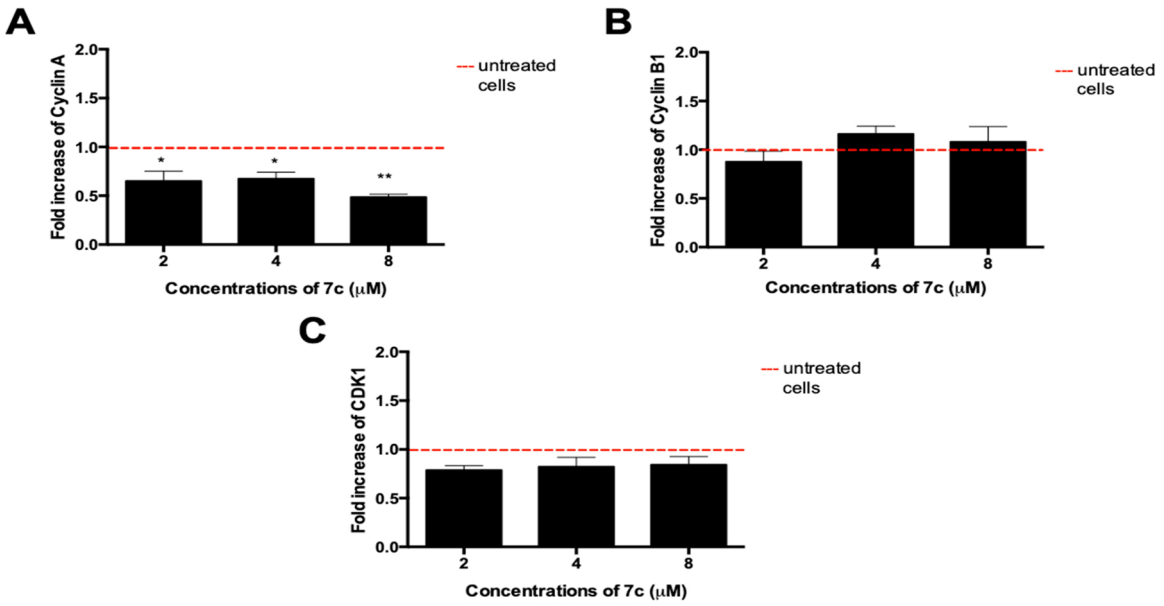

Fig. 8. Expression of cyclin A (A), cyclin B1 (B), and CDK1 (C), indicated as fold increase *versus* untreated cells, following 24 h treatment of Jurkat cells with increasing concentration of **7c**. *p < 0.05; **p < 0.01 *versus* untreated cells.

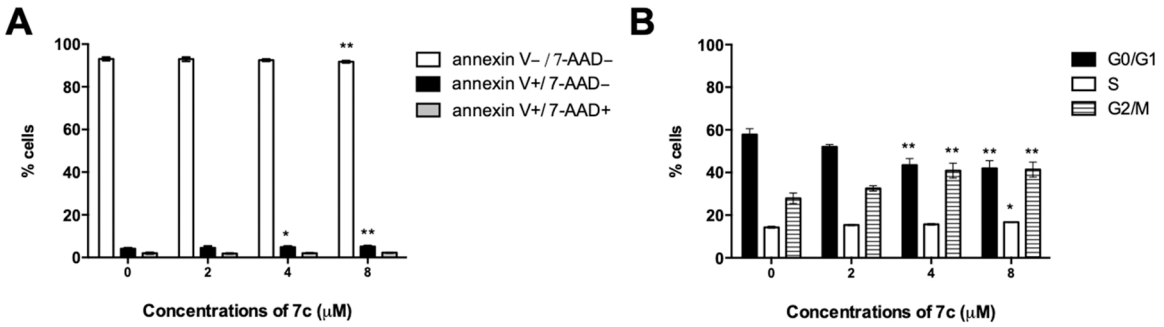

Fig. 9. Percentage (%) of viable (annexin V^-/7-AAD^-), early apoptotic (annexin V^+/7-AAD^-), and late apoptotic or necrotic (annexin V^+/ 7-AAD^+) cells (A) and cell-cycle distribution (B) following 6 h treatment of Jurkat cells with increasing concentrations of **7c**. *p < 0–05; **p < 0.01 *versus* untreated cells.

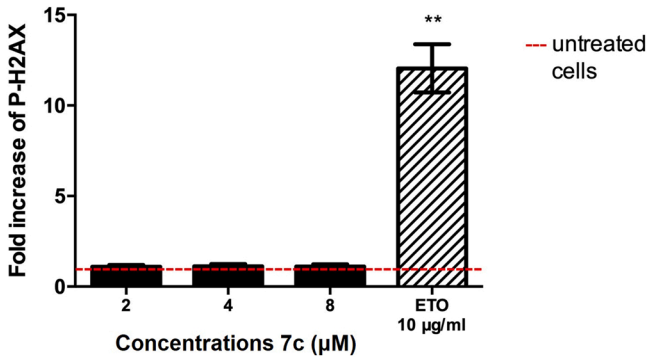

Fig. 10. Relative expression of P-H2AX following 5 h treatment of Jurkat cells with increasing concentrations of **7c**. Etoposide (ETO) 10 μg/mL was used as positive control. **p < 0.01 *versus* untreated cells.

(Nohmi, 2018). The eventual genotoxic activity of **7c** was verified by analyzing the phosphorylation of H2A.X (P-H2A.X) at Serine 139. P-H2A.X is considered an early cellular response to DNA double-strand breaks; hence, the analysis of this event is useful to detect the ability of a compound to induce DNA damage (Mah et al., 2010). Following 5 h treatment of Jurkat cells with **7c**, no significant increase in H2A.X phosphorylation was observed at any tested concentration (Fig. 10). Our results are in contrast with what has been observed for other indole derivatives. Indeed, a series of indole hydrazide (Kilic-Kurt et al., 2020) and bis-indolinone derivatives (Amato et al., 2014) induced DNA damage in breast adenocarcinoma MCF-7 cells and in human transformed fibroblasts (BJ-EHLT), as shown by a significant increase in H2AX phosphorylation (Kilic-Kurt et al., 2020; Amato et al., 2014).

3.9. Effect of 7c in normal cells

To investigate the effect of **7c** on cancer cells compared to normal, we treated 293 T cells with 0.5 mM of **7c** and performed a dead test using ethidium bromide stain over a period of 48 h. The results showed that **7c** was more cytotoxic against L1210 (3 μM), CEM (1.5 μM) and HeLa (3.4 μM) compared to 293 T normal cells (7.5 μM) (Fig. S1). This suggests that **7c** can effectively kill cells with a high rate of growth which is a hallmark of cancer cells.

3.10. Physicochemical properties and ADME parameters

The physicochemical properties, ADME parameters and the violations of drug-likeness rules of synthesized compounds were listed in Table 2. In here, the evaluated physicochemical properties are: the molecular weight (MW), topological polar surface area (tPSA), Molar

Table 2
Pharmaceutical properties of compounds **7a–x**.

Comp.	BindingAffinity	Physicochemical Properties							Lipophilicity						Water Solubility		Violation of Drug-likeness filters						
		MW (g/mol)	Fsp^3	RB	HBA	HBD	MR	tPSA	iLogP	XLogP	WLogP	MLogP	SILICOS-IT	Consensus LogP	ESOL	Class	Lipinski	Ghose	Veber	Egan	Muegge	Bioavailability Score	Log K_p (cm/s)
7a	-10.9	408.45	0.08	6	4	1	122.45	69.04	3.36	3.76	3.57	3.18	4.18	3.61	-4.89	Moderately	0	0	0	0	0	0.55	-6.12
7b	-10.7	442.90	0.08	6	4	1	127.46	69.04	3.67	4.39	4.22	3.65	4.82	4.15	-5.49	Moderately	0	0	0	0	0	0.55	-5.88
7c	-11.1	422.48	0.12	6	4	1	127.41	69.04	3.54	4.12	3.87	3.38	4.71	3.93	-5.19	Moderately	0	0	0	0	0	0.55	-5.95
7d	-10.3	487.35	0.06	6	4	1	130.15	69.04	3.65	4.45	4.33	3.75	4.86	4.21	-5.80	Moderately	0	2	0	0	0	0.55	-6.11
7e	-11.0	442.90	0.08	6	4	1	127.46	69.04	3.71	4.39	4.22	3.65	4.82	4.16	-5.49	Moderately	0	0	0	0	0	0.55	-5.88
7 f	-10.7	442.90	0.08	6	4	1	127.46	69.04	3.61	4.39	4.22	3.65	4.82	4.14	-5.49	Moderately	0	0	0	0	0	0.55	-5.88
7 g	-10.9	487.89	0.08	7	6	1	136.28	114.86	3.35	4.22	4.13	3.58	2.65	3.59	-5.55	Moderately	0	2	0	0	0	0.55	-6.28
7 h	-10.5	532.35	0.08	7	6	1	138.97	114.86	3.44	4.28	4.24	3.69	2.69	3.67	-5.86	Moderately	1	2	0	0	0	0.55	-6.51
7i	-10.8	487.89	0.08	7	6	1	136.28	114.86	3.16	4.22	4.13	3.58	2.65	3.55	-5.55	Moderately	0	2	0	0	0	0.55	-6.28
7j	-10.7	487.89	0.08	7	6	1	136.28	114.86	3.14	4.22	4.13	3.58	2.65	3.54	-5.55	Moderately	0	2	0	0	0	0.55	-6.28
7k	-10.6	453.45	0.08	7	6	1	131.27	114.86	3.08	3.59	3.47	3.11	2.01	3.05	-4.95	Moderately	0	1	0	0	0	0.55	-6.52
7 l	-10.8	467.48	0.12	7	6	1	136.23	114.86	3.35	3.95	3.78	2.50	2.54	3.23	-5.25	Moderately	0	1	0	0	0	0.55	-6.35
7 m	-10.9	422.48	0.12	6	4	1	127.41	69.04	3.60	4.12	3.87	3.38	4.71	3.94	-5.19	Moderately	0	0	0	0	0	0.55	-5.95
7 n	-10.6	456.92	0.12	6	4	1	132.42	69.04	3.80	4.75	4.53	3.85	5.34	4.45	-5.79	Moderately	0	1	0	0	0	0.55	-5.71
7o	-11.5	436.51	0.15	6	4	1	132.38	69.04	3.70	4.49	4.18	3.59	5.23	4.24	-5.49	Moderately	0	1	0	0	0	0.55	-5.77
7p	-10.8	501.37	0.12	6	4	1	135.11	69.04	3.86	4.81	4.64	3.95	5.38	4.53	-6.10	Moderately	1	2	0	0	0	0.55	-5.94
7q	-10.9	456.92	0.12	6	4	1	132.42	69.04	3.92	4.75	4.53	3.85	5.34	4.48	-5.79	Moderately	0	1	0	0	0	0.55	-5.71
7r	-10.4	456.92	0.12	6	4	1	132.42	69.04	3.90	4.75	4.53	3.85	5.34	4.48	-5.79	Moderately	0	1	0	0	0	0.55	-5.71
7 s	-10.7	442.90	0.08	6	4	1	127.46	69.04	3.62	4.39	4.22	3.65	4.82	4.14	-5.49	Moderately	0	0	0	0	0	0.55	-5.88
7 t	-10.9	477.34	0.08	6	4	1	132.47	69.04	3.76	5.01	4.87	4.12	5.46	4.64	-6.08	Moderately	0	1	0	0	1	0.55	-5.65
7 u	-10.8	521.79	0.08	6	4	1	135.16	69.04	3.88	5.08	4.98	4.22	5.49	4.73	-6.40	Moderately	2	2	0	0	1	0.17	-5.88
7 v	-11.3	456.92	0.12	6	4	1	132.42	69.04	3.78	4.75	4.53	3.85	5.34	4.45	-5.79	Moderately	0	1	0	0	0	0.55	-5.71
7w	-11.0	477.34	0.08	6	4	1	132.47	69.04	3.81	5.01	4.87	4.12	5.46	4.65	-6.08	Moderately	0	1	0	0	1	0.55	-5.65
7x	-10.8	477.34	0.08	6	4	1	132.47	69.04	3.94	5.01	4.87	4.12	5.46	4.68	-6.08	Moderately	0	1	0	0	1	0.55	-5.65
Melphalan	-8.0	313.26	1.00	8	4	3	80.01	69.72	2.79	1.25	1.35	1.56	1.72	1.73	-2.04	Soluble	0	0	0	0	0	0.55	-7.32
Co-ligand	-8.1	364.55	1.00	2	4	2	99.73	35.50	0.00	4.01	2.95	3.49	1.02	2.29	-4.49	Moderately	0	0	0	0	0	0.55	-5.68

MW: molecular weight, Fsp^3:fraction of sp^3 carbon atoms, RB: rotatable bonds,HBD: hydrogen bonds donor, HBA: hydrogen bond acceptor, MR: molecular refractivity,tPSA: topological polar surface, LogP: indicator of lipophilicity,ESOL: solubility parameter, Log K_p: skin permeation.

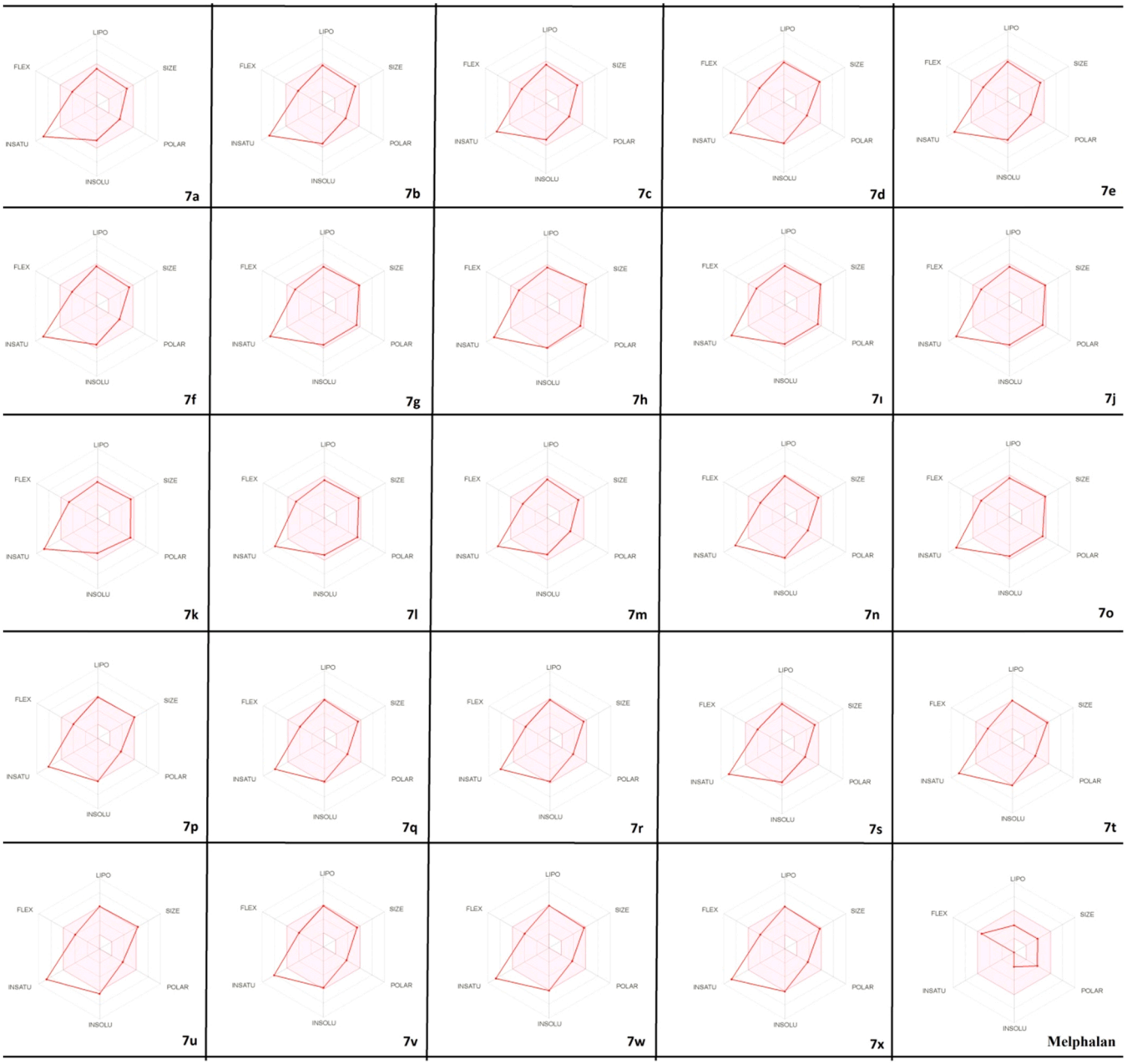

Fig. 11. The bioavailability radar schemes of all synthesized compounds.

Refractivity (MR), fraction of sp^3 carbon atoms (Fsp^3) and some Hydrogen Bond properties. tPSA is defined as the sum of surface areas of polar atoms in a molecule and is used to estimate drug transport properties. Low tPSA values in molecules correspond to a higher propensity for transport and tPSA values obtained for all compounds are within the range of values recommended by various drug-likeness filters. Fsp^3 is a newer parameter (Lovering et al., 2009) used to evaluate drug-likeness properties of molecules. As reported in Table 2, Fsp3 values of all compounds are lower than co-ligand and melphalan. MR is defined as a measure the overall polarity of a molecule and is expected to be in the range from 40 to 130. According to Table 2, MR values for all compounds are within this range. On the other hand, lipophilicity is a valuable parameter that affects drug activity in the human body. LogP values are the most widely used measure of lipophilicity and represent an indicator of drugs permeability to reach the target tissue in the body. The LogP values used by the different drug-likeness filters (MLogP for Lipinski filter (Lipinski et al., 1997), WLogP for Ghose (Ghose et al., 1999) and Egan filters (Egan et al., 2000)), XLogP for Muegge filter (Muegge et al., 2001) and their mean values (consensus LogP) were shown in the Table 2. The obtained LogP values vary a lot depending on the method used for the prediction and the acceptability limits of the LogP values differ according to drug filters approaches.In this context, when the LogP values are examined in the Table 2, it is observed that the compounds **7t** (XLogP=5.01), **7u** (XLogP=5.08), **7w** (XLogP=5.01) and **7x** (XLogP=5.01) slightly exceed the acceptability limit (XLogP< 5) determined by the Muegge filter. On the other hand, it can be said that all other LogP values meet general standards. ESOL is aqueous solubility parameter of molecules proposed by Delaney (Delaney, 2004) and is considered one of the key physical properties in drug discovery. We observed that ESOL values of all synthesized compound belong to moderately water-soluble class.

On the other hand, there are a lot of filter approach in the literature that suggest a set of rules to evaluate drug-likeness profiles ofmolecules. The filters discussed in this paper and their rules are as follows.

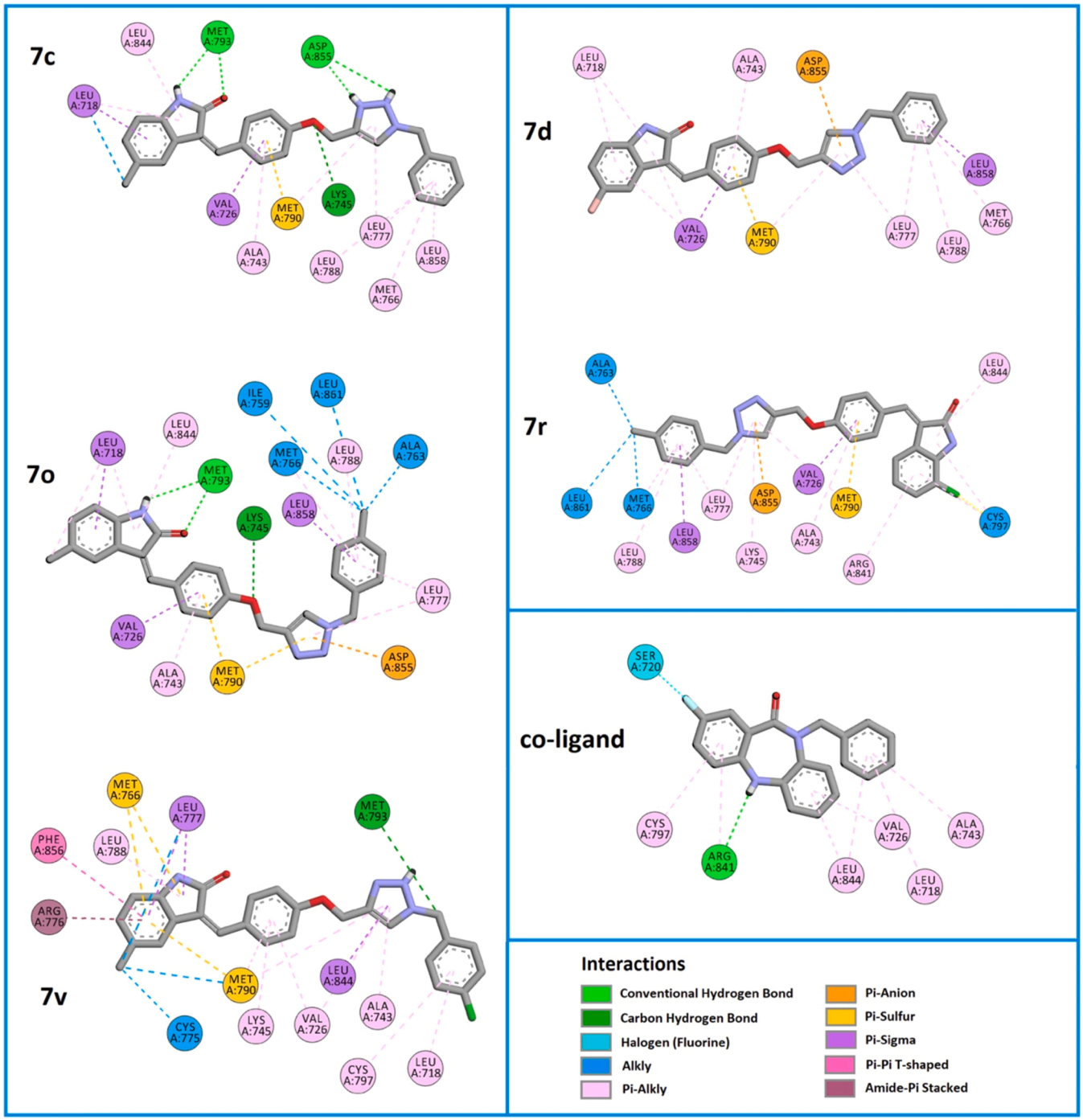

Fig. 12. 2D interaction diagram between 6P8Q receptor and compounds **7c, 7d, 7o, 7r, 7 v**, and co-ligand.

- Lipinski (Pfizer) filter (Lipinski et al., 1997): MW≤ 500; MLogP ≤ 4.15; HBA≤ 10; HBD≤ 5
- Ghose filter (Ghose et al., 1999): 160 ≤MW≤ 480; − 0.4 ≤WLogP ≤ 5.6; 40 ≤MR≤ 130; 20 ≤atoms≤ 70
- Egan (Pharmacia) filter (Egan et al., 2000): WLogP≤ 5.88; tPSA≤ 131.6
- Muegge (Bayer) filter (Muegge et al., 2001): 200 ≤MW≤ 600, − 2 ≤XLogP≤ 5; tPSA≤ 157; HBA≤ 10; HBD≤ 5; RB ≤ 15; Number of rings≤ 7; Number of carbons> 4; Number of heteroatoms> 1
- Veber (GSK) filter (Veber et al., 2002): RB≤ 10; tPSA≤ 140

In here, the filters generally state that an orally active drug should not violate the above criteria more than once. According to Table 2, it is observed that compound **7u** violates twice both Lipinski and Ghose filters. For all synthesized compounds except compound **7u**, it can be inferred that the rules of drug-likeness filters are followed. On the other hand, bioavailability score estimate the probability of a compound to have oral bioavailability in rat or measurable Caco-2 permeability and the bioavailability score value of a compound in the rat is expected to be > 0.10 (Martin, 2005). A poor bioavailability results in lower activity of the molecule and higher inter-individual variability, and thus causes an unexpected response of a drug.The bioavailability score value of only compound **7u** is 0.17 and F values for all the synthesized compounds, co-ligand and melphalan are is 0.55. Log Kp presented in Table 2 is skin permeation parameter suggested by Potts (Potts and Guy, 1992);high negative Log Kp value of the molecule indicates that the molecule has

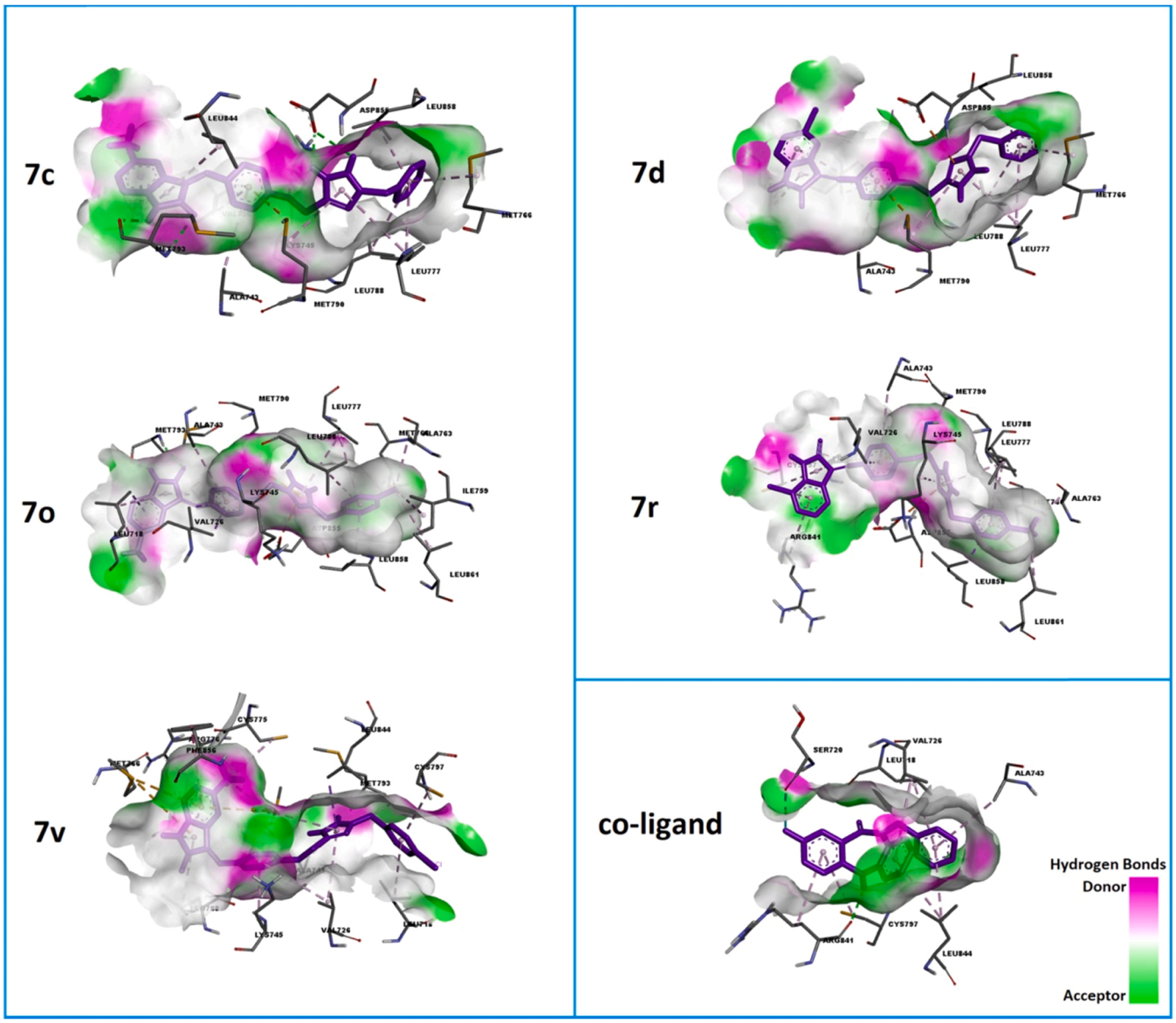

Fig. 13. 3D interactions on the Hydrogen Bond surface between 6P8Q receptor and compounds **7c**, **7d**, **7o**, **7r**, **7v**, and co-ligand.

less penetration into the skin. Accordingly, it is observed that all the synthesized compounds have higher skin permeability than melphalan.

In summary, Table 2 shows the physicochemical properties, lipophilicity and water solubility values of the compounds used by various drug filters. When the violation values of the drug filter criteria are examined, as general trend, the synthesized compounds appears to be drug-likeness. Moreover, the favorable bioavailability scores of the synthesized compounds and the higher skin absorption relative to the reference drug relative to the LogKp values indicate that these compounds can be potential drug candidates.

Moreover, we depicted the bioavailability radar scheme in Fig. 11 using SwissADME webserver. The bioavailability radar allows a rapid and more clear assessment of drug similarity of compounds. In the radar scheme, the red colored zone shows the suitable physicochemical space for oral bioavailability of molecules by taking into criteria such as flexibility, lipophilicity, saturation, size, polarity, and solubility. Validity limits of the criteria are for Lipophilicity: $-0.7 < XLogP < +5.0$, Size: $150 < MW < 500$, Polar: $20 < tPSA < 130$, Insolu: $0 < ESOL < 6$, Insatu: $0.25 < Fsp^3 < 1.00$ and Flex: $0 < RB < 9$. According to radar scheme, it is observed that all criteria except Insatu for all synthesized compounds remain within the red colored region. Lower Fsp3 values, in other words, the decrease of molecule saturation, is associated with lower solubility in water and this situation can be also seen from Table 2. It can be said that the oral bioavailability of the compounds synthesized according to the radar schemes is at an acceptable level.In summary, ADME predictions discussed in the paper shows that all synthesized compounds meet the criteria for being a possible drug candidate.

3.11. Molecular docking calculations

As mentioned before, EGFR is involved in the development of different cancer types. Therefore, the ability of potential new anticancer agents to target and eventually inhibit EGFR activity is considered an effective antitumor strategy, especially for solid tumors (Wykosky et al., 2011). For this reason, we also performed molecular docking simulations to identify the possible binding sites on the EGFR receptor. The highest binding affinity values obtained for all molecules were added to Table 2. It was observed that all compounds had higher docking scores than co-ligand (10-benzyl-2-fluoro-5,10-dihydro-11*H*-dibenzo[*b,e*][1,4] diazepin-11-one), an inhibitor of the 6P8Q EGFR receptor. Therefore, it can be inferred that these compounds could act as EGFR inhibitors. When the values are examined, we also observe that docking affinity

values are in good agreement with *in vitro* cytotoxicity results. When the values are examined, it can be also observed that affinity values are in good agreement with the experimental activity results. The three compounds with the highest binding affinity are **7c** (−11.1 kcal/mol), **7o** (−11.5 kcal/mol) and **7v** (−11.3 kcal/mol) while the two compounds with the lowest binding affinity are compounds **7d** (−10.3 kcal/mol) and **7r** (−10.4 kcal/mol). Considering both these results and *in vitro* cytotoxicity results, we displayed the 2D interaction of these compounds and co-ligand with the 6P8Q EGFR receptor (Fig. 12). It is seen in the diagram that all of the compounds **7c**, **7o**, and **7v** have, in common, hydrogen bond with MET793, Pi-Sulfur with MET790 and Pi-Alkyl type interactions with LEU788, ALA743. Therefore, it can be said that these residues play a key role for high binding affinity. On the other hand, compounds **7p** and **7r** with the lowest binding affinity have common eight interactions with the 6P8Q receptor. These interactions are Pi-Sigma with ALA726 and LEU 858, Ala743, LEU777, LEU788, Pi-Alky with MET790, Pi-Anion with ASP855, Pi-Sulfur with MET790. These common interactions could be an important finding for low binding affinity.

Due to the importance of hydrogen bonds in terms of the pharmacological properties of molecules, we also demonstrated the 3D interactions of the above-mentioned compounds and the co-ligand along with a hydrogen bond surface (Fig. 13). From the figure, acceptor and donor surface areas can be seen easily.

4. Conclusion

A series of indolin-2-one linked 1,2,3-triazole derivatives **(7a-x)** was synthesized in good yield and evaluated for their cytotoxicity after due characterization. Most of the compounds were potent cytotoxic agents against CEM and HeLa cells with IC_{50} ranging from 1.5 to 67 μM and 3.4–133 μM respectively, whereas for L1210 cells, compounds **7a, 7c, 7o** and **7v** showed cytotoxicity between 3 and 8.1 μM. Compound**7c** was found to be equipotent with standard melphalan. Further studies carried out on Jurkat cells unveiled that **7c** induces apoptosis by activating both the intrinsic and the extrinsic apoptotic pathway. Thepro-apoptotic activity of **7c** showed to be closely associated with its ability to block the proliferation of cancer cells in the G2/M phase of cell cycle. Interestingly, compound **7c** did not show any genotoxic activity. In addition, the ADME properties of all the synthesized compounds were investigated and docking simulations were conducted to observe their inhibition effect on the 6P8Q EGFR receptor. The docking affinity results showed a good coherence with *in vitro* cytotoxicity results, observing also that all compounds possess higher docking scores compared with the co-ligand of 6P8Q EGFR receptor. As far as the potency of compounds **7c**, **7o,** and **7v** is concerned, it was determined that the residues MET793, MET790, LEU788 and ALA743 of 6P8Q EGFR receptor had a key role. The ADME predictions showed that all synthesized compounds meet the criteria for being a possible drug candidate. Structure activity relationship study showed that presence of methyl group is preferred at position 5 of indolin-2-one against murine L1210 cells. Substitution made at position 5, 6 or 7 of indolin-2-one and position 4 of benzyl group increases the cytotoxic activity, against CEM cells. Replacement of hydrogen with $-CH_3$, -Cl and $-NO_2$ group on the position 4 of benzyl group improves cytotoxicity towards HeLa cells. In general, substitution on position 5, 6 or 7 of indoline-2-one increases cytotoxicity against HeLa cells.

CRediT authorship contribution statement

Arnika Das and Sujeet Kumar prepared the compounds, Giulia Greco, and Elena Catanzaro performed experiments to understand the mechanism of action, Dominique Schols performed cytotoxicity study, Rita Morigi, Alessandra Locatelli, and Carmela Fimognari designed the *in vitro* experiments, Hakan Alici, Hakan Tahtaci performed the in silico studies, Subhas S. Karki designed the scheme, interpreted the spectra, Arnika Das, Subhas S. Karki, and Carmela Fimognari wrote the paper.

Competing interest statement

The authors declare no conflict of interest.

Acknowledgement

We would like to thank Agilent Technologies, Bengaluru (India) for LC-MS and NMR Research Centre-Indian Institute of Science, Bengaluru (India) for $^{1}H/^{13}C$ NMR spectral data.

Appendix A. Supporting information

Supplementary data associated with this article can be found in the online version at doi:10.1016/j.compbiolchem.2022.107641.

References

Amato, J., Iaccarino, N., Pagano, B., Morigi, R., Locatelli, A., Leoni, A., Rambaldi, M., Zizza, P., Biroccio, A., Novellino, E., Randazzo, A., 2014. Bis-indole derivatives with antitumor activity turn out to be specific ligands of human telomeric G-quadruplex. Front. Chem. 2, 54. https://doi.org/10.3389/fchem.2014.00054.

Atulya, N., Guntuku, L., Guggilapu, S.D., Danthi Bai, K., Gannoju, S., Naidu, V.G.M., Bathini, N.B., 2016. Synthesis and apoptosis inducing studies of triazole linked 3-benzylidene isatin derivatives. Eur. J. Med. Chem. 124, 782–793. https://doi.org/10.1016/j.ejmech.2016.09.009.

Baraldi, P.G., del Carmen Nunez, M., Tabrizi, M.A., De Clercq, E., Balzarini, J., Bermejo, J., Estévez, F., Romagnoli, R., 2004. Design, synthesis, and biological evaluation of hybrid molecules containing α-methylene-γ-butyrolactones and polypyrrole minor groove binders. J. Med. Chem. 47 (11), 2877–2886. https://doi.org/10.1021/jm031104y.

Behbehani, H., Ibrahim, H.M., Makhseed, S., Mahmoud, H., 2011. Applications of 2-arylhydrazononitriles in synthesis: Preparation of new indole containing 1,2,3-triazole, pyrazole and pyrazolo[1,5-a]pyrimidine derivatives and evaluation of their antimicrobial activities. Eur. J. Med. Chem. 46 (5), 1813–1820. https://doi.org/10.1016/j.ejmech.2011.02.040.

Behnisch-Cornwell, S., Bandaru, S.S.M., Napierkowski, M., Wolff, L., Zubair, M., Urbainsky, C., Lillig, C., Schulzke, C., Bednarski, P.J., 2020. Pentathiepins: A novel class of glutathione peroxidase 1 inhibitors that induce oxidative stress, loss of mitochondrial membrane potential and apoptosis in human cancer cells. ChemMedChem 15 (16), 1515–1528. https://doi.org/10.1002/cmdc.202000160.

Biovia, D.S., 2017. Discovery Studio Modeling Environment. Dassault Systèmes, San Diego.

Bonandi, E., Christodoulou, M.S., Fumagalli, G., Perdicchia, D., Rastelli, G., Passarella, D., 2017. The 1,2,3-triazole ring as a bioisostere in medicinal chemistry. Drug Discov. Today 22 (10), 1572–1581. https://doi.org/10.1016/j.drudis.2017.05.014.

Bradford, M.M., 1976. A rapid and sensitive method for the quantitation of microgram quantities of protein utilizing the principle of protein-dye binding. Anal. Biochem. 72 (1), 248–254. https://doi.org/10.1016/0003-2697(76)90527-3.

Cao, J.Y., Dixon, S.J., 2016. Mechanisms of ferroptosis. Cell Mol. Life Sci. 73 (11), 2195–2209. https://doi.org/10.1007/s00018-016-2194-1.

Carroux, C.J., Rankin, G.M., Moeker, J., Bornaghi, L.F., Katneni, K., Morizzi, J., Charman, S.A., Vullo, D., Supuran, C.T., Poulsen, S.-A., 2013. A prodrug approach toward cancer-related carbonic anhydrase inhibition. J. Med. Chem. 56 (23), 9623–9634. https://doi.org/10.1021/jm401163e.

Chen, J., Kos, R., Garssen, J., Redegeld, F., 2019. Molecular insights into the mechanism of necroptosis: the necrosome as a potential therapeutic target. Cells 8 (12), 1486. https://doi.org/10.3390/cells8121486.

Chen, M., Lu, S., Yuan, G., Yang, S., Du, X., 2000. Synthesis and antibacterial activity of some heterocyclic β-enamino ester derivatives with 1,2,3-triazole. Heterocycl. Commun. 6 (5), 421–426. https://doi.org/10.1515/HC.2000.6.5.421.

Chen, Y., Lopez-Sanchez, M., Savoy, D.N., Billadeau, D.D., Dow, G.S., Kozikowski, A.P., 2008. A series of potent and selective, triazolylphenyl-based histone deacetylases inhibitors with activity against pancreatic cancer cells and plasmodium falciparum. J. Med. Chem. 51 (12), 3437–3448 doi.org/10.1021/jm701606b.

Daina, A., Michielin, O., Zoete, V., 2014. iLOGP: a simple, robust, and efficient description of n-octanol/water partition coefficient for drug design using the GB/SA approach. J. Chem. Inf. Model. 54 (12), 3284–3301. https://doi.org/10.1021/ci500467k.

Daina, A., Michielin, O., Zoete, V., 2017. SwissADME: a free web tool to evaluate pharmacokinetics, drug-likeness and medicinal chemistry friendliness of small molecules. Sci. Rep. 7, 42717. https://doi.org/10.1038/srep42717.

Dallakyan, S., Olson, A.J., 2015. Small-molecule library screening by docking with PyRx. Chemical biology. Springer,, pp. 243–250. https://doi.org/10.1007/978-1-4939-2269-7_19.

D'Arcy, M.S., 2019. Cell death: a review of the major forms of apoptosis, necrosis and autophagy. Cell Biol. Int. 43 (6), 582–592. https://doi.org/10.1002/cbin.11137.

Das, A., Kumar, S., Persoons, L., Daelemans, D., Schols, D., Alici, H., Tahtaci, H., Karki, S. S., 2021. Synthesis, in silico ADME, molecular docking and in vitro cytotoxicity evaluation of stilbene linked 1,2,3-triazoles. Heliyon 7 (1), e05893. https://doi.org/10.1016/j.heliyon.2020.e05893.

De Clercq, D.J.H., Heppner, D.E., To, C., Jang, J., Park, E., Scott, D.A., 2019. Discovery and optimization of dibenzodiazepinones as allosteric mutant-selective EGFR inhibitors. ACSMed. Chem. Lett. 10 (11), 1549–1553. https://doi.org/10.1021/acsmedchemlett.9b00381.

Delaney, J.S., 2004. ESOL: estimating aqueous solubility directly from molecular structure. J. Chem. Inf. Model 44 (3), 1000–1005. https://doi.org/10.1021/ci034243x.

Duan, Y.-C., Ma, Y.-C., Zhang, E., Shi, X.-J., Wang, M.-M., Ye, X.-W., Liu, H.-M., 2013. Design and synthesis of novel 1,2,3-triazole-dithiocarbamate hybrids as potential anticancer agents. Eur. J. Med. Chem. 62 11–19. https://doi.org/10.1016/j.ejmech.2012.12.046.

Egan, W.J., Merz, K.M., Baldwin, J.J., 2000. Prediction of drug absorption using multivariate statistics. J. Med. Chem. 43 (21), 3867–3877. https://doi.org/10.1021/jm000292e.

Erol, D.D., Çaliş, Ü., Demirdamar, R., Yuluğ, N., Ertan, M., 1995. Synthesis and biological activities of some 3,6-disubstituted thiazolo[3,2-b][1,2,4]triazoles. J. Pharm. Sci. 84 (4), 462–465. https://doi.org/10.1002/jps.2600840414.

Fulda, S., 2009. Tumor resistance to apoptosis. Int. J. Cancer 124 (3), 511–515. https://doi.org/10.1002/ijc.24064.

Galluzzi, L., Vitale, I., Aaronson, S.A., Abrams, J.M., Adam, D., Agostinis, P., Alnemri, E. S., Altucci, L., Kroemer, G., 2018. Molecular mechanisms of cell death: recommendations of the nomenclature committee on cell death. Cell Death Differ. 25 (3), 486–541. https://doi.org/10.1038/s41418-017-0012-4.

Ghose, A.K., Viswanadhan, V.N., Wendoloski, J.J., 1999. A knowledge-based approach in designing combinatorial or medicinal chemistry libraries for drug discovery. 1. A qualitative and quantitative characterization of known drug databases. J. Comb. Chem. 1 (1), 55–68. https://doi.org/10.1021/cc9800071.

Grandis, J.R., Melhem, M.F., Gooding, W.E., Day, R., Holst, V.A., Wagener, M.M., Drenning, S.D., Tweardy, D.J., 1998. Levels of TGF-α and EGFR protein in head and neck squamous cell carcinoma and patient survival. . J. Nat. Cancer Inst. 90 (11), 824–832. https://doi.org/10.1093/jnci/90.11.824.

Greco, G., Catanzaro, E., Fimognari, C., 2021. Natural Products as Inducers of Non-Canonical Cell Death: A Weapon against Cancer. Cncers 13 (2), 1–64. https://doi.org/10.3390/cancers13020304. In this issue.

Gujjar, R., Marwaha, A., El Mazouni, F., White, J., White, K.L., Creason, S., Shackleford, D.M., Baldwin, J., Charman, W.N., Buckner, F.S., Charman, S., Rathod, P.K., Phillips, M.A., 2009. Identification of a metabolically stable triazolopyrimidine-based dihydroorotate dehydrogenase inhibitor with antimalarial activity in mice. J. Med. Chem. 52 (7), 1864–1872. https://doi.org/10.1021/jm801343r.

Hafez, H., Abbas, H.-A., El-Gazzar, A.-R., 2008. Synthesis and evaluation of analgesic, anti-inflammatory and ulcerogenic activities of some triazolo- and 2-pyrazolyl-pyrido[2,3-d]-pyrimidines. Acta Pharm. 58 (4), 359–378. https://doi.org/10.2478/v10007-008-0024-1.

Hanwell, M.D., Curtis, D.E., Lonie, D.C., Vandermeersch, T., Zurek, E., Hutchison, G.R., 2012. Avogadro: an advanced semantic chemical editor, visualization, and analysis platform. . J. Chemin.-. 4 (1), 17. https://doi.org/10.1186/1758-2946-4-17.

Hochegger, H., Takeda, S., Hunt, T., 2008. Cyclin-dependent kinases and cell-cycle transitions: does one fit all? Nat. Rev. Mol. Cell Biol. 9 (11), 910–916. https://doi.org/10.1038/nrm2510.

Holla, B.S., Mahalinga, M., Karthikeyan, M.S., Poojary, B., Akberali, P.M., Kumari, N.S., 2005. Synthesis, characterization and antimicrobial activity of some substituted 1,2,3-triazoles. Eur. J. Med. Chem. 40 (11), 1173–1178. https://doi.org/10.1016/j.ejmech.2005.02.013.

Hong, L., Lin, W., Zhang, F., Liu, R., Zhou, X., 2013. Ln[N(SiMe$_3$)$_2$]$_3$-catalyzed cycloaddition of terminal alkynes to azides leading to 1,5-disubstituted 1,2,3-triazoles: new mechanistic features. Chem. Commun. 49, 5589–5591. https://doi.org/10.1039/C3CC42534G.

Hussain, M., Qadri, T., Hussain, Z., Saeed, A., Channar, P.A., Shehzadi, S.A., Hassan, M., Larik, F.A., Mahmood, T., Malik, A., 2019. Synthesis, antibacterial activity and molecular docking study of vanillin derived 1,4-disubstituted 1,2,3-triazoles as inhibitors of bacterial DNA synthesis. Heliyon 5 (11), E02812. https://doi.org/10.1016/j.heliyon.2019.e02812.

Huey, R., Morris, G.M., Olson, A.J., Goodsell, D.S., 2007. A semiempirical free energy force field with charge-based desolvation. J. Comput. Chem. 28 (6), 1145–1152. https://doi.org/10.1002/jcc.20634.

Iyer, D., Vartak, S.V., Mishra, A., Goldsmith, G., Kumar, S., Srivastava, M., Hegde, M., Gopalakrishnan, V., Glenn, M., Velusamy, M., Choudhary, B., Kalakonda, N., Karki, S.S., Surolia, A., Raghavan, S.C., 2016. Identification of a novel BCL2-specific inhibitor that binds predominantly to the BH1 domain. FEBS J. 283 (18), 3408–3437. https://doi.org/10.1111/febs.13815.

Jain, P., Singh, V., Ali, S., Tripathi, V., Saraswat, U., 2018. Synthesis, characterization, molecular docking and biological activity of 5,6-bis-(4-fluoro-phenyl)-3,4,7,8-tetraaza-bicyclo[8.3.1]tetradeca-1(13) 4,6,10(14),11-pentaene-2,9-dione and its transition metal complexes. J. Saudi Chem. Soc. 22 (5), 546–557. https://doi.org/10.1016/j.jscs.2017.09.005.

Jia, Y., Wen, X., Gong, Y., Wang, X., 2020. Current scenario of indole derivatives with potential anti-drug-resistant cancer activity. Eur. J. Med. Chem. 200, 112359 https://doi.org/10.1016/j.ejmech.2020.112359.

Johns, B.A., Weatherhead, J.G., Allen, S.H., Thompson, J.B., Garvey, E.P., Foster, S.A., Jeffrey, J.L., Miller, W.H., 2009. 1,3,4-oxadiazole substituted naphthyridines as HIV-1 integrase inhibitors. part 2: SAR of the C5 position. Bioorg. Med. Chem. Lett. 19 (6), 1807–1810. https://doi.org/10.1016/j.bmcl.2009.01.089.

Kalyankrishna, S., Grandis, J.R., 2006. Epidermal growth factor receptor biology in head and neck cancer. J. Clin. Oncol. 24 (17), 2666–2672. https://doi.org/10.1200/JCO.2005.04.8306.

Kilic-Kurt, Z., Acar, C., Ergul, M., Bakar-Ates, F., Altuntas, T.G., 2020. Novel indole hydrazide derivatives: Synthesis and their antiproliferative activities through inducing apoptosis and DNA damage. Arch. Pharm. 353 (8), 2000059 https://doi.org/10.1002/ardp.202000059.

Kumar, D., Beena, Khare, G., Kidwai, S., Tyagi, A.K., Singh, R., Rawat, D.S., 2014. Synthesis of novel 1,2,3-triazole derivatives of isoniazid and their in vitro and in vivo antimycobacterial activity evaluation. Eur. J. Med. Chem. 81, 301–313. https://doi.org/10.1016/j.ejmech.2014.05.005.

Kumar, R., Arora, J., Prasad, A.K., Islam, N., Verma, A.K., 2013. Synthesis and antimicrobial activity of pyrimidine chalcones. Med. Chem. Res. 22, 5624–5631. https://doi.org/10.1007/s00044-013-0555-y.

Lipinski, C.A., Lombardo, F., Dominy, B.W., Feeney, P.J., 1997. Experimental and computational approaches to estimate solubility and permeability in drug discovery and development settings. Adv. Drug. Deliv. Rev. 23 (1–3), 3–25. https://doi.org/10.1016/s0169-409x(00)00129-0.

Martin, Y.C., 2005. A bioavailability score. J. Med. Chem. 48 (9), 3164–3170. https://doi.org/10.1021/jm0492002.

Lovering, F., Bikker, J., Humblet, C., 2009. Escape from flatland: increasing saturation as an approach to improving clinical success. J. Med. Chem. 52 (21), 6752–6756. https://doi.org/10.1021/jm901241e.

Mady, M.F., Awad, G.E.A., Jørgensen, K.B., 2014. Ultrasound-assisted synthesis of novel 1,2,3-triazoles coupled diaryl sulfone moieties by the CuAAC reaction, and biological evaluation of them as antioxidant and antimicrobial agents. Eur. J. Med. Chem. 84 433–443. https://doi.org/10.1016/j.ejmech.2014.07.042.

Mah, L.J., El-Osta, A., Karagiannis, T.C., 2010. γH2AX: a sensitive molecular marker of DNA damage and repair. Leukemia 24 (4), 679–686. https://doi.org/10.1038/leu.2010.6.

Mellinghoff, I.K., Wang, M.Y., Vivanco, I., Haas-Kogan, D.A., Zhu, S., Dia, E.Q., Lu, K.V., Yoshimoto, K., Huang, J.H.Y., Chute, D.J., Mischel, P.S., 2005. Molecular determinants of the response of glioblastomas to EGFR kinase inhibitors. N. Engl. J. Med 353 (19), 2012–2024. https://doi.org/10.1056/NEJMoa051918.

Mitsudomi, T., Yatabe, Y., 2010. Epidermal growth factor receptor in relation to tumor development: EGFR gene and cancer. FEBS J. 277 (2), 301–308. https://doi.org/10.1111/j.1742-4658.2009.07448.x.

Mohammad, R.M., Muqbil, I., Lowe, L., Yedjou, C., Azmi, A.S., 2015. Broad targeting of resistance to apoptosis in cancer. Semin. Cancer Biol. 35, S78–S103. https://doi.org/10.1016/j.semcancer.2015.03.001.

Morrison, J., Haldar, K., Kehoe, S., Lawrie, T.A., 2012. Chemotherapy versus surgery for initial treatment in advanced ovarian epithelial cancer. Cochrane Database Syst. Rev. 8, CD005343 https://doi.org/10.1002/14651858.CD005343.pub3.

Nagata, S., 2018. Apoptosis and clearance of apoptotic cells. Annu. Rev. Immunol. 36 (1), 489–517. https://doi.org/10.1146/annurev-immunol-042617-053010.

Narsimha, S., Satheesh, K.N., Kumara, S.B., Reddy, N.V., Althaf Hussain, S.K., Rao, M.S., 2016. Indole-2-carboxylic acid derived mono and bis 1,4-disubstituted 1,2,3-triazoles: Synthesis, characterization and evaluation of anticancer, antibacterial, and DNA-cleavage activities. Bioorg. Med. Chem. Lett. 26 (6), 1639–1644. https://doi.org/10.1016/j.bmcl.2016.01.055.

Nielsen, J.S., Jakobsen, E., Holund, B., Bertelsen, K., Jakobsen, A., 2004. Prognostic significance of p53, Her-2, and EGFR overexpression in borderline and epithelial ovarian cancer. Int. J. Gynecol. Cancer 14 (6), 1086–1096. https://doi.org/10.1111/j.1048-891X.2004.14606.x.

Muegge, I., Heald, S.L., Brittelli, D., 2001. Simple selection criteria for drug-like chemical matter. J. Med. Chem. 44 (12), 1841–1846. https://doi.org/10.1021/jm015507e.

Nohmi, T., 2018. Thresholds of genotoxic and non-genotoxic carcinogens. Toxicol. Res 34 (4), 281–290. https://doi.org/10.5487/TR.2018.34.4.281.

Patpi, S.R., Pulipati, L., Yogeeswari, P., Sriram, D., Jain, N., Sridhar, B., Murthy, R., Anjana, D.T., Kalivendi, S.V., Kantevari, S., 2012. Design, Synthesis, and structure–activity correlations of novel dibenzo[b,d]furan, dibenzo[b,d]thiophene, and n-methylcarbazole clubbed 1,2,3-triazoles as potent inhibitors of mycobacterium tuberculosis. J. Med. Chem. 55 (8), 3911–3922. https://doi.org/10.1021/jm300125e.

Pearce, S., 2017. The importance of heterocyclic compounds in anti-cancer drug design. 66 Available online: ⟨https://www.ddw-online.com/therapeutics/p320375-the-importance-of-heterocyclic%20compounds-in-anti-cancer-drug-design.html⟩.

Potts, R.O., Guy, R.H., 1992. Predicting skin permeability. Pharm. Res 9 (5), 663–669. https://doi.org/10.1023/a:1015810312465.

Qin, X., Ma, D., Tan, Y.-x, Wang, H.-y, Cai, Z., 2019. The role of necroptosis in cancer: A double-edged sword? Biochim. Biophys. Acta Rev. Cancer 1871 (2), 259–266. https://doi.org/10.1016/j.bbcan.2019.01.006.

Rao, P.S., Kurumurthy, C., Veeraswamy, B., Santhosh Kumar, G., Poornachandra, Y., Ganesh Kumar, C., Vasamsetti, S.B., Kotamraju, S., Narsaiah, B., 2014. Synthesis of novel 1,2,3-triazole substituted-N-alkyl/aryl nitrone derivatives, their anti-inflammatory and anticancer activity, Eur. J. Med. Chem. 80, 184–191. https://doi.org/10.1016/j.ejmech.2014.04.052.

Sheehan, D.J., Hitchcock, C.A., Sibley, C.M., 1999. Current and emerging azole antifungal agents. Clin. Microbiol. Rev. 12 (1), 40–79. https://doi.org/10.1128/CMR.12.1.40.

Sigismund, S., Avanzato, D., Lanzetti, L., 2018. Emerging functions of the EGFR in cancer. Mol. Oncol. 12 (1), 3–20. https://doi.org/10.1002/1878-0261.12155.

Solis, F.J., Wets, R.J.-B., 1981. Minimization by random search techniques. Math. Oper. Res. 6 (1), 19–30. https://doi.org/10.1287/moor.6.1.19.

Soriano, D.S., 1993. Example of the Wolff-Kishner reduction procedure suitable for an undergraduate organic lab experiment: Preparation of oxindole. J. Chem. Educ. 70 (4), 332. https://doi.org/10.1021/ed070p332.

Sztanke, K., Pasternak, K., Rzymowska, J., Sztanke, M., Kandefer-Szerszeń, M., 2008. Synthesis, structure elucidation and identification of antitumoural properties of

novel fused 1,2,4-triazine aryl derivatives. Eur. J. Med. Chem. 43 (5), 1085–1094. https://doi.org/10.1016/j.ejmech.2007.07.009.

Sujeet, K., Mahesh, H., Vidya, G., Vinaya, K.R., Sureshbabu, A.R., Erik De, C., Dominique, S., Anil, K.G.N., Sathees, C.R., Subhas, S.K., 2014. 2-(4-Chlorobenzyl)-6-arylimidazo[2,1-b][1,3,4]thiadiazoles: Synthesis, cytotoxic activity and mechanism of action, Eur. J. Med. Chem. 84, 687–697. https://doi.org/10.1016/j.ejmech.2014.07.054.

Tait, S.W.G., Ichim, G., Green, D.R., 2014. Die another way – non-apoptotic mechanisms of cell death. J. Cell Sci. 127 (10), 2135. https://doi.org/10.1242/jcs.093575.

To, C., Jang, J., Chen, T., Park, E., Mushajiang, M., De Clercq, D.J.H., Janne, P.A., 2019. Single and dual targeting of mutant Egfr with an allosteric inhibitor. Cancer Discov. 9 (7), 926–943. https://doi.org/10.1158/2159-8290.CD-18-0903.

Trott, O., Olson, A.J., 2010. AutoDock Vina: improving the speed and accuracy of docking with a new scoring function, efficient optimization, and multithreading. J. Comput. Chem. 31 (2), 455–461. https://doi.org/10.1002/jcc.21334.

Ulloora, S., Shabaraya, R., Adhikari, A.V., 2013. Facile synthesis of new imidazo[1,2-a] pyridines carrying 1,2,3-triazoles via click chemistry and their antiepileptic studies. Bioorg. Med. Chem. Lett. 23 (11), 3368–3372. https://doi.org/10.1016/j.bmcl.2013.03.086.

Veber, D.F., Johnson, S.R., Cheng, H.-Y., Smith, B.R., Ward, K.W., Kopple, K.D., 2002. Molecular properties that influence the oral bioavailability of drug candidates. J. Med. Chem. 45 (12), 2615–2623. https://doi.org/10.1021/jm020017n.

Velázquez, S., Alvarez, R., Pérez, C., Gago, F., De Clercq, E., Balzarini, J., Camarasa, M.J., 1998. Regiospecific synthesis and anti-human immunodeficiency virus activity of novel 5-substituted n-alkylcarbamoyl and n,n-dialkyl carbamoyl 1,2,3-triazole-TSAO analogues. Antivir. Chem. Chemother. 9 (6), 481–489. https://doi.org/10.1177/095632029800900604.

Verhaak, R.G., Hoadley, K.A., Purdom, E., Wang, V., Qi, Y., Wilkerson, M.D., Miller, C.R., Ding, L., Golub, T., Mesirov, J.P., Alexe, G., Lawrence, M., O'Kelly, M., HayesD, N., 2010. Cancer Genome Atlas Research, Integrated genomic analysis identifies clinically relevant subtypes of glioblastoma characterized by abnormalities in PDGFRA, IDH1, EGFR, and NF1. Cancer Cell 17 (1), 98–110. https://doi.org/10.1016/j.ccr.2009.12.020.

Walker, F., Abramowitz, L., Benabderrahmane, D., Duval, X., Descatoire, V., Henin, D., Lehy, T., Aparicio, T., 2009. Growth factor receptor expression in anal squamous lesions: modifications associated with oncogenic human papillomavirus and human immunodeficiency virus. Hum. Pathol. 40 (11), 1517–1527. https://doi.org/10.1016/j.humpath.2009.05.010.

Wan, Y., Li, Y., Yan, C., Yan, M., Tang, Z., 2019. Indole: A privileged scaffold for the design of anti-cancer agents. Eur. J. Med. Chem. 183, 111691 https://doi.org/10.1016/j.ejmech.2019.111691.

Wykosky, J., Fenton, T., Furnari, F., Cavenee, W.K., 2011. Therapeutic targeting of epidermal growth factor receptor in human cancer: successes and limitations. Chin. J. Cancer 30 (1), 5–12. https://doi.org/10.5732/cjc.010.10542.

Yan, S.-J., Liu, Y.-J., Chen, Y.-L., Liu, L., Lin, J., 2010. An efficient one-pot synthesis of heterocycle-fused 1,2,3-triazole derivatives as anti-cancer agents. Bioorg. Med. Chem. Lett. 20 (17), 5225–5228. https://doi.org/10.1016/j.bmcl.2010.06.141.

Yempala, T., Sridevi, J.P., Yogeeswari, P., Sriram, D., Kantevari, S., 2014. Rational design and synthesis of novel dibenzo[b,d]furan-1,2,3-triazole conjugates as potent inhibitors of mycobacterium tuberculosis. Eur. J. Med. Chem. 71, 160–167. https://doi.org/10.1016/j.ejmech.2013.10.082.

Zimmermann, M., Meyer, N., 2011. Annexin V/7-AAD staining in keratinocytes. In: Stoddart, M.J. (Ed.), Mammalian Cell Viability: Methods and Protocols. Humana Press, Totowa, NJ, pp. 57–63. https://doi.org/10.1007/978-1-61779-108-6_8.

Heliyon 7 (2021) e05893

Contents lists available at ScienceDirect

Heliyon

journal homepage: www.cell.com/heliyon

Research article

Synthesis, in silico ADME, molecular docking and in vitro cytotoxicity evaluation of stilbene linked 1,2,3-triazoles

Arnika Das [a,b,1], Sujeet Kumar [a,1], Leentje Persoons [c], Dirk Daelemans [c], Dominique Schols [c], Hakan Alici [d], Hakan Tahtaci [e], Subhas S. Karki [a,b,*]

[a] Department of Pharmaceutical Chemistry, KLE College of Pharmacy, Bengaluru, 560010, Karnataka, India
[b] Dr Prabhakar B Kore Basic Science Research Centre, Off-Campus, KLE College of Pharmacy, A Constituent Unit of KLE Academy of Higher Education and Research-Belagavi, Bengaluru, 560010, Karnataka, India
[c] Rega Institute for Medical Research, Department of Microbiology, Immunology and Transplantation, Laboratory of Virology and Chemotherapy, KU Leuven, B-3000, Leuven, Belgium
[d] Department of Physics, Faculty of Arts and Sciences, Zonguldak Bulent Ecevit University, 67100, Zonguldak, Turkey
[e] Department of Chemistry, Faculty of Science, Karabuk University, 78050, Karabuk, Turkey

ARTICLE INFO

Keywords:
Wittig reaction
1,2,3-Triazole
Cytotoxicity
ADME
Molecular docking

ABSTRACT

Series of (*E*)-1-benzyl-4-((4-styrylphenoxy)methyl)-1*H*-1,2,3-triazoles **7a-x** were obtained by Wittig reaction between 4-((1-benzyl-1*H*-1,2,3-triazol-4-yl)methoxy)benzaldehydes **5a-d** and benzyl triphenylphosphonium halides **6a-f** in benzene. The structures of the synthesized compounds were confirmed by FTIR, NMR (^{1}H and ^{13}C NMR) spectroscopy, and mass spectrometry. All synthesized compounds were screened for their cytotoxic activity against human cancer cell lines including pancreatic carcinoma, colorectal carcinoma, lung carcinoma, and leukemias such as acute lymphoblastic, chronic myeloid, and non-Hodgkinson lymphoma cell lines. *In vitro* cytotoxicity data showed that compounds **7c**, **7e**, **7h**, **7j**, **7k**, **7r**, and **7w** were moderately cytotoxic (11.6–19.3 μM) against the selected cancer cell lines. These cytotoxicity findings were supported using molecular docking studies of the compounds against 1TUB receptor. The drug-likeness properties of the compounds evaluated by *in silico* ADME analyses. Resveratrol linked 1,2,3-triazoles were more sensitive towards human carcinoma cell lines but least sensitive towards leukemia and lymphoma cell lines.

1. Introduction

Cancer is a group of diseases responsible for one in six deaths worldwide. To overcome this threat, effective methods such as immunotherapy, chemotherapy, surgery, and radiotherapy are needed. Each method has its advantages and disadvantages. Chemotherapeutic agents used to kill or inhibit the growth of cancer cells often have serious side effects, whereas radiotherapy and surgery are limited [1]. To fill this void, there is always a need for better alternatives. It is a daunting task to develop a new anticancer compound with improved pharmaceutical properties. The role of heterocyclic chemistry is commendable in this regard. Low toxicity, high regeneration, and better receptor binding make nitrogen (N) -containing heterocycle the first choice between synthons in the drug discovery process [2].

Three nitrogens and two carbon atoms of triazole contain a five heterocyclic compound ring, a 1,2,3-triazole ring exhibits a variety of biological functions, including antiviral, anti-inflammatory, antimicrobial and anti-tubercular. In addition, 1,4-disubstituted 1,2,3-triazoles show significant anticancer activity [3, 4, 5]. Recently Kaushik et al, developed and synthesized amide linked 1,4-disubstituted 1,2,3-triazoles (**I**) as an anticancer agents [6]. Murugavel et al, have been linked to the production of thiophen containing 1,2,3-triazole (**II**) and pyridine moiety as a potential for topoisomerase IIα inhibiting anticancer agents [7]. A series of connected chalcone 1,2,3 triazoles (**III**) was synthesized using a green chemical method and tested as anticancer agents [8].

Stilbene based compounds have attracted biologists and chemists because they are widely available in nature. They have a variety of biological functions [9, 10]. Hydroxylated stilbenes have been found in

* Corresponding author.
E-mail address: subhasskarki@gmail.com (S.S. Karki).
[1] Authors contributed equally.

https://doi.org/10.1016/j.heliyon.2020.e05893
Received 6 October 2020; Received in revised form 17 December 2020; Accepted 29 December 2020

medicinal plants but plain stilbene is not found in nature. *Trans*-3,5, 4′-trihydroxy stilbene (resveratrol) (**IV**) is found in grapes and plays a role in preventing coronary heart disease associated with the use of red wine [11, 12, 13]. This resveratrol exhibits the activity of many biological agents, such as chemopreventive [14] antioxidant [15] antineoplastic [16] and antiestrogenic [17]. Various extracts/structures of stilbenes show anticancer activity [18, 19, 20, 21].

In recent times, the molecular hybridization approach is a widely used techniques in drug discovery, which forms new molecular entities by incorporating stilbenes by linker through the methylene with 1,2,3-triazoles. These integrated or cohesive systems may have advanced biological properties related to specific substances. As the continuation of our work in small nitrogenous heterocyclic compounds, a series of E stilbene linked to 1,4-disubstituted-1,2,3-triazole derivatives (**7a-x**) were synthesized, identified, and in vitro cytotoxicity is performed in this paper (see Figure 1).

Furthermore, *in silico* ADME properties were investigated to determine the drug-likeness properties of the synthesized compounds using the SwissADME webserver [22, 23]. We also conducted docking simulations both to support the *in vitro* cytotoxicity studies of the compounds and to identify their binding sites on the 1TUB receptor (tubulin-docetaxel complex) [24].

2. Experimental

2.1. General information and instrumentation

Reagents and solvents were tested for purity before use. Melting points (m.p.) were measured by open capillary tube method in liquid paraffin (heavy) and are uncorrected. FTIR spectra were recorded using infrared (IR) grade potassium bromide (KBr) by diffuse reflectance technique on a JASCO 460 + instrument. The ^{1}H NMR spectra were recorded in deuterated dimethyl sulfoxide (DMSO-d_6) and chloroform ($CDCl_3$) in the range of 400–500 MHz (MHz) on Bruker (Ultraspec AMX 400) and JEOL RESONANCE instruments. Chemical shift (δ) values in ppm were expressed using tetramethylsilane (TMS) as the reference. Compound purity was determined by an Agilent 1100 HPLC coupled to an Agilent mass spectrometry detector (MSD) with electrospray ionization in positive mode. 4-(Prop-2-ynyloxy)benzaldehyde (**3**) and aryl azides (**4a-d**) were prepared as per literature [25] and 4-((1-arylmethyl-1*H*-1,2,3-triazol-4-yl)methoxy)benzaldehydes (**5a-d**) were synthesized as per the literature [26]. Various aryltriphenylphosphonium chlorides (**6a-f**) were prepared as per the literature [27].

2.2. Synthesis

General procedure for synthesis of (E)-1-benzyl-4-((4-styrylphenoxy)methyl)-1H-1,2,3-triazoles (7a-x)

Sodium hydride (0.0478 g, 2 mmol) was added in part to an equimolar mixture of different benzyltriphenylphosphonium halides (**6a-f**) and 4-((1-benzyl-1*H*-1,2,3-triazol-4-yl)methoxy) benzaldehydes **(5a-d)** at 0–5 °C in dry benzene. The resulting mixture was stirred for 16 h at room temperature. Excess sodium hydride was quenched in anhydrous methanol (10 mL) followed by extraction with a chloroform-water mixture. The organic layer was dried over anhydrous Na_2SO_4 and removed under vacuum. The crude mass thus obtained was purified from hot ethanol to get the ***E*** isomeric forms of **7a-x** while ***Z*** remained in the solution.

(E)-1-benzyl-4-((4-styrylphenoxy) methyl)-1H-1,2,3-triazole (7a). White amorphous mass, IR (KBr) *ν*: = 3010, 2873, 1602, 1510, 1455, 1243 cm^{-1}. ^{1}H NMR (400 MHz, DMSO-d_6): δ = 5.15 (2H, s, –CH_2-), 5.61 (2H, s, –OCH_2-), 7.04 (2H, d, J = 8.8 Hz, Ar–H), 7.11 (1H, d, *J* = 16.4 Hz, styryl –CH=C-), 7.17–7.25 (2H, md, *J* = 16.4 Hz, styryl –C=CH-), 7.30–7.39 (7H, m, Ar–H), 7.54 (4H, m, Ar–H), 8.27 (1H, s, Triazole-H). ^{13}C NMR (400 MHz, DMSO-d_6): δ = 52.82, 61.12, 114.97, 124.66, 126.16, 126.30, 127.06, 127.19, 127.75, 127.93, 128.13, 128.63, 128.74, 157.72. +MS (ESI) m/z: 369.1 (368.4).

(E)-1-benzyl-4-((4-(4-fluorostyryl)-phenoxy)methyl)-1H-1,2,3-triazole (7b). White amorphous mass, IR (KBr) *ν*: = 3074, 2790, 1605, 1514, 1455, 1266 cm-^{1}. ^{1}H NMR (400 MHz, DMSO-d_6): δ = 5.15 (2H, s, –CH_2-), 5.60 (2H, s, –OCH_2-), 7.04 (2H, d, *J* = 11.6 Hz, Ar–H), 7.12 (2H, d, *J* = 6.8 Hz, Ar–H), 7.16–7.20 (2H, m, Ar–H), 7.30–7.39 (5H, m, Ar–H), 7.53 (2H, d, *J* = 11.2 Hz, Ar–H), 7.58–7.61 (2H, m, Ar–H), 8.27 (1H, s, Triazole-H). ^{13}C NMR (400 MHz, DMSO-d_6): δ = 52.84, 61.11, 114.97, 115.43, 115.60, 124.72, 125.15, 127.73, 127.91, 127.96, 128.01, 128.17, 128.78, 129.95, 133.97, 136.02, 142.94, 157.73, 160.43, 162.37. +MS (ESI) m/z: 386.1 (386.4).

(E)-1-benzyl-4-((4-(4-chlorostyryl)phenoxy)methyl)-1H-1,2,3-triazole (7c). White crystals, IR (KBr) *ν*: = 3033, 2918, 1603, 1509, 1467, 1249 cm-^{1}. ^{1}H NMR (400 MHz, DMSO-d_6): δ = 5.15 (2H, s, –CH_2-), 5.60 (2H, s, –OCH_2-), 7.03 (2H, d, *J* = 8.4 Hz, Ar–H), 7.11 (1H, d, J = 16.8 Hz, styryl –CH=C-), 7.23 (1H, d, *J* = 16.8 Hz, styryl –C=CH-),

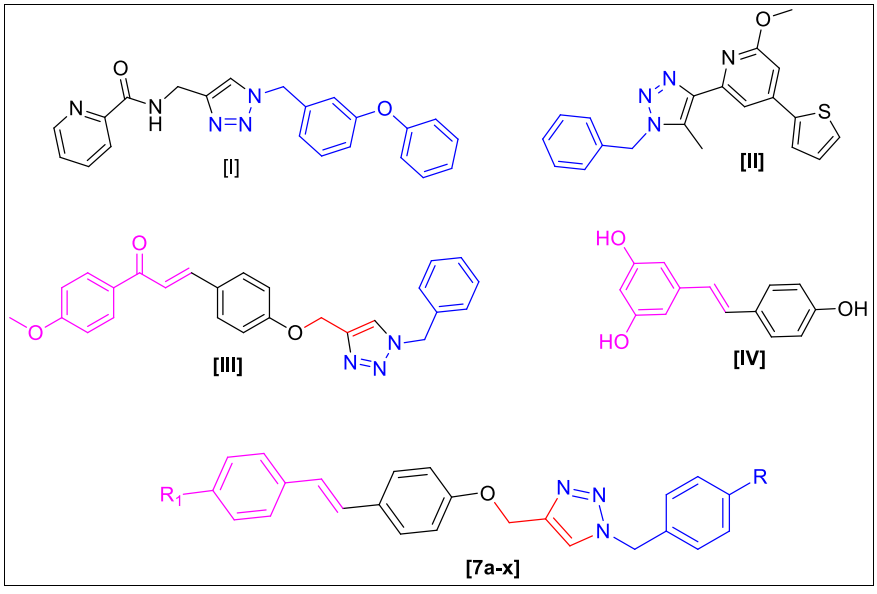

Figure 1. Pharmacologically hybridized/linked 1,2,3-triazole derivatives such as amide linked 1,4-disubstituted 1,2,3-triazoles I, thiophen containing 1,2,3-triazole pyridine II, chalcone linked 1,2,3-triazole III, resveratrol IV and resveratrol linked 1,2,3-triazoles 7a-x.

7.29–7.38 (3H, m, Ar–H), 7.45 (2H, d, $J = 8.8$ Hz, Ar–H), 7.55 (2H, d, $J = 8.8$ Hz, Ar–H), 7.54 (2H, d, $J = 8.8$ Hz, Ar–H), 8.27 (1H, s, Triazole-H). ^{13}C NMR (400 MHz, DMSO-d_6): δ = 53.37, 61.66, 115.53, 125.25, 125.51, 128.35, 128.44, 128.49, 128.70, 129.17, 129.31, 129.42, 130.30, 131.94, 136.55, 136.90, 139.73, 143.44, 158.43. +MS (ESI) m/z: 402.1 (402.9).

(E)-1-benzyl-4-((4-(4-methylstyryl)phenoxy)methyl)-1H-1,2,3-triazole (7d). White crystals, IR (KBr) ν: = 3070, 2964, 1603, 1514, 1476, 1244 cm-^{1}. ^{1}H NMR (400 MHz, DMSO-d_6): δ = 2.29 (3H, s, –CH_3), 5.14 (2H, s, –CH_2-), 5.60 (2H, s, 2H, –OCH_2-), 7.03 (2H, d, $J = 8.8$ Hz, Ar–H), 7.06 (1H, d, $J = 16.8$ Hz, styryl –CH=C-), 7.10 (1H, d, $J = 16.8$ Hz, styryl –C=CH-), 7.17 (2H, d, $J = 8$ Hz, Ar–H), 7.29–7.39 (4H, m, Ar–H), 7.45 (2H, d, $J = 8$ Hz, Ar–H), 7.52 (2H, d, $J = 8.8$ Hz, Ar–H), 8.27 (1H, s, Triazole-H). ^{13}C NMR (400 MHz, DMSO-d_6): = δ 20.78, 52.81, 61.10, 124.65, 126.08, 126.23, 126.39, 127.57, 127.92, 128.12, 128.73, 129.23, 130.13, 134.53, 135.98, 136.50, 143.05, 157.59, 178.69. +MS (ESI) m/z: 382.1 (382.5).

(E)-1-benzyl-4-((4-(4-methoxystyryl)phenoxy)methyl)-1H-1,2,3-triazole (7e). White amorphous mass, IR (KBr) ν: = 3034, 2837, 1606, 1514, 1467, 1384, 1253 cm-^{1}. ^{1}H NMR (400 MHz, DMSO-d_6): δ = 3.76 (3H, s, –OCH_3), 5.14 (2H, s, –CH_2-), 5.60 (2H, s, –OCH_2-), 6.93 (2H, d, $J = 8.8$ Hz, Ar–H), 6.99–7.03 (4H, m, Ar–H), 7.30–7.39 (5H, m, Ar–H), 7.49 (4H, d, $J = 8$ Hz, Ar–H), 8.27 (1H, s, Triazole-H). ^{13}C NMR (400 MHz, DMSO-d_6): δ = 52.82, 55.11, 61.11, 114.11, 114.93, 124.65, 125.69, 125.95, 127.37, 127.42, 127.93, 128.13, 128.74, 129.97, 130.36, 135.99, 142.96, 157.38, 158.65. +MS (ESI) m/z: 398.1 (398.5).

(E)-1-benzyl-4-((4-(4-nitrostyryl) phenoxy)methyl)-1H-1,2,3-triazole (7f). Yellow crystals, IR (KBr) ν: = 3101, 2838, 1591, 1513, 1178 cm-^{1}. ^{1}H NMR (400 MHz, DMSO-d_6): δ = 5.18 (2H, s, –CH_2-), 5.61 (2H, s, –OCH_2-), 7.09 (2H, d, $J = 8.8$ Hz, Ar–H), 7.29 (1H, d, $J = 16.4$ Hz, styryl –CH=C-), 7.30–7.39 (5H, m, Ar–H), 7.50 (1H, d, $J = 16.4$ Hz, styryl –C=CH-), 7.63 (2H, d, $J = 8.8$ Hz, Ar–H), 7.82 (2H, d, $J = 8.8$ Hz, Ar–H), 8.22 (2H, d, $J = 8.8$ Hz, Ar–H), 8.28 (1H, s, Triazole-H). ^{13}C NMR (400 MHz, DMSO-d_6): δ = 53.40, 61.70, 115.65, 124.61, 124.75, 125.32, 127.47, 128.52, 128.73, 129.18, 129.33, 129.81, 133.52, 136.56, 143.37, 145.04, 146.37, 159.13. +MS (ESI) m/z: 413.1 (413.4).

(E)-1-(4-nitrobenzyl)-4-((4-styrylphenoxy)methyl)-1H-1,2,3-triazole (7g). Yellow amorphous powder, IR (KBr) ν: = 3087, 2872, 1606, 1515, 1447, 1219 cm-^{1}. ^{1}H NMR (400 MHz, DMSO-d_6): δ = 5.18 (2H, s, –CH_2-), 5.80 (2H, s,–OCH_2–), 7.05 (2H, d, $J = 8.8$ Hz, Ar–H), 7.11 (1H, d, $J = 16.4$ Hz, styryl –CH=C-), 7.21 (1H, d, $J = 16.8$ Hz, styryl –C=CH-), 7.25 (1H, d, $J = 7.2$ Hz, Ar–H), 7.35 (2H, t, $J = 15.6$ Hz, Ar–H), 7.51–7.56 (5H, m, Ar–H), 8.25 (2H, d, $J = 8.0$ Hz, Ar–H), 8.38 (1H, s, Triazole-H). ^{13}C NMR (400 MHz, DMSO-d_6): δ = 51.92, 61.10, 114.99, 123.95, 125.16, 126.19, 126.34, 127.23, 127.79, 127.95, 128.67, 129.05, 130.05, 137.33, 143.12, 143.42, 147.25, 157.69. +MS (ESI) m/z: 414.1 (413.4).

(E)-4-((4-(4-fluorostyryl)phenoxy)methyl)-1-(4-nitrobenzyl)-1H-1,2,3-triazole (7h). Light yellow crystals, IR (KBr) ν: = 3098, 2874, 1607, 1517, 1458, 1217 cm-^{1}. ^{1}H NMR (400 MHz, DMSO-d_6): δ 5.18 (2H, s, –CH_2-), 5.80 (2H, s, –OCH_2-), 7.05 (d, 2H, $J = 9.2$, Hz Ar–H), 7.12 (2H, d, $J = 6.4$ Hz, Ar–H), 7.16–7.20 (2H, m, Ar–H), 7.51–7.54 (4H, m, Ar–H), 7.57–7.61 (2H, m, Ar–H), 8.24 (2H, d, $J = 8.8$ Hz, Ar–H), 8.35 (1H, s, Triazole-H). ^{13}C NMR (400 MHz, DMSO-d_6): δ = 51.92, 61.11, 115.00, 115.19, 115.39, 115.56, 123.90, 125.10, 125.17, 127.71, 127.87, 127.92, 127.99, 129.01, 129.98, 131.75, 133.91, 143.12, 143.36, 147.24, 157.67, 160.41, 162.35. +MS (ESI) m/z: 431.1 (431.4).

(E)-4-((4-(4-chlorostyryl)phenoxy)methyl)-1-(4-nitrobenzyl)-1H-1,2,3-triazole (7i). Yellow amorphous mass, IR (KBr) ν: = 3084, 2781, 1604, 1514, 1457, 1348, 1256 cm-^{1}. ^{1}H NMR (400 MHz, DMSO-d_6): δ = 5.18 (2H, s, –CH_2-), 5.80 (2H, s, –OCH_2-), 7.05 (2H, d, $J = 8.8$ Hz, Ar–H), 7.11 (1H, d, $J = 16.8$ Hz, styryl –CH=C-), 7.24 (1H, d, $J = 16.8$ Hz, styryl –C=CH-), 7.41 (2H, d, $J = 8.8$ Hz, Ar–H), 7.51–7.55 (4H, m, Ar–H), 7.58 (2H, d, $J = 8.4$ Hz, Ar–H), 8.24 (2H, d, $J = 8.8$ Hz, Ar–H), 8.35 (1H, s, Triazole-H).^{13}C NMR (400 MHz, DMSO-d_6): δ = 51.94, 61.11, 115.04, 123.96, 125.01, 125.18, 127.83, 127.94, 128.65, 128.87, 129.06, 129.82, 131.44, 136.37, 143.11, 143.42. +MS (ESI) m/z: 448.0 (447.9).

(E)-4-((4-(4-methylstyryl)phenoxy)methyl)-1-(4-nitrobenzyl)-1H-1,2,3-triazole (7j). Yellow crystals, IR (KBr) ν: = 3087, 2912, 1604, 1515, 1453, 1349, 1255 cm^{-1}. ^{1}H NMR (400 MHz, DMSO-d_6): δ = 2.29 (3H, s, –CH_3), 5.17 (2H, s, –CH_2-), 5.80 (2H, s, –OCH_2-), 7.04 (2H, d, $J = 8.8$ Hz, Ar–H), 7.06 (1H, s, $J = 16$ Hz, styryl –CH=C-), 7.10 (1H, s, $J = 16$ Hz, styryl –C=CH-), 7.17 (2H, d, $J = 8.0$ Hz, Ar–H), 7.45 (2H, d, $J = 8.0$ Hz, Ar–H), 7.50–7.54 (4H, dd, Ar–H), 8.24 (2H, d, $J = 8.8$ Hz, Ar–H), 8.35 (1H, s, Triazole-H). ^{13}C NMR (400 MHz, DMSO-d_6): δ = 20.80, 51.91, 61.08, 114.97, 123.92, 125.13, 126.27, 126.92, 127.61, 129.03, 129.25, 130.19, 134.53, 136.53, 143.13, 143.39, 147.24, 157.52. +MS (ESI) m/z: 427.1 (427.5).

(E)-4-((4-(4-methoxystyryl)phenoxy)methyl)-1-(4-nitrobenzyl)-1H-1,2,3-triazole (7k). Yellow amorphous mass, IR (KBr) ν: = 3087, 2836, 1607, 1516, 1462, 1349, 1254 cm^{-1}. ^{1}H NMR (400 MHz, DMSO-d_6): δ = 3.76 (3H, s, –OCH_3), 5.17 (2H, s, –CH_2-), 5.79 (2H, s, –OCH_2-), 6.93 (2H, d, $J = 8$ Hz, Ar–H), 7.00–7.03 (4H, m, Ar–H), 7.49 (4H, d, $J = .$ 8.4 Hz, Ar–H), 7.53 (2H, d, $J = 9$ Hz, Ar–H), 8.24 (2H, d, $J = 8.8$ Hz, Ar–H), 8.34 (1H, s, Triazole-H).^{13}C NMR (400 MHz, DMSO-d_6): δ = 51.91, 55.11, 61.08, 114.11, 114.96, 123.92, 125.11, 125.07, 126.02, 127.43, 129.03, 129.96, 130.41, 143,15, 143.39, 147.24, 157.34, 158.65. +MS (ESI) m/z: 444.1 (443.5).

(E)-1-(4-nitrobenzyl)-4-((4-(4-nitrostyryl)phenoxy)methyl)-1H-1,2,3-triazole (7l). Yellow amorphous mass, IR (KBr) ν: = 3050, 2936, 1588, 1507, 1176 cm^{-1}. ^{1}H NMR (400 MHz, DMSO-d_6): δ = 5.20 (2H, s, –CH_2-), 5.80 (2H, s, –OCH_2-), 7.09 (2H, d, $J = 8.8$ Hz, Ar–H), 7.29 (1H, d, $J = 16.4$ Hz, styryl –CH=C-), 7.50 (1H, d, $J = 16.4$ Hz, styryl –C=CH-), 7.54 (2H, d, $J = 8.4$ Hz, Ar–H), 7.63 (2H, d, $J = 8.8$ Hz, Ar–H), 7.82 (2H, d, $J = 8.8$ Hz, Ar–H), 8.22 (2H, d, $J = 9.2$ Hz, Ar–H), 8.25 (2H, d, $J = 8.8$ Hz, Ar–H), 8.36 (1H, s, Triazole-H).^{13}C NMR (400 MHz, DMSO-d_6): δ = 51.93, 61.14, 115.13, 123.92, 124.03, 124.23, 125.16, 126.90, 128.62, 129.04, 129.29, 132.93, 143.00, 143.37, 144.46, 145.82, 158.52. +MS (ESI) m/z: 458.0 (458.4).

(E)-1-(4-methylbenzyl)-4-((4-styrylphenoxy) methyl)-1H-1,2,3-triazole (7m). White crystals, IR (KBr) ν: = 3027, 2872, 1602, 1509, 1462, 1380, 1243 cm^{-1}. ^{1}H NMR (400 MHz, DMSO-d_6): δ = 2.27 (3H, s, –CH_3), 5.14 (2H, s, –CH_2-), 5.54 (2H, s, –OCH_2-), 7.04 (2H, d, $J = 8.8$ Hz, Ar–H), 7.07 (1H, d, $J = 16.4$ Hz, styryl –CH=C-), 7.16–7.25 (6H, m, Ar–H), 7.35 (2H, t, $J = 16.0$ Hz, Ar–H), 7.55 (4H, t, $J = 16.8$ Hz, Ar–H), 8.23 (1H, s, Triazole-H).^{13}C NMR (400 MHz, DMSO-d_6): δ 20.67, 52.63, 61.11, 114.96, 124.54, 126.16, 126.29, 127.20, 127.76, 127.99, 128.65, 129.28, 129.98, 132.99, 137.33, 137.49, 142.88, 157.72. +MS (ESI) m/z: 382.0 (382.5).

(E)-4-((4-(4-fluorostyryl)phenoxy)methyl)-1-(4-methylbenzyl)-1H-1,2,3-triazole (7n). White amorphous powder, IR (KBr) ν: = 3077, 2872, 1605, 1514, 1454, 1213 cm-^{1}. NMR (400 MHz, DMSO-d_6): δ = 2.27 (3H, s, –OCH_3), 5.14 (2H, s, –CH_2-), 5.54 (2H, s, –OCH_2-), 7.04 (2H, d, $J = 8.8$ Hz, Ar–H), 7.12 (2H, d, $J = 6.8$ Hz, Ar–H), 7.16–7.22 (6H, m, Ar–H), 7.52 (2H, d, $J = 8.4$ Hz, Ar–H), 7.57–7.61 (2H, m, Ar–H), 8.23 (1H, s, Triazole-H). ^{13}C NMR (400 MHz, DMSO-d_6): δ 20.63, 52.60, 61.10, 114.95, 115.34, 115.55, 124.47, 125.11, 127.67, 127.88, 127.95, 129.24, 129.91, 132.95, 133.93, 137.45, 142.85, 157.68. +MS (ESI) m/z: 400.1 (400.5).

(E)-4-((4-(4-chlorostyryl)phenoxy) methyl)-1-(4-methylbenzyl)-1H-1,2,3-triazole (7o). White amorphous mass, IR (KBr) ν: = 3077, 2877, 1605, 1510, 1457, 1177 cm^{-1}. ^{1}H NMR (400 MHz, DMSO-d_6): δ = 2.27 (3H, s, –CH_3), 5.14 (2H, s, –CH_2-), 5.54 (2H, s, –OCH_2-), 7.04 (2H, d, $J = 8.8$ Hz, Ar–H), 7.11 (1H, d, $J = 16.4$ Hz, styryl –CH=C-), 7.16–7.23 (5H, m, Ar–H), 7.40 (2H, d, $J = 8.8$ Hz, Ar–H), 7.54 (2H, d, $J = 8.8$ Hz, Ar–H), 7.59 (2H, d, $J = 8.8$ Hz, Ar–H), 8.23 (1H, s, Triazole-H). ^{13}C NMR (400 MHz, DMSO-d_6): δ = 20.67, 52.62, 61.09, 114.95, 115.41, 115.58, 124.54, 125.13, 127.70, 127.93, 127.99, 129.28, 129.92, 132.99, 133.93, 137.50, 142.87, 157.70, 160.41, 162.32. +MS (ESI) m/z: 416.1 (416.9).

(E)-1-(4-methylbenzyl)-4-((4-(4-methylstyryl)phenoxy)methyl)-1H-1,2,3-triazole (7p). White crystals, IR (KBr) ν: = 3023, 2734, 1602, 1515, 1455, 1388, 1240 cm^{-1}. ^1H NMR (400 MHz, DMSO-d_6): δ = 2.27 (3H, s, $–CH_3$), 2.29 (3H, s, $–CH_3$-), 5.13 (2H, s, $–CH_2$-), 5.40 (2H, s,$–OCH_2–$), 7.02 (2H, d, J = 8.8 Hz, Ar–H), 7.06 (1H, s, J = 16.8 Hz, styryl –CH=C-), 7.10 (1H, s, J = 16.8 Hz, styryl –C=CH-), 7.15–7.22 (6H, m, Ar–H), 7.45 (2H, d, J = 8.0 Hz, Ar–H), 7.51 (2H, d, J = 8.8 Hz, Ar–H), 8.23 (1H, s, Triazole-H). ^{13}C NMR (400 MHz, DMSO-d_6): δ 20.65, 20.78, 52.61, 61.1.0, 113.70, 114.94, 124.49, 126.08, 126.22, 126.93, 127.57, 127.97, 129.22, 129.26, 130.25, 133.01, 134.50, 136.49, 137.59, 142.89, 157.55. +MS (ESI) m/z: 396.1 (396.5).

(E)-4-((4-(4-methoxystyryl)phenoxy)methyl)-1-(4-methylbenzyl)-1H-1,2,3-triazole (7q). White amorphous mass, IR (KBr) ν: = 3079, 2840, 1605, 1515, 1395, 1249 cm^{-1}. ^1H NMR (400 MHz, DMSO-d_6): δ = 2.27 (3H, s, $–CH_3$), 3.76 (3H, s, 3H, $–OCH_3$), 5.13 (2H, s, $–CH_2$-), 5.54 (2H, s, $–OCH_2$-), 6.93 (2H, d, J = 8.8 Hz, Ar–H), 6.99–7.02 (4H, m, Ar–H), 7.16–7.22 (4H, m, Ar–H), 7.47–7.50 (4H, m, Ar–H), 8.23 (1H, s, Triazole-H). ^{13}C NMR (400 MHz, DMSO-d_6): δ = 20.66, 52.62, 55.11, 61.10, 114.11, 114.93, 124.49, 125.69, 125.98, 127.37, 127.41, 127.97, 129.27, 129.97, 130.35, 132.99, 137.48, 142.92, 157.37, 158.64. +MS (ESI) m/z: 412.1 (412.5).

(E)-1-(4-methylbenzyl)-4-((4-(4-nitrostyryl)phenoxy)methyl)-1H-1,2,3-triazole (7r). White crystals, IR (KBr) ν: = 3075, 2926, 1592, 1509, 1465, 1388, 1219 cm^{-1}. ^1H NMR (400 MHz, DMSO-d_6): δ = 2.27 (3H, s, $–CH_3$), 5.17 (2H, s, $–CH_2$-), 5.54 (2H, s, $–OCH_2$-), 7.08 (2H, d, J = 8.4 Hz, Ar–H), 7.18 (2H, d, J = 8 Hz, Ar–H), 7.22 (2H, d, J = 8 Hz, Ar–H), 7.29 (1H, d, J = 16.4 Hz, styryl –CH=C-), 7.50 (1H, d, J = 16.4 styryl –C=CH-), 7.63 (2H, d, J = 8.8 Hz, Ar–H), 7.82 (2H, d, J = 9.2 Hz, Ar–H), 8.22 (2H, d, J = 8.8 Hz, Ar–H), 8.24 (1H, s, Triazole-H). ^{13}C NMR (400 MHz, DMSO-d_6): δ = 20.67, 52.64, 61.13, 115.09, 124.03, 124.18, 124.58, 126.89, 127.99, 128.61, 129.29, 132.96, 137.51, 142.76, 144.47, 145.81, 158.56. +MS (ESI) m/z: 427.1 (427.5).

(E)-1-(4-chlorobenzyl)-4-((4-styrylphenoxy)methyl)-1H-1,2,3-triazole (7s). White crystals, IR (KBr) ν: = 3023, 2791, 1606, 1516, 1459, 1258 cm^{-1}. ^1H NMR (400 MHz, DMSO-d_6): δ = 5.15 (2H, s, $–CH_2$-), 5.61 (2H, s, $–OCH_2$-), 7.04 (2H, d, J = 8.8 Hz, Ar–H), 7.11 (1H, d, J = 16.4 Hz, styryl –CH=C-), 7.21 (1H, d, J = 16.4 Hz, styryl –C=CH-), 7.25 (1H, d, J = 7.2 Hz, Ar–H), 7.32–7.37 (4H, m, Ar–H), 7.45 (2H, d, J = 8.4 Hz, Ar–H), 7.56 (4H, t, J = 15.2 Hz, Ar–H), 8.28 (1H, s, Triazole-H). ^{13}C NMR (400 MHz, DMSO-d_6): δ = 51.01, 61.11, 114.97, 115.19, 124.73, 126.16, 126.31, 127.19, 127.76, 127.95, 128.63, 128.75, 129.89, 130.01, 131.75, 132.87, 134.98, 137.32, 142.99, 157.70, 191.38. +MS (ESI) m/z: 402.1 (402.9).

(E)-1-(4-chlorobenzyl)-4-((4-(4-fluorostyryl)phenoxy)methyl)-1H-1,2,3-triazole (7t). White crystals, IR (KBr) ν: = 3064, 2790, 1607, 1515, 1459, 1216 cm^{-1}. ^1H NMR (400 MHz, DMSO-d_6): δ 5.15 = (3H, s, $–CH_2$), 5.61 (2H, s, $–OCH_2$-), 7.04 (2H, d, J = 8.8 Hz, Ar–H), 7.12 (2H, d, J = 6.4 Hz, Ar–H), 7.16–7.20 (2H, m, Ar–H), 7.34 (2H, d, J = 10.8 Hz, Ar–H), 7.45 (2H, d, J = 8.4 Hz, Ar–H), 7.53 (2H, d, J = 11.6 Hz, Ar–H), 7.58–7.61 (2H, m, Ar–H), 8.28 (1H, s, Triazole-H). ^{13}C NMR (400 MHz, DMSO-d_6): = δ 52.0, 61.10, 114.97, 115.40, 115.57, 124.73, 125.15, 127.70, 127.88, 127.92, 127.99, 128.75, 129.89, 129.95, 132.86, 133.92, 134.98, 142.98, 157.69, 160.41, 162.34. +MS (ESI) m/z: 420.0 (420.9).

(E)-1-(4-chlorobenzyl)-4-((4-(4-chlorostyryl)phenoxy)methyl)-1H-1,2,3-triazole (7u). White crystals, IR (KBr) ν: = 3059, 2937, 1606, 1514, 1492, 1258 cm^{-1}. ^1H NMR (400 MHz, DMSO-d_6): δ = 5.15 (2H, s, $–CH_2$-), 5.61 (2H, s, $–OCH_2$-), 7.05 (2H, d, J = 8.8 Hz, Ar–H), 7.11 (1H, d, J = 16.8 Hz, styryl –CH=C-), 7.24 (1H, d, J = 16.8 Hz, styryl –C=CH-), 7.34 (2H, d, J = 8.4 Hz, Ar–H), 7.38–7.46 (4H, dd, J = 8.8, 8.8 Hz, Ar–H), 7.52–7.59 (4H, dd, J = 8.4, 8.8 Hz, Ar–H), 8.20 (1H, s, Triazole-H). ^{13}C NMR (400 MHz, DMSO-d_6): δ = 52.01, 61.11, 124.74, 124.97, 127.78, 127.88, 128.61, 128.75, 128.86, 129.77, 129.89, 131.39, 132.86, 134.98, 136.34, 142.95, 157.86. +MS (ESI) m/z: 437.0 (437.3).

(E)-1-(4-chlorobenzyl)-4-((4-(4-methylstyryl)phenoxy)methyl)-1H-1,2,3-triazole (7v). White crystals, IR (KBr) ν: = 3087, 2921, 1604, 1514, 1459, 1336, 1253 cm^{-1}. ^1H NMR (400 MHz, DMSO-d_6): δ = 2.29 (3H, s, $–CH_3$), 5.15 (2H, s, $–CH_2$-), 5.61 (2H, s, $–OCH_2$-), 7.02 (2H, d, J = 8.8 Hz, Ar–H), 7.06 (1H, d, J = 16 Hz, styryl –CH=C-), 7.10 (1H, d, J = 16 Hz, styryl –C=CH-), 7.17 (2H, d, J = 7.6 Hz, Ar–H), 7.36 (2H, d, J = 8.4 Hz, Ar–H), 7.45 (4H, d, J = 8.4 Hz, Ar–H), 7.51 (2H, d, J = 8.8 Hz, Ar–H), 8.27 (1H, s, Triazole-H). ^{13}C NMR (400 MHz, DMSO-d_6): δ = 20.78, 51.99, 61.10, 114.95, 124.71, 126.09, 126.25, 126.93, 127.85, 128.74, 129.23, 129.88, 130.16, 132.85, 134.53, 134.97, 136.51, 143.0, 157.54. +MS (ESI) m/z: 416.1 (416.9).

(E)-1-(4-chlorobenzyl)-4-((4-(4-methoxystyryl)phenoxy)methyl)-1H-1,2,3-triazole (7w). White amorphous mass, IR (KBr) ν: = 3077, 2841, 1606, 1516, 1388, 1251 cm^{-1}. ^1H NMR (400 MHz, DMSO-d_6): δ = 3.76 (3H, s, $–OCH_3$), 5.14 (2H, s, $–CH_2$-), 5.61 (2H, s, $–OCH_2$-), 6.93 (2H, d, J = 8.8 Hz, Ar–H), 7.00–7.03 (4H, m, Ar–H), 7.34 (2H, d, J = 8.4 Hz, Ar–H), 7.45 (2H, d, J = 8.4 Hz, Ar–H), 7.50 (4H, d, J = 8.8 Hz, Ar–H), 8.28 (1H, s, Triazole-H). ^{13}C NMR (400 MHz, DMSO-d_6): δ = 51.99, 55.10, 61.10, 114.10, 114.94, 124.68, 125.68, 125.99, 127.36, 128.74, 129.88, 129.96, 130.37, 132.85, 134.97, 143.02, 157.35, 158.64. +MS (ESI) m/z: 432.1 (432.9).

(E)-1-(4-chlorobenzyl)-4-((4-(4-nitrostyryl)phenoxy)methyl)-1H-1,2,3-triazole (7x). Yellow crystals, IR (KBr) ν: = 3089, 2826, 1634, 1587, 1509, 1427, 1217 cm^{-1}. ^1H NMR (400 MHz, DMSO-d_6): δ = 5.18 (2H, s, $–CH_2$-), 5.62 (2H, s, $–OCH_2$-), 7.09 (2H, d, J = 8.8 Hz, Ar–H), 7.29 (1H, d, J = 16.4 Hz, styryl –CH=C-), 7.35 (2H, d, J = 8.4 Hz, Ar–H), 7.45 (2H, d, J = 8.4 Hz, Ar–H), 7.50 (1H, d, J = 16.4 Hz, styryl –C=CH-), 7.63 (2H, d, J = 8.8 Hz, Ar–H), 7.83 (2H, d, J = 8.8 Hz, Ar–H), 8.22 (2H, d, J = 8.8 Hz, Ar–H), 8.29 (1H, s, Triazole-H). ^{13}C NMR (400 MHz, DMSO-d_6): δ = 52.02, 61.14, 115.11, 124.23, 124.83, 126.92, 128.63, 128.79, 129.27, 129.93, 132.96, 134.35, 135.01, 142.88, 144.49, 145.82, 158.56. +MS (ESI) m/z: 447.1 (447.9).

2.3. Bio-evaluation

2.3.1. Cytostatic assays

All tumor cell lines were acquired from the American Type Culture Collection (ATCC, Manassas, VA, USA), except for the DND-41 cell line, which was purchased from Deutsche Sammlung von Mikroorganismen und Zellkulturen (DSMZ Leibniz-Institut, Braunschweig, Germany). All cell lines were cultured as recommended by the suppliers. Media were purchased from GIBCO Life Technologies, USA, and supplemented with 10% fetal bovine serum (HyClone, GE Healthcare Life Sciences, USA). For real-time monitoring, adherent cell lines HCT-116, NCI–H460, and Capan-1 were seeded at a density between 500 and 1500 cells per well in 384-well clear-bottomed tissue culture plates (Greiner). After overnight incubation, cells were treated with the test compounds at seven different concentrations ranging from 100 to 6.4 × 10^{-3} μM. Suspension cell lines K-562, Z-138, and DND-41 were seeded at densities ranging from 2500 to 5000 cells per well in 384-well clear-bottomed tissue culture plates containing the test compounds at the same seven concentration points. The plates were incubated and monitored at 37 °C for 72 h in the IncuCyte® system (Essen BioScience Inc., Ann Arbor, MI, USA) for real-time imaging. Images were taken every 3 h, with one field imaged per well under 10× magnification. Cell growth was then quantified based on percent cellular confluence as analyzed by the IncuCyte® image analysis software and used to determine the IC_{50} values.

2.3.2. Methodology for in silico studies

The 3D structures of all compounds were prepared using Avogadro v1.2.0 [28] and their energies were minimized with the MMFF94s force field. The ADME properties, pharmacokinetic properties, and drug-likenesses of the compounds were then investigated with the SwissADME webserver [22, 23]. Finally, docking simulations of all compounds were performed with the crystal structure of a tubulin heterodimer (PDB ID: 1TUB) [24]. All ligands and the target were

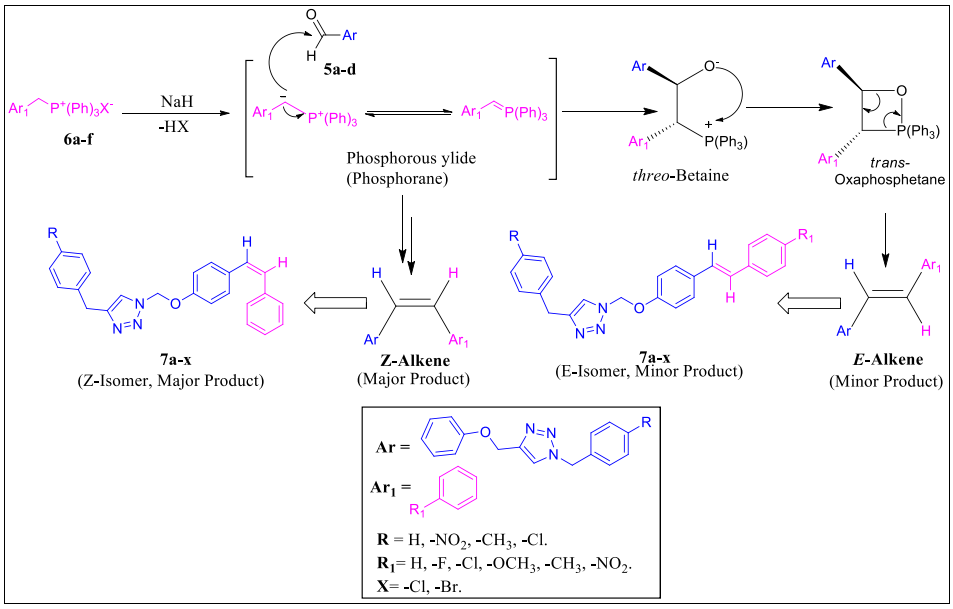

Figure 2. Mechanism of synthesis for 7a-x.

prepared using PyRx software [29] and the docking experiments were subsequently carried out using AutoDock Vina software [30] with the Lamarckian genetic algorithm (LGA) [31, 32]. The visualizations of docking simulation results were conducted using the Discovery studio [33].

3. Results and discussion

3.1. Chemistry

Series of (*E*)-1-benzyl-4-((4-styrylphenoxy)methyl)-1*H*-1,2,3-triazoles (**7a-x**) were obtained by Wittig reaction (Figure 2) [34] between the

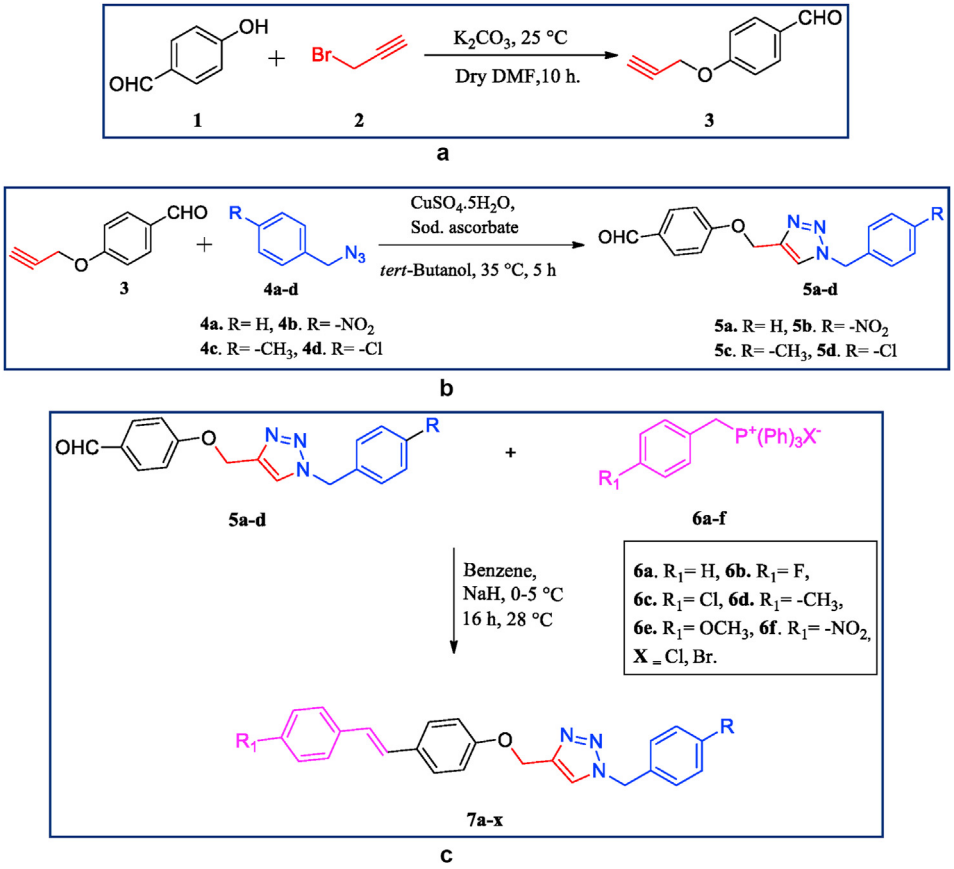

Scheme 1. a. Synthesis of 4-(prop-2-yn-1-yloxy)benzaldehyde (3). b. Synthesis of 4-((1-benzyl-1*H*-1,2,3-triazol-4-yl)methoxy)benzaldehydes (5a-d). c. Synthesis of *(E)*-1-benzyl-4-((4-styrylphenoxy)methyl)-1*H*-1,2,3-triazoles (7a-x).

Table 1. Synthesized stilbene linked 1,2,3-triazole analogues (**7a-x**).

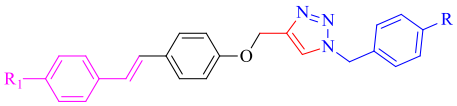

Compound	R_1	R	Molecular weight	Molecular formula	Melting point (°C)	Yield (%)	Purity (%)
7a	H	H	367.44	$C_{24}H_{21}N_3O$	202–204	35	100
7b	F	H	385.43	$C_{24}H_{20}FN_3O$	180–182	45	100
7c	Cl	H	401.89	$C_{24}H_{20}ClN_3O$	229–230	39	100
7d	CH_3	H	381.47	$C_{25}H_{23}N_3O$	102–104	28	100
7e	OCH_3	H	397.47	$C_{24}H_{23}N_3O_2$	190–192	39	100
7f	NO_2	H	412.44	$C_{24}H_{20}N_4O_3$	176–177	36	100
7g	H	NO_2	412.44	$C_{24}H_{20}N_4O_3$	145–147	45	100
7h	F	NO_2	430.43	$C_{24}H_{19}FN_4O_3$	182–184	32	100
7i	Cl	NO_2	446.89	$C_{24}H_{19}ClN_4O_3$	190–192	28	100
7j	CH_3	NO_2	426.47	$C_{25}H_{22}N_4O_3$	208–211	42	100
7k	OCH_3	NO_2	442.47	$C_{25}H_{22}N_4O_4$	207–209	28	100
7l	NO_2	NO_2	457.44	$C_{24}H_{19}N_5O_5$	207–208	33	100
7m	H	CH_3	381.47	$C_{25}H_{23}N_3O$	174–176	32	100
7n	F	CH_3	399.46	$C_{25}H_{22}FN_3O$	204–206	42	100
7o	Cl	CH_3	415.91	$C_{25}H_{22}ClN_3O$	187–190	42	100
7p	CH_3	CH_3	395.50	$C_{26}H_{25}N_3O$	200–202	35	100
7q	OCH_3	CH_3	411.50	$C_{26}H_{25}N_3O_2$	166–168	42	100
7r	NO_2	CH_3	426.47	$C_{25}H_{22}N_4O_3$	148–150	34	91
7s	H	Cl	401.89	$C_{24}H_{20}ClN_3O$	170–171	42	88
7t	F	Cl	419.88	$C_{24}H_{19}ClFN_3O$	170–172	36	100
7u	Cl	Cl	436.33	$C_{24}H_{19}Cl_2N_3O$	128–130	35	100
7v	CH_3	Cl	415.91	$C_{24}H_{22}ClN_3O$	165–166	42	100
7w	OCH_3	Cl	431.91	$C_{25}H_{22}ClN_3O_2$	192–194	35	100
7x	NO_2	Cl	446.89	$C_{24}H_{19}ClN_4O_3$	174–176	39	100

respective 4-((1-benzyl-1*H*-1,2,3-triazol-4-yl)methoxy) benzaldehydes (**5a-d**) and benzyltriphenylphosphonium halides (chlorides and bromide) (**6a-f**). Compounds **5a-d** were obtained *via* copper (Cu)-catalyzed regioselective 1,3-dipolar cycloaddition of 4-(prop-2-ynyloxy)benzaldehyde (**3**) with benzyl azides (**4a-d**), while the reaction between 4-hydroxybenzaldehyde (**1**) and propargyl bromide (**2**) led to compound **3**. Schemes 1a-c represent the synthetic routes and Table 1 contains the structures of **7a-x**. Structural confirmation was performed with Fourier transform infrared (FTIR), nuclear magnetic resonance (NMR) spectroscopy and mass spectrometry.

The FTIR spectra of compounds **7a-x** showed stretching peaks in the ranges of 3010–3101 (-CH, ar.), 2734–2964 (-CH, ali.), 1513–1634 (>C=N-), 1507–1516 (>C=C<), and 1176–1266 (-O-) cm^{-1} for the groups given in parentheses. Methylene ($–CH_2–$) bending peaks appeared in the range of 1427–1492 cm^{-1}. Compounds **7d**, **7e**, **7j**, **7k**, **7m-r**, **7v**, and **7w** showed methyl ($-CH_3$) bending peaks in the range of 1336–1395 cm^{-1}, while the nitro ($-NO_2$) stretching in **7f-l**, **7r**, and **7x** appeared between 1514 and 1592 cm^{-1}.

^{1}H NMR spectra showed singlet triazole ring protons in the range of 8.20–8.38 δ ppm. The aromatic protons appeared between 6.93 and 8.25 δ ppm while two doublet peaks appeared in the range of 7.06–7.50 δ ppm for ***E***-CH=CH of styryl moiety [35, 36]. Peaks at 5.40–5.80 and 5.13–5.20 δ ppm represent -N–CH_2– and –OCH_2-, respectively. The –CH_3 protons of **7d**, **7j**, **7m-r**, and **7v** appeared between 2.27 and 2.29 δ ppm along with -O-CH_3 protons of **7e**, **7k**, **7q**, and **7w** at 3.76 δ ppm. The nature of the carbon in **7a-x** was ascertained by the respective ^{13}C NMR spectral data. Absence of the –C≡CH proton of **3** at 1.56 δ ppm and presence of additional -N–CH_2– protons at 5.52 δ ppm along with singlet triazole-H at 7.59 δ ppm in **5a** confirmed the reaction between **3** and **4a**. Table 1 contains details of compounds **7a-x** such as molecular weight, molecular formula, yield, percentage purity, and physical constant.

3.2. Biological study

In vitro cellular cytotoxicity evaluations of derivatives **7a-x** were performed using six different human cancer cell lines (Capan-1, HCT-116, NCI–H460, DND-41, K-562, and Z-138) in 384-well micro-titer plates [37]. The tubulin inhibitor docetaxel [38] and the pan-kinase inhibitor staurosporine (STS) [39] were used as reference compounds and dimethyl sulfoxide (DMSO) as a solvent. The cytotoxicity data summarized in Table 2 represent 50% inhibitory concentrations (IC_{50}).

Irrespective of the substituents on the aromatic ring system, compounds **7a-x** were found to be poorly cytotoxic towards acute lymphoma (**DND-41**), chronic myeloid leukemia (**K-562**), Non Hodgin lymphoma (**Z-138**) and moderate cytotoxic against pancreatic adeno carcinoma (**Capan-1**), colorectal carcinoma (**HCT-116**), lung carcinoma (**NCI–H460**). In general, among the tested derivatives, **7a** and **7c** showed some cytotoxic chronic myeloid leukemia (**K-562**) cells. Most of the compounds displayed some sort of cytotoxic activity 31–96 μM against pancreatic adeno carcinoma (**Capan-1**) cells except compounds **7d**, **7g**, **7v** and **7x**. For colorectal carcinoma cells (**HCT-116**), the cytotoxic activity exhibited by many compounds of the series ranging from 12-87 μM. Among this series, **7e**, **7h** and **7k** were the most potent with IC50 at 12–13 μM, many compounds such as **7a**, **7g**, **7i**, **7q** and **7r** were cytotoxic in the range of 20–30 μM. For lung carcinoma (**NCI–H460**) cells, 12–16 μM cytotoxicity activity showed by compounds **7h**, **7r** and **7w,** whereas remaining compounds exhibited the activity ˃30 μM. In case of acute lymphoblastc leukemia (**DND-41**), very limited compounds namely **7a**, **7g** and **7o** displayed some cytotoxic activity 60–80 μM, remaining all compounds did not display any cytotoxic activity. Even for the chronic myeloid leukemia (**K-562**) cells also not showed any activity by the synthesized compounds except **7a** and **7c** with 40 and 19 μM. Similarly, for Non Hodgin lymphoma (**Z-138**), one compound that is **7d** showed some cytotoxic activity with IC50 60μM, and remaining compounds in

Table 2. *In-vitro* cytotoxicity data of synthesized stilbene linked 1,2,3-triazoles **7a-x** (μM).

Compound	Capan-1	HCT-116	NCI–H460	DND-41	K-562	Z-138
	Pancreatic adeno-carcinoma	Colorectal carcinoma	Lung carcinoma	Acute lymphoblastic leukemia	Chronic myeloid leukemia	Non-Hodgkin lymphoma
7a	46.7	29.1	34.3	61.4	39.9	>100
7b	30.7	46.7	31.7	>100	>100	>100
7c	96.4	36.1	>100	>100	19.3	>100
7d	>100	>100	81.7	>100	>100	60.3
7e	55.3	13.5	35.1	>100	>100	>100
7f	45.3	62.4	40.7	>100	>100	>100
7g	>100	26.1	78.5	82.1	>100	>100
7h	40.2	12.2	11.6	>100	>100	>100
7i	62.3	21.3	31.3	>100	>100	>100
7j	62.3	>100	98.3	>100	>100	>100
7k	50.2	12.6	95.4	>100	>100	>100
7l	70.3	76.7	44.3	>100	>100	>100
7m	45.9	>100	41.7	>100	>100	>100
7n	73.4	>100	>100	>100	>100	>100
7o	51.8	>100	47.3	81.2	>100	>100
7p	52.4	87.4	60.8	>100	>100	>100
7q	34.6	30.5	37.1	>100	>100	>100
7r	39.5	21.3	16.2	>100	>100	>100
7s	80.6	33	61.1	>100	>100	>100
7t	67.3	71.5	91.9	>100	>100	>100
7u	41.3	36.5	33.8	>100	>100	>100
7v	>100	57.3	>100	>100	>100	>100
7w	48.9	36	12.4	>100	>100	>100
7x	>100	55.8	72.5	>100	>100	>100
Docetaxel	0.0063	0.0008	0.0001	0.0019	0.0034	0.0019
STS	0.0046	0.0003	0.0032	0.0064	0.0298	0.0003

the series failed to display activity. By looking at the cytotoxicity results from Table 2, the most of the compounds tested in the series were cytotoxic only against carcinoma cells but not active or cytotoxic to leukemia and lymphoma but none of the tested compounds was not potent as compared to both the drug standards. The compounds shown in Figure 3 are the most active members of the series.

3.3. *In silico analyses*

Table 3 shows the physicochemical properties, ADME parameters, and violations of drug-likeness rules of the synthesized compounds. Calculated physicochemical and lipophilicity parameters are used by various filters to evaluate the drug-likeness of synthesized compounds and, in this paper, we evaluated the drug-likeness properties of the compounds with the most significant filtering approaches in the literature. The filters used here and their rules are as follows:

- Lipinski (Pfizer) filter [40]: MW $\leq$ 500; MLOGP $\leq$4.15; HBA $\leq$10; HBD $\leq$5
- Ghose filter [41]: 160 $\leq$ MW $\leq$ 480; -0.4 $\leq$ WLOGP $\leq$5.6; 40 $\leq$ MR $\leq$ 130; 20 $\leq$ atoms $\leq$70
- Veber (GSK) filter [42]: RB $\leq$ 10; TPSA $\leq$140
- Egan (Pharmacia) filter [43]: WLOGP $\leq$5.88; TPSA $\leq$131.6
- Muegge (Bayer) filter [44]: 200 $\leq$ MW $\leq$ 600, -2 $\leq$ XLOGP $\leq$5; TPSA $\leq$157; HBA $\leq$10; HBD $\leq$5; RB $\leq$ 15; number of rings $\leq$7; number of carbons >4; number of heteroatoms >1.

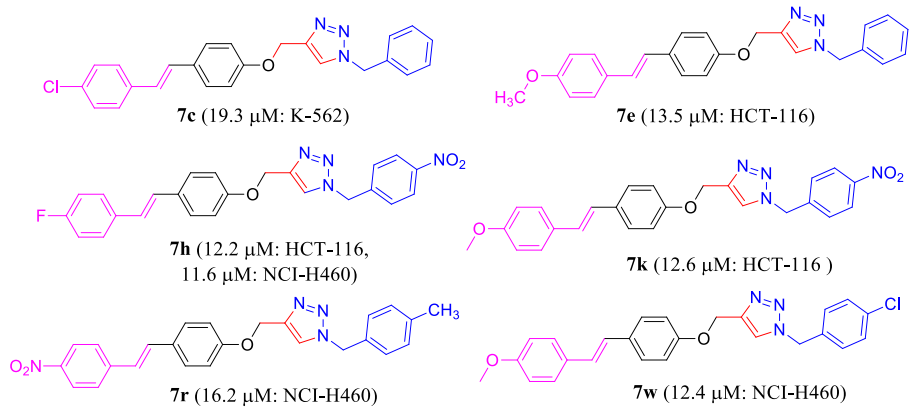

Figure 3. Biologically active stilbene linked 1,2,3-triazole derivatives.

Table 3. Physicochemical and pharmacokinetic properties of stilbene linked 1,2,3-triazoles.

Comp.	Binding affinity	Physicochemical Properties							Lipophilicity						Drug-likeness					Water Solubility		Pharmacokinetics	
		MW (g/mol)	Fsp^3	RB	HBA	HBD	MR	tPSA	ilogP	XlogP3	WlogP	MlogP	SILICOS-IT	Consensus logP	Lipinski	Ghose	Veber	Egan	Muegge	ESOL	Class	Log K_p (cm/s)	F
7a	-10.3	367.44	0.08	7	3	0	112.12	39.94	3.83	5.05	4.71	4.01	4.86	4.49	0	0	0	0	1	-5.45	Moderately	-4.96	0.55
7b	-9.9	385.43	0.08	7	4	0	112.08	39.94	3.84	5.15	5.27	4.38	5.27	4.78	1	0	0	0	1	-5.60	Moderately	-4.99	0.55
7c	-10.6	401.89	0.08	7	3	0	117.13	39.94	4.18	5.68	5.36	4.49	5.49	5.04	1	0	0	0	1	-6.04	Poorly	-4.72	0.55
7d	-10.4	381.47	0.12	7	3	0	117.09	39.94	4.03	5.42	5.01	4.22	5.38	4.81	1	0	0	0	1	-5.74	Moderately	-4.78	0.55
7e	-10.3	397.47	0.12	8	4	0	118.61	49.17	4.23	5.03	4.71	3.66	4.91	4.51	0	0	0	0	1	-5.51	Moderately	-5.15	0.55
7f	-10.1	412.44	0.08	8	5	0	120.94	85.76	3.50	4.88	4.61	3.86	2.68	3.91	0	0	0	0	0	-5.49	Moderately	-5.35	0.55
7g	-9.7	412.44	0.08	8	5	0	120.94	85.76	3.53	4.88	4.61	3.86	2.68	3.91	0	0	0	0	0	-5.49	Moderately	-5.35	0.55
7h	-11.2	430.43	0.08	8	6	0	120.90	85.76	3.55	4.98	5.17	4.24	3.10	4.21	1	0	0	0	0	-5.65	Moderately	-5.39	0.55
7i	-10.2	446.89	0.08	8	5	0	125.95	85.76	3.74	5.51	5.27	4.34	3.32	4.44	1	0	0	0	1	-6.09	Poorly	-5.11	0.55
7j	-10.5	426.47	0.12	8	5	0	125.91	85.76	3.84	5.25	4.92	3.26	3.21	4.10	0	0	0	0	1	-5.80	Moderately	-5.17	0.55
7k	-10.3	442.47	0.12	9	6	0	127.43	94.99	3.72	4.85	4.62	2.74	2.75	3.74	0	0	0	0	0	-5.56	Moderately	-5.56	0.55
7l	-10.1	457.44	0.08	9	7	0	129.76	131.58	3.29	4.71	4.52	3.01	0.53	3.21	0	0	0	0	0	-5.55	Moderately	-5.75	0.55
7m	-9.6	381.47	0.12	7	3	0	117.09	39.94	4.09	5.42	5.01	4.22	5.38	4.83	1	0	0	0	1	-5.74	Moderately	-4.78	0.55
7n	-10.2	399.49	0.12	7	4	0	117.04	39.94	4.28	5.52	5.57	4.59	5.80	5.15	1	0	0	0	1	-5.90	Moderately	-4.82	0.55
7o	-10.2	415.91	0.12	7	3	0	122.10	39.94	4.42	6.05	5.67	4.69	6.02	5.37	1	1	0	0	1	-6.34	Poorly	-4.54	0.55
7p	-10.5	395.50	0.15	7	3	0	122.05	39.94	4.27	5.78	5.32	4.42	5.91	5.14	1	0	0	0	1	-6.04	Poorly	-4.61	0.55
7q	-10.5	411.50	0.15	8	4	0	123.58	49.17	4.54	5.39	5.02	3.86	5.44	4.85	0	0	0	0	1	-5.81	Moderately	-4.98	0.55
7r	-10.9	426.47	0.12	8	5	0	125.91	85.76	3.87	5.25	4.92	3.26	3.21	4.10	0	0	0	0	1	-5.80	Moderately	-5.17	0.55
7s	-9.3	401.89	0.08	7	3	0	117.13	39.94	4.14	5.68	5.36	4.49	5.49	5.03	1	0	0	0	1	-6.04	Poorly	-4.72	0.55
7t	-9.7	419.88	0.08	7	4	0	117.09	39.94	4.21	5.78	5.92	4.86	5.91	5.33	1	1	0	1	1	-6.19	Poorly	-4.76	0.55
7u	-10.0	436.33	0.08	7	3	0	122.14	39.94	4.34	6.31	6.01	4.96	6.13	5.55	1	1	0	1	1	-6.63	Poorly	-4.48	0.55
7v	-10.2	415.91	0.12	7	3	0	122.10	39.94	4.27	6.05	5.67	4.69	6.02	5.34	1	1	0	0	1	-6.34	Poorly	-4.54	0.55
7w	-10.4	431.91	0.12	8	4	0	123.62	49.17	4.44	5.65	5.37	4.13	5.55	5.03	0	0	0	0	1	-6.10	Poorly	-4.92	0.55
7x	-10.5	446.89	0.08	8	5	0	125.95	85.76	3.73	5.51	5.27	4.34	3.32	4.43	1	0	0	0	1	-6.09	Poorly	-5.11	0.55
Docetaxel	-9.4	807.88	0.56	14	14	5	205.25	224.45	4.30	2.81	2.94	1.06	3.51	2.92	2	3	2	1	3	-5.85	Moderately	-9.23	0.17
STS	-10.8	466.53	0.32	2	4	2	139.39	69.45	3.19	3.24	3.39	2.60	3.02	3.09	0	1	0	0	1	-5.06	Moderately	-6.85	0.55

Molecular weight: MW, topological polar surface area: tPSA, Molar Refractivity: MR, fraction of sp^3 carbon atoms: Fsp^3, HBD: hydrogen bonds donor, HBA: hydrogen bond acceptor, RB: rotatable bonds, LogP values: indicator of Lipophilicity, ESOL: aqueous solubility parameter, Log K_p: skin permeation, F: Bioavailability Score.

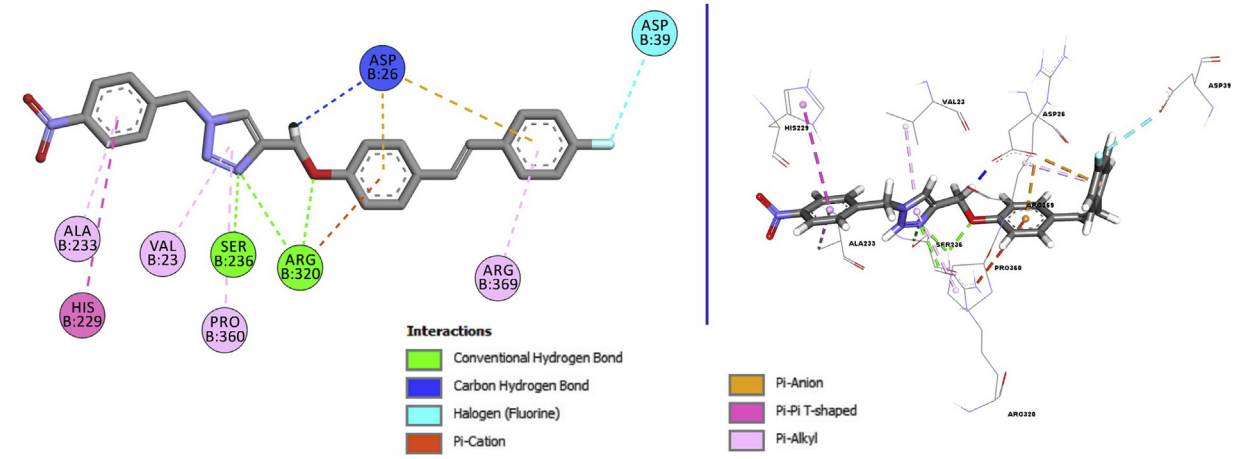

Figure 4. The 2D and 3D representations of interactions between compound **7h** and 1TUB receptor.

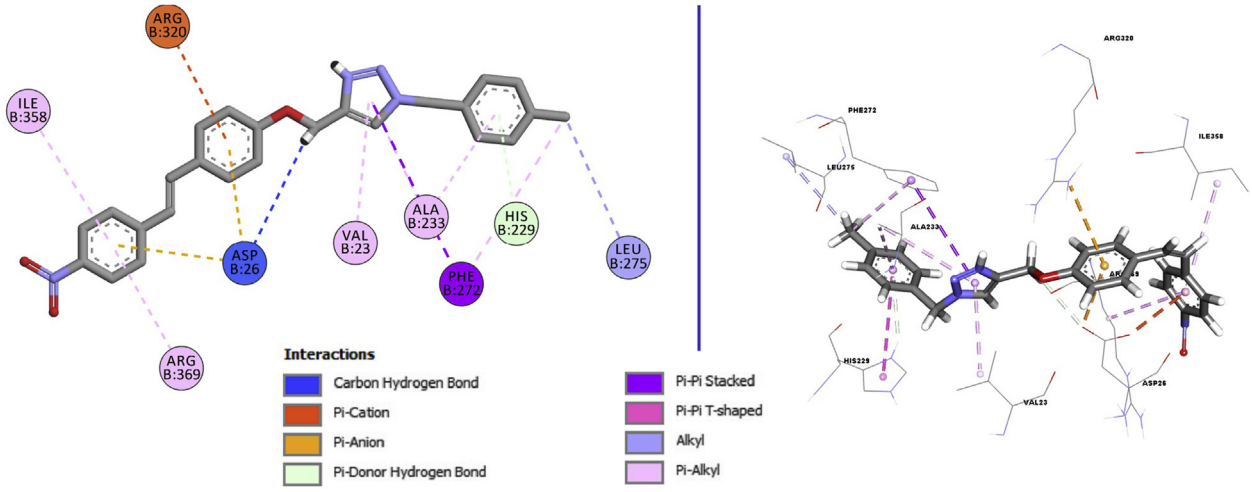

Figure 5. The 2D and 3D representations of interactions between compound **7r** and 1TUB receptor.

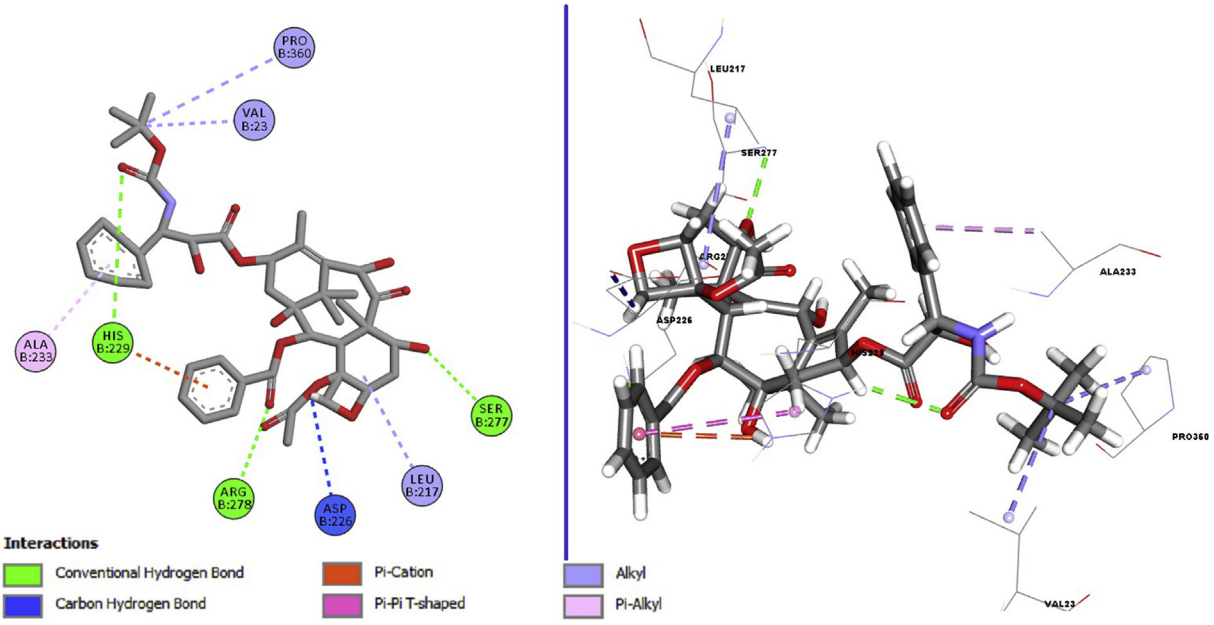

Figure 6. The 2D and 3D representations of interactions between docetaxel (co-ligand) and 1TUB receptor.

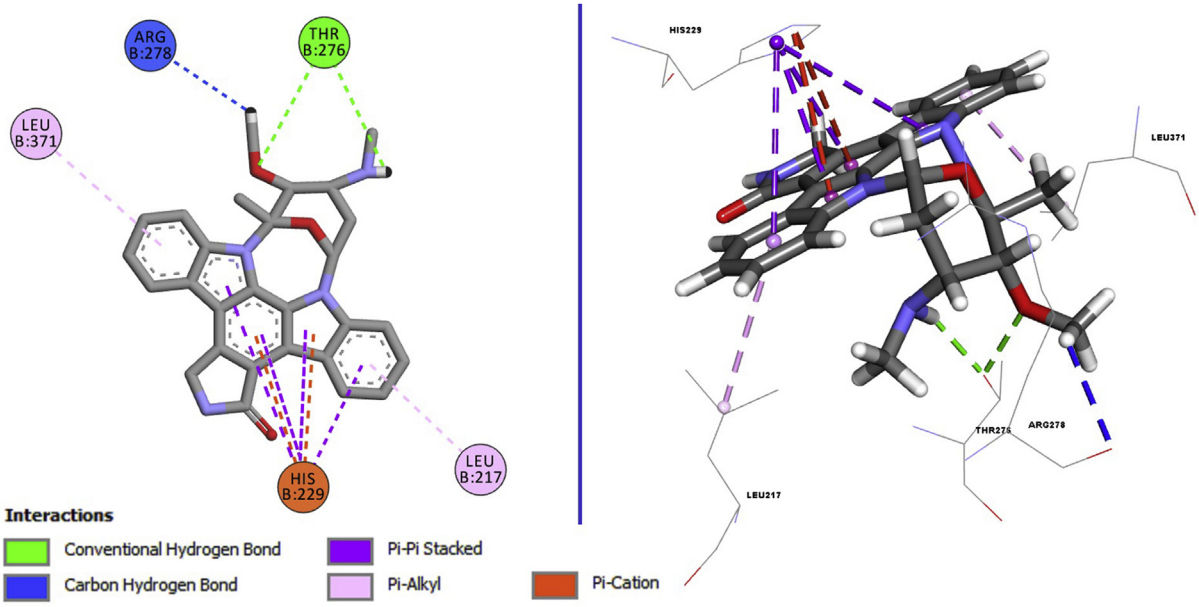

Figure 7. The 2D and 3D representations of interactions between STS and 1TUB receptor.

The filters generally assume that an orally active drug should not violate the above criteria more than once. When Table 3 is examined, it can be said that all newly synthesized compounds and the reference drug STS meet these criteria. However, the other reference drug, docetaxel, is observed to violate all filters more than once, except the Muegge filter.

Fsp^3 is another newly introduced parameter [45] to interpret the drug-likeness properties of molecules. According to Table 3, the Fsp^3 values of all compounds are lower than those of docetaxel and STS. Furthermore, we observed that the ESOL values of all synthesized compounds belonged to the moderately water-soluble class. Compounds **7c**, **7j**, **7o**, **7p**, **7s**, **7t**, **7u**, **7v**, **7w**, and **7x** have values greater than -6; thus, they are in the poorly soluble class. On the other hand, other newly synthesized compounds and reference drugs are in the moderately soluble class. Log K_p in the table is the skin permeation parameter suggested by Potts et al. [46], and a low negative log K_p value of a compound corresponds to higher absorption into human skin. Accordingly, all newly synthesized compounds have higher levels of skin absorption than the reference drugs. In the table, the bioavailability score (F) of the compounds signifies the probability that a compound will have oral bioavailability in rats [47]. The newly synthesized compounds and STS have higher F scores than docetaxel.

We also conducted molecular docking simulations to help elucidate the anticancer activities of the synthesized compounds. In the docking simulations, we utilized the crystal structure of the tubulin-docetaxel complex [24] (PDB ID: 1TUB) as the target. The binding affinity values obtained as a result of the docking studies are shown in Table 3. As is seen there, compounds **7h** and **7r**, which show good cytotoxicity *in vitro*, have the highest binding energy values. It was also observed that the reference drug STS had a higher binding affinity than the other reference drug, docetaxel, which is also the co-ligand of 1TUB. In this context, to identify the binding regions of **7h, 7r**, STS, and docetaxel, we display the two-dimensional (2D) interaction diagrams and 3D interactions between these compounds and 1TUB in Figures 4, 5, 6, and 7.

As seen in Figures 4, 5, 6, and 7, compound **7h** has a total of 4 hydrogen bond interactions, including 3 conventional hydrogen bonds (coHB) and 1 carbon hydrogen bond (caHB). Compound **7h** also has 3 electrostatic interactions (2 pi-anion (PA), 1 pi-cation (PC)), 5 hydrophobic interactions (1 pi-pi T-shaped (PT), 3 pi-alkyl (PAl)), and 1 halogen interaction. On the other hand, compound **7r** has 2 hydrogen bonds (1 coHB, 1 pi-donor hydrogen bond (pdHB)), 3 electrostatic interactions (1 PC, 2 PA), and 9 hydrophobic interactions (2 PT, 6 PAl, 1 Alkyl (Al)).

For reference compounds docetaxel and STS, it can be said that docetaxel has 3 hydrogen bonds (3 coHB, 1 caHB), 1 electrostatic interaction (1 PC), and 8 hydrophobic interactions (1 PT, 2 PAl, 5 Al), whereas STS has 2 hydrogen bonds (3 coHB, 1 caHB), 2 electrostatic interactions (1 PC), and 6 hydrophobic interactions (2 PAl, 4 pi-pi stacked (PSt)). In this case, the PSt interactions of STS may have caused STS to show higher affinity for 1TUB than docetaxel.

4. Conclusions

24 derivatives of resveratrol linked 1,2,3-triazole (**7a-x)** were synthesized, characterized by ^1H, ^{13}C NMR, Mass Spectrometry and FTIR. All the compounds tested for their cytotoxic study against three carcinoma, two leukemia and one lymphoma human cancer cell lines. Most of the compounds tested in the series were cytotoxic towards all three types of carcinoma cells but were not cytotoxic to leukemia and lymphoma. In the docking simulations, we docked all the compounds with protein 1TUB. Compounds **7h** and **7r**, which showed good cytotoxicity *in vitro*, have the highest binding energy values. We identified according to docking results that compound **7h** has four hydrogen bond, three electrostatic interactions, five hydrophobic interactions, and one halogen interaction while another compound **7r** has two hydrogen bonds, three electrostatic interactions, and nine hydrophobic interactions. Therefore, resveratrol linked 1,2,3-triazoles were more sensitive towards human carcinoma cell lines but least sensitive towards leukemia and lymphoma cell lines. Hence, further optimization is required to obtain an effective lead molecule against cancer.

Declarations

Author contribution statement

A. Das: Performed the experiments; Contributed reagents, materials, analysis tools or data.

D. Daelemans: Performed the experiments.

L. Persoons: Performed the experiments.

D. Schols: Analyzed and interpreted the data; Contributed reagents, materials, analysis tools or data; Wrote the paper.

S. S Karki: Conceived and designed the experiments; Analyzed and interpreted the data; Wrote the paper.

S. Kumar: Contributed reagents, materials, analysis tools or data; Wrote the paper.

H. Alici: Conceived and designed the experiments; Performed the experiments; Contributed reagents, materials, analysis tools or data.

H. Tahtaci: Analyzed and interpreted the data; Wrote the paper.

Funding statement

This work was supported by Federal funds from the Division of Microbiology and Infectious Diseases, National Institute of Allergy and Infectious Diseases, National Institutes of Health, Department of Health and Human Services, under Contract No. 75N93019D00005.

Data availability statement

Data will be made available on request.

Declaration of interests statement

The authors declare no conflict of interest.

Additional information

Supplementary content related to this article has been published online at https://doi.org/10.1016/j.heliyon.2020.e05893.

References

[1] V. Schirrmacher, From chemotherapy to biological therapy: a review of novel concepts to reduce the side effects of systemic cancer treatment, Int. J. Oncol. 54 (2019) 407–419.
[2] P. Simon, The importance of heterocyclic compounds in anti-cancer drug design, Drug Discov. World Summer (2017) 66–70.
[3] X.-L. Wang, K. Wan, C.-H. Zhou, Synthesis of novel sulfanilamide-derived 1,2,3-triazoles and their evaluation for antibacterial and antifungal activities, Eur. J. Med. Chem. 45 (2010) 4631–4639.
[4] Y.-W. He, C.-Z. Dong, J.-Y. Zhao, L.-L. Ma, Y.-H. Li, H.A. Aisa, 1,2,3-Triazole-containing derivatives of rupestonic acid: clickchemical synthesis and antiviral activities against influenza viruses, Eur. J. Med. Chem. 76 (2014) 245–255.
[5] D. Dheer, V. Singh, R. Shankar, Medicinal attributes of 1,2,3- triazoles: current developments, Bioorg. Chem. 71 (2017) 30–54.
[6] C.P. Kaushik, J. Sangwan, R. Luxmi, D. Kumar, D. Kumar, A. Das, A. Kumar, D. Singh, Design, synthesis, anticancer and antioxidant activities of amide linked 1,4-disubstituted 1,2,3- triazoles, J. Mol. Struct. 1226 (2021) 129255.
[7] S. Murugavel, C. Ravikumar, G. Jaabil, Ponnuswamy Alagusundaram, Synthesis, computational quantum chemical study, in silico ADMET and molecular docking analysis, in vitro biological evaluation of a novel sulfur heterocyclic thiophene derivative containing 1,2,3- triazole and pyridine moieties as a potential human topoisomerase IIα inhibiting anticancer agent, Comput. Biol. Chem. 79 (2019) 73–82.
[8] P. Yadav, K. Lal, A. Kumar, S.K. Guru, S. Jaglan, S. Bhushan, Green synthesis and anticancer potential of chalcone linked-1,2,3-triazoles, Eur. J. Med. Chem. 126 (2017) 944–953.
[9] J.H. Hart, Role of phytostilbenes in decay and disease resistance, Annu. Rev. Phytopathol. 19 (1991) 437–458.
[10] J. Burns, T. Yokota, H. Ashihara, M.E. Lean, A. Crozier, Plant foods and herbal sources of resveratrol, J. Agric. Food Chem. 50 (2002) 3337–3340.
[11] G.J. Soleas, E.P. Diamandis, D.M. Goldberg, Resveratrol: a molecule whose time has come? and gone? Clin. Biochem. 30 (1997) 91–113.
[12] H.B. Zhou, J.J. Chen, W.X. Wang, J.T. Cai, Q. Du, Anticancer activity of resveratrol on implanted human primary, World J. Gastroenterol. 11 (2005) 280–284.
[13] C.R. Pace-Asciak, S. Hahn, E.P. Diamandis, G. Soleas, D.M. Goldberg, The red wine phenolics trans-resveratrol and quercetin block human platelet aggregation and eicosanoid synthesis implications for protection against coronary heart disease, Clin. Chim. Acta 235 (1995) 207–219.
[14] J. Griggs, J.C. Metcalfe, R. Hesketh, Targeting tumour vasculature: the development of combretastatin A4, Lancet Oncol. 2 (2001) 82–87.
[15] M. Mokni, S. Elkahoui, F. Limam, M. Amri, E. Aouani, Effect of resveratrol on antioxidant enzyme activities in the brain of healthy rat, Neurochem. Res. 32 (2007) 981–987.
[16] D. Simoni, M. Roberti, F.P. Invidiata, E. Aiello, S. Aiello, P. Marchetti, R. Baruchello, M. Eleopra, A.D. Cristina, S. Grimaudo, N. Gebbia, L. Crosta, F. Dieli, M. Tolomeo, Stilbene- based anticancer agents: resveratrol analogues active toward HL 60 leukemic cells with a non-specific phase mechanism, Bioorg. Med. Chem. Lett 16 (2006) 3245–3248.
[17] A. Cirla, J. Mann, Combretastatins: from natural products to drug discovery, Nat. Prod. Rep. 20 (2003) 558–564.
[18] R. Cassano, F. De Amicis, C. Servidio, F. Curcio, S. Trombino, Preparation, characterization and in vitro evaluation of resveratrol-loaded nanospheres potentially useful for human breast carcinoma, J. Drug Deliv. Sci. Technol. 57 (2020) 101748.
[19] K.-Y. Kang, J.-K. Shin, S.-M. Lee, Pterostilbene protects against acetaminophen-induced liver injury by restoring impaired autophagic flux, Food Chem. Toxicol. 123 (2019) 536–545.
[20] M. Rostami, M. Ghorbani, M.A. Mohammadi, M. Delavar, M. Tabibiazar, S. Ramezani, Development of resveratrol loaded chitosan-gellan nanofiber as a novel gastrointestinal delivery system, Int. J. Biol. Macromol. 135 (2019) 698–705.
[21] X. Zheng, L.Y. Yu, X. Yao, B. Lv, Z.H. Yang, Q.T. Zheng, H.Y. Duan, C. Song, H.L. Xie, Synthesis and anti-cancer activities of resveratrol derivatives, Open J. Med. Chem. 6 (2016) 51–57.
[22] A. Daina, O. Michielin, V. Zoete, SwissADME: a free web tool to evaluate pharmacokinetics, drug-likeness and medicinal chemistry friendliness of small molecules, Sci. Rep. 7 (2017) 42717.
[23] A. Daina, O. Michielin, V. Zoete, iLOGP: a simple, robust, and efficient description of n-octanol/water partition coefficient for drug design using the GB/SA approach, J. Chem. Inf. Model. 54 (2014) 3284–3301.
[24] E. Nogales, S.G. Wolf, K.H. Downing, Erratum: structure of the αβ tubulin dimer by electron crystallography, Nature 393 (1998) 191, 191.
[25] L. Hong, W. Lin, F. Zhang, R. Liua, X. Zhou, Ln[N(SiMe3)2]3-catalyzed cycloaddition of terminal alkynes to azides leading to 1,5-disubstituted 1,2,3-triazoles: new mechanistic features, Chem. Commun. 49 (2013) 5589–5591.
[26] K. Lal, P. Yadav, A. Kumar, Synthesis, characterization and antimicrobial activity of 4-((1-benzyl/phenyl-1*H*-1,2,3-triazol-4-yl)methoxy)benzaldehyde analogues, Med. Chem. Res. 25 (2016) 644–652.
[27] S.S. Karki, S.R. Bhutle, G.S. Pedgaonkar, P.K. Zubaidha, R.M. Shaikh, C.G. Rajput, G.S. Shendarkar, Synthesis and biological evaluation of some stilbene-based analogues, Med. Chem. Res. 20 (2011) 1158–1163.
[28] M.D. Hanwell, D.E. Curtis, D.C. Lonie, T. Vandermeersch, E. Zurek, G.R. Hutchison, Avogadro: an advanced semantic chemical editor, visualization, and analysis platform, J. Cheminf. 4 (2012) 17.
[29] S. Dallakyan, A.J. Olson, Small-molecule Library Screening by Docking with PyRx, Chemical Biology, Springer, 2015, pp. 243–250.
[30] O. Trott, A.J. Olson, AutoDock Vina, Improving the speed and accuracy of docking with a new scoring function, efficient optimization, and multithreading, J. Comput. Chem. 31 (2010) 455–461.
[31] F.J. Solis, R.J.-B. Wets, Minimization by random search techniques, Math. Oper. Res. 6 (1981) 19–30.
[32] R. Huey, G.M. Morris, A.J. Olson, D.S. Goodsell, A semiempirical free energy force field with charge-based desolvation, J. Comput. Chem. 28 (2007) 1145–1152.
[33] D.S. Biovia, Discovery Studio Modeling Environment, Dassault Systèmes, San Diego, 2017.
[34] B.E. Maryanoff, A.B. Reitz, M.S. Mutter, R.R. Whittle, R. Olofson, Stereochemistry and mechanism of the Wittig reaction. Diasteromeric reaction intermediates and analysis of the reaction course, J. Am. Chem. Soc. 108 (1986) 7664–7678.
[35] V. Srivastava, H. Lee, Synthesis and bio-evaluation of novel quinolino-stilbene derivatives as potential anticancer agents, Bioorg. Med. Chem. 23 (2015) 7629–7640.
[36] Y.-C. Duan, Y.-Y. Guan, X.-Y. Zhai, L.-N. Ding, W.-P. Qin, D.-D. Shen, X.-Q. Liu, X.-D. Sun, Y.-C. Zheng, H.-M. Liu, Discovery of resveratrol derivatives as novel LSD1 inhibitors: design, synthesis and their biological evaluation, Eur. J. Med. Chem. 126 (2017) 246–258.
[37] K. Pavić, I. Perković, P. Gilja, F. Kozlina, K. Ester, M. Kralj, D. Schols, D. Hadjipavlou-Litina, E. Pontiki, B. Zorc, Design, synthesis and biological evaluation of novel primaquine-cinnamic acid conjugates of the amide and acylsemicarbazide type, Molecules 21 (2016) 1629.
[38] A. Montero, F. Fossella, G. Hortobagyi, V. Valero, Docetaxel for treatment of solid tumours: a systematic review of clinical data, Lancet Oncol. 6 (2005) 229–239.
[39] A. Gescher, Analogs of staurosporine: potential anticancer drugs? Gen. Pharmacol. 31 (1998) 721–728.
[40] C.A. Lipinski, F. Lombardo, B.W. Dominy, P.J. Feeney, Experimental and computational approaches to estimate solubility and permeability in drug discovery and development settings, Adv. Drug Deliv. Rev. 23 (1997) 3–25.
[41] A.K. Ghose, V.N. Viswanadhan, J.J. Wendoloski, A knowledge-based approach in designing combinatorial or medicinal chemistry libraries for drug discovery. 1. A qualitative and quantitative characterization of known drug databases, J. Comb. Chem. 1 (1999) 55–68.
[42] D.F. Veber, S.R. Johnson, H.-Y. Cheng, B.R. Smith, K.W. Ward, K.D. Kopple, Molecular properties that influence the oral bioavailability of drug candidates, J. Med. Chem. 45 (2002) 2615–2623.
[43] W.J. Egan, K.M. Merz, J.J. Baldwin, Prediction of drug absorption using multivariate statistics, J. Med. Chem. 43 (2000) 3867–3877.
[44] I. Muegge, S.L. Heald, D. Brittelli, Simple selection criteria for drug-like chemical matter, J. Med. Chem. 44 (2001) 1841–1846.
[45] F. Lovering, J. Bikker, C. Humblet, Escape from flatland: increasing saturation as an approach to improving clinical success, J. Med. Chem. 52 (2009) 6752–6756.
[46] R.O. Potts, R.H. Guy, Predicting skin permeability, Pharm. Res. (N. Y.) 9 (1992) 663–669.
[47] Y.C. Martin, A bioavailability score, J. Med. Chem. 48 (2005) 3164–3170.